NOVEL NEAR-IR PHOTOSENSITIZERS FOR PHOTODYNAMIC THERAPY & DESIGNING HEAVY ATOM FREE PHOTOSENSITIZERS FOR THE PHOTODYNAMIC THERAPY

A THESIS SUBMITTED TO
THE GRADUATE SCHOOL OF ENGINEERING AND SCIENCE
OF BİLKENT UNIVERSITY
IN PARTIAL FULFILLMENT OF THE REQUIREMENTS FOR
THE DEGREE OF
DOCTOR OF PHILOSOPHY
IN
MATERIALS SCIENCE AND NANOTECHNOLOGY

By
Bilal Kılıç
March 2016

NOVEL NEAR-IR PHOTOSENSITIZERS FOR PHOTODYNAMIC THERAPY & DESIGNING HEAVY ATOM FREE PHOTOSENSITIZERS FOR THE PHOTODYNAMIC THERAPY

By Bilal KILIÇ

March 2016

We certify that I have read this thesis and that in my opinion it is fully adequate, in scope and in quality, as a dissertation for the degree of doctor of philosophy.

_____

Engin U. Akkaya (Advisor)

_____

Mehmet Bayındır

_____

Özdemir Doğan

Zeynel Seferoğlu

Serdar Atılgan

Approved for the Graduate School of Engineering and Science:

Levent Onural

Director of the Graduate School

ABSTRACT

NOVEL NEAR-IR PHOTOSENSITIZERS FOR PHOTODYNAMIC THERAPY & DESIGNING HEAVY ATOM FREE PHOTOSENSITIZERS FOR THE PHOTODYNAMIC THERAPY

Bilal Kılıç

Ph.D. in Materials Science and Nanotechnology

Advisor: Engin U. Akkaya

March 2016

Photodynamic therapy (PDT) is a promising and emerging noninvasive treatment modality for the treatment of a great number of malignant and non-malignant diseases. Therapeutic strategy in PDT is performed by combining a photosensitizer which can potently and specifically kill diseased cell and a light source, preferentially near-IR light (650-800 nm). In spite of the fact that numerous studies have been published and notable progress has been made in tumor biology and photochemistry which let us to design novel therapeutic agents, the number of the new therapeutic agents which have been recently got approval for clinical application are relatively low. We aimed to produce novel photosensitizers. In the chapters 3, 4 and 5 BODIPY dyes which are amenable to functionalization have been used to produce a novel series of BODIPY-based photosensitizers. We synthesized and characterized a series of novel BODIPY-based photosensitizers. The first part describes novel near-IR BODIPY-based photosensitizers. In the second part, the main goal was to design and synthesize heavy atom free BODIPY-based photosensitizers. In this respect, a new modification of the BODIPY dyes, novel orthogonal BODIPYs were synthesized and their computational analysis were done. A cell culture assay with cancer cell lines was performed in order to demonstrate photocytotoxicity of the orthogonal BODIPY. The third study underlines the importance of micelle-embedded BODIPY-based photosensitizers for photodynamic therapy.

Keywords: photodynamic therapy, singlet oxygen, boradiazaindacene

ÖZET

FOTODİNAMİK TERAPİ İÇİN KIZIL ÖTESİ IŞIĞI SOĞURABİLEN YENİ FOTODUYARLAŞTIRICI VE AĞIR ATOM İÇERMEYEN FOTODUYARLAŞTIRICILARIN TASARLANMASI

Bilal Kılıç

Malzeme Bilimi ve Nanoteknoloji, Doktora

TEZ DANIŞMANI: ENGİN UMUT AKKAYA

Mart 2016

Fotodinamik terapi kanserli ve kötü huylu olmayan birçok hastalığın tedavisinde kullanılan yaygın ve umut vaat eden bir tedavi yöntemidir. Tedavi yöntemi, hasta hücreyi seçici ve etkili bir şekilde öldüren bir fotoduyarlaştırıcı ve bir ışık kaynağının, tercihen yakın kızıl ötesi (650-800 nm), kullanılması ile gerçekleştirilir. Son yıllarda yayınlanan çok sayıda çalışmaya ve bizlere yeni fotouyarıcılar dizayn etmemize olanak sağlayan tümör biyolojisindeki ve fotokimyadaki gelişmelere rağmen, klinik uygulamaları için onay alan terapi ajanı sayısı oldukça azdır. Bu tezde yeni fotoduyarlaştırıcılar sentezlemeyi hedefledik. Üçüncü dördüncü beşinci bölümlerde çeşitlendirilmeye oldukça uygun olan BODIPY boyar maddeleri kullanılarak bir seri yeni BODIPY temelli fotoduyarlaştırıcılar sentezlendi ve karakterize edildi. Birinci bölüm yeni yakın kızıl ötesi ışığı soğurabilen BODIPY temelli fotoduyarlaştırıcıları içermektedir. İkinci kısım ise, ağır atom içermeyen BODIPY temelli fotoduyarlaştırıcıların dizaynı ve sentezini içermektedir. Bu doğrultuda BODIPY boyar maddelerinin yeni bir türevi olan, bir birine dik BODIPY türevleri sentezlenmiş ve bu boyar maddelerin teorik çalışmaları da yapılmıştır. Bir birine dik BODIPY türevlerinin ışık sitotoksisitesini göstermek amacıyla hücre kültürü deneyleri gerçekleştirilmiştir. Misel içerisine yerleştirilmiş BODIPY temelli fotoduyarlıştırıcıların önemine ise üçüncü çalışmada vurgu yapılmaktadır.

Anahtar Sözcükler: foto dinamik terapi , boradiazaindasen, singlet oksijen

ACKNOWLEDGEMENTS

I would like to express my heartfelt thanks and deepest appreciation to my supervisor Prof. Dr. Engin U. Akkaya for his unremitting support, infinite patience, encouragement and guidance during the course of this research. I am also heartily grateful to him for demonstrating us how to become a good scientist and mentor. Without his guidance and cheerfulness and positive attitude towards me this thesis would not have been possible. I will never forget his support and personality throughout my life.

I am deeply grateful Prof. Dr. Özdemir Doğan for his significant advices and discussions.

I would like to also appreciatively acknowledge my PhD thesis committee members, Assoc. Prof. Dr. Zeynel Seferoğlu and Assoc. Prof. Dr. Serdar Atılgan for their grateful support and positive attitudes towards me.

I owe special thanks to Dr. Ruslan Guliyev and Dr. Nisa Yesilgül for his support, advices from the very beginning.

I would like to express my special thanks to Dr. Safacan Kölemen, Dr. Ziya Köstereli, Dr. Seda Demirel, Bilal Uyar and Ahmet Atılgan for their partnership in my PhD studies.

My gratitude also goes to our present and previous group members H. Eser Iden, Merve Türkşanlı Kaplan, Gizem Çeltek, Şeyma Öztürk Guliyeva, Dr. Fazlı Sözmen, Tugrul Nalbantoglu, Tuba Yaşar, Ahmet Bekdemir, Elif Ertem Bekdemir, Tuğçe Durgut, Tuğçe Karataş, Cansu Kaya, Ceren Çamur, Darika Okeava, Hale Atılgan, Jose Bila and rest of the SCL (Supramolecular Chemistry Laboratory) members for great friendships, grateful collaborations, and wonderful atmosphere in the laboratory.

I also owe grateful thanks to Dr. Lale Doğan, Dr. Dicle Güç for their notable efforts during the cell culture studies.

I would like to thank to Dr. Yavuz Dede and Selin Duman Muhammed Buyuktemiz for their helpful discussions, collaborations and computational studies

I would like to express my special thanks to UNAM (Institute of Materials Science and Nanotechnology) for their support.

I would like to thank to TÜBİTAK (The Scientific and Technological Research Council of Turkey) for financial support

Finally, the most special thanks go to my family for their unremitting support, love and understanding. Without their support and belief none of this would have been possible.

LIST OF ABBREVIATIONS

BODIPY	**:**	4,4-difluoro-4-bora-3a,4a-diaza-s-indacene
CASSCF	**:**	Complete active-space self consistent field methodology
$CHCl_3$	**:**	Chloroform
DCM	**:**	Dichloromethane
DS-TR	**:**	Doubly substituted-tetra radicalic
DFT	**:**	Density functional theory
ISC	**:**	Intersystem crossing
HOMO	**:**	Highest occupied molecular orbital
LUMO	**:**	Lowest unoccupied molecular orbital
MS	**:**	Mass spectrometry
NMR	**:**	Nuclear magnetic resonance
NOON	**:**	Natural orbitals and occupation numbers
PDT	**:**	Photodynamic therapy
PS	**:**	Photosensitizer
SS	**:**	Singly substituted
TLC	**:**	Thin layer chromatography

TABLE OF CONTENTS

LIST OF FIGURES

LIST OF TABLES

CHAPTER 1

INTRODUCTION

Cancer also known as a malignant tumor is a challenging and terrifying disease and its most widely used treatment modalities are chemotherapy, radiation therapy and surgery. These treatment modalities frighten patients due to the side effects that up to know could not be obviated. A novel treatment modality, Photodynamic therapy that has been used clinically for around 25 years has been emerged and widely used as an alternative method for treatment of the malignant and nonmalignant diseases. Photodynamic therapy has numerous advantages compared to the conventional treatment modalities owing to the fact that it is noninvasive and selective treatment method. Over the past decade, there have been great number studies showing the application of PDT for the treatment of various diseases and there is an important impetus to produce novel and efficient photodynamic therapy agents. The only know side effects of the current photodynamic therapy agents, mostly porphyrin based photosensitizers is the skin photosensitization. To overcome this drawback, novel photosensitizers that absorb light in the near-IR region of the electromagnetic spectrum, where the deepest tissue penetration is available, are required to perform more effective therapeutic action.

With this consideration in mind, we design and synthesized a novel series of BODIPY based photosensitizers which absorb light in the therapeutic window of the electromagnetic spectrum (650-800 nm). BODIPY dyes are pertinent to functionalization on their core. Furthermore, BODIPY dyes have high fluorescence quantum yields, straightforward synthetic methods and high

absorption coefficients. Therefore, we introduced novel BODIPY-based photosensitizers in Chapter 3.

The choice of the photosensitizer plays an important role in the photodynamic therapy. It is a well-known fact that incorporation of the heavy atoms to the core of the BODIPY confer inter system crossing (ISC), yielding cytotoxic singlet oxygen. However, an effective photosensitizer should be non-toxic in the absence of light or has low dark-toxicity. Incorporation of the heavy atoms gives rise to an increase in dark toxicity of the photosensitizers. We have been at pains to find out a method in order to produce cytotoxic single oxygen without introducing singlet oxygen to the core of the BODIPY which alleviate the dark toxicity of the photosensitizers. In chapter 4, we introduced novel BODIPY derivatives which have orthogonal arrangement. This arrangement has a doubly substituted tetra radical state (DS-TR) that has a relationship with $S_1 \rightarrow T_1$ intersystem crossing, resulting in generation of cytotoxic singlet oxygen. In the chapter 5, we targeted Bodipy derivatives with heavy atom substitutions which would facilitate intersystem crossing. In addition, to ensure that these compounds would prefer a micellar structure as opposed to bulk aqueous solution, we incorporated long alkyl chains at the *meso* positions (C-8) of the Bodipy dye

CHAPTER 2

BACKGROUND

2.1 Photodynamic Therapy

2.1.1 General Information

Photodynamic therapy (called PDT, photoirradiation therapy, phototherapy, or photochemotherapy) is one of the most promising and minimally invasive treatment modality for certain cancers such as bladder cancer, skin cancer, gynecological, head and neck cancer, gastrointerstinal cancer cervical cancer and gastric cancer and for many other certain diseases like psoriasis, basal cell carcinoma[1]. Furthermore, PDT is used as a treatment modality in cardiology[2].

The PDT strategy is based on the preferential localization of the certain photosensitizers in tumor tissues upon systematic administration. After the administration of the photosensitizer into the body, the sensitizer is activated by red or near infrared (NIR) which leads to generation of reactive oxygen species (ROS) including singlet oxygen ($^1O_2$) and thus irreversibly damaging tumor cells. These PSs are harmless in the absence of light and the phototoxicity of these photosensitizers mainly relies on the generation of the singlet oxygen, which is converted from its triplet state to its singlet state by the exited-state dye. Photosensitizing agents, which is also known as photosensitizer, are administrated locally or intravenously

Moreover, the photosensitizer is selectively absorbed and retained within the targeted tissues[3]. When the target tissue is illuminated by a certain light source at an appropriate wavelength, especially in the therapeutic window, the nearby normal tissues which contain little amount of photosensitizer or no photosensitizer are prevented from photodamage and injury.

Over the past decade, significant progress has been made in the development of novel photosensitizers[4]. However, the efficacy and properties of these materials must be improved in order to meet treatment requirements.

The first property relevant to the PS is its absorption maximum which determines its efficiency with regard to the singlet oxygen generation. It is a well-known fact that photosensitization relies on the absorption of light of the correct wavelength by a photosensitizer

A convenient photodynamic therapy agent should have absorption maxima in the spectral region 700- 900 nm which is known as therapeutic window. Because of the fact that below 700 nm light array cannot penetrate deeply into the tissue and water into the body begins to absorb light above 900 nm, a well-designed photosensitizer should absorb light in the therapeutic window[5].

Another key issue influencing the photodynamic capability of a photosensitizer is the efficiency of the singlet oxygen generation. Singlet oxygen is one of the most important parameters for PDT which is very reactive and causes cell death.

2.1.2 History of the Photodynamic therapy

Although light has been used a therapeutic agent for thousands of years in order to heal malignant and non-malignant diseases, photodynamic therapy was initially observed more than hundred years ago[6,7]. Light was widely used by ancient Egyptian, Indian and Chinese civilization as a treatment modality for various diseases such as psoriasis, rickets and skin cancer[8].

In 1900, Oscar Raab has showed that the use of organic photosensitizer acridine orange in combination with day light gives rise to the cytotoxic effect on infusoria[7]. In the same year, scientist J.Prime has discovered that patients suffered from dermatitis when they were exposure to the sunlight after treatment which was executed by using eosin[9].

In 1901, Niels Finsen has reported that smallpox and cutaneous tuberculosis was treated by using light. In 1903, he was awarded Nobel Prize for his work on phototherapy[10] .

In the same year, Herman Von Tappeiner, director of the Institute of Pharmacology at the University of Munich and A. Jesionek, the dermatologist, have demonstrated that skin tumors successfully treated by using eosin which is applied topically in the presence of light. It was then named as photodynamic action. The term "photodynamic" was firstly used by von Tappeiner and A. Jodbauer in 1907[11].

In 1911, W. Hausmann has reported that paramecium and red blood cells were treated with light and hematoporphyrin which was a derivative of the most widely studied photosensitizers, porphyrins, in the mid-nineteenth century. He also reported that the treated mice showed skin reactions, such as extensive edama and erythema[12].

In 1913, the German physician Friedrich Meyer-Bertz conducted a study with hematoporphyrin to treat a human. He delivered the photosensitizer, 200 mg hematoporphyrin, into his hand intravenously and he suffered from pain and

swelling after the exposure to the sun light. It was the first reported photodynamic therapy experiment on humans[13].

In 1942, the German scientist Auler and Banzer reported that hematoporphyrin in the malignant tissues has higher fluorescence compared to the surrounding tissues and these malignant tissues were killed by necrosis after illumination with a powerful quartz lamp[14].

In 1955, Dr Samuel Schwartz reported that he developed a new hematoporphyrin derivative (HPD)[15]. It was shown that HPD was twice as phototoxic as hematoporphyrin[16]. This compound, HPD, was used by Richard Lipson and coworkers in their studies[17]. They demonstrated that hematoporphyrin derivatives can be used as a diagnostic tool[16].

In 1972, first in vivo study was accomplished by I. Diamond and their coworkers. They reported by performing PDT to treat tumors which was implanted in rats, tumor growth was inhibited for approximately 20 days[18].

In 1975, Thomas Dougherty and colleagues reported that they managed to eradicate malignant tissues in mice by using hematoporphyrin derivative (HpD) and red light.

J.F.Kelly and colleagues published a study in the same year. It revealed that bladder carcinoma in mice could be treated by using HPD in combination with light[19].

Clinical trials with HPD were initiated in 1976[1]. Kelly and colleagues performed a successful study which was the first human trials with hematoporphyrin derivative. This most widely used photosensitizer was used to treat recurrent bladder cancer. Malignant tissue growth was slowed down and these tissues were killed by necrosis. Following this study, Dougherty and coworkers treated 25 patients by using similar approach[20]. Y.Hayata and coworkers reported that PDT was used to treat obstructing malignant tissues, lung cancer. The result of this trial was not impressive but only around 7% of tumor of the patients was eradicated successfully[21].

In 1984, J.S. Mc Caughan and coworkers reported that PDS was used as a treatment modalitiy for the oesphageal cancer[22]. Only one year after this breakthrough study, gastric cancer was cured with PDT by Y.Hayata and coworkers[23].

Thereafter, photodynamic therapy was also used for the treatment of the pancreatic carcinoma[24], cholangioma[25], mesothelium carcinoma[26] , skin carcinoma[27], head and neck tumors[28] , and brain tumors[29] . According to these breakthrough studies, it was revealed that PDT treatment could be effectively applied on early-stage cancers[30] .

In the late 1980s, there have been a great number of studies on PDT that results in microvascular collapse, subsequently this mircrovascular collapse gives rise to the severe tissue hypoxia and anoxia[31,32].

In 1993, the most frequently used photosensitizer porfimer sodium (Photofrin), a purified hematoporphyrin derivative, was used to treat bladder cancer and its approval was reported in the same year in Canada. It was the first photosensitizer which was for approved for photodynamic therapy (Figure 1)[33].

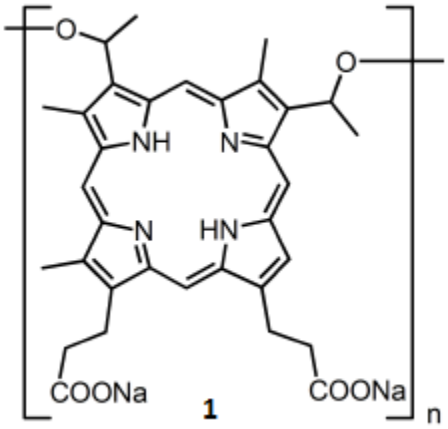

Figure 1 : Chemical structure of porfimer sodium

In the following years, other photosensitizers have been reported which employed in the photodynamic milieu and they were FDA approved. One of them is temoporfin (Foscan) which gained its approval in Europe and is used for the treatment of the head and neck tumor, brain tumor and skin carcinoma (Figure 2)[34].

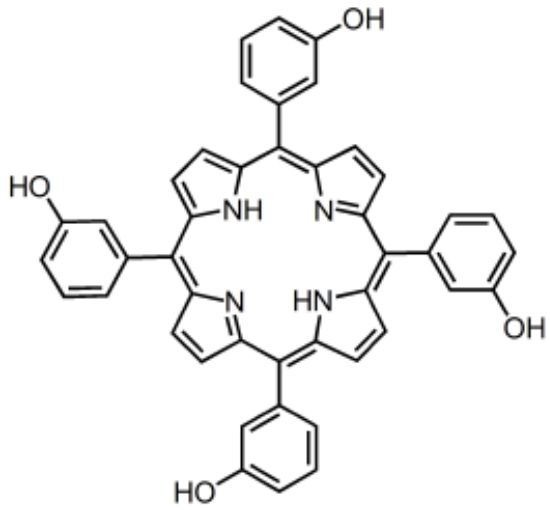

2

Figure 2: Chemical Structure of the temoporfin

2.1.3 Working Principle of PDT

Photodynamic therapy includes various photophysical processes. Figure 3 graphically demonstrates the process of light absorption and energy transfer, which is essential for the photodynamic therapy. After the activation of the photosensitizer upon absorption of the light transforms the photosensitizer from its ground state (^{1}PS) to its excited single state (^{1}PS*,Fig. 3) .This is a short-lived (nanoseconds) species and may decay from this excited state to ground state and during this decay the fluorescence emits. We can use this property clinically for photodetection[35]. The PS can undergo electron spin conversion to its long –lived (microseconds) triplet state (^{3}PS*). Because of the fact that the loss of energy by emission of light (phosphorescence) is a spin forbidden process the photosensitizer triplet state has a long lifetime.

Because of the dependence on a long-lived triplet excited state, the synthesis of the photosensitizers are encouraged in order to improve this feature usually by attaching the heavy halogens to the photosensitizers, i.e. via the heavy atom effect. In this case we can obtain better results in terms of therapeutic effect.

Reactive oxygen can be generated through two types of reaction. In the type 2 reaction, the excited state photosensitizer reacts with molecular oxygen, yielding singlet oxygen. In the type one reaction the excited photosensitizer can react with a substrate either by proton or by electron transfer and form radical or radical ions. After the formation of these radicals, they can react with oxygen and produce oxygenated products[36,37].

The second type reaction illustrates that the energy of the excited photosensitizer can be transferred to oxygen and the singlet oxygen, which is a cytotoxic species, is formed[38.]

The ratio between these two types of reactions is concentrations and oxygen dependent.

Owing to the fact that reactive oxygen species are highly reactive and have short half-life, only tissues in close proximity to the location, where reactive oxygen species are produced, are treated with photodynamic therapy.

As a result, the activated photosensitizer and energy transfer result in apoptosis and necrosis of targeted either malignant or nonmalignant tissue.

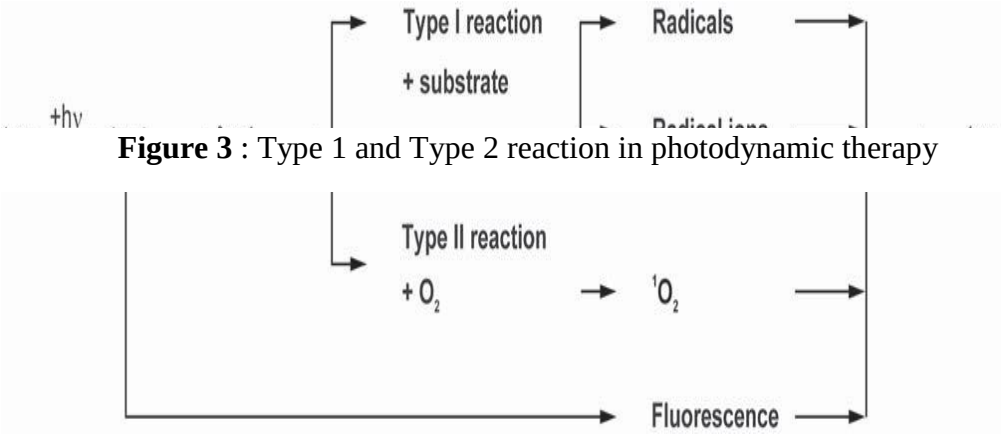

Figure 3 : Type 1 and Type 2 reaction in photodynamic therapy

Because of the fact that the effectiveness of the nearly all photosensitizers depends on oxygen, photodynamic action of the photosensitizers does not happen in the area of tissues where they lack oxygen[39].

Location of photodamage belongs to the type of the photosensitizer. Therefore, a great photodynamic agent would be diversely gathered in the target tissue. It is worth to address that specifity of destruction of cancer cells can be achieved by selective application of the photosensitizer, selective uptake of the photosensitizer, high quantum yields of singlet oxygen, which is produced during reactions we discussed above, and by the selective exposure of malignant tissue to the active light[40]. There are numerous drawbacks of photodynamic therapy.

One of them is the prolonged skin photosensitization[41]. Another one is that the patient needs to stay away from the sunlight exposure for a certain time (1-4 weeks).

Generally, efficiency of the photodynamic therapy and cytotoxic effect depends on administration of the photosensitizer, light exposure doses, interval between illumination of the tissues by a certain light source and administrations of the photosensitizer into the body, light source and type of photosensitizers[42].

2.1.4 Photodynamic Effect and Cell Death Mechanism

Photodynamic therapy has three major components. These are photosensitizers, clinically known as drug, light source and oxygen. To obtain photodynamic action and to generate cytotoxic oxygen, singlet oxygen, all of these three components are required. Reactive singlet oxygen gives rise to the cellular destruction by means of direct cellular damage, vascular shutdown, activation of immune response system. After the generation of the reactive singlet oxygen, it directly reacts with cellular components, such as nucleic acids, lipids and proteins[43]. As a result, oxidative stress occurs, causing cellular destruction.

There are two types of cellular death. One of them is apoptosis and another one is necrosis. The type of the cellular death depends on localization of the photosensitizer. It is also dependent upon the quantity of the reactive singlet oxygen[44]. Patterson et al. has reported that photosensitizers which localized especially in the mitochondria or endoplasmic reticulum mostly gives rise to the apoptosis. On the other hand, photosensitizers that localized in lysosomes or in the plasma membrane is likely to cause necrosis[45]. Photodynamic therapy can also cause cellular destruction by means of acute local inflammation[46].

There are a number of factors that affect efficiency of the treatment. Localization of the photosensitizer is one of the most widely known factors that determine

efficiency of the photodynamic therapy action. In order to improve efficacy of the treatment, a great number of study have been performed and published in recent years. To obtain better localization in the cancerous cells, selectivity of the photosensitizers should be improved. Photodynamic therapy with localized and targeted photosensitizer is a smart treatment option owing to the fact that only targeted cells are treated without any side effect.

By designing and synthesizing photosensitizer through conjugation to different type of targeting peptides, targeting for photosensitizers uptake into cancerous cells has been accomplished[47]. Other approaches that are used to improve localization of the photosensitizers are conjugation of small targeting ligands and protein conjugation. These types of photosensitizers are commonly known as third generation photosensitizers[48].

In recent years, selectivity of the photosensitizers and designing novel activatable photosensitizers has been the focus of the extensive research[4].

Akkaya group reported that near-IR absorbing BODIPY-based photosensitizers were selectively activated once they were inside the cells. In this study, they synthesized a series of BODIPY based photosensitizers that are in caged form, i.e. they cannot produce singlet oxygen. However, once these BODIPY-based chromophores are inside the cells, they become activated because of the fact that cancer cells have high intracellular glutathione concentration, photosensitizers become active after the quencher has been cleaved by intracellular glutathione[3].

2.1.5 Light in Photodynamic Therapy

Light is one of the three essential components of the photodynamic therapy as it is essential for the life

It is a well-known fact that UV-light radiates at short-wavelength of the electromagnetic spectrum and it is a high-energy radiation. Also, it is an undeniable fact that all human beings are exposed to the UV-light during their daily life. Therefore, some precautions have to be taken against the UV-light during our daily life. This high energy ray is capable of remove electrons from

DNA and serious damage can occur, including tumor formation. During exposure to the UV-light, skin behaves like a protective coating. Melanin absorbs UV-light in order to impede its effect and the color of our skin is changed since the pigmentation occurs since melanin absorbs light in the region of the electromagnetic spectrum where sunlight radiates (Figure 4).

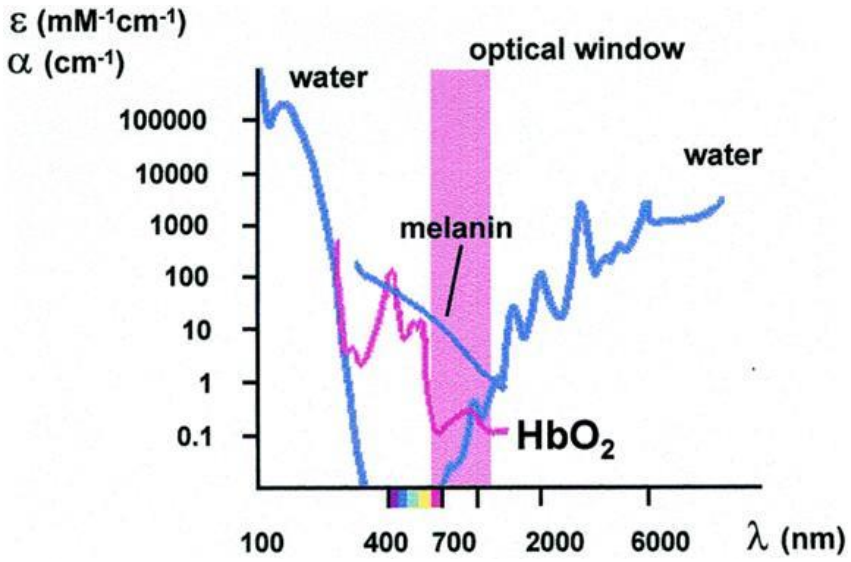

Figure 4 : Absorption spectra of major intracellular absorbers

On the other hand, there are another biomolecules absorbing UV-light in the skin, such as hemoglobin and amino acids which contain aromatic molecules in their chemical structure[49].

Intracellular absorption is therefore especially important considering the activation of the photosensitizer under a certain light source and at a certain wavelength. As a result, selection of the light source and its wavelengths range are of great importance in terms of skin sensitivity during the treatment of photodynamic therapy action. Long-wavelength light is essential to the sufficient tissue penetration due to the intracellular absorption and light scattering. In the

last decade, considerable effort has been devoted to delivering of light to the tumor site, including interstitial and superficial illumination.

It was reported in the literature that photosensitizer, ALA, was used for treatment of the squamous cell carcinoma. It was applied topically and light source was superficially delivered to the tumor. For treatment of the thicker cancerous tissues, it can be necessary to administrate the photosensitizers into the body intravenously and light is required to deliver via implanted optical-fiber light sources.

2.2 Photosensitizers

2.2.1 Photosensitizers based on BODIPY Dyes

As mentioned in the previous chapter, photosensitizer is one of the key components of the photodynamic therapy. In order to generate more effectively singlet oxygen which is another key component of the photodynamic therapy, the selection of an appropriate photosensitizer is of paramount importance. In recent years, production of the novel and effective photosensitizers has been the focus of extensive research[4]. There are a great number of clinically approved photosensitizers, such as HPD-photofrin, verteporfin, Foscan etc. However, there has not been yet any approval for the use of BODIPY-based photosensitizers in clinical treatment, but BODIPY-based photosensitizers have important features that will most probably provide clinical approval for their use in photodynamic therapy application in the near future[3].

One of the most widely used photosensitizers, photofrin has a number disadvantages. Since its activation by light occurs at *ca*. 630 nm, light rays cannot penetrate into tissue more than few millimeters. Besides that, illumination of the skin at this wavelength gives rise to the painful edema which is known as photosensitivity[50].

Due to the abovementioned drawbacks of phorphyrin-based photosensitizers, researchers have extensively attempted to develop novel photosensitizers and many studies have been focused on design and synthesis of the new photosensitizers in recent times[51].

It is a well-known fact that a photosensitizer should be nontoxic in the absence of light and have low side effects and absorption especially at long wavelengths of the electromagnetic spectrum for deeper tissue penetration. Furthermore, photosensitizers should be resistance to photobleaching.

BODIPY (4, 4-difluoro-4-bora-3a, 4a-diaza-s-indacene) dyes have attracted much attention as a photosensitizer over last decade owing to its characteristics which are particularly required for the effective photosensitizers and photodynamic

action. In 1968, BODIPY was for the first time synthesized and reported by Treibs and Kreuzer[52].

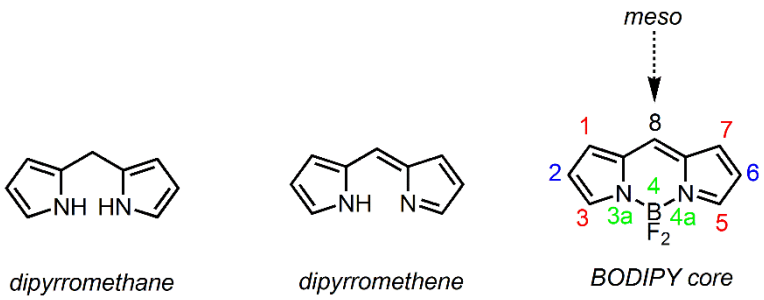

Figure 5 : Molecular structures of BODIPY and its precursors.

BODIPY dyes have attracted much attention as photosensitizers and fluorescent molecular sensors over the past few decades because of the fact that they have sharp absorption, high fluorescence quantum yields, high excitation coefficients, light to dark toxicity ratios[53] and high stability[54]. Since BODIPY dyes have distinctive characteristics, they have been used for the application as solar cells[55], fluorescent imaging probe[56] and chemical sensor.[57]

Furthermore, BODIPY dyes are amenable to the modifications on their core (Figure 5) . Their absorption and fluorescence emission can be easily tuned. By utilizing these properties of the BODIPY dyes, their derivatives have been synthesized and different derivatives have developed over the past two decade by using substitution on the BODIPY core, by reacting an aldehyde with methyl groups on the 3 and 5-position of the BODIPY core (Knovenagel condensation reaction) [58] and by displacing the fluorine atoms with boron atoms on the 4-position of the BODIPY core[59]. Another modification option has been applied at the 8-position (meso) of the BODIPY core.[60,61] Prasad and coworker have reported that meso-phenyl and meso-naphtalenyl substituted BODIPY derivatives

were synthesized by utilizing the distinctive feature of the BODIPY dyes which is straightforward synthesis and functionalization.[62]

All of these distinctive properties of the BODIPY dyes have inspired efforts to develop BODIPY based photosensitizers.[63]

Nagano and coworkers have shown that a halogenated BODIPY derivative can generate cytotoxic singlet oxygen. It was the first BODIPY which was reported as a photosensitizer in 2005. In this work, they introduced iodine atoms to the core of BODIPY in order to achieve ISC for the production of singlet oxygen. After the synthesis and characterization of the diiodo-BODIPY (**3**), singlet oxygen quantum yield was measured by using a trap molecule which is 1,3-diphenylisobenzofuran (DBPF) (Figure 6).

3

Figure 6 : Halogenated BODIPYderivative

Cell culture studies were performed by using HeLa cells. According to the results of singlet oxygen generation experiments with cell culture, this halogenated BODIPY derivative is photocytotoxic under the light illumination.[64]

In 2010, Burgess and coworkers have reported a study. This work presents another new BODIPY based photosensitizer. In this study, a functional group, ethylene-carboxylic acid was introduced to the meso-position of the BODIPY unit. After synthesis and characterization of the halogenated and meso-substituted BODIPY

derivative (**4**), cell culture studies were carried out. It is a noteworthy fact that this BODIPY derivative has high singlet oxygen quantum yield and high-to-dark phototoxicity (Figure 7).

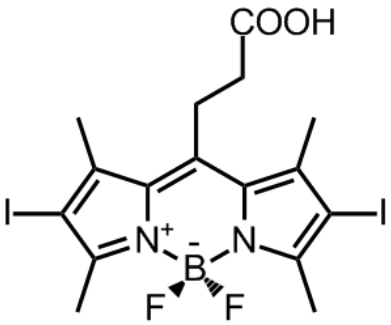

4

Figure 7: Molecular structure of the BODIPY-based photosensitizer

HSC-2 cells were treated with this BODIPY-based photosensitizer under the illumination of light source at wavelength 525nm for 2 hours. It was shown that photosensitizer **4** was delivered in the mitochondria and gave rise to the cell death via apoptosis.[53]

In 2012, Arbeloa and colleagues have prepared a BODIPY-based photosensitizer by introducing iodine atoms at the 2- and 6-positions and 3- and 5-positions of the BODIPY unit. (Compound **5**,**6** and **7**)

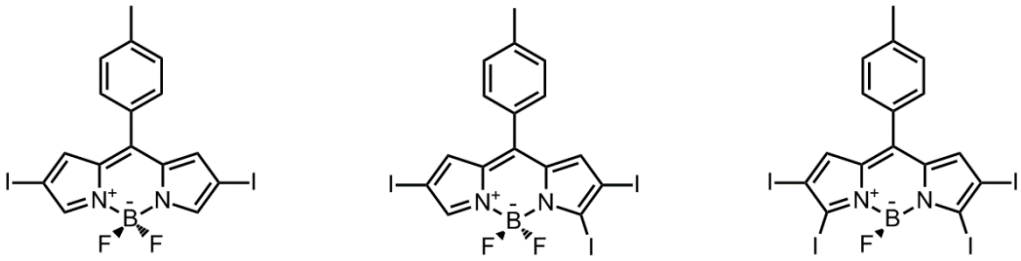

5 6 7

It was shown that attachment of the iodine atoms to the 3-and 5- position of the

Figure 8 : Molecular structures of the BODIPY based photosensitizers (5, 6 and 7)

BODIPY cores give rise to an increase in fluorescence of the molecule and they have high singlet oxygen quantum yield. It was experimentally proved that these photosensitizers are highly stable against light.[65]

Suzuki and coworkers reported that they synthesized and characterized heteroaryl-fused BODIPY derivatives (Figure 9 and 10). In this study, singlet oxygen generation experiments of the BODIPY-based photosensitizers were performed by using DPBF. It was found that they have high singlet oxygen yield.

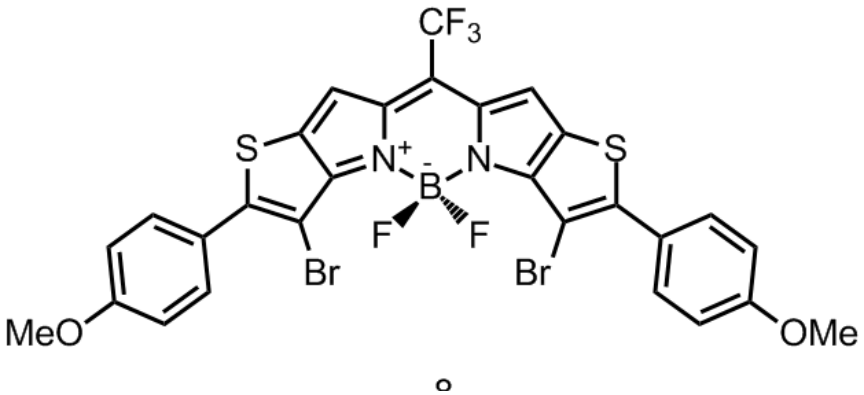

Figure 9 : Molecular structure of the heteroaryl-fused BODIPY based photosensitizer (Compound **8**)

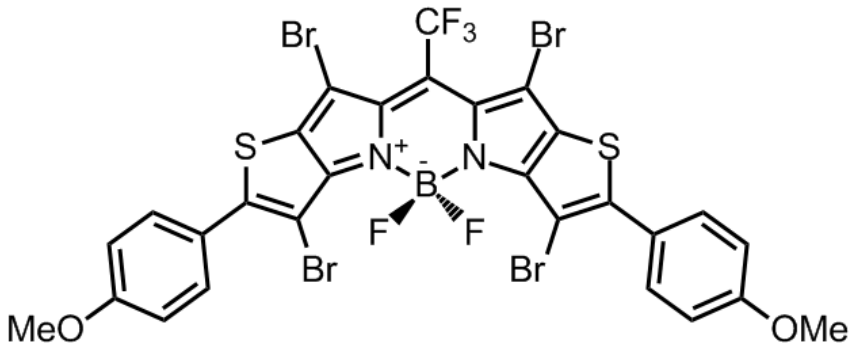

9

Figure 10: Molecular structure of the heteroaryl-fused BODIPY-based photosensitizer (Compound **9**)

These novel photosensitizers (**8** and **9**) have absorption maxima in the near-IR range of the electromagnetic spectrum. The absorption maximum of the compound **8** is at 720 nm and its emission is at 754 nm. The absorption maximum of the compound **9** is at 766 nm and it emission is at 820 nm. Furthermore, it has been shown that these BODIPY derivatives can be used as imaging probe and photosensitizer at the same time due to fact that they are enough fluorescent for the imaging purpose even if they were brominated.[66]

Akkaya and coworkers reported a pioneering study in 2007 by synthesizing 3 novel water soluble styryl-substituted BODIPY derivatives[67]. In this study, it was shown that introduction of the styryl groups to the 3-and 5-position of the BODIPY core gives rise to the spectacular red shifts in the absorption maximum of the related BODIPY dye. These photosensitizers have absorption maximum in the 590-660 nm region. Water solubility of these photosensitizers was improved by introducing amphiphilic triethylenglycol groups to the BODIPY molecules (Figure 11).

The singlet oxygen generation experiments were performed by using 1,3-diphenylisobenzofuran (DPBF) which is the most widely used singlet oxygen trap molecule.

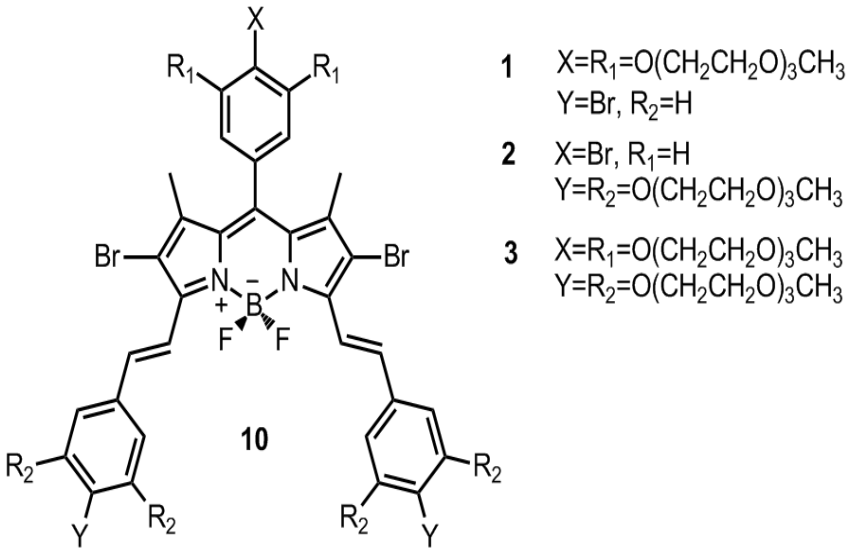

Figure 11 : Molecular structures of the water soluble styryl-substituted BODIPY derivatives

Cell culture experiments were carried out by using standard MTT assay (K562 Cells). The experiment performed in the dark and with photosensitizer exhibited no cell death. Besides that, experiment carried out in the dark without photosensitizer did not demonstrate any cytotoxic result either. Fluorescence microscope images showed that BODIPY based photosensitizer is effective photodynamic therapy agent (Figure 12).

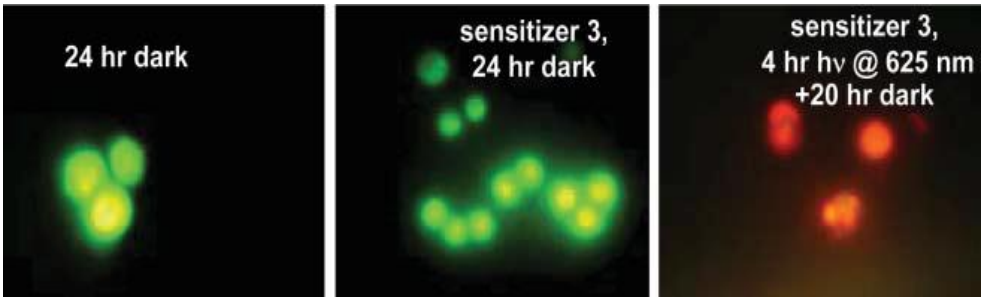

Figure 12: Fluorescence microscope images of acridine orange (AO) and propidium iodide (PI) stained K562 cells,
Live cells were preferentially stained with AO (green) and dead cells with PI (red) due to increased cellular permeability

In 2011, Ng and colleagues reported a similar study. A series of BODIPY-based photosensitizers have been synthesized[67]. They are similar to the photosensitizers which were reported by Akkaya group in 2006. In this work, iodine atoms were incorporated to the core of the BODIPY instead of bromine atoms which was used by Akkaya group for the heavy atom effect (Figure 13).

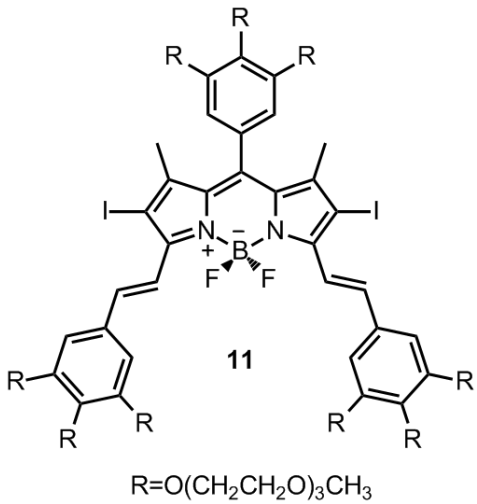

Figure 13 : Molecular structure of iodinated styryl-substituted BODIPY derivative

Halogenated aza-BODIPY based

photosensitizers were reported by O'Shea *et al*[68]. They synthesized and characterized a new series of photodynamic therapy agents which can be excited in the therapeutic window of the electromagnetic spectrum (650-800nm, beyond the absorptivity region of body tissue) (Figure 14).

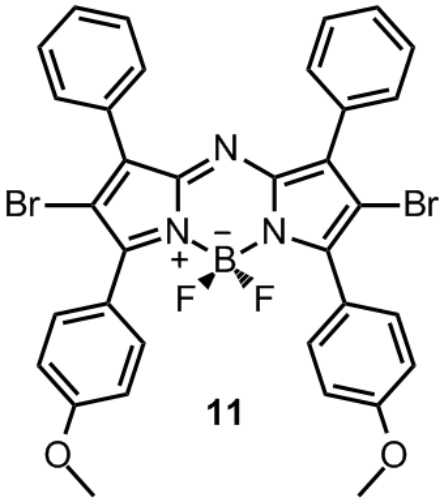

Figure 14 : Molecular structure of the halogenated aza-BODIPY based photosensitizer

After the synthesis and characterization of the BODIPY dyes, *in vitro* cellular uptake was investigated. Singlet oxygen generation efficiency of the photosensitizers was evaluated. 1,3-diphenylisobenzofuran (DPBF) was used as a trap molecule for the singlet oxygen generation experiments. *In vivo* assays and human tumor cell lines have prepared for the evaluation of the cytotoxicity of the compound **11.** Activation of sensitizer resulted in the generation of the photoinduced cytotoxic singlet oxygen, causing cell death via apoptosis and necrosis[69].

In 2010, another aza-BODIPY based photodynamic therapy agents were reported by Ramaiah and coworkers. In this work, iodine atoms were introduced to the BODIPY cores in order to improve intersystem crossing efficacy (Figure 15). As a result, it was found that the target compounds were highly cytotoxic and promising singlet oxygen generators.

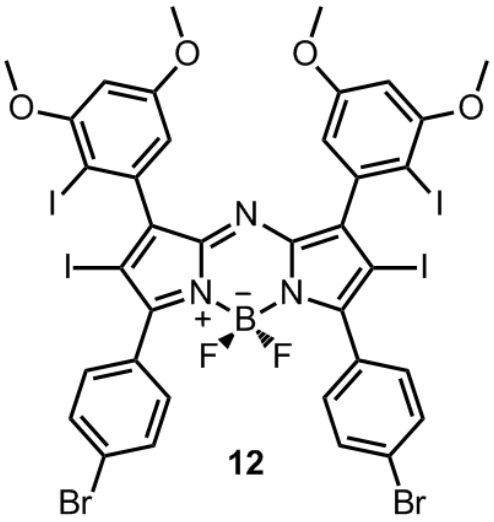

12

Figure 15: Molecular structure of the tetraiododibromo aza-BODIPY based photosensitizer

The absorption maximum of the compound **12** is at 666 nm and its emission is at 694 nm. As a result of the heavy atom incorporation, up to 70 % singlet oxygen generation efficiency was acquired.

In 2015, a glutathione activated BODIPY based photosensitizer (**13**) was reported by Akkaya *et al* [70](Figure 16). The singlet oxygen generation of this BODIPY based photosensitizer can be turned ON/OFF by using intracellular glutathione. It is a noteworthy fact that this BODIPY based photosensitizer can discern between concentrations in normal and malignant cells.

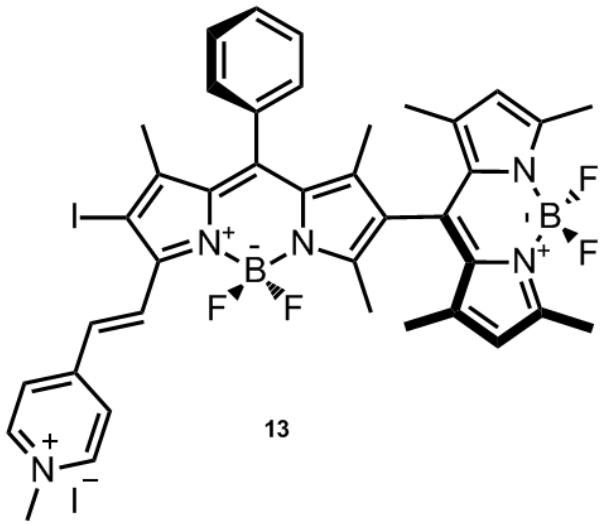

Figure 16 : Molecular Structure of the glutathione activated BODIPY

2.2.2 Photosensitizers based on other Dyes

There are a great number of photosensitizers based on various chromophores. As mentioned in the previous section of this chapter, the first clinically approved photosensitizer is Photofrin and it's a porphyrin derivative (Table 1). In 1993, it was clinically approved in Canada and it is now most widely used photosensitizers for the photodynamic therapy application in many countries including USA. Even photofrin is a most widely used photosensitizer in the photodynamic milieu, it has some drawbacks. In order to overcome side effects and deficiencies of this most widely used photosensitizer, development of the novel photosensitizers have been the focus of extensive research. In recent years, many photosensitizers have been extensively developed and reported[71].

5-Aminolaevulinic acid (5-ALA) is another clinically approved photosensitizer for the photodynamic therapy application. It is a porphyrin precursor (Protoporphyrin IX) and mainly used for the treatment of skin and bladder cancer. Clinical use of the ALA was reported in 1990 by Kennedy coworkers. It was shown that skin reaction after the treatment did not last as long as photofrin did.[72]

Texaphyrins, expanded porphyrins, are a new class of photosensitizers was reported in 1988 by Sessler *et al.*[73].They have many of features in common with porphyrins, such as aromatic molecular structure and colorfulness. They have mainly absorption in the near-IR region of the electromagnetic spectrum. There are five coordinating nitrogen atoms in their central core which confer them to react with the lanthanides in more stable manner.

In 2000, clinical applications of two texaphyrin derivatives, the gadolinium (III) and lutetium (III) were reported by J.L. Sessler and R.A. Miller[74]. The latter one, Lutetium (III) derivative is water soluble and has absorption maximum at 732 nm in the near-IR region of the electromagnetic spectrum (Figure 16). Its administration is performed intravenously by using injection. At this wavelength, light can deeply penetrate into the mammalian tissue.

It is found that this texaphyrin derivative, Lu-Tex, has high singlet oxygen quantum yield. Furthermore, it shows low dark toxicity and lower skin

photoinduced cytotoxicity compared to the Photofrin because of the fact that this photosensitizers can leave the human body faster than Photofrin.[75,76] Phase trials of these photosensitizers have been performed for the treatment of breast cancer and atherosclerosis vascular diseases.

In 1998, cadmium coordinating texaphyrin , Cadmium (II) texaphyrin, derivatives was reported by Maiya *et al.* The absorption maximum of one of these derivatives was at 864 nm[77].

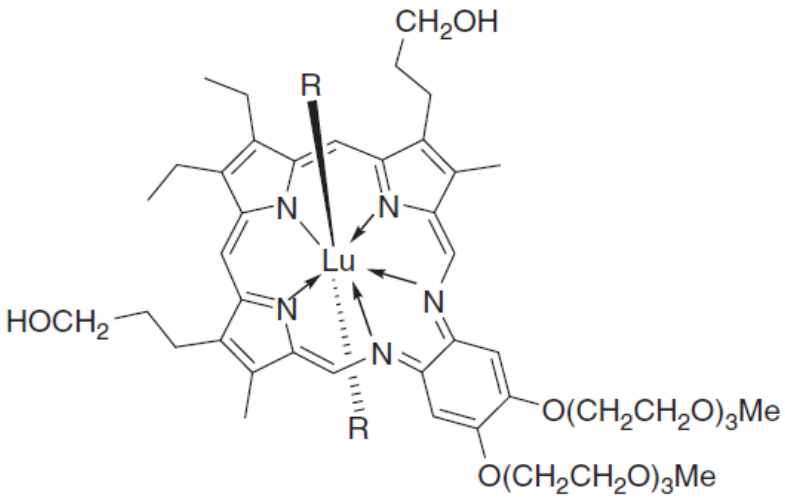

Figure 17 : Molecular Structure of the Lutetium texaphyrins

Chlorin based photosensitizers have attracted much attention due to their potential as a putative cytotoxic singlet oxygen generator and they can make conjugation

with proteins. These features endow the chlorins potential photodynamic therapy agents[78].

A novel series of chlorin based photosensitizer reported by Shan *et al.* in 2006[79].

Bacteriochlorins are another group of photosensitizers absorbing lights in the near-IR range of the electromagnetic spectrum. In 2006, a series of bacteriochlorins were reported by Sharonov *et al.* They have absorption maximum between 760 and 830 nm, at longer wavelengths compared to the photofrin and chlorins[80].

Table 1 : Clinically Approved Photodynamic therapy agenst[1,81].

Photosensitizer	Structure	Wavelength	Approved	Trial	Type of Cancer
HPD-Pormier sodium (Photofrin)	Porphyrin	630 nm	Worldwide		Cervical, Endobronchial, Esophageal, Gastric,bladder,brain.ovarian
ALA (Levulan)	Porphyrin	635 nm	Worldwide		Skin, head and neck, gynaecological
5-ALA-methylesther (Metvix)	Porphyrin	635 nm	Europe		Basal cell carcinoma, bladder
5-ALA-benzylesther (Benzvix)	Porphyrin	635 nm	Europe		Gastrointestinal
5-ALA-hexylester (Hexvix)	Porphyrin	375-400 nm	Europe		Diagnosis of bladder tumors
Verteporfin	Chlorine	690 nm	Worlwide		Basal cell carcinoma, pancreatic
Temoporfin (Foscan)	Chlorine	652 nm	Europe		Head and neck, lung, brain, skin, bile duct
SnEt2	(Purlytin)	664 nm		USA	Skin, breast, prostate Kaposi's sarcoma
Motexafin Lutetium (Lutex)	Texaphyrin	732 nm		USA	Breast

Padoporfin (TOOKAD)	Bacteriochlorin	762 nm		USA	Prostate
Silicon phtalocyanine (Pc4)	Phatolocyanine	675 nm		USA	Cutaneous T-Cell lymphoma
Ce6-PVP (Fotolon), Ce6 derivetives (Radachlorin,Photodithazine	Chlorin	660 nm		Belarus, Russia	Nasopharyngeal, Sarcoma, brain

2.3 Application of PDT in medicine

In the last decade the application of photodynamic therapy has increased and acquired growing acceptance around the world. Cancer is one of the most problematic disease and many people have suffered from various cancer types like cancers of the lung[82], gastrointestinal tract[83], bladder[84], head and neck region[85], prostate[86] and nonmelanoma skin cancers and actinic keratosis.[87,88,89,90,.91,92]

Photodynamic therapy gives complete response in a high percentage of patients. There are also ex vivo procedure which has been used for treating bone marrow and hematopoietic stem cell grafts.[93,94,95.96]

Photodynamic therapy is also used as a treatment modality for the nonmalignant diseases such as age related macular degeneration and psoriasis[97]. Furthermore, some successful PDT treatment of the atherosclerosis plaque has been reported in recent years[80]

CHAPTER 3

NOVEL NEAR-IR PHOTOSENSITIZERS FOR PHOTODYNAMIC THERAPY

Kilic, B.; Yesilgül, N. ; Akkaya, E. U.

3.1 Objective

In this project, four different types of novel BODIPY based photosensitizers were designed and synthesized which fulfill a great number of criteria for the PDT in terms of singlet oxygen generation, low dark toxicity, tissue penetration and solubility. All target compounds were synthesized by using standard BODIPY chemistry. Owing the fact that BODIPY dyes have remarkable features, such as high quantum yields, good solubility, photostability etc., BODIPY dyes were used for the design and synthesis of the target compounds as promising near-IR photosensitizer for the PDT.

3.2 Introduction

By considering the important parameters, which is essential for an ideal photosensitizer, our aim was to synthesize novel near-IR photodynamic therapy agents which will fulfil the requirement for an ideal photosensitizer and maximize the efficiency of the method.

The reason why we have used BODPY dyes (4,4-difluoro-4-bora-3a,4a-diaza-s-indacene) in order to obtain an ideal photosensitizer is that they have many distinctive properties such as high fluorescence quantum yield, photostability, long wavelength absorption and emission, high molar absorption coefficient and their simple synthesis method[59].

The chemical and photochemical stabilities of BODIPY dyes, which are higher than those of many other chromophores, are other important factors that we took into consideration for the design of the photosensitizers. Modifications on the BODIPY core can be carried out by introduction of different groups which afford red-shifted BODIPY derivatives[98,3]. It was shown that the strongly electron-withdrawing group CF_3 on the meso position of the BODIPY core resulted in a large bathochromic shift compared to that of the congeners with aryl substituents in this position[99].

By taking account the above information, we have designed meso-CF_3-substituted BODIPY dyes having aryl substituents. The usual BODIPY molecules have absorption maximum at around 500 nm, which is not suitable for an effective light penetration into the tissue[61]. Thus, we have designed a general effective route to a novel family of the meso-CF_3-3,5-diaryl-BODIPY dyes which is composed of 4 different target BODIPY molecules. These molecules have heavy atom functionalization on the 3, 5-positions of their BODIPY cores. This functionalization gives rise to the effective singlet oxygen generation for serving as a potential photodynamic therapy agent.[62,100]

Nagano et al. have recently shown that substitution of the BODIPY with iodine gives rise to a radical increase in the intersystem crossing efficiency[62]. On the other hand, several studies have recently shown that BODIPY dyes without heavy atom functionalization can be used as effective photosensitizers providing that they are synthesized as orthogonal dimers.[101,102]

Synthetic pathway for the target compounds is shown below (Figure 18 and Figure 19)

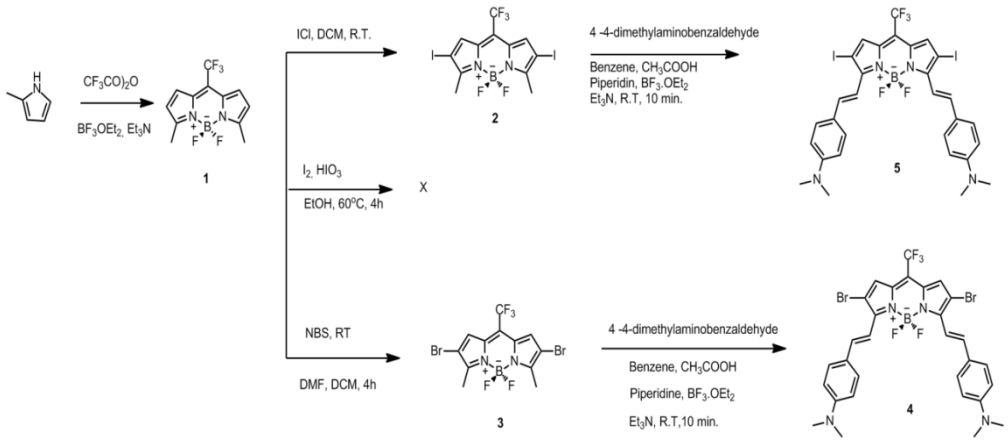

Figure 18 : Synthetic pathway of target compounds **4** and **5**

3.3 Result and Discussion

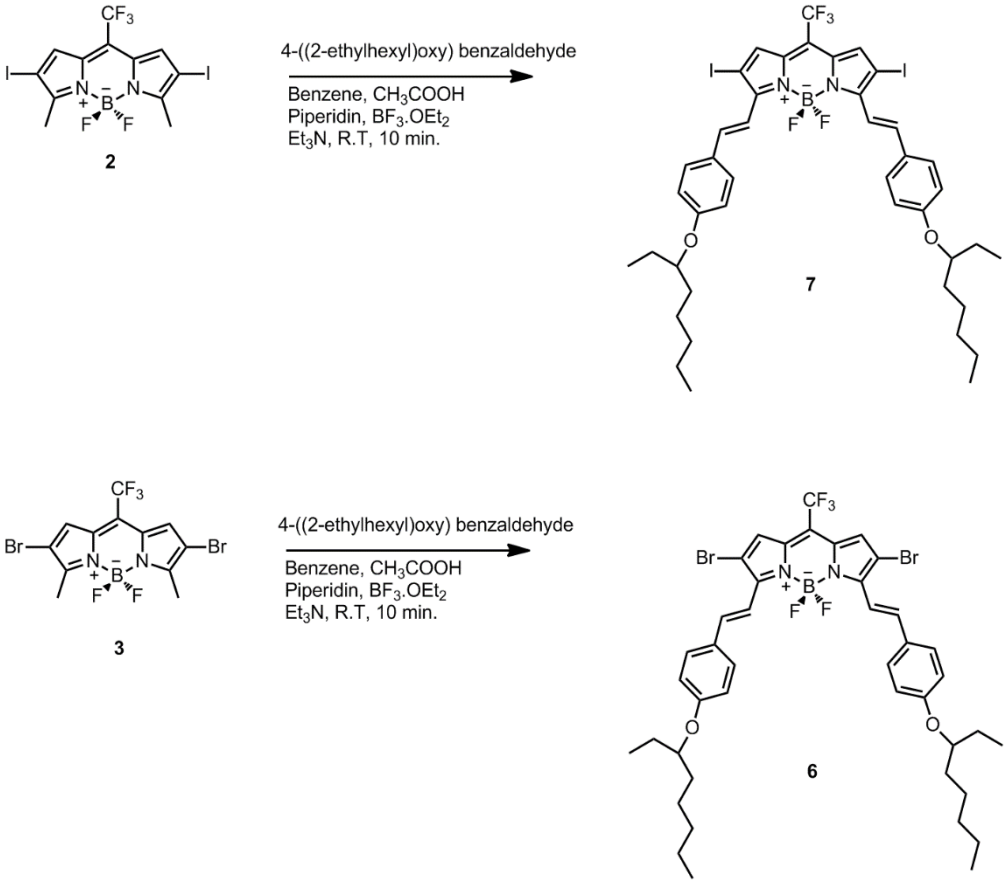

Figure 19: Synthetic pathway of target compounds **6** and **7**

In this study, we have designed four different novel photosensitizers and they were successfully synthesized and characterized. The **TM1** (Compound **4**) and **TM2** (Compound **5**) were obtained from the common precursor meso-CF_3-substituted and brominated BODIPY. The **TM3** (Compound **6**) and TM4 (Compound **7**) were also prepared from another common precursor meso-CF_3-substituted and iodinated BODIPY.

First, we synthesized 2-methyl pyrrole via Wolf-Kischner reduction starting with pyrrole-2-carboxaldehyde (Figure 20).

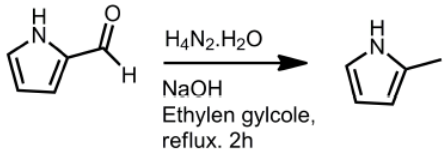

Figure 20 : Synthesis of the 2-methyl pyrrole

After the synthesis of the 2-methyl pyrrole, we synthesized meso-CF_3-substituted BODIPY. The absorption λmax of meso-CF_3-substituted BODIPY is at 543 nm and its emission is at 550 nm (Figure 21). After the completion of the synthesis of the meso-CF_3-substituted BODIPY, well-known heavy atoms Iodine and Bromine were introduced to the BODIPY cores because of the fact that intersystem crossing of a photosensitizer is an important parameter for PDT action.

During the synthesis of the iodinated meso-CF_3-substituted BODIPY we encountered a synthetic problem. The Iodination of the meso-CF_3-substituted BODIPY with iodic acid and I_2 was the problematic step and did not work. Following another procedure, we managed to synthesize the iodinated meso-CF_3-substituted BODIPY in good yields. Synthesis of the iodinated BODIPY by using this procedure was straightforward.

Since our aim was to design and synthesize photosensitizers for PDT presenting absorption maxima especially in the near-IR region of the spectrum, we introduced electron donating terminal groups to the BODIPY cores via Knoevenagel condensation which allows the extension of the conjugation at the same time.

As has been mentioned above, the first target molecule **TM1**, compound 4, has been synthesized via Knoevenagel condensation and the ^{1}H NMR, ^{13}C NMR spectra and high resolution mass spectrum (HRMS) of the target compound have been evaluated. We obtained absorption spectrum of the target molecule **TM1**

using a Varian spectrophotometer. It has absorption maximum at 890 nm (Figure 22). The attachment of the electron donating group 4,4-dimethylaminobenzaldehyde to the meso-CF_3-substituted and brominated BODIPY gives rise to a spectacular 304 nm red shift.

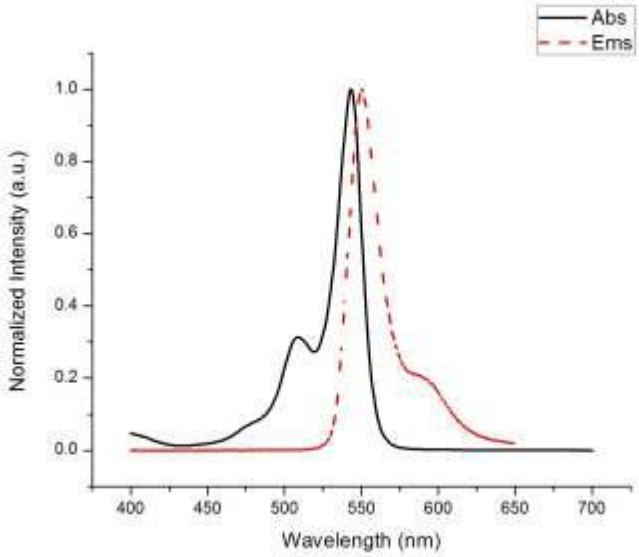

Figure 21 : The absorbance and emission spectra of the meso-CF_3-substituted BODIPY

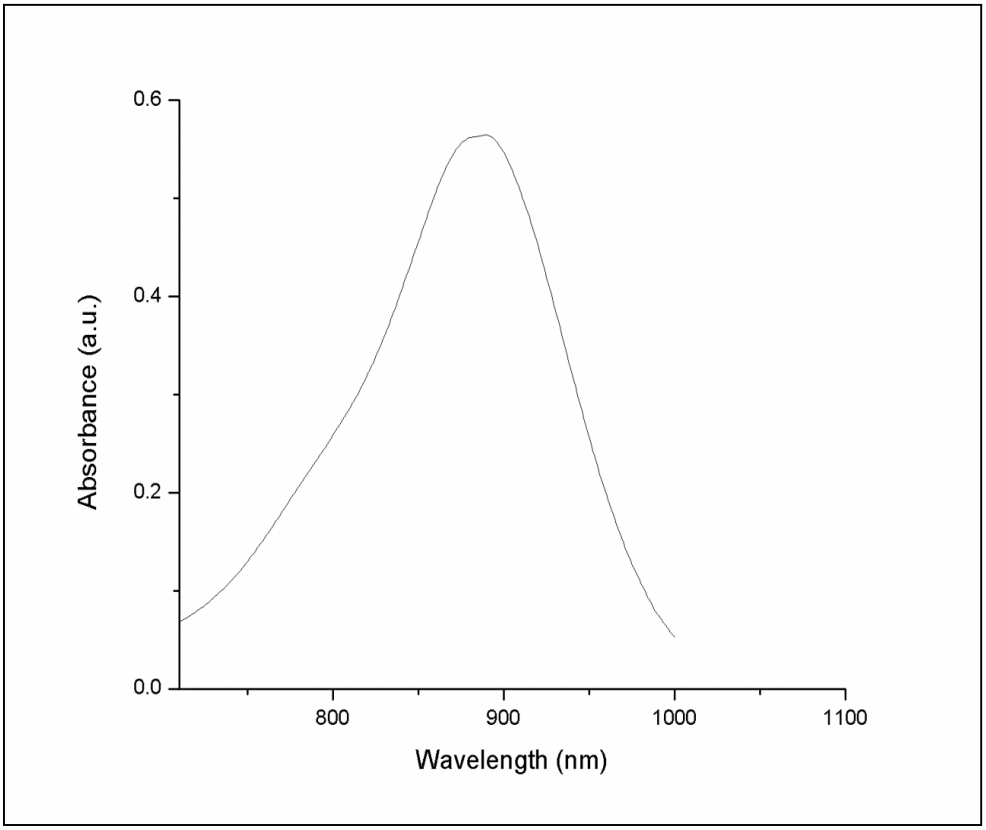

Figure 22 : Absorbance spectrum of the target molecule **TM1** in CH_2Cl_2

After the completion of the synthesis of the target molecule **TM1,** we searched for the suitable trap molecule in order to determine the ability of the target molecule **TM1** to convert ground state triplet oxygen to the reactive and cytotoxic singlet oxygen. We opted for the compound diphenylisobenzofuran (DPBF) as a trap molecule in order to assess singlet oxygen measurements. This trap molecule is ideal when the measurement is carried out in organic media.

We carried out the measurement in order to demonstrate the singlet oxygen generation capacity of the target molecule **TM1** by using 1,3-diphenylisobenzofuran as a trap molecule and when examined carefully it has been shown that singlet oxygen producing ability of the target compound is rather good.

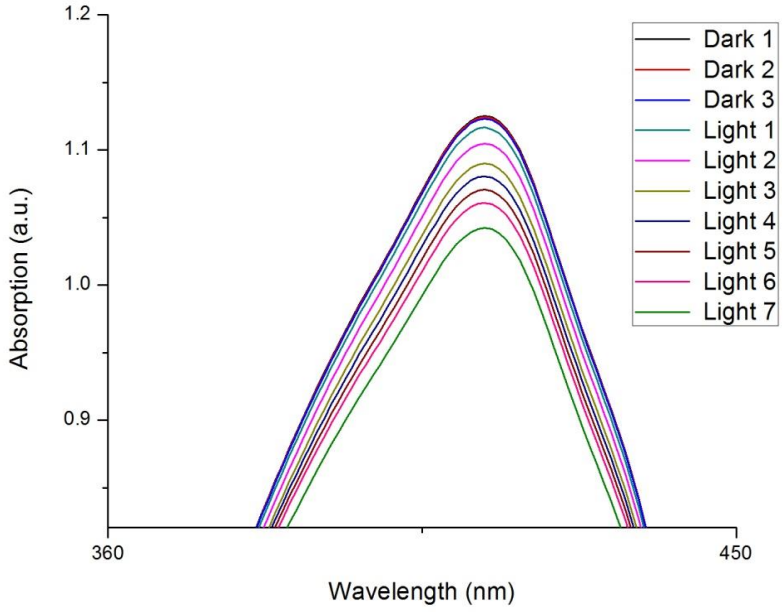

Figure 23 : Absorbance spectrum of trap molecule diphenylisobenzofuran (DPBF) in dichloromethane under light and Photosensitizer (**Target molecule 1**)

Air saturated DCM was obtained by bubbling the air for 5 minutes. Excitation of the target molecule was carried out with a near-IR light emitting diode (LED) source. The decrease of the absorbance band of the trap molecule at 410 nm was monitored.

This decrease of the absorbance band is caused by the oxidation of the trap molecule with reactive oxygen species such as singlet oxygen.

The experiment was performed at the concentration of $2x10^{-6}$ M of PS and $50x10^{-6}$ M of DPBF over a period of 50 min. For the first 15 minutes sample was kept at dark, then irradiated at 890 nm light for 35 minutes. Absorbance was measured in 5 minutes intervals (Figure 23).

As noted above, the second target molecule **TM2**, compound 5, has been synthesized via Knoevenagel condensation and the ^{1}H and ^{13}C NMR spectra and high resolution mass spectrum (HRMS) of the target compound have been evaluated. We obtained absorption spectrum of the target molecule **TM2** using a Varian spectrophotometer. It has absorption maximum at 886 nm (Figure 24). The attachment of the electron donating group 4, 4-dimethylaminobenzaldehyde to the meso-CF_3-substituted and iodinated BODIPY gives rise to a spectacular 290 nm red shift.

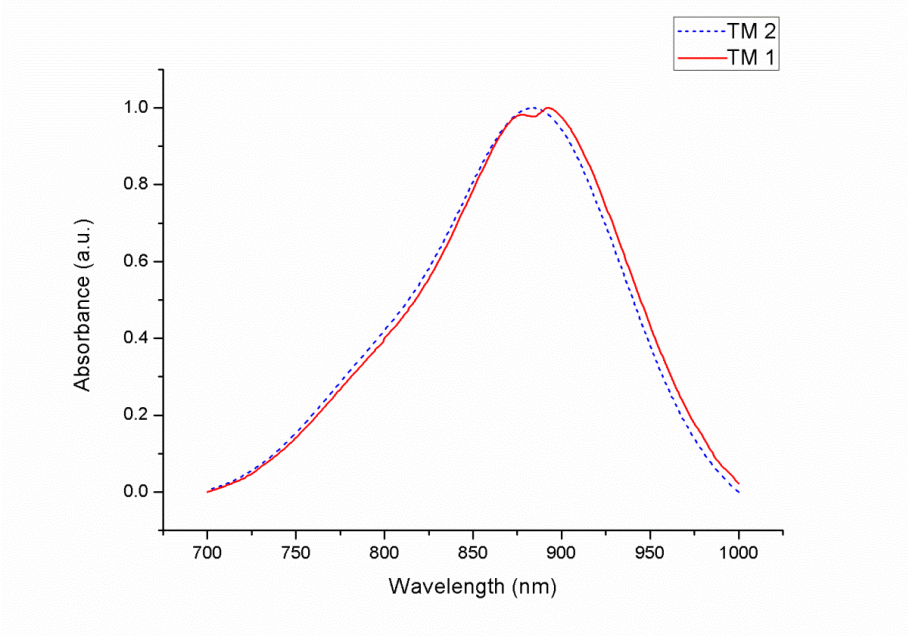

Figure 24: The absorbance spectra of the Target molecules **1** and **2** in CH_2Cl_2 (**TM1** and **TM2**)

Maximum absorbance wavelength of target molecules **TM1** and **TM2** is determined to be 886 and 890 nm respectively (Figure 24). All wavelengths of our target compounds correspond to near IR region is very appropriate for the PDT applications because of the fact that it is the region of the electromagnetic spectrum where the deepest penetration of the light into the mammalian tissues is occurred

We carried out the same measurement in order to demonstrate the singlet oxygen generation capacity of the target molecule **TM2** by using 1,3-diphenylisobenzofuran as a trap molecule

Figure 25 : Absorbance spectrum of trap molecule diphenylisobenzofuran (DPBF) in dichloromethane under light and PS (Target molecule **2**)

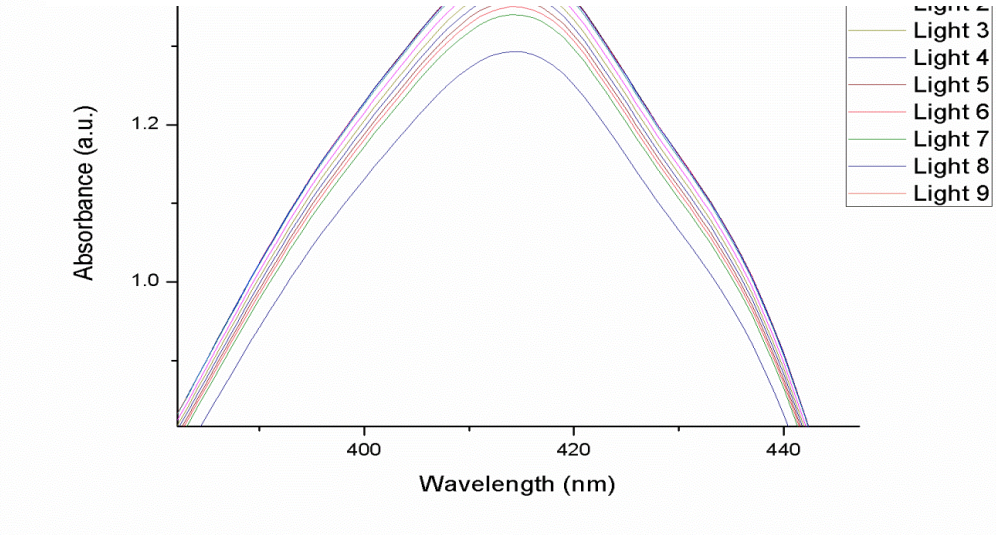

Excitation of the target molecule was carried out with a near-IR light emitting diode (LED) source. 890 nm light was exposed from 20 cm cell distance. The decrease of the absorbance band of the trap molecule at 410 nm was monitored (Figure 25). This decrease of the absorbance band is caused by the oxidation of the trap molecule with reactive oxygen species such as singlet oxygen (Figure 26).

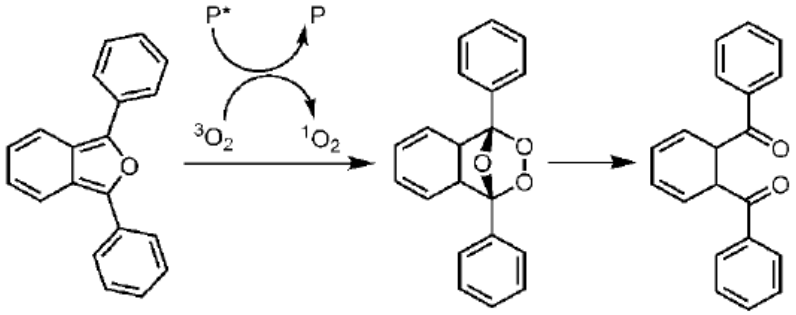

Figure 26 : Photobleaching of DPFB

The experiment was performed at the concentration of $2x10^{-6}$ M of PS and $50x10^{-6}$ M of DPBF over a period of 50 min. For the first 15 minutes sample was kept at dark, then irradiated at 890 nm light for 40 minutes. Absorbance was measured in 5 minutes intervals.

After this regular irradiation, the sample was irradiated for 1h and the absorbance was measured (Light 9 in Figure 25).

The quest to obtain more effective PDT agent has led to us to introduce another electron donating group 4-(2-ethylhexyl)oxybenzaldehyde to the meso-CF_3-substituted and brominated BODIPY which allows the extension of the conjugation and fulfills a great number of criteria to be an efficient photodynamic therapy agent such as singlet oxygen photosensitization in the near-IR region of the electromagnetic spectrum and photostability.

After the completion of the singlet oxygen measurement of these two target molecules, we synthesized target molecule **TM3**, compound **6**, according to the synthetic pathway.

The ^{1}H and ^{13}C NMR spectra and high resolution mass spectrum (HRMS) of the target compound have been evaluated. The same singlet oxygen generation experiments were carried out to show the singlet oxygen generation capacity of the target molecule **TM3**. As a trap molecule, 1,3-diphenylisobenzofuran was used

Excitation of the target molecule was carried out with a near-IR light emitting diode (LED) source. 760 nm light was exposed from 20 cm cell distance. The decrease of the absorbance band of the trap molecule at 410 nm was monitored. This decrease of the absorbance band is caused by the oxidation of the trap molecule with reactive oxygen species such as singlet oxygen

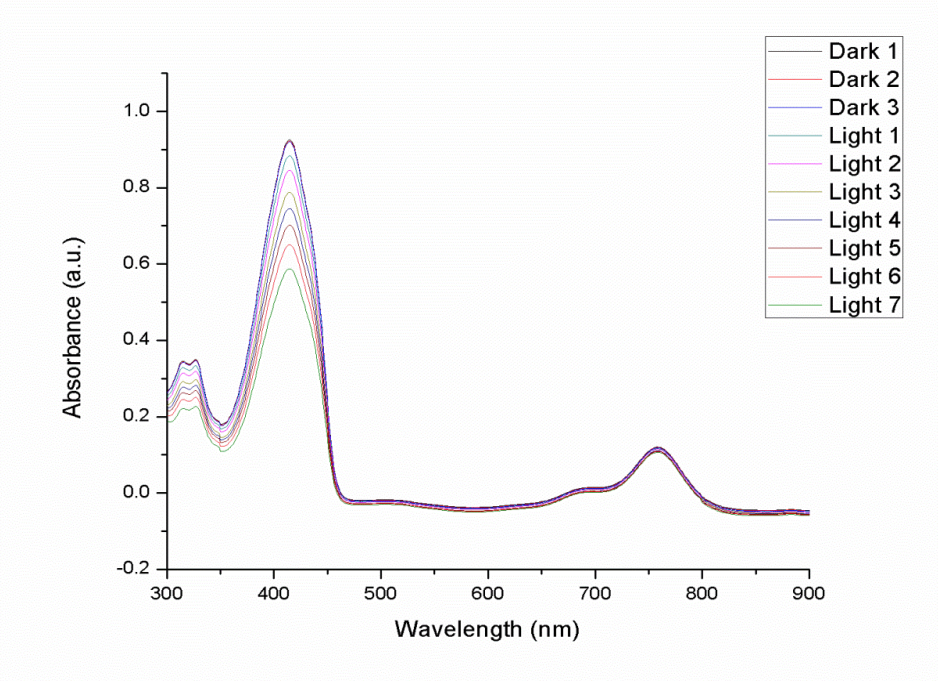

Figure 27 : Absorbance spectrum of trap molecule diphenylisobenzofuran (DPBF) in dichloromethane under light and PS (Target molecule **3**)

The experiment was performed at the concentration of $2x10^{-6}$ M of PS and $50x10^{-6}$ M of DPBF over a period of 10 min. For the first 3 minutes sample was kept at dark, then irradiated at 760 nm light for 7 minutes. Absorbance was measured in 1 minute intervals (Figure 27).

After the completion of the singlet oxygen measurement of target molecule 3 **TM3**, we synthesized target molecule **TM4**, compound **7**, according to the synthetic pathway. The ^{1}H and ^{13}C NMR spectra and high resolution mass spectrum (HRMS) of the target compound have been evaluated. The same singlet oxygen generation experiments were carried out to show the singlet oxygen generation capacity of the target molecule **TM4**. As a trap molecule, 1, 3-diphenylisobenzofuran was used.

Excitation of the target molecule was carried out with a near-IR light emitting diode (LED) source. 760 nm light was exposed from 20 cm cell distance. The decrease of the absorbance band of the trap molecule at 410 nm was monitored. This decrease of the absorbance band is caused by the oxidation of the trap molecule with reactive oxygen species such as singlet oxygen

The experiment was performed at the concentration of $2x10^{-6}$ M of PS and $50x10^{-6}$ M of DPBF over a period of 10 min. For the first 3 minutes sample was kept at dark, then irradiated at 760 nm light for 7 minutes. Absorbance was measured in 1 minute intervals (Figure 28).

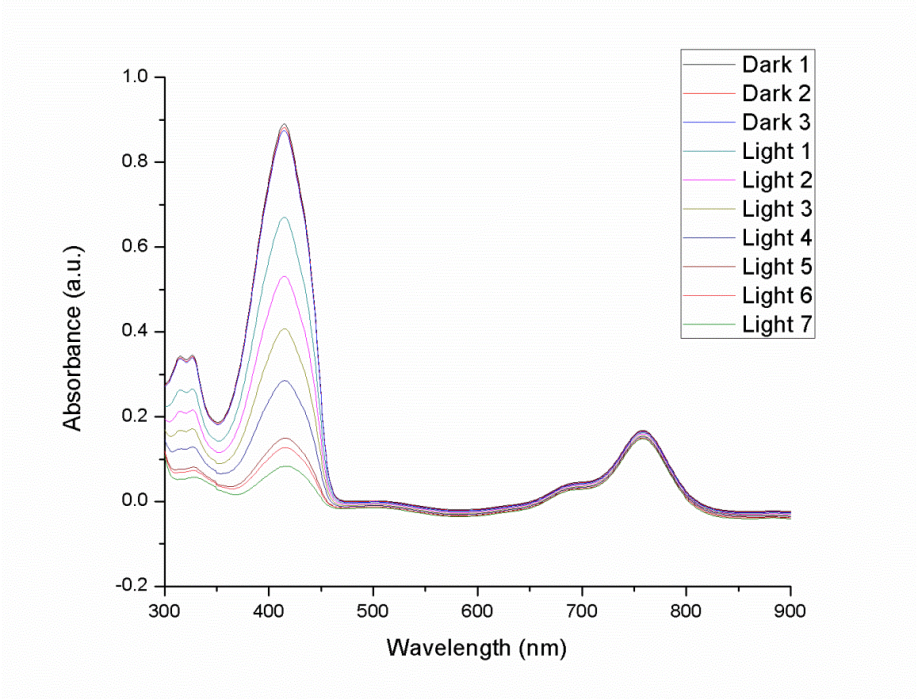

Figure 28 : Absorbance spectrum of trap molecule diphenylisobenzofuran (DPBF) in dichloromethane under light and PS (Target molecule **4**)

Control experiment was performed with trap molecule (without any photosensitizer). The solution of the trap molecule was irradiated at 890 nm for 30 minutes. The absorbance of the trap molecule was measured in 10 minutes intervals (Figure 29).

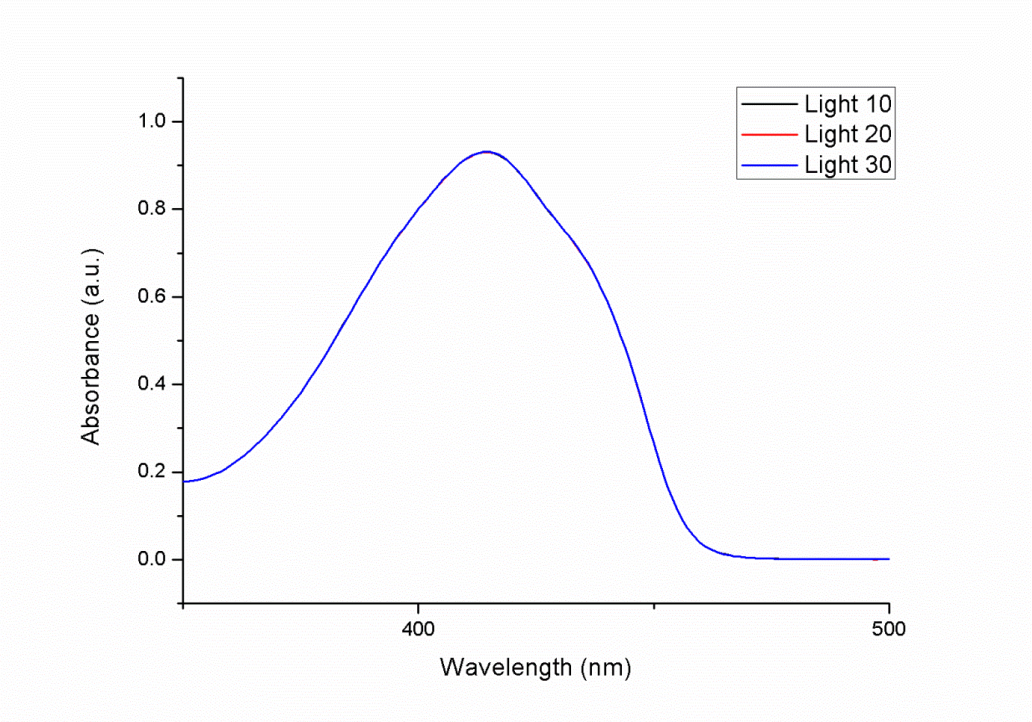

Figure 29 : The absorbance spectrum of the trap molecule in CH_2Cl_2. There is no decrease in absorbance spectrum of the trap molecule diphenylbenzoisofuran under the light irridiation of 890 nm LED.

3.4 Conclusion

To sum up, we have successfully synthesized and characterized four novel BODIPY-based photosensitizer that have absorption maximum in the near –IR region of the electromagnetic spectrum as we envisaged at the design phase of this study.

To best of our knowledge, it is the first time that a BODIPY-based photosensitizer has an absorption maximum at 890 nm. By introducing an electron donating group to the BODIPY core, a substantial amount of red shift has been encountered. It is clearly shown that introduction of the electron donation group, alkoxy group to the 3 and 5 positions gives rise to lesser amount of red shift compared to dialkyamino group. This can be seen by comparing the absorption maxima of the target compounds.

We performed singlet oxygen generation experiments with four different novel photosensitizers. The results are very promising in terms of photodynamic activity in the near-IR region of the electromagnetic spectrum. For further demonstration of the singlet oxygen generation capacity and phototoxicity of our target molecules, a cell culture assay with cancer cell lines experiments are in progress.

3.5 Experimental Procedures

General: ^{1}H NMR and ^{13}C NMR spectra were recorded on Bruker DPX-400 (operating at 400 MHz for ^{1}H NMR and 100 MHz for ^{13}C NMR) in $CDCl_3$ with tetramethylsilane as internal standard. All spectra were recorded at $25^{0}C$ and coupling constants (*J* values) are given in Hz. Chemical shifts are given in parts per million (ppm). Absorption spectra were performed by using a Varian Cary-100 spectrophotometer. Fluorescence measurements were conducted on a Varian Eclipse spectrofluorometer. Mass spectra were recorded on Agilent Technologies 6530 Accurate-Mass Q-TOF LC/MS. Reactions were monitored by thin layer chromatography using Merck TLC Silica gel 60 F254. Silica gel column chromatography was performed over Merck Silica gel 60 (particle size: 0.040-0.063 mm, 230-400 mesh ASTM).. All other reagents and solvents were purchased from Aldrich and used without further purification.

Synthesis of the meso-CF3 substituted BODIPY (Compound 1)

Trifluroaceticacidanhydride (5.85 mmol, 0.82mL) was dropwise added into a 200 mL round bottom flask containing 2-methyl pyrrole(11.71 mmol, 950 mg). The reaction solution was stirred for 20 min. at room temperature. The combined organic mixture was dissolved in 200 mL argon-degassed CH_2Cl_2 and was stirred for 1h. After that, to the reaction mixture 1.5 mL Et_3N and 1.5 mL $BF_3.OEt_2$ were sequentially added and it was stirred for 1h. The resulting solution was washed three times with water and dried over anhydrous Na_2SO_4. The solvent was removed in *vacuo* and then silica gel column chromatography was carried out to purify the residue (as eluent $CHCl_3$). The orange colored fraction was collected (495 mg, 29 %).

^{1}H NMR (400 MHz, $CDCl_3$): δH = 7.25 (s, 2H), 6.36 (s, 2H), 2.68 (s, 6H)

^{13}C NMR (100 MHz, $CDCl_3$): δC = 161.7, 131.6, 130.3, 123.8, 121.6, 29.6, 15.4

HRMS (ESI) calculated for $C_{18}H_{14}BF_2N_3$ (M-H) 287.0779, found 287.0804 Δ = 8.7 ppm

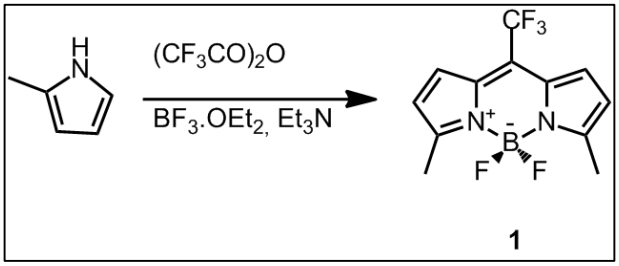

Figure 30 : Synthesis of the meso-CF_3 substituted BODIPY

Synthesis of the iodinated meso-CF_3 substituted BODIPY (Compound 2)

Compound **1** (100mg, 1.47 mmol) was dissolved in 10 ml of DCM. ICl (2.21 mmol, 0.36 g) in 10 ml of DCM was added dropwise to solution at room temperature. After stirring 1 h, saturated $Na_2S_2O_3$ solution in water was added to reaction mixture. Then mixture was extracted into CH_2Cl_2 and it was dried over Na_2SO_4. The residue was purified by silica gel column chromatography (EtOAc). Brown liquid was obtained (0.55 g, 69%).

^{1}H NMR (400 MHz, $CDCl_3$, 300K): δH = 7.42 (s, 2H), 2.61 (s, 6H)

^{13}C NMR (100 MHz, $CDCl_3$): δC = 162.8 , 136.4, 132.2,123.4, 120.7, 68.1, 16.0

HRMS (ESI) calculated for $C_{12}H_8BF_5I_2N_2$ (M-H) 537.8785, found 537.8753 Δ = 5.9 ppm

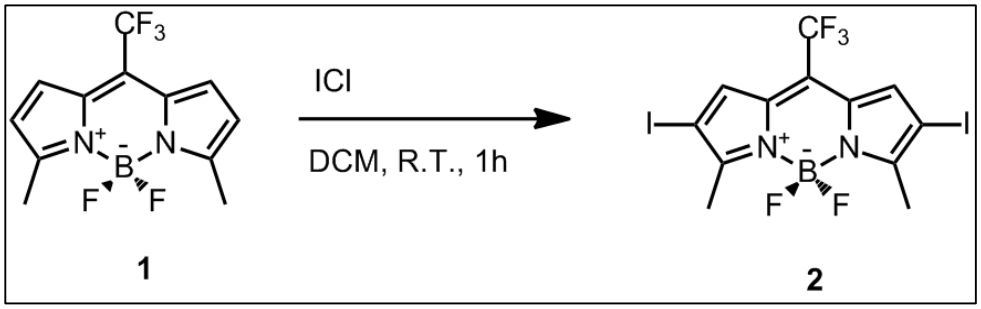

Figure 31 : Synthesis of the iodinated meso-CF_3 substituted BODIPY

Synthesis of the brominated meso-CF_3 substituted BODIPY (Compound 3)

Compound **1** (100 mg, 0.35 mmol) was dissolved in a mixture of DMF/DCM (25ml:25ml). Then N-bromosuccinimide (185 mg, 1.04 mmol) dissolved in DCM (25ml) It was added to the reaction mixture dropwise in 15 min. The reaction mixture was stirred at room temperature for 2 hours. Followed by thin layer chromatography the reaction was stopped and the extraction was done with water and DCM. The organic phase was dried with Na_2SO_4 and evaporated by using rotary evaporator. The purification was done by silica gel column by using chloroform/ hexane mixture (3:1 v/v). Fraction that contains brominated meso-CF_3 substituted BODIPYwas collected then the solvent was evaporated by using rotary evaporator (120 mg, 77%).

^{1}H NMR (400 MHz, $CDCl_3$,): δH = 7.25 (s, 2H), 2.58 (s, 6H)

^{13}C NMR (100 MHz, $CDCl_3$): δC = 213.4, 160.1, 130.0,121.0, 111.6, 29.7, 13.9

HRMS (ESI) calculated for $C_{12}H_8BBr_2F_5N_2$ (M-H) 441.9031, found 441.8991 Δ = 9.1 ppm

Figure 32 : Synthesis of the brominated meso-CF_3 substituted BODIPY

Synthesis of the Target Molecule 1 (Compound 4)

Compound **3** (0.112 mmol, 50 mg) and 4,4- dimethylaminobenzaldehyde (0.336 mmol, 78.85 mg) were dissolved in benzene (20ml). To the reaction mixture piperidine (0.5 ml) and glacial acetic acid (0.5 ml) were successively added and refluxed for 10 minutes in a Dean-Stark apparatus. The progress of the reaction was monitored by TLC (eluent $CHCl_3$ /Hexane) (1:1). Crude product was concentrated under vacuum and purified by using silica gel column chromatography (eluent $CHCl_3$/Hexane) (1:1) (40 mg, 50.58 %)

^1H NMR (400 MHz, $CDCl_3$): δH = 8.26 (d, 2H, J= 16,0), 7.60 (d, 4H, J=7.52 Hz), 7.58 (d, 2H, J=16,0 Hz), 7.30 (s, 2H), 6.75 (d, 4H, J= 8.28 Hz), 3.10 (s, 12H)

HRMS (ESI) calculated for $C_{30}H_{26}BBr_2F_5N_4$ (M-H) 705.0606, found 705,05792
Δ = 3.77 ppm

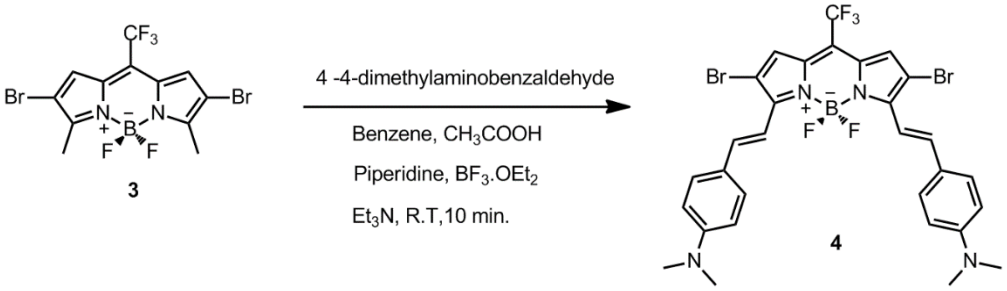

Synthesis of the Target Molecule 2 (Compound 5)

Compound **2** (0.185mmol, 100 mg) and 4,4- dimethylaminobenzaldehyde (0.555 mmol, 130.25 mg) were dissolved in benzene(20ml). To the reaction mixture piperidine (0.5 ml) and glacial acetic acid (0.5 ml) were successively added and refluxed for 10 minutes in a Dean- Stark apparatus. The progress of the reaction was monitored by TLC (eluent $CHCl_3$/Hexane) (1:1). Crude product was concentrated under vacuum and purified by using silica gel column chromatography (eluent CHCl3/Hexane) (1:1) (40 mg, 26.96 %)

^{1}H NMR (400 MHz, $CDCl_3$): δH = 8.35 (d, 2H, J= 16,0), 7.65 (d, 4H, J=8.68 Hz), 7.60 (d, 2H, *J*=16,0 Hz), 7.50 (s, 2H), 6.75 (d, 4H, J= 8.68 Hz), 3.10 (s, 12H)

HRMS (ESI) calculated for $C_{30}H_{26}BF_5I_2N_4$ (M+H) 803.0260, found 803.0255 Δ = 0.6 ppm

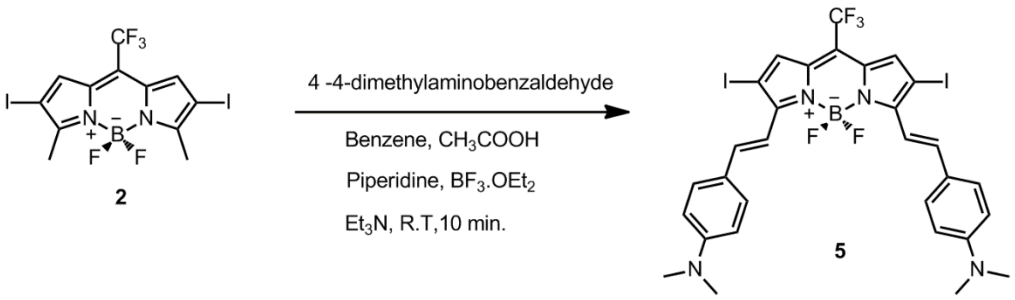

Figure 34 : Synthesis of the Target Molecule 2

Synthesis of the Target Molecule 3 (Compound 6)

Compound **3** (0.225 mmol, 100 mg) and 4-(2 ethylhexyl)oxybenzaldehyde (0.450mmol, 105.61 mg) were dissolved in benzene(20mL). To the reaction mixture piperidine (0.5 mL) and glacial acetic acid (0.5 mL) were successively added and refluxed for 10 minutes in a Dean-Stark apparatus. The progress of the reaction was monitored by TLC (eluent $CHCl_3$/Hexane) (1:1). Crude product was concentrated under vacuum and purified by using silica gel column chromatography (eluent $CHCl_3$/Hexane) (1:1) (40 mg, 20.98 %)

^{1}H NMR (400 MHz, $CDCl_3$): δH = 8.35 (d, J = 16.4 Hz, 2H), 7.70-7.61 (m, 6H), 7.38 (s, 2H) ,7.01 (d, 8.6 Hz, 4H), 3.95 (d, 5.7 Hz, 4H), 1.82-1.70(m, 2H), 1.60-1.32 (m, 16H), 1.02-0.90 (m, 12H)

^{13}C NMR (100 MHz, $CDCl_3$): δC = 161.6, 151.80, 141.72, 132.0, 130.6, 130.0, 129.0,125.27, 124.15, 115.7, 115.1, 109.5, 70.7, 39.4, 30.5, 29.0, 23.8, 23.0, 14.0, 11.1

HRMS (ESI) calculated for $C_{42}H_{48}BBr_2F_5N_2O_2$ (M+H) 877.20958, found 877.21070
Δ = 1.27 ppm

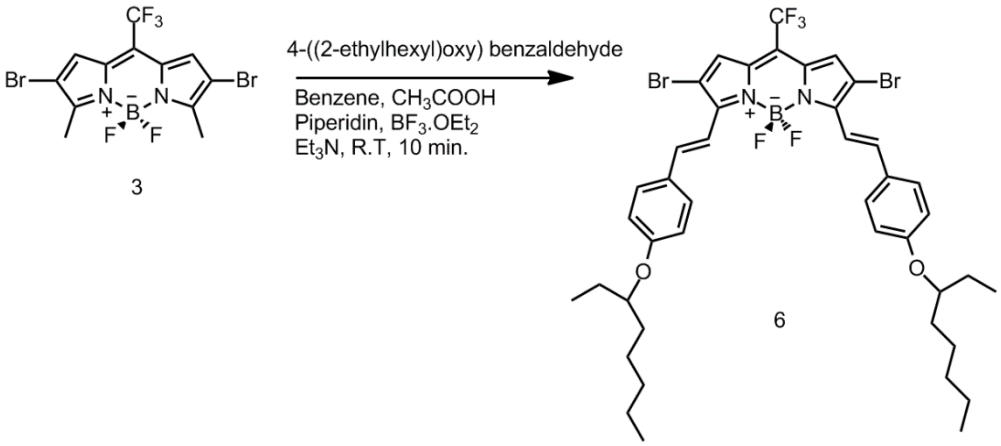

Figure 35 : Synthesis of Target Molecule 3

Synthesis of the Target Molecule 4 (Compound 7)

Compound **2** (0.185 mmol, 100 mg) and 4-(2-ethylhexyl)oxybenzaldehyde (0.450 mmol, 105.61 mg) were dissolved in benzene(20mL). To the reaction mixture piperidine (0.5 mL) and glacial acetic acid (0.5 mL) were successively added and refluxed for 10 minutes in a Dean- Stark apparatus. The progress of the reaction was monitored by TLC (eluent CHCl3/Hexane) (1:1). Crude product was concentrated under vacuum. The progress of the reaction was monitored by TLC (eluent $CHCl_3$/Hexane) (1:1). Crude product was concentrated under vacuum and purified by using silica gel column chromatography (eluent $CHCl_3$/Hexane) (1:1) (45 mg, 25 %)

^{1}H NMR (400 MHz, $CDCl_3$): δH = ^{1}H NMR (400 MHz, $CDCl_3$, 300K): δH = 8.36 (d, J = 16.4 Hz, 2H), 7.75-7.60 (m, 6H), 7.51 (s, 2H) , 6.97 (d, 8.4 Hz, 4H), 3.97 (d, 5.7 Hz, 4H), 1.85-1.75(m, 2H), 1.62-1.40 (m, 16H), 1.05-0.90 (m, 12H)

^{13}C NMR (100 MHz, $CDCl_3$): δC = 161.6, 153.95, 141.77, 137.61, 136.58 130.29, 130.01, 129.44, 128.94, 116.23, 115.14, 115.00, 70.80, 39.34, 30.51, 29.08, 23.86, 23.03, 14.06, 11.10

HRMS (ESI) calculated for $C_{42}H_{48}BBr_2F_5N_2O_2$ (M+H) 973.18184, found 973.18384

Δ = 2.0 ppm

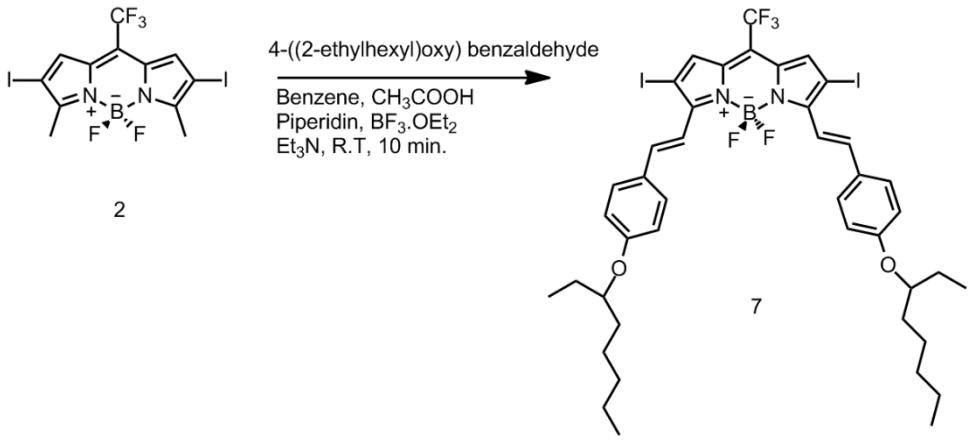

Figure 36 : Synthesis of Target Molecule 4

CHAPTER 4

Designing Heavy Atom Free Photosensitizers for the Photodynamic Therapy

The discussions on this chapter are partially based on the following publications:

Cakmak, Y.; Kolemen, S.; Duman, S.; Dede, Y.; Dolen, Y.; **Kilic, B**.; Kostereli, Z.; Yildirim, L. T.; Dogan, L.; Guc, D.; Akkaya, E. U. *Angew. Chem. Int. Ed.*, **2011**, 50, 11937.

4.1 Objective

In this project[101], we have designed and synthesized three different bis-BODIPYs. Their S_0, S_1, and T_1 states were studied by multireference quantum chemical approaches. According to the calculations on the orthogonal 8,8' and 8,2' bis-BODIPYs , it was clearly shown that these orthogonal BODIPY derivatives can be used as heavy atom free photosensitizers for Photodynamic therapy application. This has been proved experimentally by singlet oxygen generation experiments and cell culture studies

4.2 Introduction

Broader acceptance by the medical community and applicability is hampered, at least in less than optimal photophysical characteristics of the porphyrin derivatives. This situation sparked a worldwide search for novel sensitizers leading to new compounds, some holding more promise than others.[46,4] The primary cytotoxic agent involved in the photodynamic action is singlet oxygen (1Dg), the efficient generation of which is linked invariably to the intersystem crossing (ISC) efficiency of the excited sensitizer. Most organic dyes have low triplet quantum yields, and in many recent candidates for photodynamic sensitizers, heavy atoms are incorporated into the structure as a strategy to improve spin–orbit coupling leading to facilitated intersystem crossing.[103,63] While this approach seems fail-safe, incorporation of heavy atoms such as bromine, iodine, selenium, and certain lanthanides very often leads to increased "dark toxicity".[52] Unlike traditional chemotherapy agents, in principle, photodynamic therapy sensitizers themselves can be nontoxic, either at cellular or organ levels, even at relatively high concentrations. We have been interested in trying to find alternative ways of achieving increased intersystem crossing without the use of heavy atoms to minimize dark toxicity, turning our attention to the excitedstate properties of the sensitizers

Designing efficient photoinduced $^1O_2$ generators requires that any existing operative fluorescence cycle of the fluorophore, which is through the $S_0 \rightarrow S_1 \rightarrow S_0$ states, has to be perturbed so as to minimize or shutdown the $S_1 \rightarrow S_0$ deactivation, and switch to the triplet surface once S_1 is accessed. A general design principle for a favourable $S_1 \rightarrow T_1$ hop from an electronic structure viewpoint would in principle, require the structural and electronic compatibility of S_1 and T_1 states to surpass that of S_1 - S_0 pair. Once multiple electronic states come into play, quantum mechanical calculations providing a detailed understanding of the electronic structure are extremely helpful. Multi-configurational self-consistent field (MCSCF) techniques are the state of the art computational chemistry tools when near degeneracies and excited states are considered. These methods may not reach chemical accuracy (±2-3 kcal/mol) for computing total energies, but are crucial for a qualitatively correct description of the excited states and are capable of providing conceptually complete picture of the photophysics taking place. Therefore, we mainly employed a popular variant of MCSCF techniques; the complete active space SCF (CASSCF) method in combination with relatively large basis sets and different active spaces

4.3 Result and Discussion

Our calculations on the parent BODIPY core showed that natural orbital occupancies of S_1 state do describe an open-shell singlet with essentially double (>1.9) or zero (<0.1) electrons for all orbitals except HOMO and LUMO that are singly occupied (figure 37).

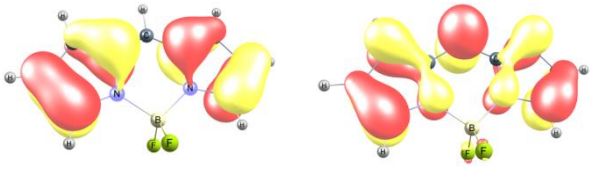

Figure 37 : Frontier molecular orbitals. HOMO (left) LUMO (right), of the parent BODIPY core at B3LYP/6-31G(d,p) level of theory. Surfaces are plotted at 0.2 a.u. Copyright © 2011, John Wiley and Sons. Reprinted with permission from ref (102)

It is no surprise to observe a fluorophore with low triplet quantum yield to have an excited state possessing only two orbitals with single occupancy, hence to achieve our goal of efficient switching to the triplet manifold, we have to access to excited states different from the ones built by simple HOMO → LUMO transitions. Among multiply excited configurations, doubly substituted ones are particularly important in enhancing S_1 - T_1 coupling as shown by the seminal work of Salem and Rowland[104] and the following work by Michl.[105] Thus, the substitutions should invoke simultaneous two electrons excitation from the ground state, guiding us to search for molecules with a pair of degenerate or near-degenerate occupied frontier orbitals correlating with a similar virtual (unoccupied) pair and pointing out a design principle of orthogonal dimeric chromophores. This foundation has two important features: (i) orthogonal placement prevents mixing of the π-systems of the two subunits leaving us with two essentially undisturbed chromophore cores. (ii) Upon irradiation, both cores are almost equally likely to undergo a HOMO → LUMO electron transfer

(referring to the original monomer MOs) yielding an excited state mainly comprised of double substitutions.

Our previous involvement with BODIPY dyes led us to seek ways to implement these design considerations using these dyes. BODIPY dyes are exceptional fluorophores with amazing versatility[59 ,106]and rich chemistry.[107,53] Heavy atom functionalized BODIPY dyes showed some promise as potential sensitizers for photodynamic activity.[61,108] It is also interesting to note that a few years ago, dimeric (albeit non-orthogonal) BODIPY derivatives with peculiar properties linked to exciton coupling between the chromophores were reported.[109] We believe orthogonality to be an important distinction in our design.

According to our calculations on the orthogonal 8-2'dimer **3**, it is clearly shown that the essentially unperturbed BODIPY HOMO and LUMO as a result of lack of mixing of orthogonal Π frameworks (Figure 38).

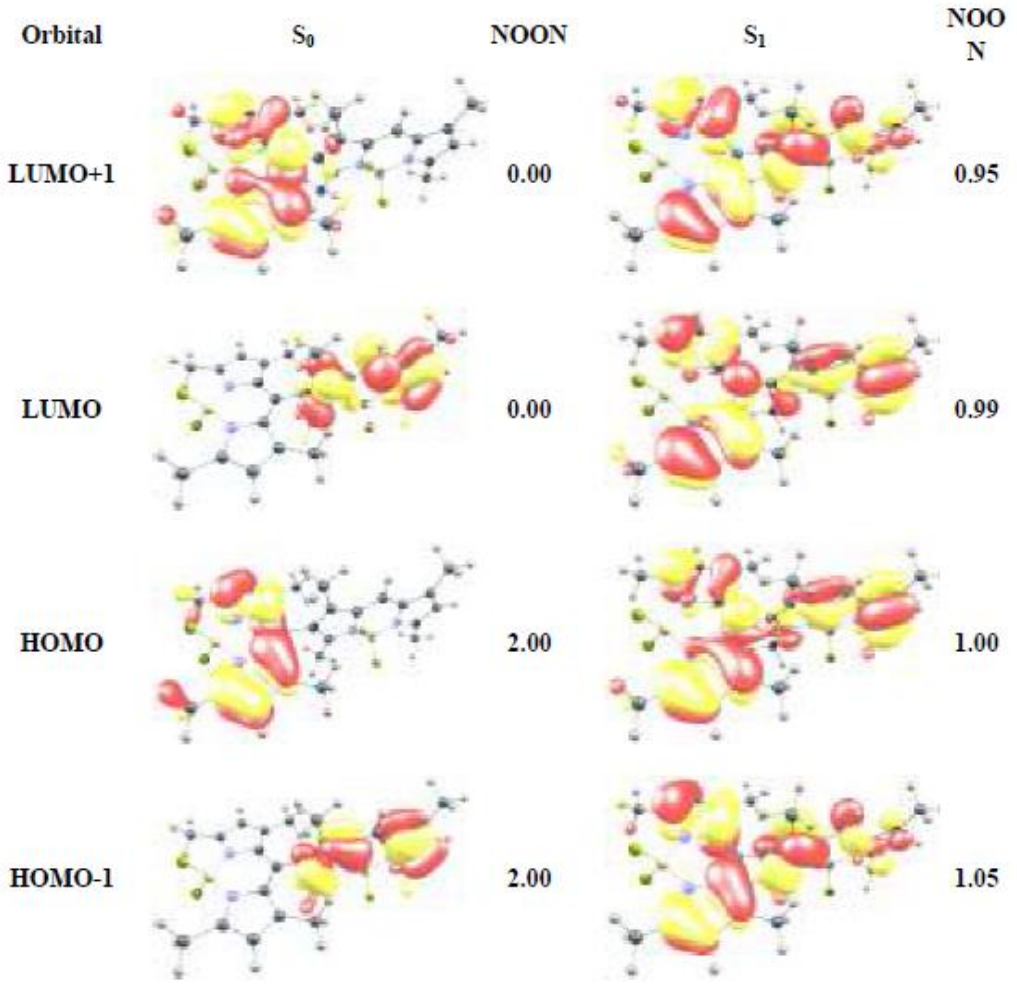

Figure 38: Frontier orbital plots and natural orbital occupation numbers (NOON) for the dimer 3. a, S_0 state. b, S_1 state. a, b, Calculations were done at CAS(6e in 6o)/cc-pVDZ level. Surfaces are plotted at 0.2 a.u. All four orbitals in both states retain characteristics of Bodipy frontier orbitals and NOONs prove tetraradicalic character of S_1. Copyright © 2011, John Wiley and Sons. Reprinted with permission from ref (101).

Orthogonality is secured by the strategic placement of the methyl substituents, resulting in a dihedral angle very close to 90° for the two BODIPY cores. Orthogonal arrangement of the BODIPY units was also experimentally verified by the X-ray diffraction of the compound **3** (Figure 39).

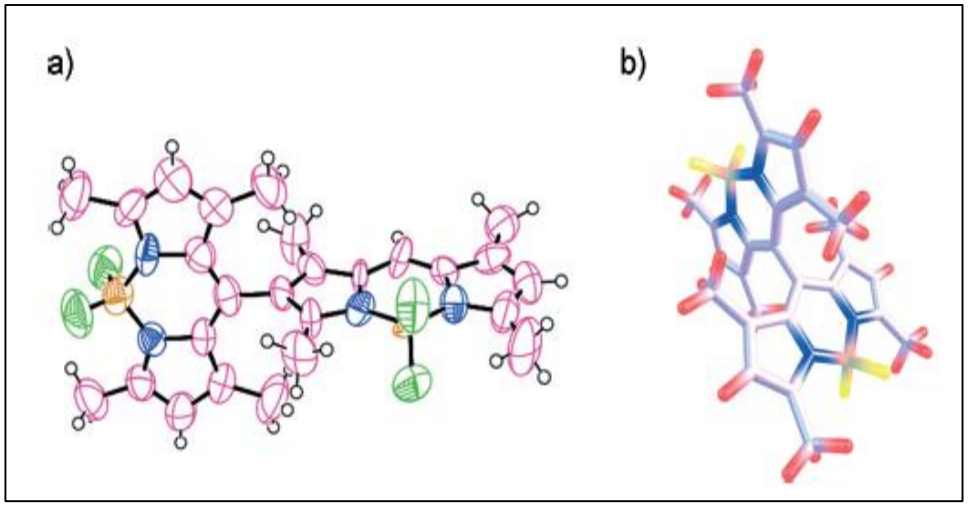

Figure 39 : Structures of the dimeric Bodipys. a) X-ray diffraction structure of the orthogonal 8,2' dimer (3). b) Optimized geometry of orthogonal 8,8' dimer (6) at CAS(6e in 6o)/cc-pVDZ level. Dihedral angle between the two Bodipy units is very close (± 0.5°) to 90° in both dimers. Copyright © 2011, John Wiley and Sons. Reprinted with permission from ref (101).

The calculated energy differences (2.96, 2.97 eV) remaining very close to HOMO – LUMO gap of Bodipy core (3.10 eV) further support our claim of Bodipy cores remaining essentially unperturbed in the dimeric form. Thus the orthogonal dimer should possess the desired features sought in the excitation process.

CASSCF calculations on the orthogonal dimer **3** show that there is a huge amount of electronic reorganization upon $S_0 \rightarrow S_1$ transition. S_1 with an equilibrium

geometry very similar to S_0 (Figure 38) lies 80 kcalmol^{-1} above the ground state (Figure 40).

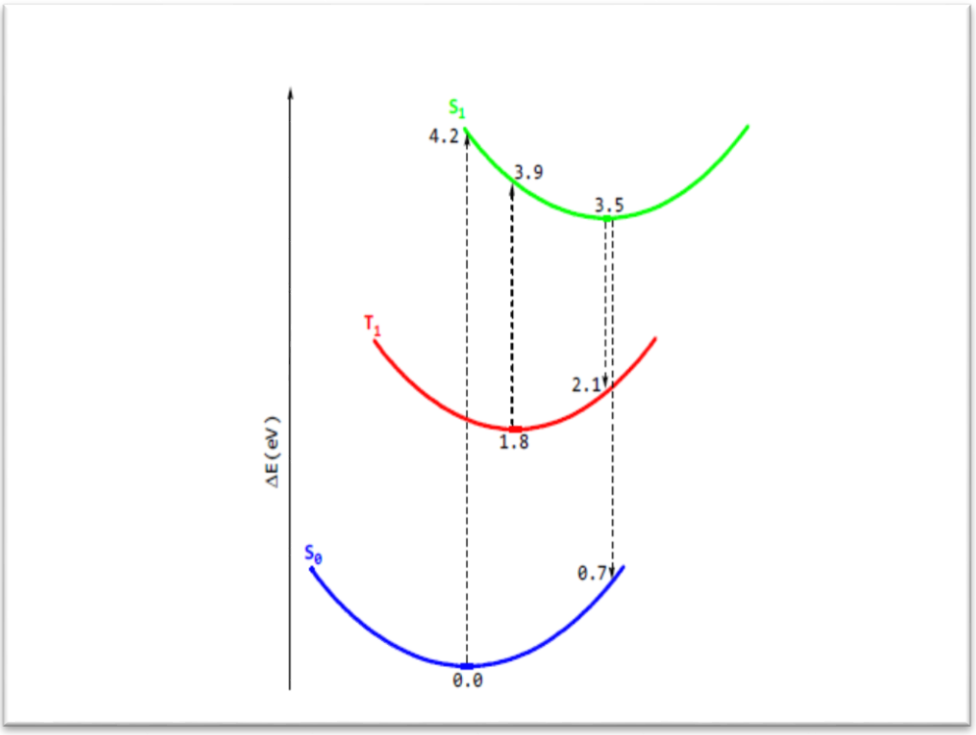

Figure 40 : Relative energies (eV) of equilibrium structures of S_0, S_1, and T_1 states of **3.** Vertical transitions computed at CAS(6e in 6o)/cc-pVDZ level

Computations of the $S_0 \leftrightarrow S_1$ vertical transitions show that only 15 kcalmol^{-1} of this difference is due to structural deformation, whereas electronic reorganization is more than four times as costly (65 kcalmol^{-1}). This finding implies that the electronic structure of S_1 is rather unusual. Natural orbital occupation numbers show four odd electrons in four very similar orbitals (Figure 38).

Thus, on excitation, both Bodipy units are essentially equally likely to undergo the inherent (Bodipy) HOMO→LUMO transition from HOMO-1 to LUMO and HOMO to LUMO+1 of Figure 3. In addition, orbitals optimized for the S_1 state

support the involvement of both cores through their clearly visible delocalized character. Thus, the S_1 state could be predicted to be comprised of a linear combination of doubly substituted configurations (with respect to the closed-shell reference) and in line with this expectation, the CASSCF wave function is almost totally made up of doubly substituted configurations, an unexpectedly large value for any chromophore (Figure 41).

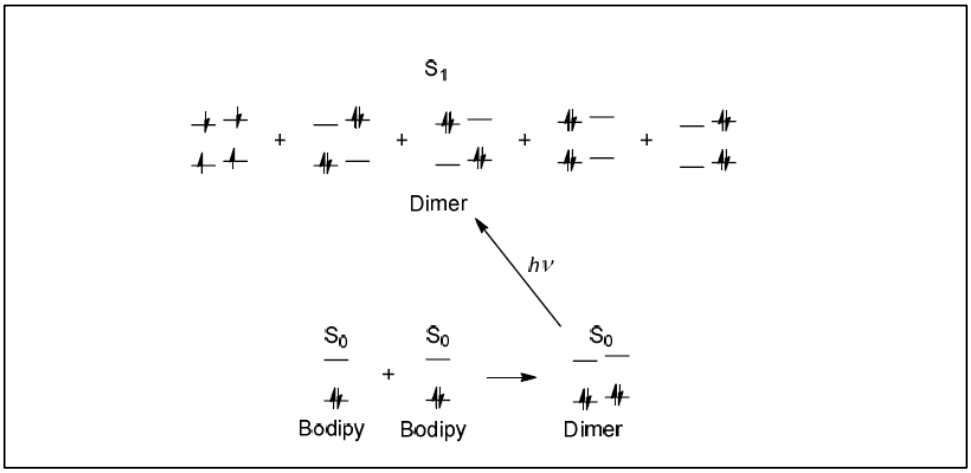

Figure 41: S_1 wave function of bis-BODIPYs **3** and **6**

Conceptual frontier MO diagram describing the building up of S1 states of the dimers **3** and **6** and dominance of doubly substituted configurations. Only the leading configurations are shown and minus signs to restrain antisymmetry in the S1 states are intentionally excluded for clarity.

As a result of spatial orthogonal arrangement HOMO and LUMO of both Bodipy cores are essentially kept in their original form (only slightly modified) in the dimers. Thus upon irradiation all the five configurations are almost equally probable and this picture is verified by CASSCF calculations. Each of the five configurations making up S_1 is termed as doubly substituted with respect to the closed shell reference S_0 state of the dimer.

The dominance of the S_1 wave function by double substitutions is in stark contrast with the S_0 wave function of the orthogonal dimer, as the latter is dominated by the reference configuration to an extent of approximately 90%. These findings suggest a severe mismatch between the S_1 and S_0 states and an enhanced transition to the T_1 state lying 1.7 eV lower (at 1.8 eV with respect to the ground state). Essentially the same electronic structure fingerprints are observed for 8, 8' dimer **6**.

Repeated calculations with different active space basis set combinations without exception, showed a Picture dominated by doubly substituted configurations and four singly occupied molecular orbitals in the S_1 state.

As a result, functionalization of the BODIPY core orthogonally, by a second BODIPY is the key to switching to the triplet manifold. Based on these clearly encouraging computational results, we were highly motivated towards the synthesis of a series of orthogonally linked dimeric BODIPYs. The synthesis procedure for compound **3** is quite straightforward, especially in view of recent contribution to BODIPY chemistry by Jiao and co-workers.[110] The parent compound **1** was formylated through Vilsmeier reaction (Figure 42). The BODIPY framework was then constructed around the formyl carbon using standard BODIPY chemistry.

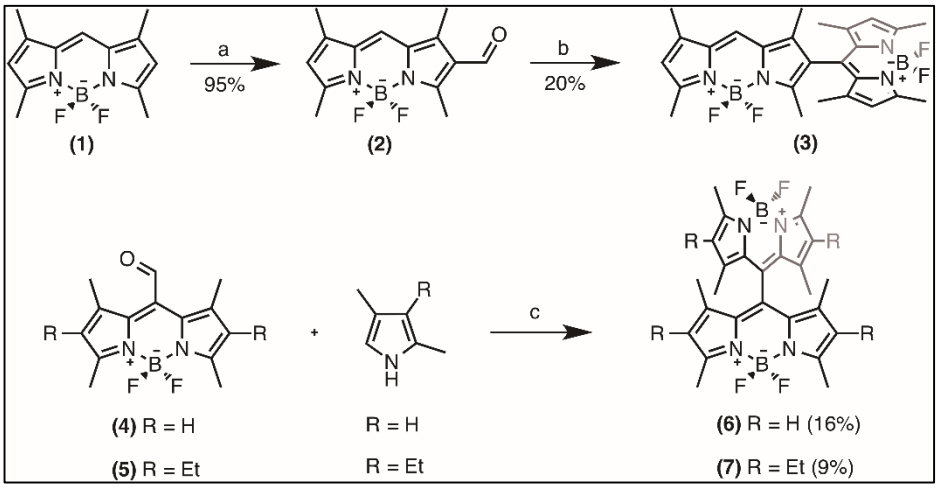

Figure 42 : Synthesis of the target photosensitizers. a) $POCl_3$, DMF, $ClCH_2CH_2Cl$, 50°C; b) 2,4-dimethylpyrrole, trifluoroacetic acid (TFA), CH_2Cl_2, p-chloranil, Et_3N, $BF_3{\cdot}OEt_2$; c) TFA, CH_2Cl_2, *p*-chloranil, Et_3N, $BF_3{\cdot}OEt_2$. Copyright © 2011, John Wiley and Sons. Reprinted with permission from ref (101).

The absorption spectrum of the product showed a single band centered around 506 nm, not much different than the parent compound (Figure 43). Organic solutions of the orange colored compound were noticeably lacking detectable fluorescence emission under ambient or hand-held UV lamp irradiation, an indication of competing excited state process(es) in action. Recent progress in the derivatization of BODIPY dyes also allowed us to synthesize two different and more symmetrical, 8,8' orthogonal dimers as well. Thus, recently reported[110] 8-formyl-BODIPY derivative was transformed into orthogonal dimers **6** and **7**, using standard protocols (figure 42).

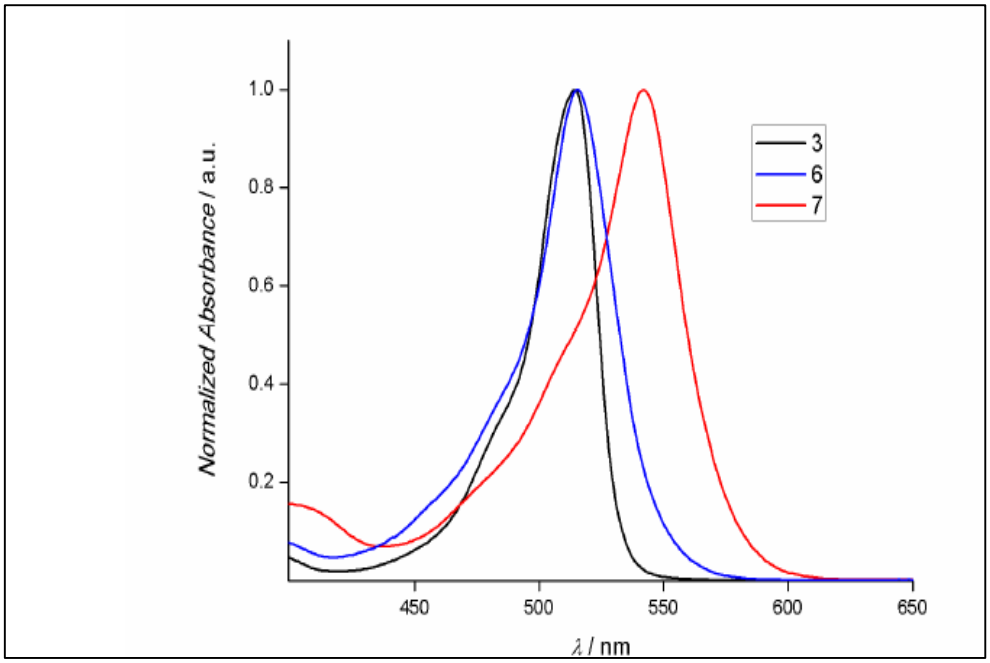

Figure 43: Absorbance spectra of the synthesized molecules **3**, **6** and **7** in $CHCl_3$

We surmised that a comparative study of compounds **1**, **3**, **6** and **7** would be instructive. First, we attempted to detect singlet oxygen phosphorescence at 1270 nm in chloroform for all four compounds excited with xenon-arc source at their respective absorption peaks, detection was done with a near IR sensitive detector. When excited at equal absorptivity concentrations for all compounds, dimer **3** yielded the strongest singlet oxygen phosphorescence emission (figure 44) at the signature wavelengths (peaking around 1270 nm), dimers **(6)** and **(7)** also showed phosphorescence peaks, but with somewhat reduced intensity. On the other hand, no such emission was observed with compound **(1) (**Figure 44).

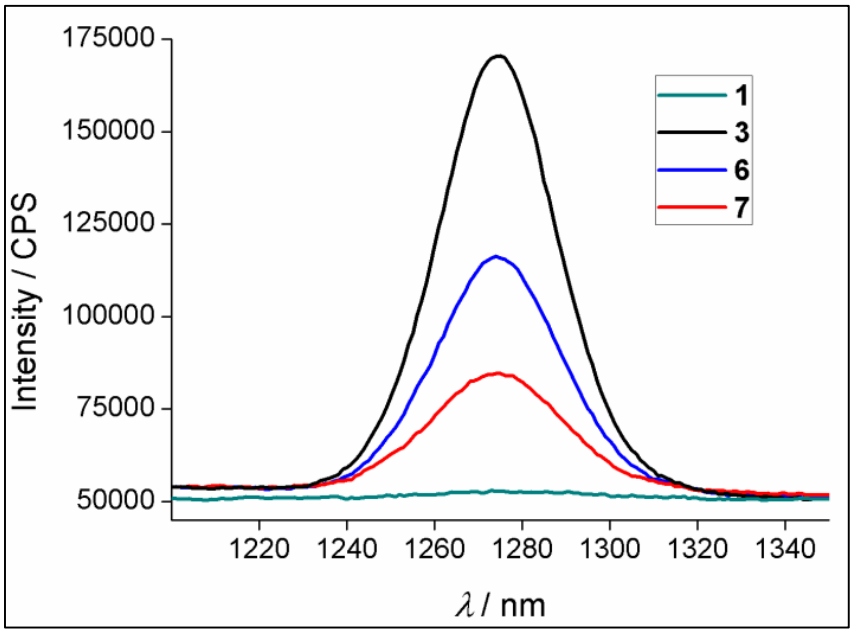

Figure 44 : Singlet oxygen phosphorescence with sensitization from BODIPY derivatives: **1** (green), **3** (blue), **6** (black) and **7** (red) in $CHCl_3$ at equal absorbances (0,2) at the wavelength of the maximum of their respective absorbances. Copyright © 2011, John Wiley and Sons. Reprinted with permission from ref (101).

Non-halogenated BODIPY dyes having low intersystem crossing efficiency, is a well-established fact[52] , indeed that is at least part of the reason for their bright fluorescence and photostability.

A list of relevant photophysical parameters for the sensitizers is placed in table 1. It is interesting to note that for the dimers **6** and **7**, significant fluorescence emission quantum yield is preserved, opening the possibility for a dual use as therapeutic and imaging agents.

Table 2. Comparative spectroscopic properties of BODIPY compounds.

Compound	λ_{abs}[a]/nm	λ_{ems}[a]/nm	ϕ_f	τ[a]/ns	ϕ_Δ[e]
1	509	514	0.80[d]	5.2	-
3	514	527	0.03[a,b]	2.5	0.51
6	515	588	0.31[a,c]	10.9	0.46
7	542	605	0.49[a,c]	5.0	0.21

[a] In $CHCl_3$. [b] In reference to Fluorescein in 0.1 M NaOH solution excited at 496 nm. [c] In reference to Rhodamine 6G in EtOH excited at 480 nm. [d] In EtOH. [e] Singlet oxygen quantum yield was determined with respect to Methylene Blue (0.57 in Dichloromethane)[113]

While integral areas under the phosphorescence emission peak is a measure of singlet oxygen quantum yield, we opted for more quantitative assessment of singlet oxygen quantum yields using 1,3-diphenylisobenzofuran as a trap molecule and with Methylene Blue as the reference compound (Methylene Blue has a singlet oxygen quantum yield of 0.57 under the conditions of the study in dichloromethane[113]) (figure 45). Excitation of the dyes was carried out by irradiation at the respective absorbance peak wavelengths with monochromatized light source, at a fluence rate around 30 $\mu W/cm^{-2}$. The quantum yield for singlet oxygen generation for **3** is 0.51 in dichloromethane, much higher than all non-halogenated BODIPY dyes and many other organic chromophores and photosensitizers, under comparable conditions. The other BODIPY dimers **6** and **7** also showed respectable singlet oxygen quantum yields of 0.46 and 0.21, respectively.

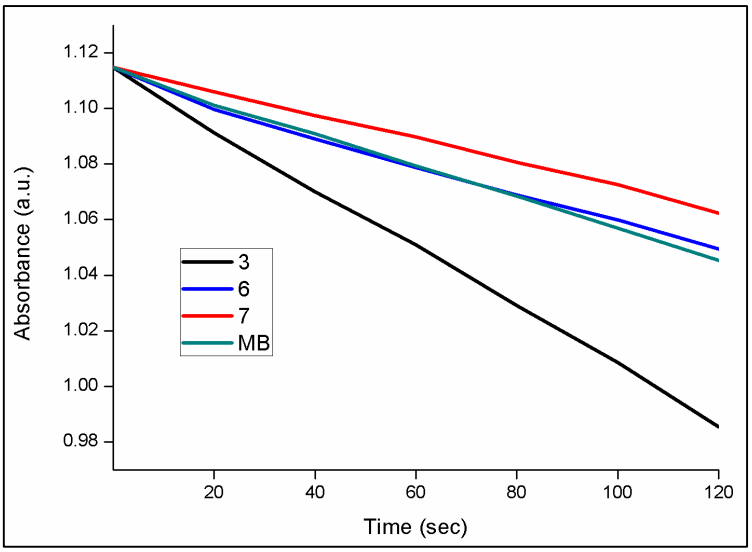

Figure 45 : Comparative singlet oxygen generation experiment. Absorbance decrease of DPBF at 414 nm with time in dichloromethane in the presence of BODIPY photosensitizers: (3) (black), (6) (blue), (7) (red) and reference photosensitizer methylene blue (green). Copyright © 2011, John Wiley and Sons. Reprinted with permission from ref (101).

For further demonstration of singlet generation capacity and photocytotoxicity of the most active dimeric dye **3**, we carried out a cell culture assay with cancer cell lines. To that end, we prepared a micellar formulation of the 8,2'-orthogonal dimeric dye using Cremophor-EL. The size distribution of the micelles was determined using electrophoretic light scattering. The size distribution reveals a median size of 100 nm for the micellar constructs (Figure 46).

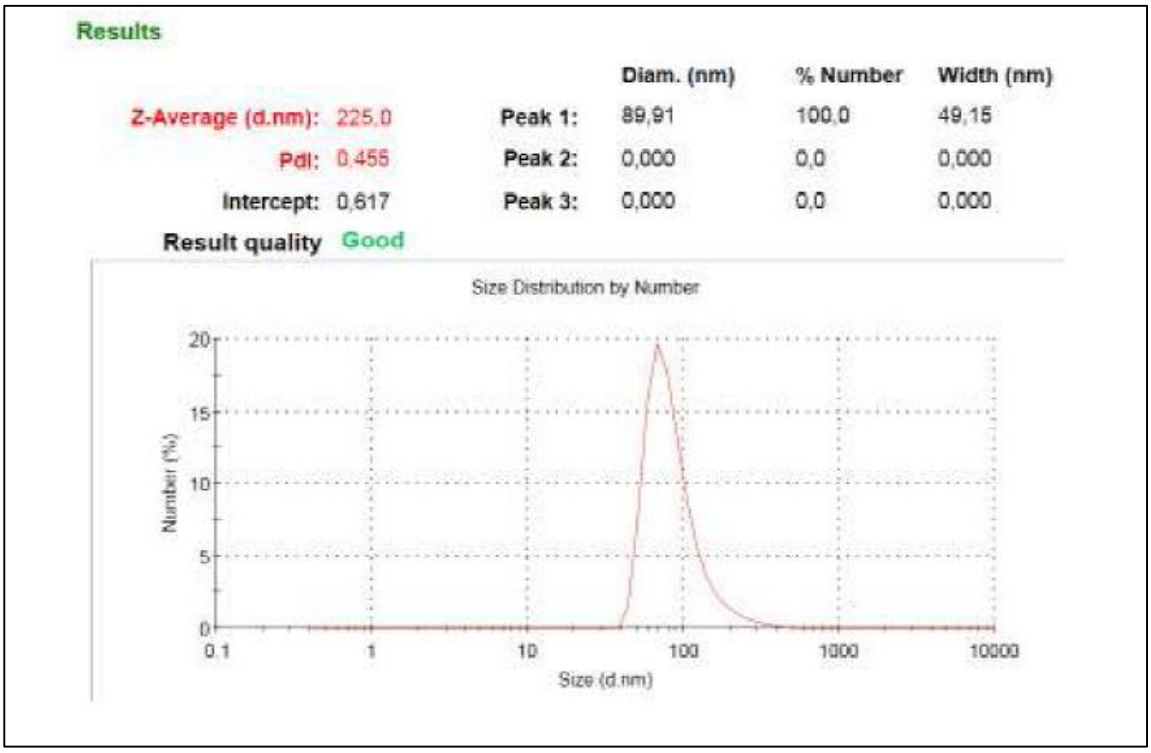

Figure 46 : Size distribution of compound micellar compound **3**. Cremophor EL was used for micelle formation

Micelle embedded dye retained high levels of singlet oxygen generation capacity as revealed by another singlet oxygen trapping experiment, this time in aqueous media, using a water soluble anthracene derivative (2,2'-(Anthracene-9,10-diylbis(methylene))dimalonic acid) (figure 47).

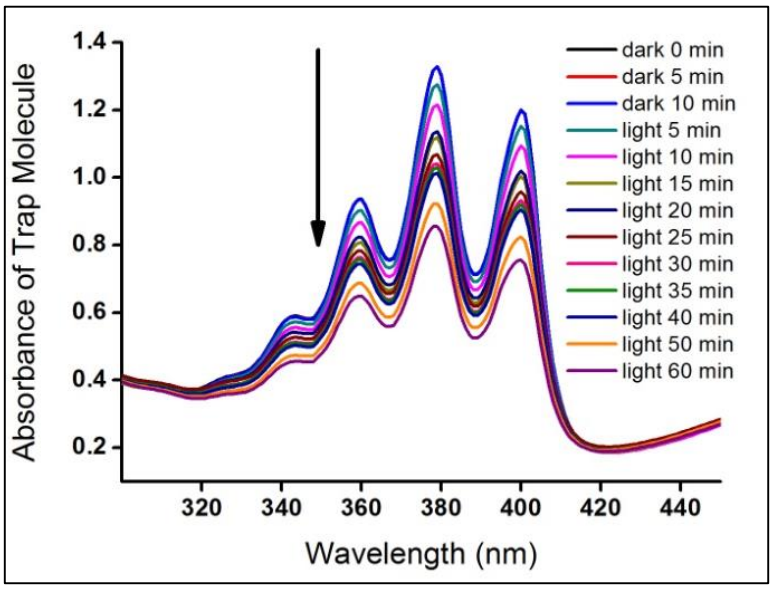

Figure 47 : Singlet oxygen generation experiment in aqueous solution. Decrease in Absorbance spectrum of trap molecule (anthracene derivative) in the presence of 1.69 μM compound **3** in phosphate buffer saline (PBS). Details are given in singlet oxygen measurements part.

Experimental verification of photocytotoxicity was carried out as follows: varying concentrations of the dimeric dye in Cremophor-EL micelles were incubated with K562 human erythroleukemia cells within a standard culture medium at 37 ºC in a humidified incubator containing 5% CO_2. Cells were irradiated with the green LED source for 4 hours, followed 44 hours of incubation in dark. The control group was incubated in dark, under otherwise identical conditions. The cell viabilities were determined using standard MTT assay (Figure 12). Even at very low concentrations of dyes (as embedded within micelles) significant decrease of cell viability was observed (green bars in figure 12) with a remarkable EC_{50} of 50 nM. No statistically significant change was observed when the cells were kept in dark, in the presence of same concentration of the photosensitizer **3** (black bars in figure 48).

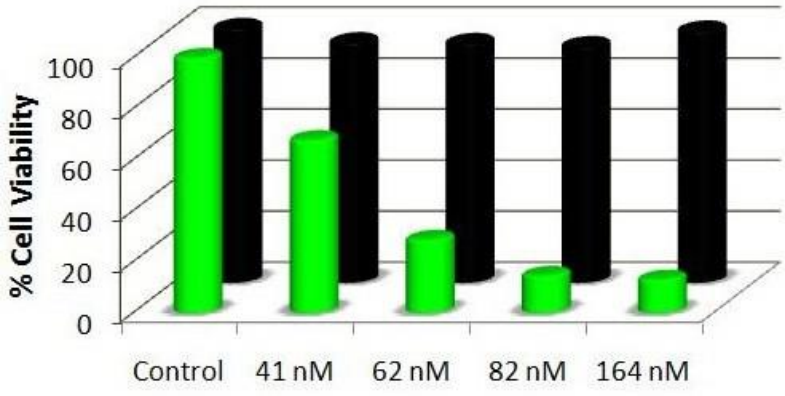

Figure 48: Photocytotoxicity of the sensitizer **3** as demonstrated by MTT assay. Cell suspensions (K562, human erythroleukemia cells) were seeded in 96-well flat-bottom plates and varying concentrations of the sensitizers were added into each well. Cells were kept either in dark, or under illumination with a green (520 nm) LED array at 2.5 mW/cm^2 fluence rate for a period of 4 h at 37^{0}C in a humidified incubator containing 5% CO_2. Copyright © 2011, John Wiley and Sons. Reprinted with permission from ref (101).

Photocytotoxicity was also revealed (figure 49) using confocal microscopy with two fluorescent probes of cell viability (acridine orange and propidium iodide). Cells incubated with the sensitizer **3** in dark show no changes as revealed by differential staining with the neutral and cell permeable acridine orange. These cells appear bright green under excitation at 488 nm. Cationic propidium iodide stains these cells only when membrane integrity is compromised; this happens only when both green LED irradiation and the sensitizer are acting on the cells. The use of excess propidium iodide results in red fluorescence in dead cells, or in cells dying via either apoptotic or necrotic pathways

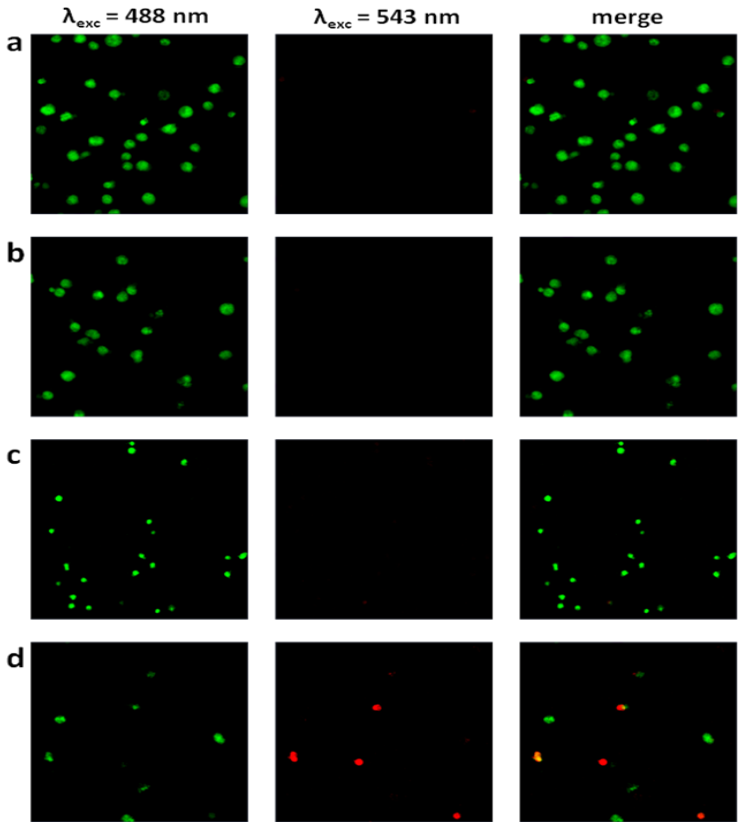

Figure 49 : Photocytotoxic activity of the dimeric BODIPY **3** visualized via confocal microscopy. Cell suspensions (K562, human erythroleukemia cells) were seeded in 24-well plates. a, Cells in Control 1 (upper plates) wells were incubated in dark for 24 hours; b, Cells in Control 2 wells (second row plates) were incubated with 500 µl/well Cremophor-EL solubilized (3) (at a final concentration of 164 nM) and kept in dark for 24 hours in the same incubator, c, Cells in Control 3 well were illuminated for 4 h without the sensitizer and incubated for a further 20 h in dark at the incubator. d, Cells in Control 4 (bottom row of plates) well were illuminated for 4 h after addition of 164 nM (3) and incubated for a further 20 h in dark at the incubator. Cells in wells were collected after 24 h and imaged at 40x magnification. Live cells are preferentially stained with acridine orange (AO, green) (a), whereas dead cells are preferentially stained with the dye propidium iodide (PI, red) due to increased cellular permeability (b). Copyright © 2011, John Wiley and Sons. Reprinted with permission from ref (101)

4.4 Conclusion

Our work demonstrated for the first time a practical example of excited state design leading to efficient cytotoxic singlet oxygen generation with a potential in photodynamic therapy. With a sound theoretical framework in design, it is only natural to expect other photosensitizers to emerge with similar line of reasoning. In this particular proof-of-principle work, excitation outside the therapeutic window is needed, but that issue can be easily addressed by the use of upconverting or persistence nanoparticles as secondary excitation sources. The other alternative is extending the conjugation in the dyes and exploring the longer wavelength extremes of the design principle has performed and published recently.[113]

4.5. Experimental Procedures

General: ^{1}H NMR and ^{13}C NMR spectra were recorded on Bruker DPX-400 (operating at 400 MHz for ^{1}H NMR and 100 MHz for ^{13}C NMR) in $CDCl_3$ solvent with tetramethylsilane as internal standard. All spectra were recorded and coupling constants (*J* values) are given in Hz. Chemical shifts are given in parts per million (ppm). Absorption spectra were performed by using a Varian Cary-100 and Varian Cary 5000 UV-VIS-NIR absorption spectrophotometer. Fluorescence measurements were conducted on a Varian Eclipse spectrofluometer. The Fluorescence decay measurements were carried out with the Horiba Jobin-Yvon Time-Resolved Fluorometer, Fluorolog FL-1057. The instrument response function was measured with an aqueous Ludox solution. Singlet oxygen phosphorescence around 1270 nm were determined by using Horiba Jobin-Yvon Fluoremeter with Hamamatsu NIR PMT module, model H-10330-75. The decays were analyzed with a multiexponential fitting function by iterative reconvolution and chi-square minimization. Mass spectra were recorded with Agilent Technologies 6224 TOF LC/MS and 6530 Accurate Mass Q-TOF LC/MS. Irradiation of photosensitizers **3**, **6** and **7** were accomplished at 520 nm by monochromatic light system composed of Spectral Products CM 110 1/8m monochromator, ASB-XE-175 Xenon light source, Newport Multi-Function Optical Meter model 1835-C. Electrophoretic Light Scattering was performed with Malvern NanoZS zeta potential. Reactions were monitored by thin layer chromatography using Merck TLC Silica gel 60 F254. Silica gel column chromatography was performed over Merck Silica gel 60 (particle size: 0.040-0.063 mm, 230-400 mesh ASTM).All other reagents and solvents were purchased from suppliers and used without further purification. Micelle has been prepared with compound **3** according to the literature[21]. In singlet oxygen measurements 1,3-Diphenylisobenzofuran was used as a singlet oxygen trap in organic solvent measurements and was purchased from supplier. 2,2'-(Anthracene-9,10-diylbis(methylene))dimalonic acid was used a singlet oxygen trap in aqueous solvent and was synthesized according to the literature[114].

Cremophor-EL solubilization : Photosensitizer **3** (5×10^{-5} moles) was dissolved in THF (1mL) treated with Cremophor EL (CrEL, 150 mg) and sonicated for 30 mins. THF was removed under reduced pressure, the remaining oil was dissolved in phosphate-buffered saline (PBS) (5mL), filtered through a 0.2 μm membrane filter and filled up to 10 mL with PBS (1X , pH= 7.4). Average size was found to be ca. 90 nm (figure 10).

Cell culture and MTT assay : K562 human erythroleukemia cells (ATCC) were cultured in 25 cm^3 culture flasks containing RPMI 1640 medium supplemented with heat inactivated 10 % fetal bovine serum, 2 mM L-glutamine,100 units.mL-1 penicillin G and 100 $\mu g.mL^{-1}$ streptomycin at 37ºC in a humidified incubator containing 5% CO_2. Micellar preparation of the sensitizer was dissolved in RPMI 1640 medium and test concentrations were prepared daily. The methlythiazolyltetrazolium (MTT) assay was used to evaluate cell viability. Briefly, 50 μL cell suspensions containing 4×10^4 K562 cells were seeded in 96-well flat-bottom plates (Costar, Cambridge, MA) and varying concentrations of Cremophor-EL solubilized dye **(3)** (Final concentrations= 41 nM - 164 nM) were added in 50 μL into each well. All dye concentrations were tested in triplicate for three times. Then, cells were kept either in dark or under illumination with a green (520 nm) LED array at 2.5 mW/cm^2 fluence rate for a period of 4 h at 37ºC in a humidified incubator containing 5% CO_2. In order to evaluate the cytotoxicity of dye, 4 h irradiated plates were kept in dark for a further 44 h and then MTT solution was added for measuring cell viability. In addition, plates kept in dark for 4 h were also incubated for an additional 44 h for control. After 48 h, 25 µL of MTT solution (1.0 mg/mL final concentration) (Sigma Chemical Co., St. Louis, MO) were added to each well, and the plates were incubated for a further 4 h. The formazan precipitate was solubilized by adding 80 μL lysing buffer (pH=4.7) composed of 23% SDS (sodium dodecyl sulfate) dissolved in a solution of 45% N,N- dimethylformamide. After an overnight incubation at 370ºC, the absorbances were read at 570 nm using a microplate reader (Spectramax Plus, Molecular Devices, Sunnyvale, California, USA). Cells incubated in culture medium alone served as a control for cell viability (nontreated wells) either in

irradiated plate or in plate that was kept in dark. Cell viability (%) was calculated as OD of treated wells/OD of nontreated cells x 100. **Cell culture and MTT assay studies were performed by Dicle Güç group at Hacettepe University, Basic Oncology Department, Ankara, Turkey**

Computational Details: Geometries were fully optimized with the *ab initio* Complete Active Space Self Consistent Field (CASSCF) methodology and B3LYP Density Functional[23] employing CEP-31G (SBKJC) and cc-pVDZ basis sets.[24] Harmonic vibrational frequencies were computed to assure that the species did not possess any imaginary frequencies and hence correspond to true minima. After a number of trial and error the active space in the CASSCF calculations were established as 6 electrons distributed over 6 valence orbitals (6,6) for the 8,2' dimer **3** and 4 electrons distributed over 4 valence orbitals (4,4) for the 8,8' dimer **6** and. Enlarged active spaces up to 12,12 also reproduced the key features presented in the main text. For the sake of consistency a 6 electrons in 6 orbitals CAS is used for both dimers. Geometries of excited states T_1 and S_1 were also fully optimized. Natural orbitals of the CASSCF wavefunction and configuration state function coefficients were analyzed to understand the nature of the electronic state as being a single electron HOMO → LUMO type or multiply substituted type. Whereas BODIPY core S_1 is a clean HOMO → LUMO dominated $\pi\pi^*$ state, S_1 states of **(3)** and **(6)** are drastically different and showed a large degree of multi-reference character. Gaussian 03[118] suite was mainly used for the DFT calculations, CASSCF calculations were mainly performed with MOLCAS[117], and GAMESS-US[27] programs. **Computational studies were performed in Dr. Yavuz Dede group at Gazi University, Department of Chemistry, Ankara, Turkey**

Singlet Oxygen Trap Experiments: In singlet oxygen measurements 1,3-Diphenylisobenzofuran (DPBF) (figure 50) was used as a singlet oxygen trap in organic solvent and was purchased from a supplier. 2,2'-(Anthracene-9,10-diylbis(methylene))dimalonic acid (ADMDA) was used a singlet oxygen trap in aqueous solvent and was synthesized according to the literature (figure 51).[54] In a typical procedure for the detection of singlet oxygen generation by using trap molecules, a photosensitizer (~1 □M) and a trap molecule (O.D ~ 1.0) were mixed in O_2 bubbled solvent. Initially several dark measurements were taken followed by irradiation of the mixture at absorption maximum of a sensitizer. Absorbance decrease of trap molecules was monitored suggesting singlet oxygen generation in the presence of light and sensitizers.

Singlet oxygen quantum yields were calculated according to the literature[103]. The relative quantum yields were calculated with reference to Methylene Blue (MB) in dichloromethane as 0.57.[112] First, dichloromethane was bubbled with air for 5 minutes. In UV cuvette absorbance of DPBF was adjusted around 1.0 using air bubbled dichloromethane. Then, photosensitizer was added to cuvette and photosentizer's absorbance was adjusted around 0.2-0.3

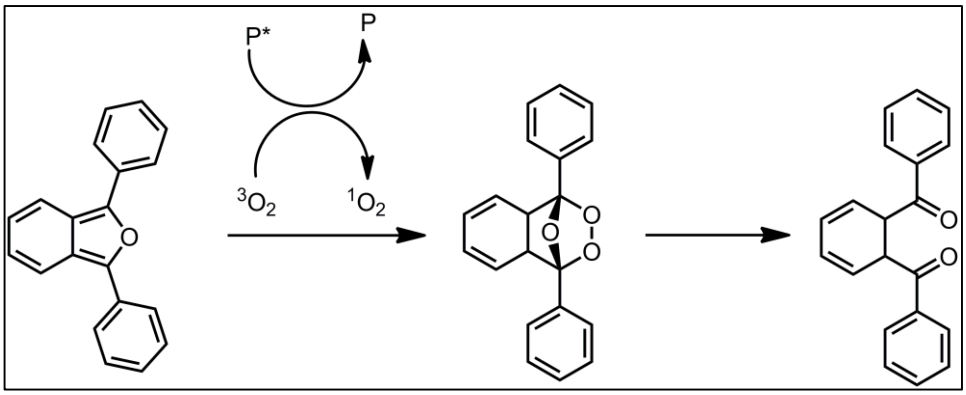

Figure 50: Reaction of singlet oxygen with 1,3-Diphenylisobenzofuran

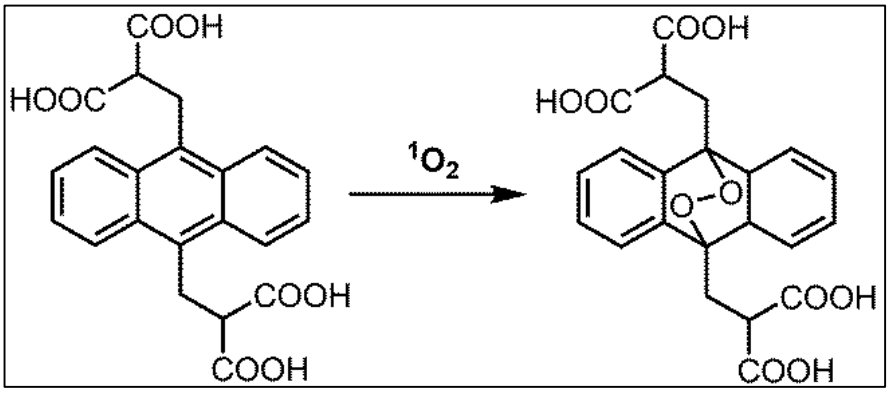

Figure 51 : Reaction of singlet oxygen with 2,2'-(Anthracene-9,10-diylbis(methylene))dimalonic acid

After, taking some measurements in dark, we took cuvette to monochromatic light system for irradiation at peak wavelength for 20 seconds. Absorbance was measured for several times after each irradiation. The graphics recorded are shown below; Figures 52 to 55. Then, slope of absorbance maxima of DPBF at 414 nm versus time graph for each photosensitizer were calculated. Singlet oxygen quantum yield were calculated according to the equation:

$$\phi_{\Delta}(\text{bod}) = \phi_{\Delta}(\text{ref}) \times \frac{\text{m (bod)}}{\text{m (ref)}} \times \frac{\text{F (ref)}}{\text{F (bod)}} \times \frac{\text{PF (ref)}}{\text{PF } (bod)}$$

where bod and ref designate the orthogonal BODIPY photosensitizer and MB respectively. m is the slope of difference in change in absorbance of DPBF (414 nm) with the irradiation time, F is the absorption correction factor, which is given by $F = 1 - 10^{-OD}$ (OD at the irradiation wavelength), and PF is absorbed photonic flux (μEinstein dm^{-3} s^{-1}).

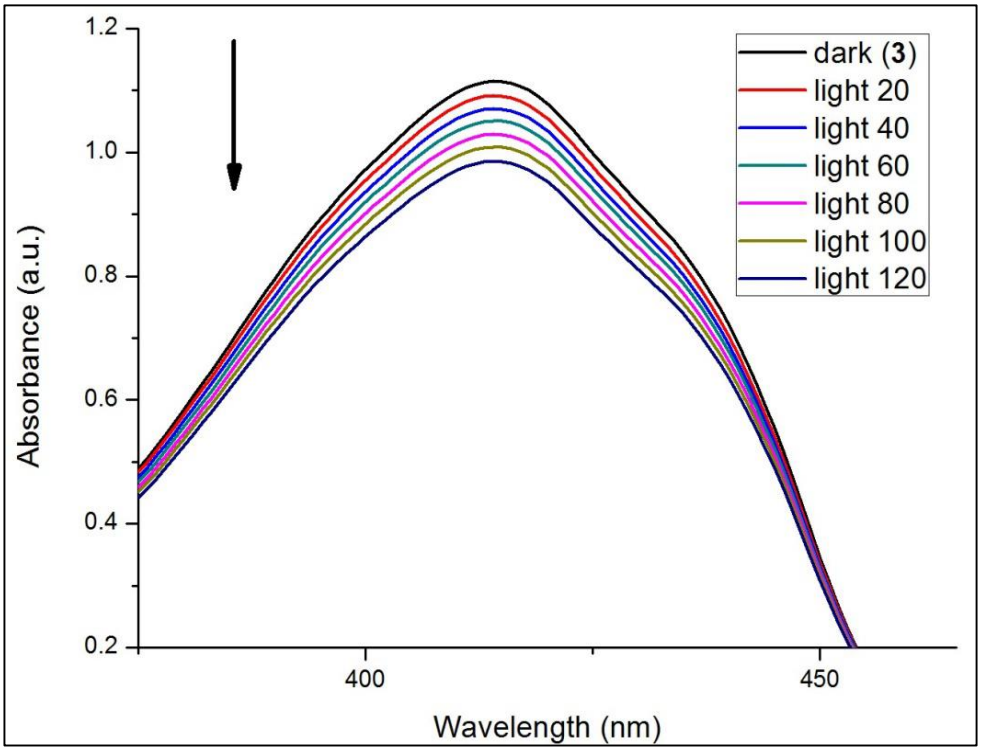
dark (3)
light 20
light 40
light 60
light 80
light 100
light 120
Absorbance (a.u.)
Wavelength (nm)
1.2
1.0
0.8
0.6
0.4
0.2
400
450

Figure 52: Decrease in absorbance of DPBF in dichloromethane in the presence of compound **3** in medium. Details are given in singlet oxygen measurements part. Copyright **.**2011, John Wiley and Sons. Reprinted with permission from ref (101).

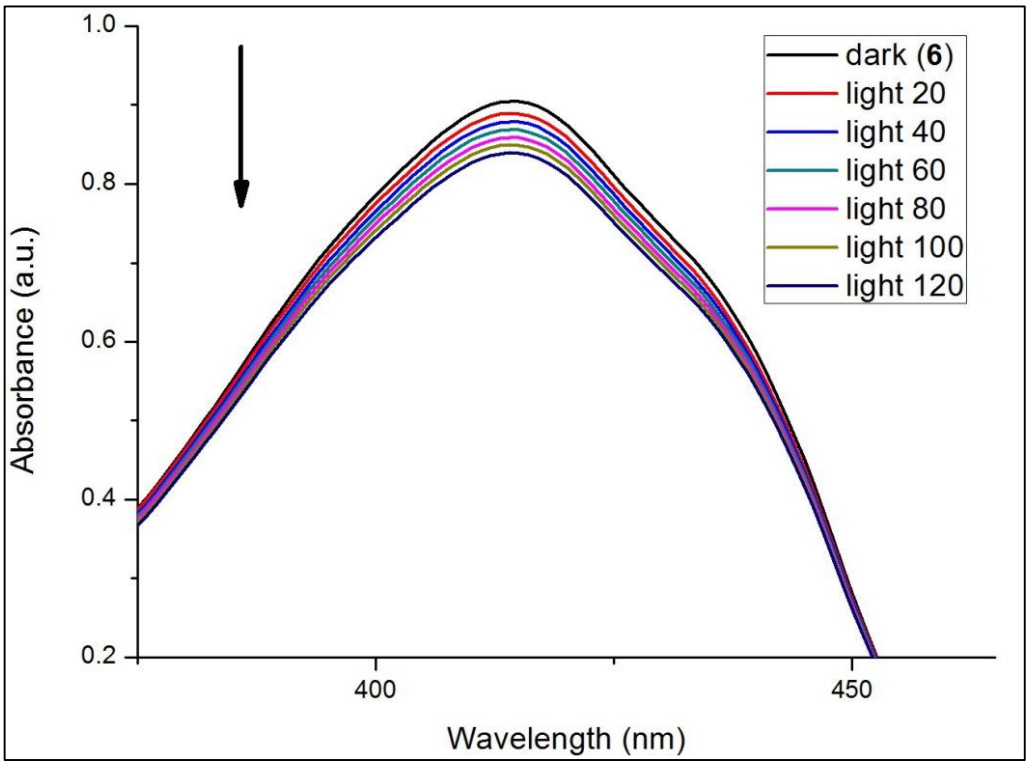

Figure 53: Decrease in absorbance of DPBF in dichloromethane in the presence of compound **6** in medium. Details are given in singlet oxygen measurements part. Copyright. 2011, John Wiley and Sons. Reprinted with permission from ref (101).

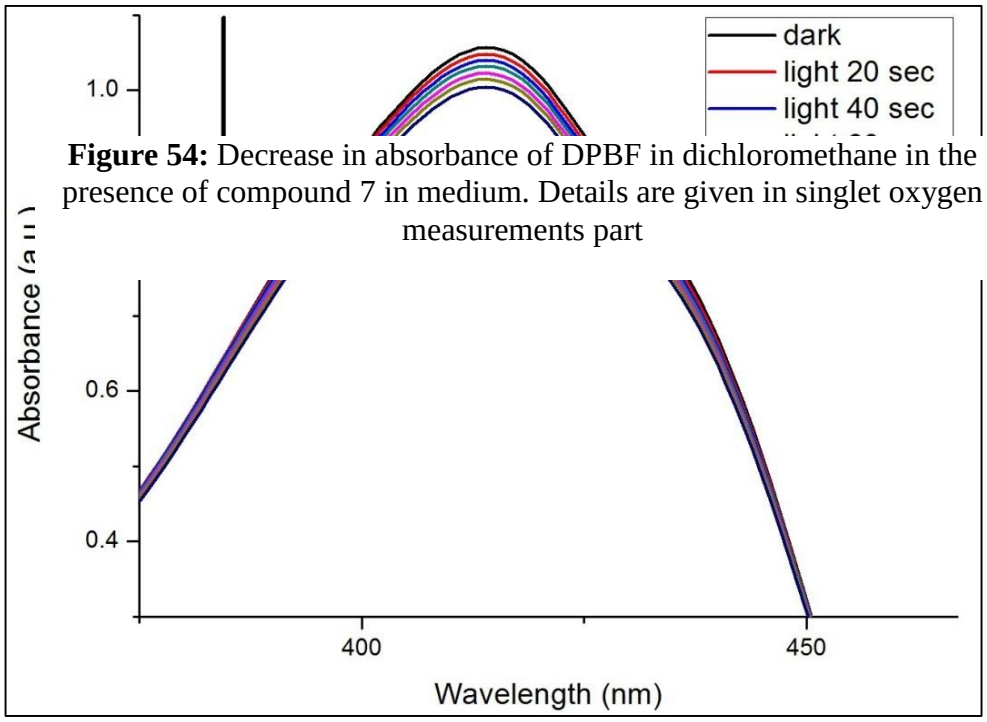

Figure 54: Decrease in absorbance of DPBF in dichloromethane in the presence of compound 7 in medium. Details are given in singlet oxygen measurements part

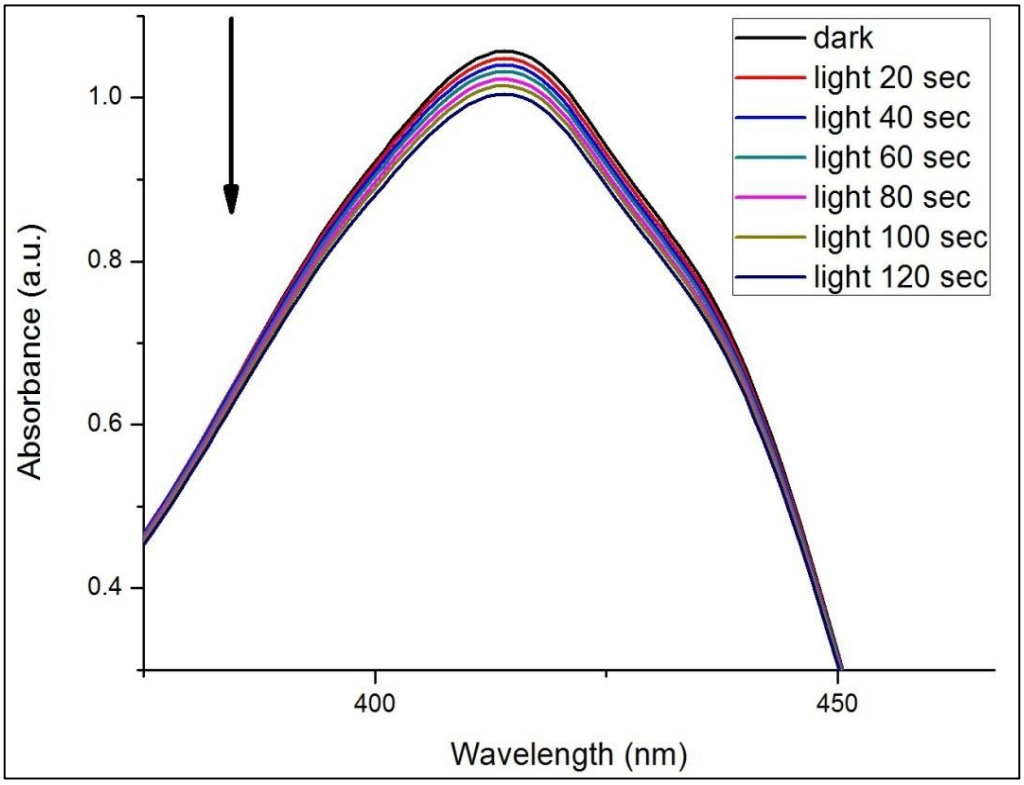

Figure 55: Decrease in absorbance of DPBF in dichloromethane in the presence of **MB** in medium. Details are given in singlet oxygen measurements part. Copyright . 2011, John Wiley and Sons. Reprinted with permission from ref (101).

Confocal Microscopy Imaging: Confocal microscopic analysis was also performed to evaluate cell viability. Briefly, 1500 μL cell suspensions containing 2 x 10^5 K562 cells/well were seeded in 24-well plates. Cells in Control 1 well were incubated in dark for 24 hours at 370ºC in a humidified incubator containing 5% CO_2. Cells in Control 2 well were incubated with 500 μL/well Cremophor-EL solubilized dye **3** (Final dye concentration = 164 nM) and kept in dark for 24 hours in the same incubator. Cells in Control 3 well were illuminated for 4 h without dye and incubated for a further 20 h in dark at the incubator. Cells in Control 4 well were illuminated for 4 h after addition of 164 nM dye **3** and incubated for a further 20 h in dark at the incubator. All conditions were studied in duplicate. Cells in wells were collected after 24 h and confocal microscopy images were acquired.

A stock solution of propidium iodide (PI) (Sigma P-4170) was prepared in distilled water, and used at a concentration of 0.5 mg/mL. Acridine orange (AO) was dissolved in phosphate buffered saline at a concentration of 100 μg/mL. One tablet of phosphate buffered saline (PBS) (Amresco) was dissolved in the distilled water to yield a pH=7.4 buffered solution.

X-ray Crystal Structure Determination: X-ray diffraction data were obtained on an Enraf-Nonius CAD4 (κ-geometry) diffractometer operating in ω/2θ scan mode using graphite-monochromated MoK_α radiation (λ = 0.71073 Å) at room temperature. The lattice parameters and their estimated standard deviations were determined by using CAD4 Express. Data reduction was carried out using XCAD4. The structures were solved by direct methods and refined by the full-matrix least-squares refinement on F^2 using the programs SHELXS97 and SHELXL97, respectively, in the WinGX package. Atomic scattering factors were taken from the International Tables for X-ray Crystallography. Hydrogen atoms bonded to carbon were placed on ideal positions and refined with fixed isotropic displacement parameters using a riding model. The molecules are held together by weak van der Waals interactions. Hydrogen bond and molecular packing

geometry of the title molecule was calculated with PLATON. The compound has one intermolecular and four intramolecular hydrogen bonds. Packing figure (figure 56) are prepared by MERCURY program.[120] **X-ray crystal structure of compound 3 was determined in Dr. Leyla Tatar Yildirim group, at Hacettepe University, Department of Physics Engineering, Ankara, Turkey.**

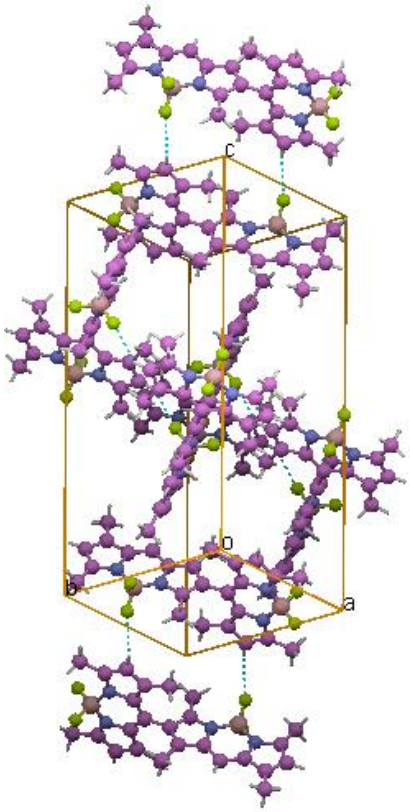

Figure 56 : Packing diagrams of compound **3**. Dashed lines indicate inter H-bond between C2 and F4 atoms. Copyright . 2011, John Wiley and Sons. Reprinted with permission from ref (101).

Synthetic Details:

Synthesis of 1: 250 mL 1,2-dichloroethane was degassed with N_2. 2,4-dimethyl pyrrole (1 mL, 11.37 mmol), triethylorthoformate (0.95 mL, 5.69 mmol) and $POCl_3$ (0.58 mL, 6.25 mmol) were added to degassed solvent. Reaction was allowed to stir for 2 hours at room temperature. Then 11.55 mL NEt_3 and 11.55 mL $BF_3.OEt_2$ were added. After 1 hour the reaction was washed with water (3x250 mL), the organic layer separated, dried on $NaSO_4$ and evaporated in vacuo. Column chromatography with $CHCl_3$ yielded the pure product as reddish solid (400 mg, 28 %). ^{1}H NMR (400 MHz, $CDCl_3$): δ_H 7.09 (1H, s, Ar*H*), 6.10 (2H, s, Ar*H*), 2.60 (6H, s, C*H*$_3$), 2.29 (6H, s, C*H*$_3$); ^{13}C NMR (100 MHz, $CDCl_3$): δ_C 156.8, 141.3, 133.5, 120.2, 119.1, 14.8, 11.2 ppm.

Synthesis of 2: 4 mL of DMF and 4 mL of $POCl_3$ was stirred in an ice bath for 5 min under argon. Then warmed to room temperature and waited for 30 minutes. To this mixture compound **(1)** (100 mg, 0.328 mmol) was added in dichloroethane (40 mL). The temperature is raised to 50 ^{0}C and stirred for 2 hours. The reaction medium was cooled and poured into 150 mL $NaHCO_3$ solution slowly under cool conditions. After cooling it was stirred for further 30 min, then washed with water 3 times. The organic layers was combined and dried over $NaSO_4$ and evaporated to dryness. The compound has been purified by column chromatography by using chloroform as an eluant and the compound has been got pure as reddish solid (95 %). ^{1}H NMR (400 MHz, $CDCl_3$): δ_H 10.02 (1H, s, C*H*O), 7.20 (1H, s, Ar*H*), 6.20 (1H, s, Ar*H*), 2.77 (3H, s, C*H*$_3$), 2.58 (3H, s, C*H*$_3$), 2.48 (3H, s, C*H*$_3$), 2.28 ppm (3H, s, C*H*$_3$); ^{13}C NMR (100 MHz, $CDCl_3$): δ_C 185.5, 163.5, 157.2, 145.4, 140.6, 136.4, 131.1, 125.8, 122.0, 121.5, 15.2, 12.9, 11.5, 10.4 ppm; MS HRMS (TOF-ESI): *m*/z calcd for $C_{14}H_{15}BF_2N_2O^+$: 275.1246 $[M+H]^+$; found: 275.1212$[M+H]^+$, Δ = 12.3 ppm.

Synthesis of 3: In N_2 bubbled 250 mL dichloromethane, 2,4-Dimethylpyrrole (50 µL, 0.478 mmol) and **(2)** (60 mg, 0.217 mmol) were mixed. 1 drop of trifluoroacetic acid has been added. The reaction mixture stirred at room

temperature overnight. Then p-chloranil (49.2 mg, 0.217 mmol) was added to the reaction. After stirring 1 hours at room temperature, NEt_3 (2 mL) and $BF_3.OEt_2$ (2 mL) was added and stirred again for 1 hour. The reaction was finished by extracting with water (3x250 mL). Column chromatography with $CHCl_3$ yielded the pure product (20 %). ^{1}H NMR (400 MHz, $CDCl_3$): δ_H 7.18 (1H, s, Ar*H*), 6.15 (1H, s, Ar*H*), 6.02 (2H, s, Ar*H*), 2.61 (3H, s, C*H*$_3$), 2.59 (3H, s, C*H*$_3$), 2.57 (3H, s, C*H*$_3$), 2.54 (3H, s, C*H*$_3$), 2.40 (3H, s, C*H*$_3$), 2.30 (3H, s, C*H*$_3$), 2.12 (3H, s, C*H*$_3$), 1.72 ppm (3H, s, C*H*$_3$); ^{13}C NMR (100 MHz, $CDCl_3$): δ_C 160.3, 155.8, 151.5, 143.7, 142.5, 136.6, 134.7, 133.4, 132.3, 131.7, 124.2, 121.3, 120.7, 120.5, 14.9, 14.7, 13.9, 12.7, 9.8, 8.7 ppm; MS HRMS (TOF-ESI): *m*/z calcd for $C_{26}H_{28}B_2F_4N_4^+$: 493.2436 $[M+H]^+$; found: 493.2417 $[M+H]^+$, Δ = 3.9 ppm.

Synthesis of 6: In N_2 bubbled 100 mL dichloromethane 2,4-Dimethylpyrrole (16.2 μL, 0.12 mmol) and **4** (20 mg, 0.06 mmol) were mixed. 1 drop of trifluoroacetic acid has been added. The reaction mixture stirred at room temperature overnight. Then p-chloranil (14.8 mg, 0.06 mmol) was added to the reaction. After stirring 1 hour at room temperature, NEt_3 (1 mL) and $BF_3.OEt_2$ (1 mL) was added and stirred again for 1 hour. The reaction was finished by extracting with water (3x100 mL). Column chromatography with $CHCl_3$ yielded the pure product (16 %). ^{1}H NMR (400 MHz, $CDCl_3$): δ_H 6.05 (4H, s, Ar*H*), 2.61 (12H, s, C*H*$_3$), 1.60 (3H, s, C*H*$_3$); ^{13}C NMR (100 MHz, $CDCl_3$): δ_C 157.2, 142.6, 121.6, 14.8, 14.3 ppm; MS HRMS (TOF-APCI): *m*/z calcd for $C_{26}H_{28}B_2F_4N_4$: 493.2358 $[M-H]^-$; 493.2385 found: $[M-H]^-$, Δ = 5.5 ppm.

Synthesis of 7: In N_2 bubbled 100 mL dichloromethane 2,4-Dimethylpyrrole (14.8 μL, 0.143 mmol) and **5** (18 mg, 0.065 mmol) were mixed. 1 drop of trifluoroacetic acid has been added. The reaction mixture stirred at room temperature overnight. Then p-chloranil (16 mg, 0.065 mmol) was added to the reaction. After stirring 1 hour at room temperature, NEt_3 (1 mL) and $BF_3.OEt_2$ (1 mL) was added and stirred again for 1 hour. The reaction was finished by

extracting with water (3x100 mL). Column chromatography with $CHCl_3$ yielded the pure product (9 %). ^1H NMR (400 MHz, $CDCl_3$): δ_H 2.54 (12H, s, C*H*$_3$), 2.36 (8H, q, J = 11.3 Hz, C*H*$_2$,), 1.82 (12H, s, C*H*$_3$), 1.10 (12H, s, C*H*$_3$); ^{13}C NMR (100 MHz, $CDCl_3$): δ_C 155.1, 137.8, 134.8, 133.2, 129.9, 17.1, 14.7, 12.8, 11.6 ppm; MS HRMS (TOF-APCI): *m*/z calcd for $C_{34}H_{43}B_2F_4N_4$: 605.3610 $[M-H]^-$; found: 605.3618 $[M-H]^-$, Δ = 1.3 ppm.

CHAPTER 5

Designing Micelle-embedded BODIPY based photosensitizers for the Photodynamic Therapy

The discussions on this chapter are partially based on the following publications:

Kilic, B.; Yesilgul, N.; Polat, V.; Gercek, Z; Akkaya, E. U., *Tetrahedron Lett.* **2016,** 57, 1317-1320

5.1 Objective

In this project, a series of novel BODIPY based photosensitizers have been designed and synthesized which fulfill a great number of criteria for the PDT in terms of singlet oxygen generation ,narrow absorption bands, low dark toxicity, tissue penetration and solubility. All target compounds were synthesized by using standard BODIPY chemistry. Because of the fact that BODIPY dyes have remarkable features, such as high quantum yields, good solubility, photostability etc., BODIPY dyes were used for the design and synthesis of the target compounds as promising photodynamic therapy agent for the photodynamic therapy application.

5.2 Introduction

It is a well-known fact that promising and effective photodynamic therapy agents should have some distinctive properties, such as efficient singlet oxygen generation, water solubility, and biocompatibility.

In this study, we have used BODIPY dyes as a photosensitizer, due to the fact that BODIPY dyes (4,4-difluoro-4-bora-3a,4a-diaza-s-indacene) have many distinctive properties such as high fluorescence quantum yield, photostability, long wavelength absorption and emission, high molar absorption coefficient and their simple synthesis method[60] and they meet important criteria for the photodynamic therapy action.

In order to overcome water solubility problem, we have prepared aqueous solution of the target compounds within Chremophor EL micelle. The micelle forming agent examined was Cremophor EL (currently known as Kolliphor EL), a synthetic, non-ionic surfactant made by the reaction of Castor oil (mostly triglyceride) with ethylene oxide, which provides a polyethylene glycol chain. Cremophor EL is widely used in pharmaceutical industry as an excipient in order to get water insoluble drugs into a water soluble and biocompatible drug[122].

It was found that as the size of the hydrophobic tail at constant temperature increases, surfactant systems show an exponential decrease in the critical micelle concentration (CMC). The CMC is dependent on the free energy which is formed by the formation of micelle. With respect to increasing the tail length, CMC decreases exponentially. It has been reported that there is a linear behavior on the logarithmic scale with respect to the number of atoms in the alkyl chain.[123] It has been shown that typical micelles should have small submicron size of lower than 200 nm in diameter[124].

We have introduced different long alky groups at the meso-position of the BODIPY cores in order to have hydrophobic groups which are located inside of the micelles and give rise to a more stable aqueous solution of the BODIPY dyes. For effective singlet oxygen generation, we have introduced heavy atoms to the 3, 5-positions of the BODIPY cores due to the fact that heavy atom functionalization results in an intersystem crossing process and effective singlet oxygen generation. [63,120]

5.3 Result and Discussion

In this study, we have three novel BODIPY-based photosensitizers synthesized and characterized. In order to achieve one of the most important parameter, water solubility of the target compounds, we have prepared aqueous solution of the target compounds in Chremephor EL micelle.

First, we have synthesized 4-decyloxybenzaldehyde starting with 4-hydroxybenzahldeyde (Figure 57).

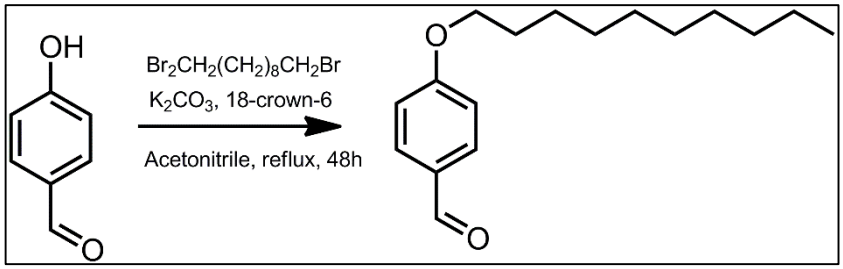

Figure 57 : Synthesis of the 4-decyloxybenzaldehyde

After the synthesis of the aldehyde, we have synthesized meso-substituted BODIPY with standard BODIPY chemistry. It was performed by the reaction of previously synthesized 4-declyoxybenzaldehyde with 2,4-dimethyl pyrrole[109]. (Figure 58)

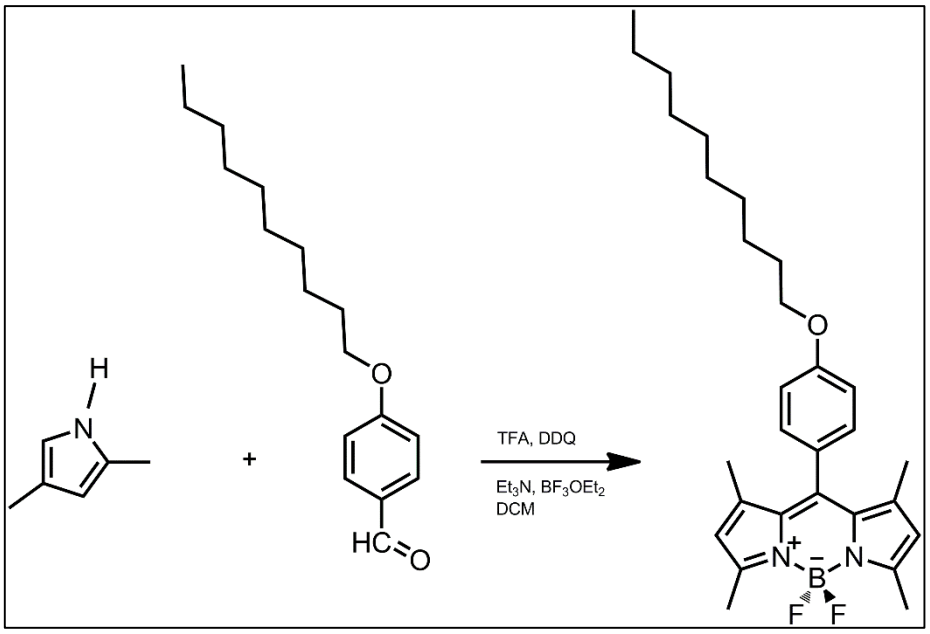

Figure 58 : Synthesis of the meso-substituted BODIPY

Then, we have introduced two different heavy atoms, Bromine and Iodine to the 3, 5-positions of the BODIPY cores successively. (Figure 59 and 62)

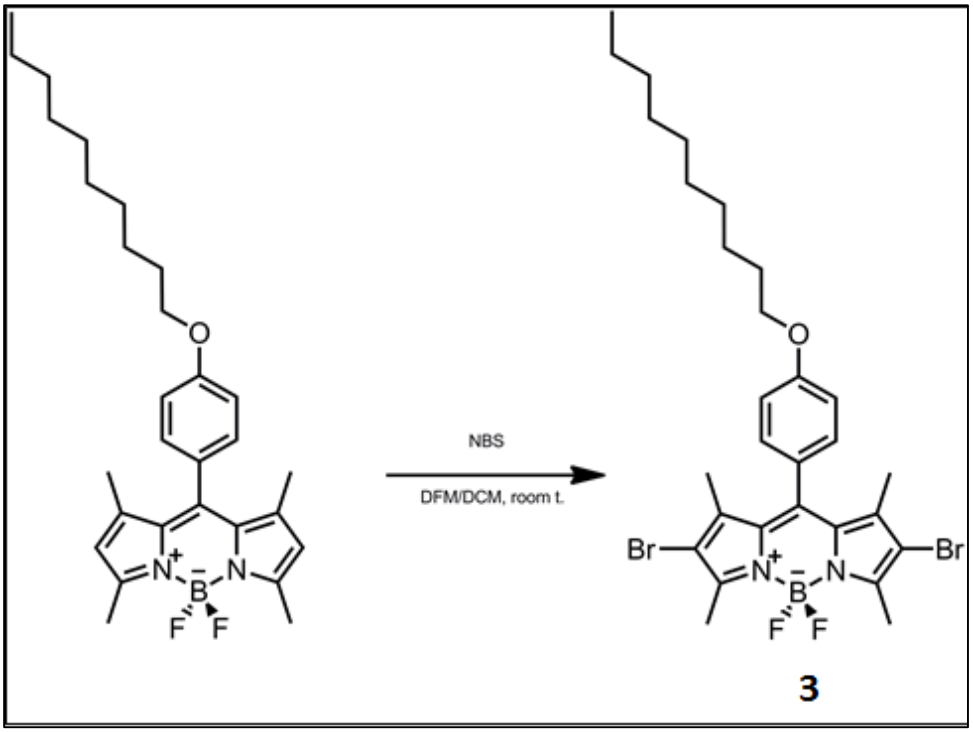

Figure 59 : Synthesis of the brominated meso-substituted BODIPY Compound **3** (Target molecule **1**)

After the synthesis and characterization of the first target compound (Compound **3**), we have prepared its micelles by using Cherephor EL and performed singlet oxygen generation experiments in aqueous medium. Average size of the micelles was found to be ca. 26.62 nm (Figure 68). As a trap molecule, water soluble 2,2'-(anthracene-9,10-diylbis(methylene)dimalonic acid was used (Figure 60). The decrease in the absorbance of the trap molecule indicates the generation of the cytotoxic singlet oxygen (Figure 61).

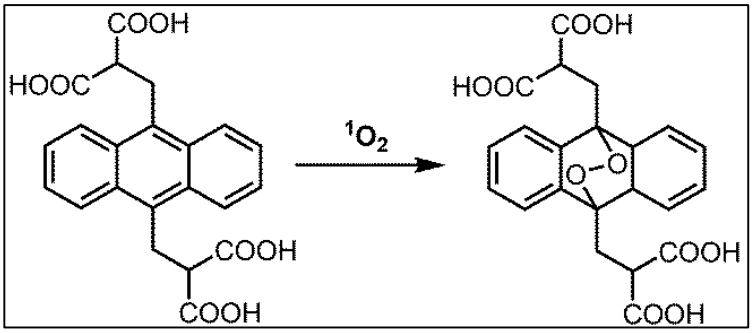

Figure 60 : Reaction scheme of trap molecule with singlet oxygen

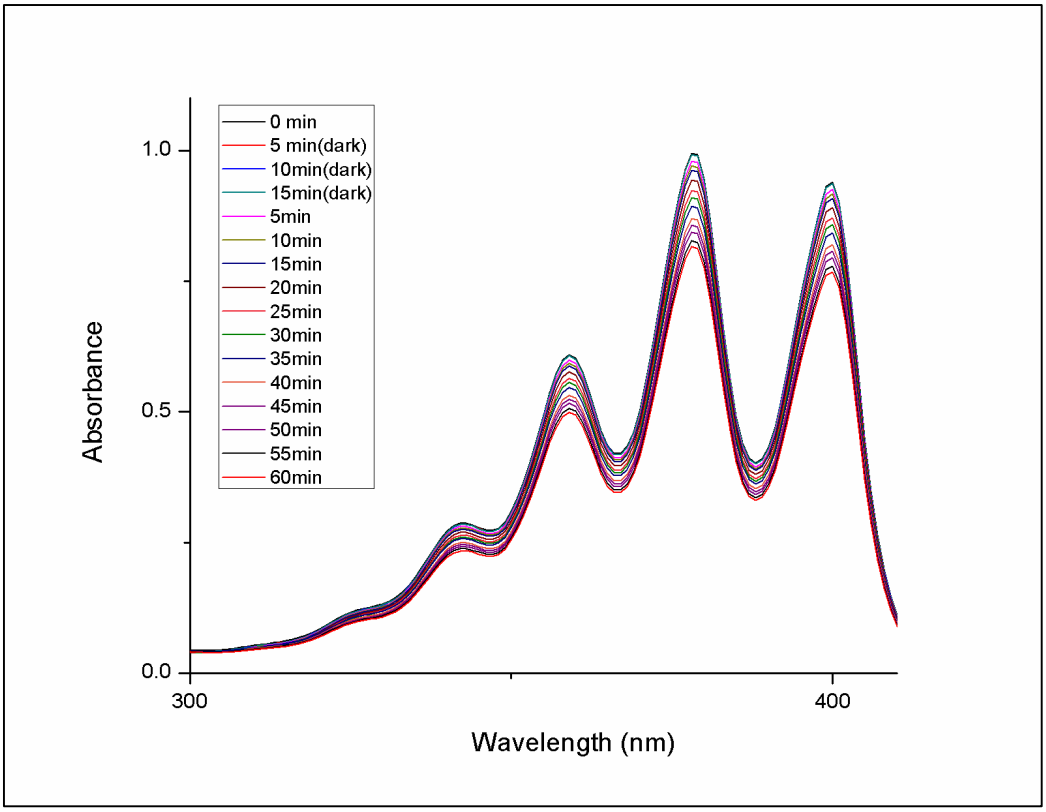

Figure 61 : Absorbance spectrum of trap molecule 2,2'-(anthracene-9,10-diylbis(methylene)dimalonic acid in water under light and Photosensitizer (Target molecule **1**)

Excitation of the target molecule was carried out with a light emitting diode (LED) source. 507 nm light was exposed from 20 cm cell distance. The decrease of the absorbance band of the trap molecule at 378 nm was monitored. This decrease of the absorbance band is caused by the oxidation of the trap molecule with reactive oxygen species such as singlet oxygen

The experiment was performed at the concentration of $2x10^{-6}$ M of PS (Target Molecule **1**) and $50x10^{-6}$ M of 2,2'-(anthracene-9,10-diylbis(methylene)dimalonic acid over a period of 75 min. For the first 15 minutes sample was kept at dark, then irradiated at 517 nm light for 60 minutes. Absorbance was measured in 5 minute intervals (Figure 61).

The decrease in the absorbance of the trap molecule at 378 nm shows that target molecule **1** is relatively effective singlet oxygen generator.

Second target molecule was synthesized by introducing iodine atoms to the 3, 5-positions of the BODIPY core. (Figure 62) . After the synthesis of the second target molecule, we have perfomed singlet oxygen generation experiments as we carried out for the first target compound. We have prepared its micelles by using Cremophor EL and average size of the micelles was found to be ca. 50.59 nm (Figure 69).

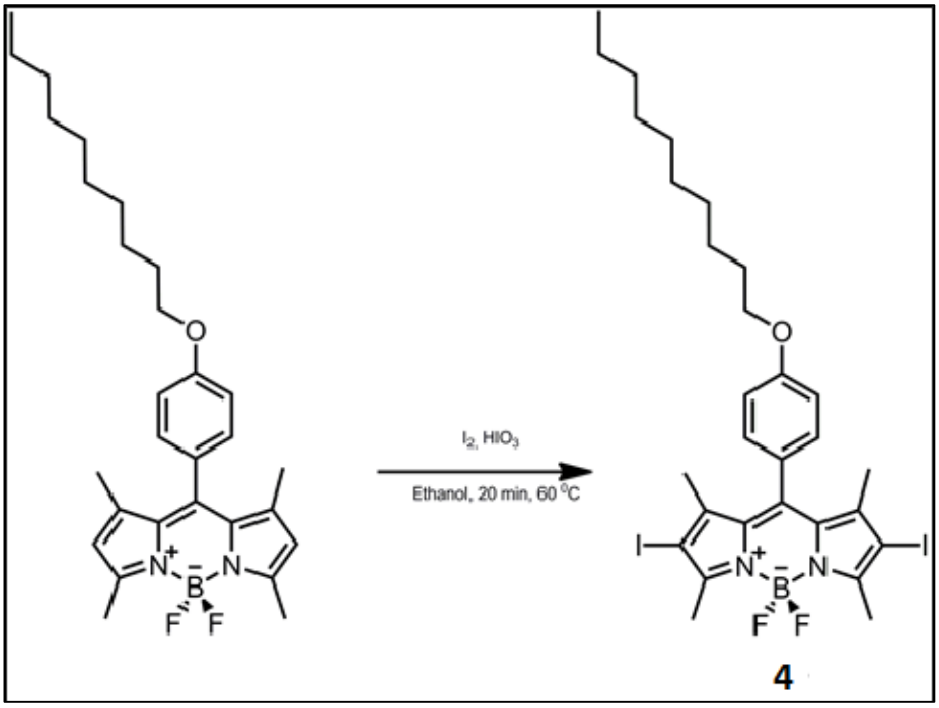

Figure 62 : Synthesis of the iodinated meso-substituted BODIPY

Excitation of the target molecule **2** (Compound **4**) was carried out with a light emitting diode (LED) source. 517 nm light was exposed from 20 cm cell distance. The decrease of the absorbance band of the trap molecule at 378 nm was monitored. This decrease of the absorbance band is caused by the oxidation of the trap molecule with reactive oxygen species such as singlet oxygen

The experiment was performed at the concentration of $2x10^{-6}$ M of PS (Target Molecule **2**) and $50x10^{-6}$ M of 2,2'-(anthracene-9,10-diylbis(methylene)dimalonic acid over a period of 75 min. For the first 15 minutes sample was kept at dark, then irradiated at 517 nm light for 60 minutes. Absorbance was measured in 5 minute intervals (Figure 63).

The decrease in the absorbance of the trap molecule at 378 nm shows that target molecule **2** is highly effective singlet oxygen generator in aqueous medium.

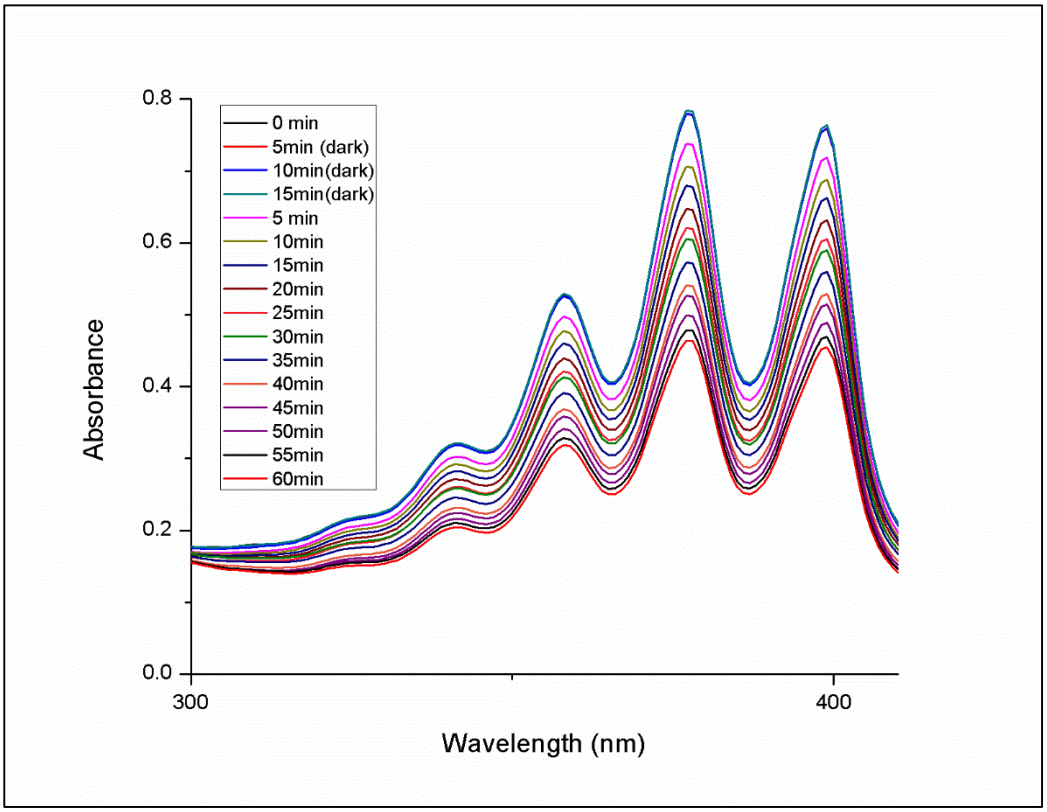

Figure 63 : Absorbance spectrum of trap molecule 2,2'-(anthracene-9,10-diylbis(methylene)dimalonic acid in water under light and Photosensitizer , Compound **4** (Target molecule **2**)

The third target compound **3** was synthesized by the reaction of 2,4-dimethyl pyrrole with palmitoylchrolide.(Figure 64)

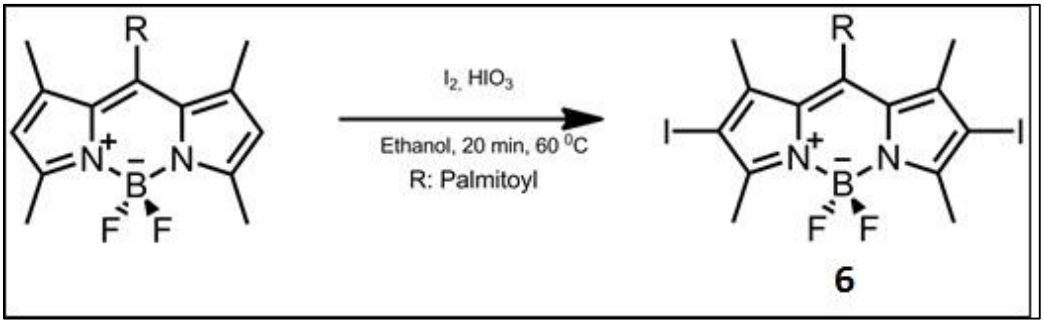

Figure 64 : Synthesis of the target molecule **3**

After the synthesis and micelle preparation of the third target molecule, Compound **6**, we have perfomed singlet oxygen generation experiments as we carried out for previous target compounds. Average size of the micelles was found to be ca. 25.20 nm (Figure 69). Absorbance decrease of the trap molecule shows that singlet oxygen was generated in the presence of light source which is LED emitting at 517 nm and photosensitizing agent which is the third BODIPY-based targer molecule of this project. (Figure 65)

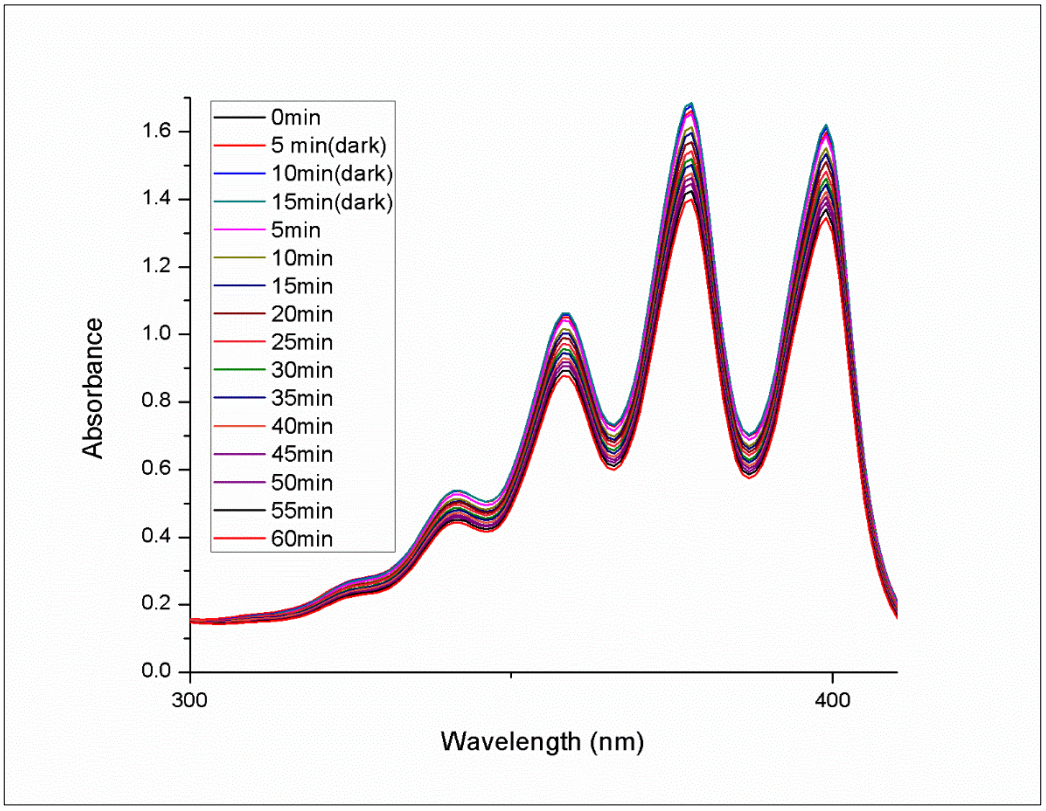

Figure 65 : Absorbance spectrum of trap molecule 2,2'-(anthracene-9,10-diylbis(methylene)dimalonic acid in water under light and Photosensitizer **,** Compund **6** (Target molecule **3**)

Before we started with singlet oxygen generation experiments of the target compounds, a control experiment was performed by using an aqueous solution of trap molecule, 2,2'-(anthracene-9,10-diylbis(methylene)dimalonic acid to check the stability of the trap molecule.

An aqueous solution of trap molecule was illuminated under the same conditions that were carried out for the singlet oxygen generation of the target compounds.

The solution was irradiated at 517 nm for 30 min and absorbance was measured in 5 minutes intervals.

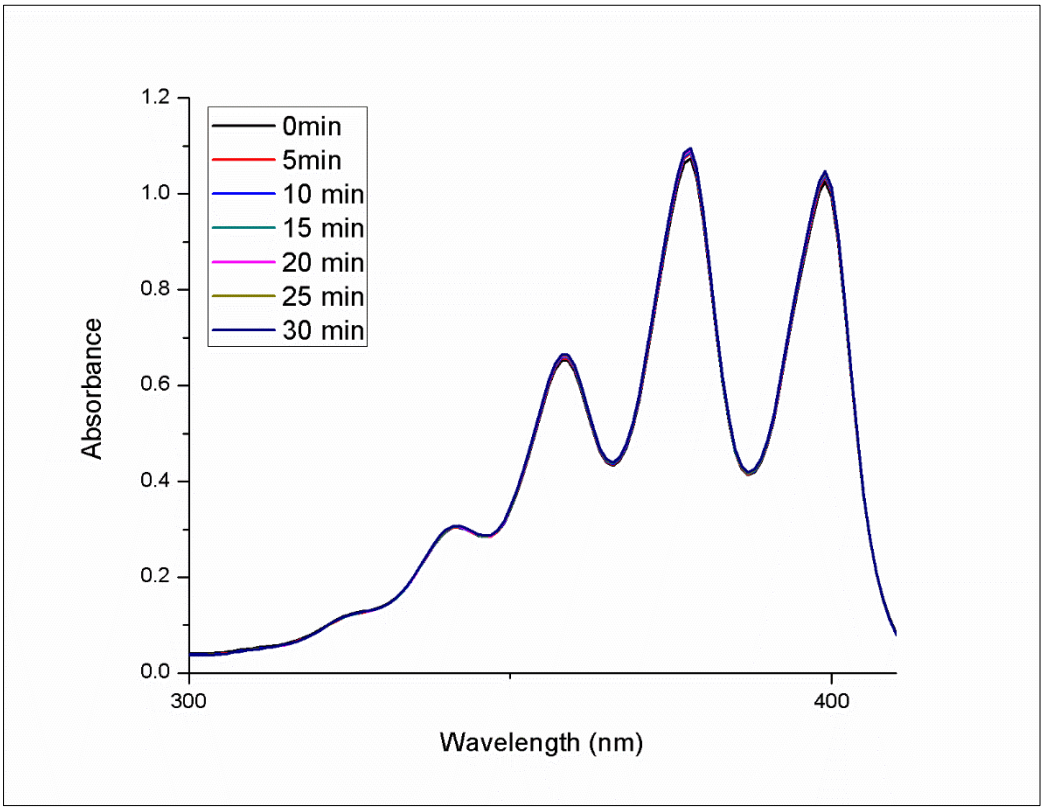

Figure 66 : Absorbance spectrum of trap molecule 2,2'-(anthracene-9,10-diylbis(methylene)dimalonic acid in water without photosensitizer

There was no decrease in the absorbance of the trap molecule that shows the trap molecule does not decompose under the light illumination and is stable (Figure 66).

To determine the emission wavelength of the LED that was used for performing singlet oxygen generation experiments, emission spectrum was performed. The emission of the LED source is at 517 nm.

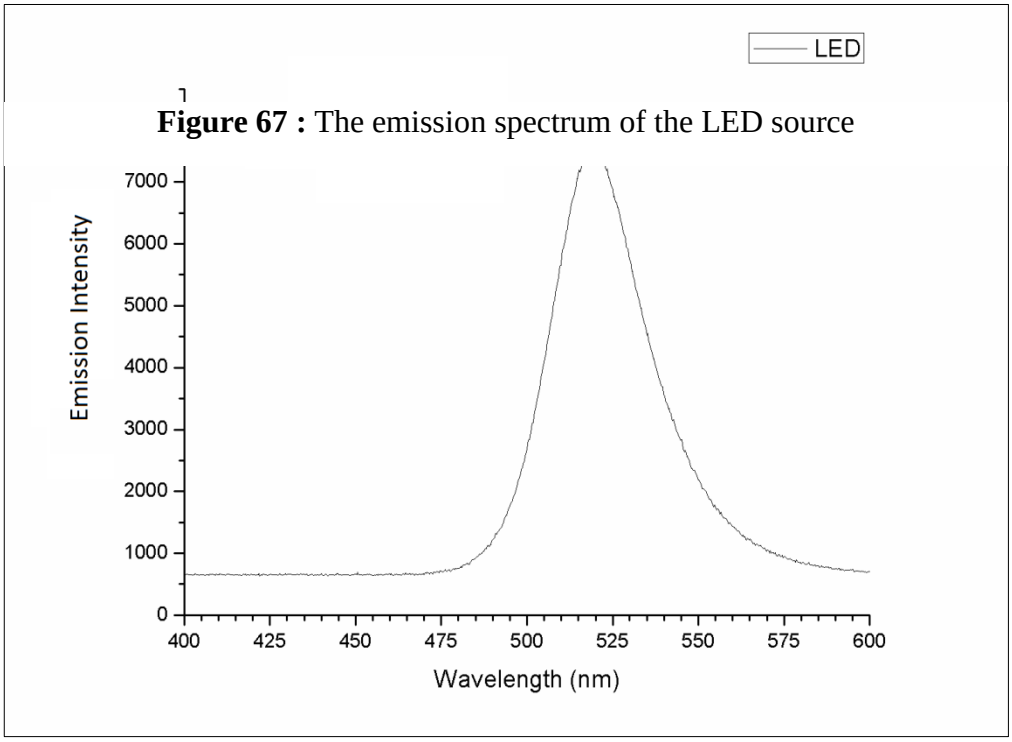

Figure 67 : The emission spectrum of the LED source

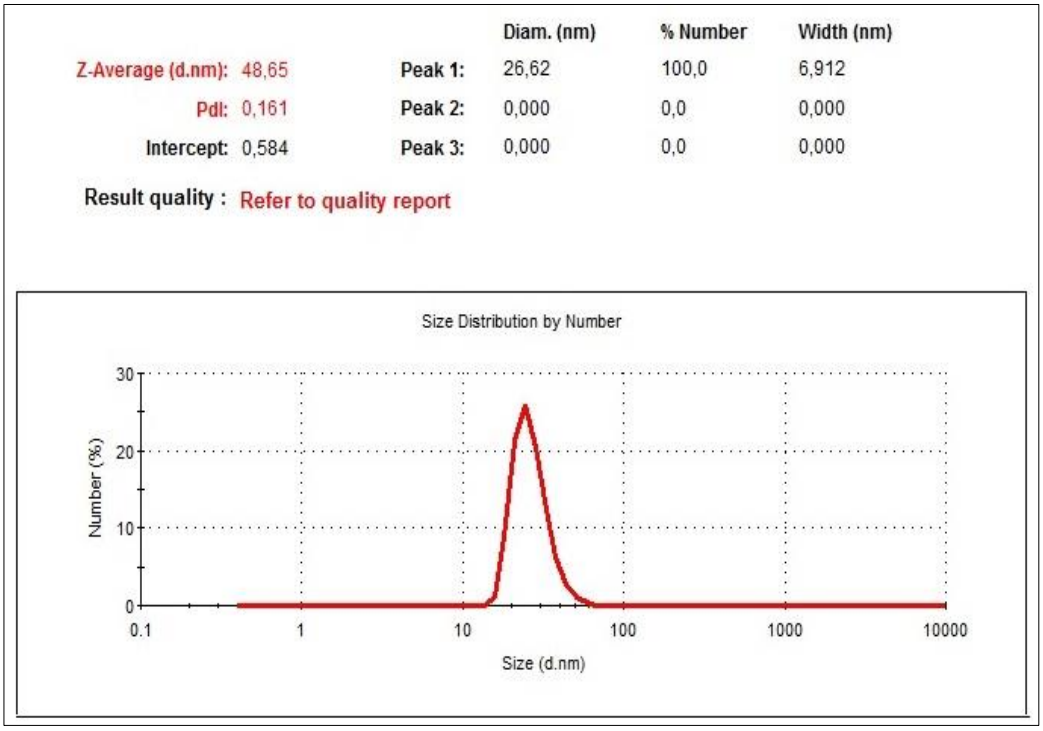

Figure 68 : Size distribution of compound micellar compound **3** (First Target Compound). Cremophor EL was used for embedding the dye.

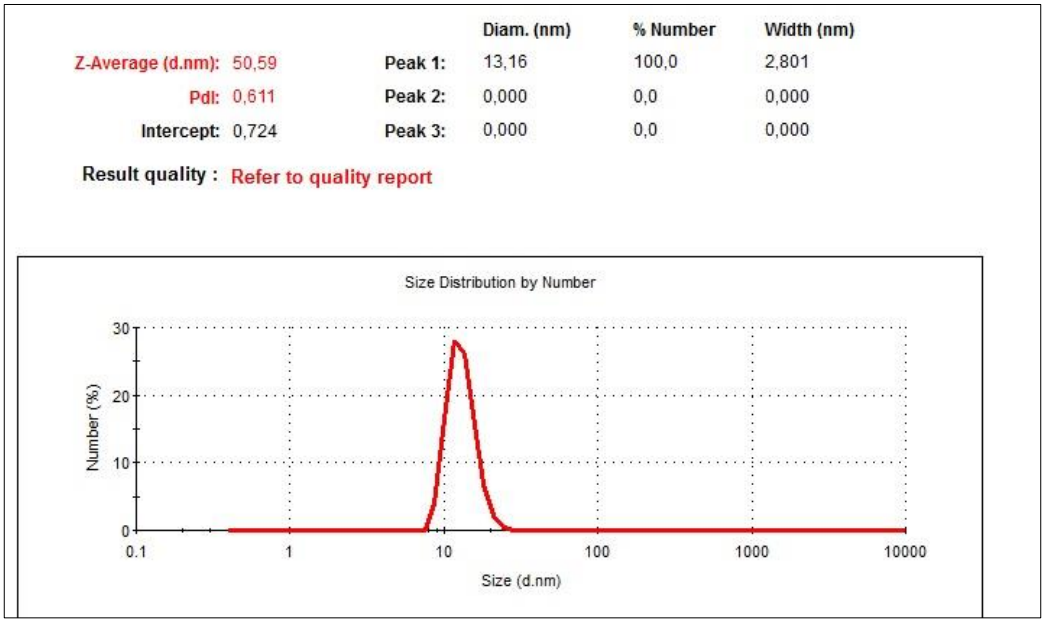

Figure 69 : Size distribution of compound micellar compound **4** (Second Target Compound). Cremophor EL was used for embedding the dye.

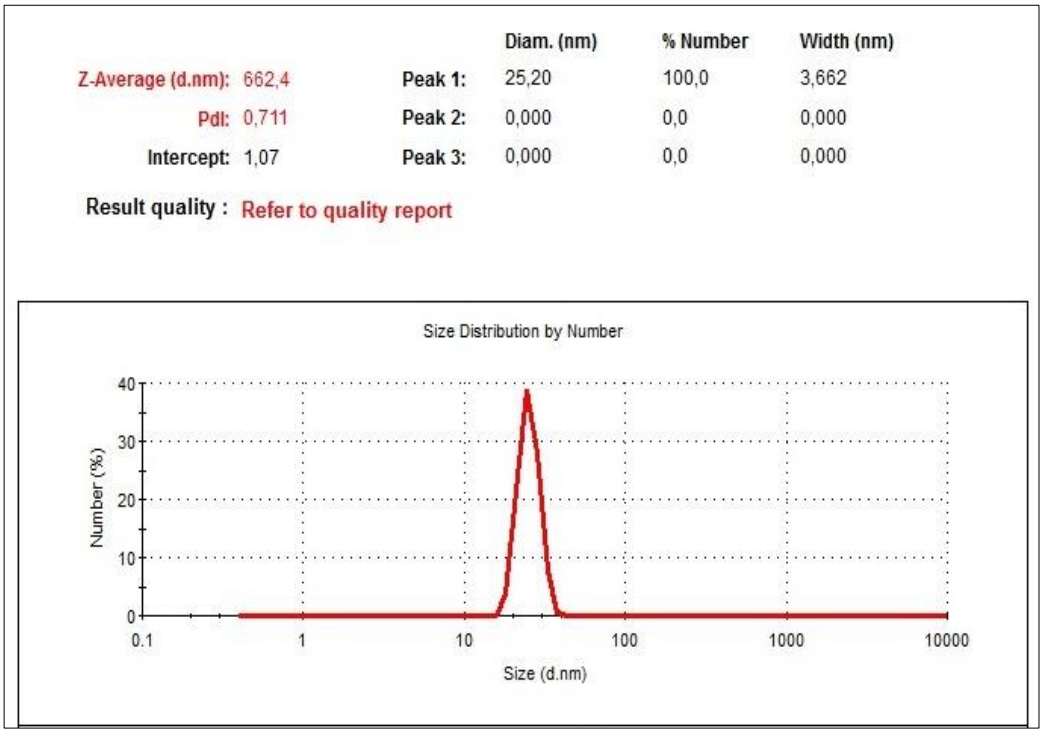

Figure 70 : Size distribution of compound micellar compound **6** (Third Target Compound). Cremophor EL was used for embedding the dye.

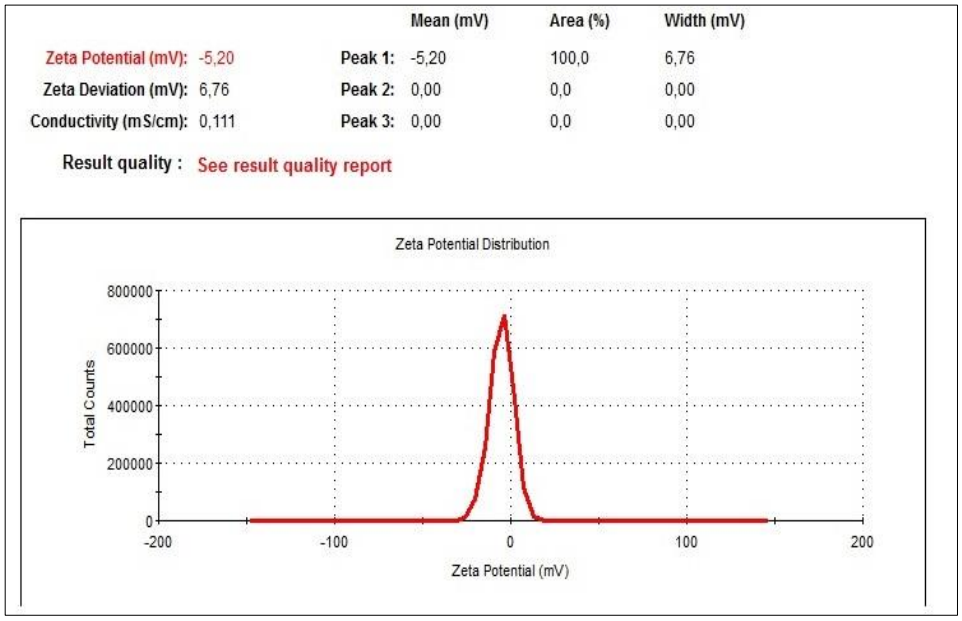

Figure 71 : : Zeta potential measurement of micellar compound **4** . Cremophor EL was used for embedding the dye.

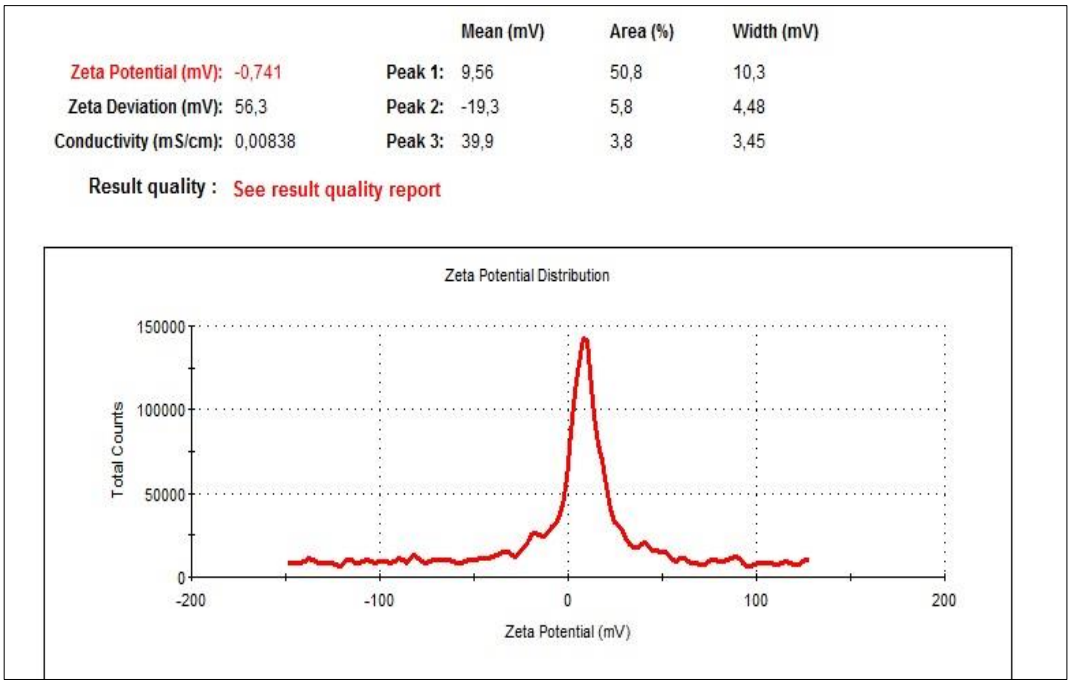

Figure 72: : Zeta potential measurement of micellar compound **3** . Cremophor EL was used for embedding the dye.

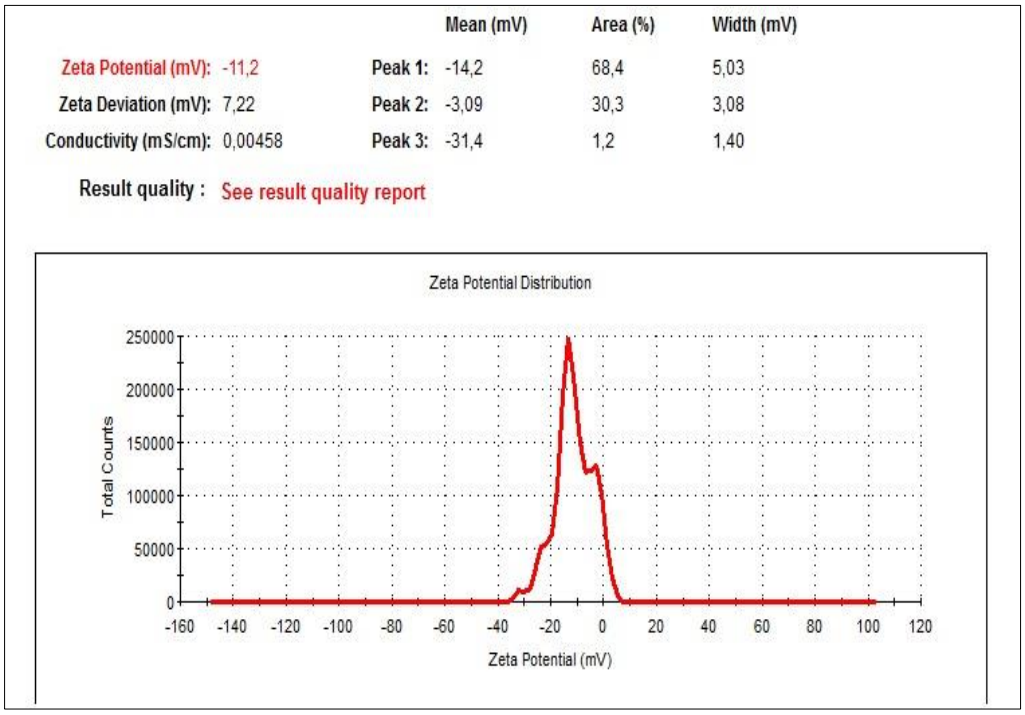

Figure 73 : Zeta potential measurement of micellar compound **6** . Cremophor EL was used for embedding the dye.

Table 3 : Characteristics of micellar compounds **3**, **4** and **6**. Cremophor EL was used for embedding the dye

Compound	**Zeta potential ζ (mV)**	***Size distribution (nm)***	**Polydispersity index (PdI)**
Compound 4	-5.20	13.16	0.611
Compound 3	-1	26.62	0.161
Compound 6	-11.2	25.20	0.711

Singlet oxygen quantum yields were calculated according to the literature.[101] The relative quantum yields were calculated with reference to Methylene Blue (MB)

in water as 0.52 [125,126] Quantum yields for singlet oxygen generation in water were determined by monitoring the photooxidation of trap molecule (2,2'-(Anthracene-9,10-diyl)bis(methylene)dimalonic acid). The absorbance of trap molecule was adjusted around 1.0 in oxygen saturated solution. Then, the photosensitizer (4μM) was added to cuvette and photosentizer's absorbance was adjusted around 0.1-0.2 in order to diminish the possibility of singlet oxygen quenching by the dyes. After, taking some measurements in dark, we exposed the cuvette to monochromatic light (521 nm) at the peak absorption wavelength. Absorbance was measured for several times after each irradiation. The graphics were plotted as the change in optical density (ΔOD) of trap molecule at 382 nm vs irradiation time for each photosensitizer.

The quantum yields of singlet oxygen generation were calculated by using the following equation The quantum yields of singlet oxygen generation were calculated by using the following equation:

$$\Phi(^1O_2)bod = \Phi(^1O_2)MB\ (m_{bod}.\ F_{MB}/\ m_{MB}.\ Fbod)\ (PF_{ref}/\ PF_{bod})$$

where superscripts 'bod' represents the photosensitizers, $\Phi(^1O_2)$ is the quantum yield of singlet oxygen, m is the slope of difference in change in the absorbance of the trap molecule (at 382 nm) with the irradiation time and F is the absorption correction factor, which is given by F=1- 10-OD (OD at the irradiation wavelength). PF is absorbed photonic flux (μEinstein dm^{-3} s^{-1}).

Table 4 : $\Phi(^1O_2)$ values of photosensitizer

Compound	$\Phi(^1O2)$
Compound 4	0.17
Compound 3	0.46
Compound 6	0.14
MB	0.52

Absorbance and emission spectra of the compound 3 were taken on a Varian Cary-100 spectrophotometer. Fluorescence measurements were conducted on a Varian Eclipse spectrofluorometer The absorption λ_{max} of compound **3** is at 529 nm and its emission is at 542 nm (Figure 74 and 75).

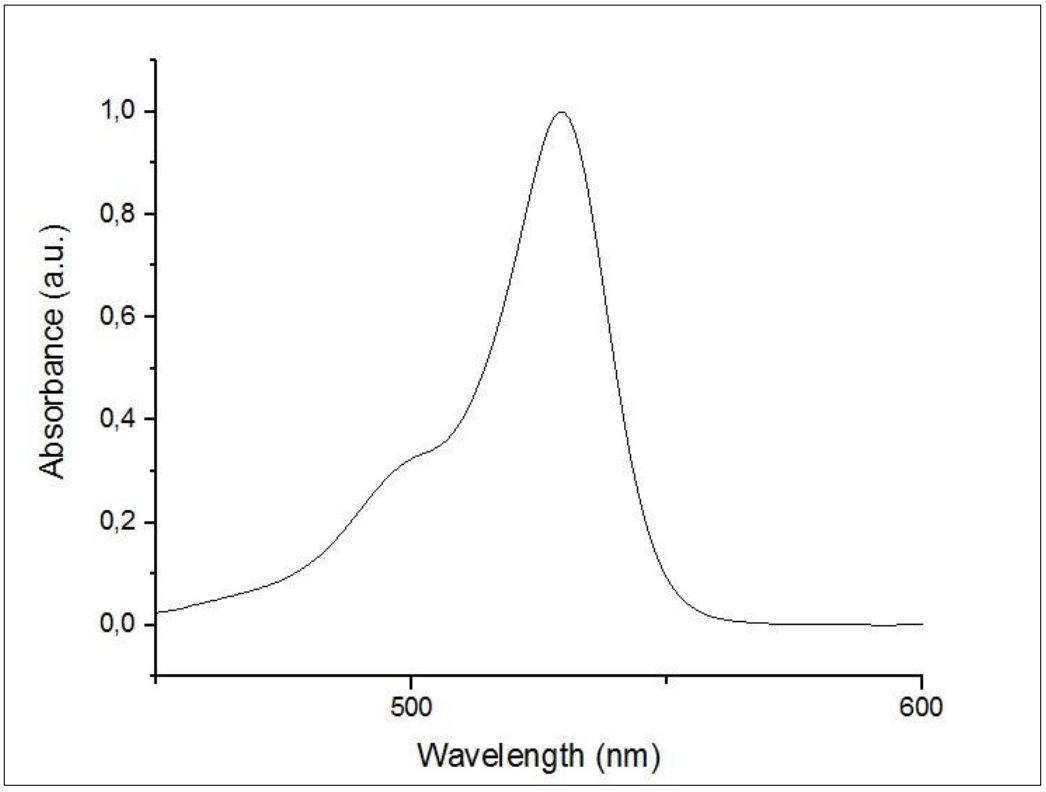

Figure 74 : Normalized absorbance spectrum of compound **3** in CH_2Cl_2

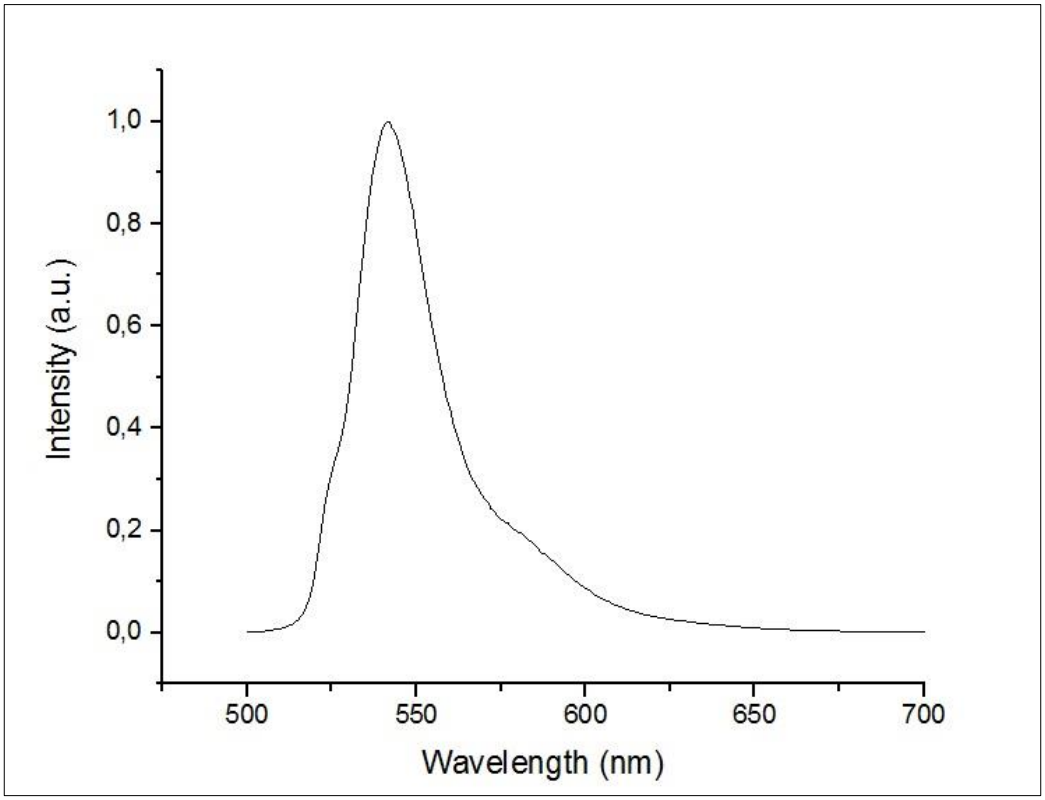

Figure 75 : The normalized fluorescence emission of Compound **3** in CH_2Cl_2

The absorption λ_{max} of compound **4** is at 535 nm and its emission is at 550 nm (Figure 76 and 77).

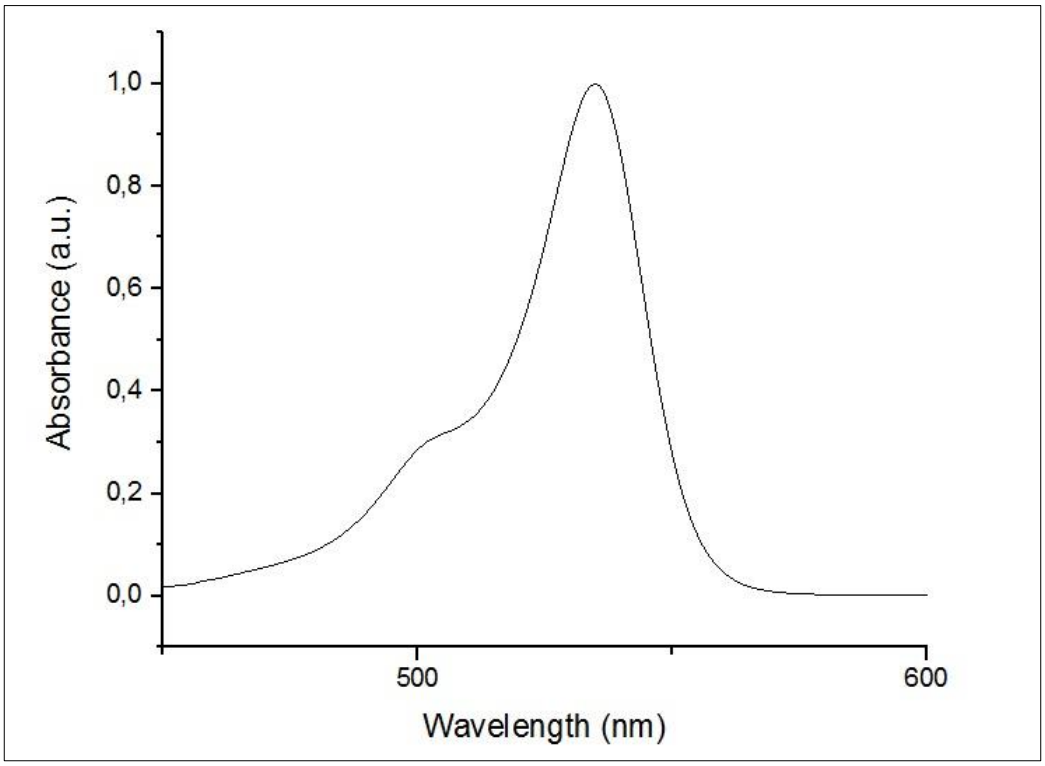

Figure 76 : Normalized absorbance spectrum of compound **4** in CH_2Cl_2

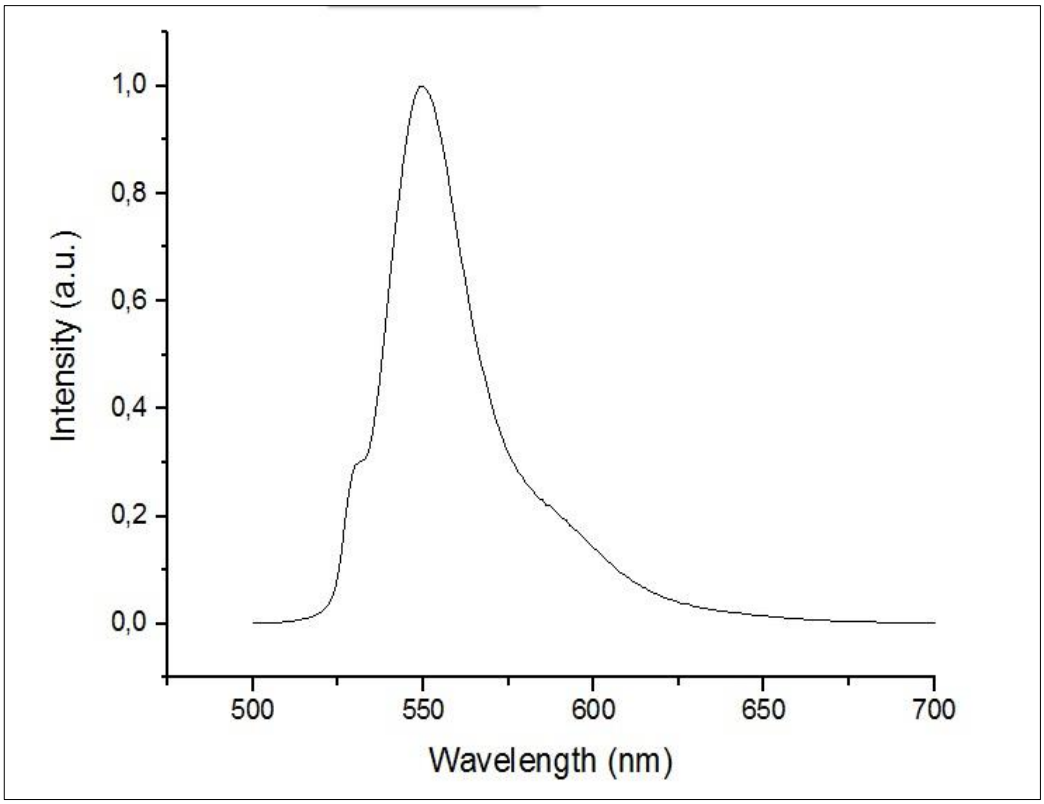

Figure 77 : The normalized fluorescence emission of Compound **4** in CH_2Cl_2

The absorption λ_{max} of compound **6** is at 531 nm and its emission is at 545 nm (Figure 78 and 79).

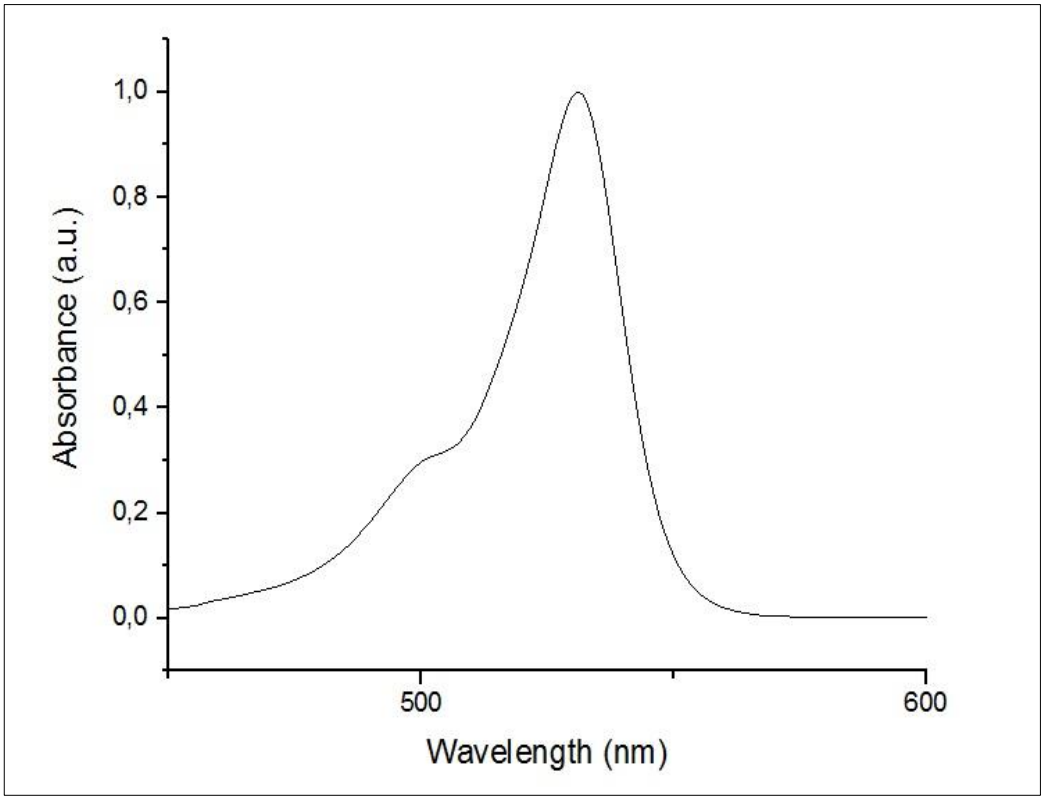

Figure 78 : Normalized absorbance spectrum of compound **4** in CH_2Cl_2

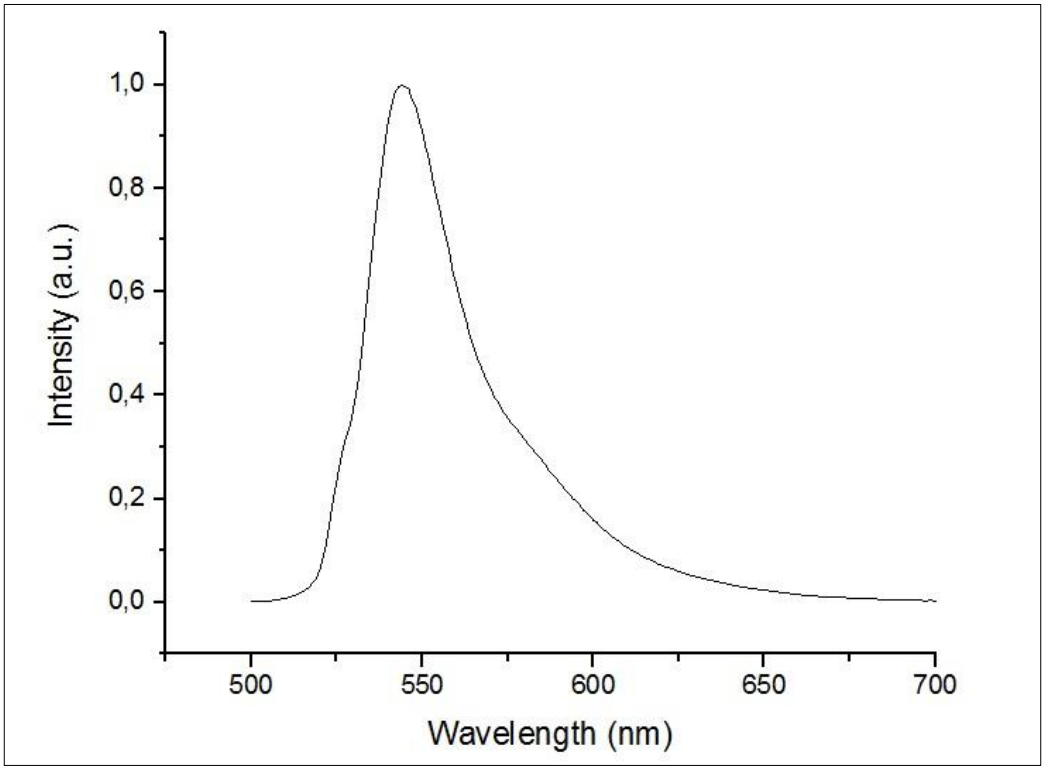

Figure 79 : The normalized fluorescence emission of Compound **4** in CH_2Cl_2

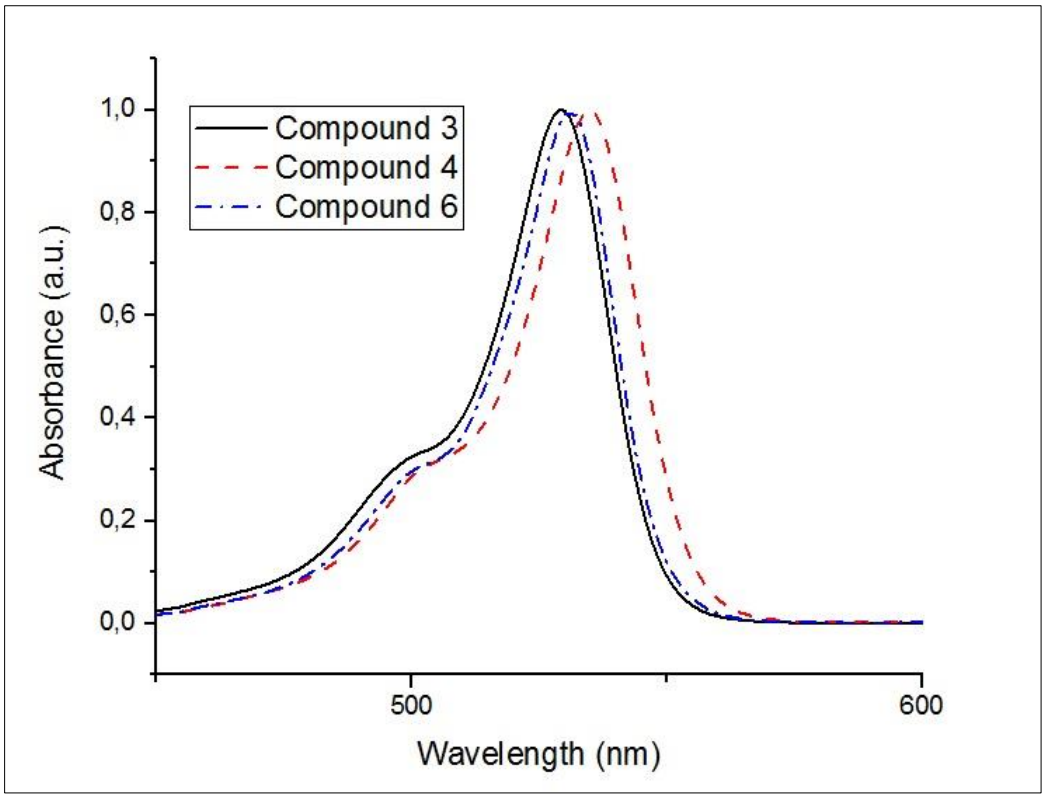

Figure 80 : The normalized absorbance spectra of the compounds **3**, **4**, and **6** in CH_2Cl_2

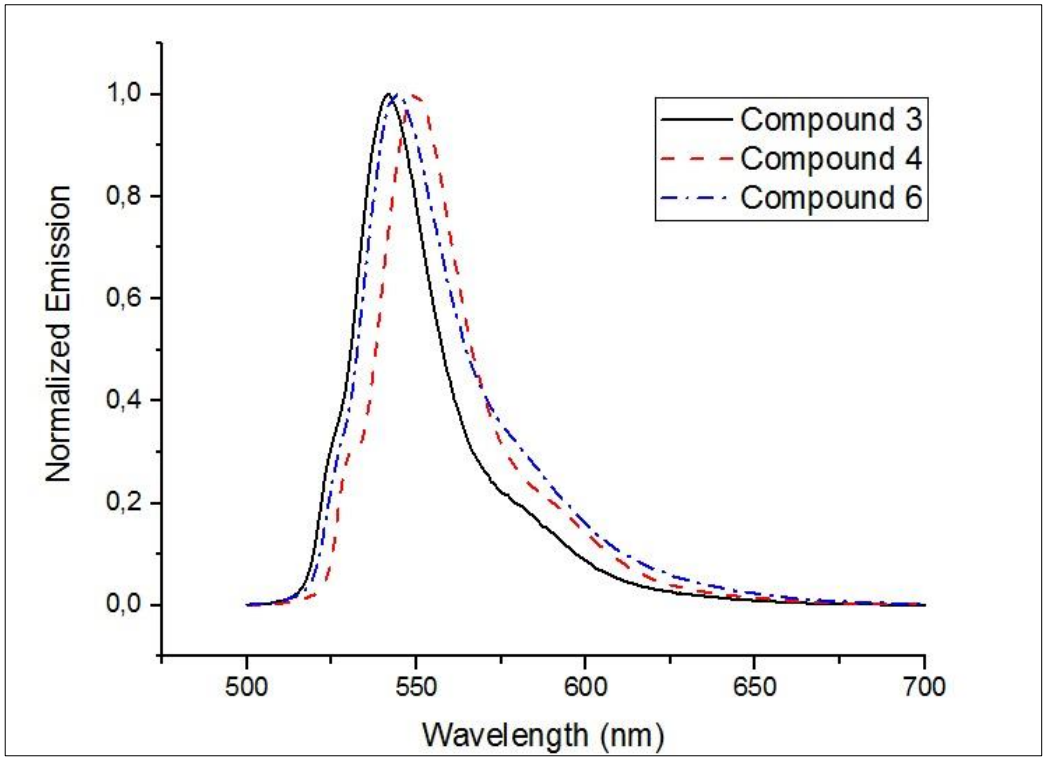

Figure 81 : The normalized fluorescence emission of Compound **3** , **4** and **6** in CH_2Cl_2

Table 5 : Comparative spectroscopic properties of BODIPY compounds

Compound	λ_{abs} [a]/nm	λ_{ems} [a]/nm
Compound 3	529	542
Compound 4	535	550
Compound 6	531	545

According to the results of the singlet oxygen generation experiments, compound **4** is the highly effective singlet oxygen generator. (Figure 82).

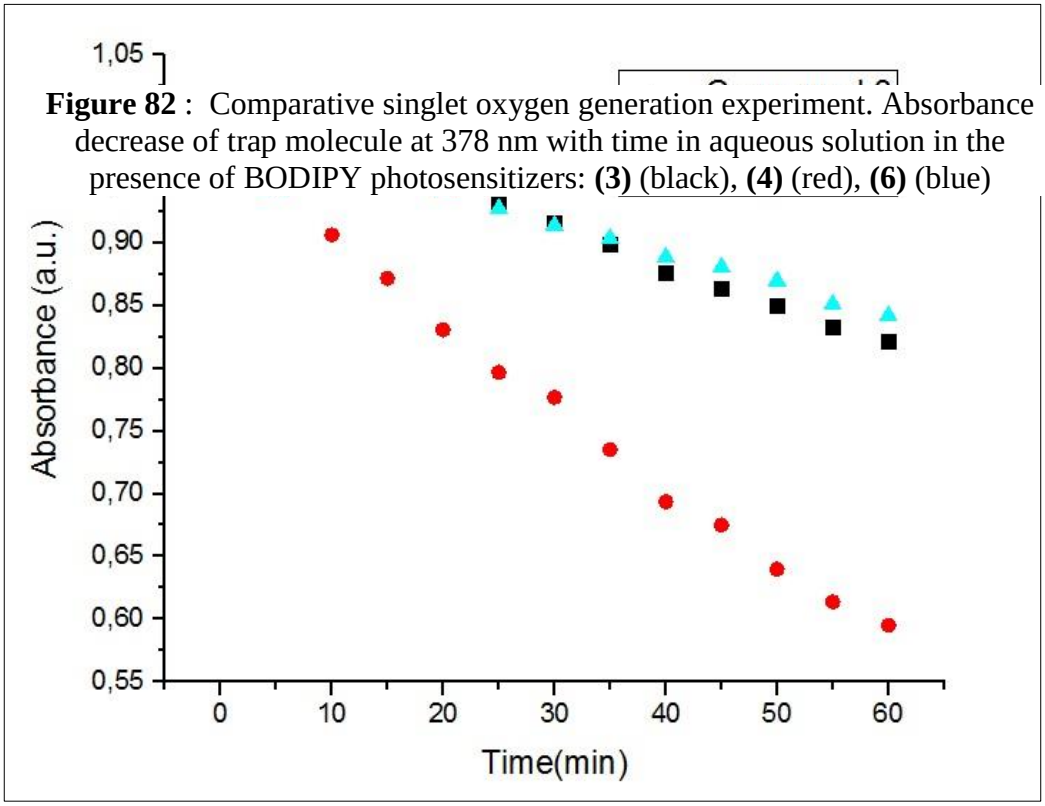

Figure 82 : Comparative singlet oxygen generation experiment. Absorbance decrease of trap molecule at 378 nm with time in aqueous solution in the presence of BODIPY photosensitizers: **(3)** (black), **(4)** (red), **(6)** (blue)

Compound 3 and 6 also demonstrated respectable singlet oxygen generation efficiency (Figure 83 and 84).

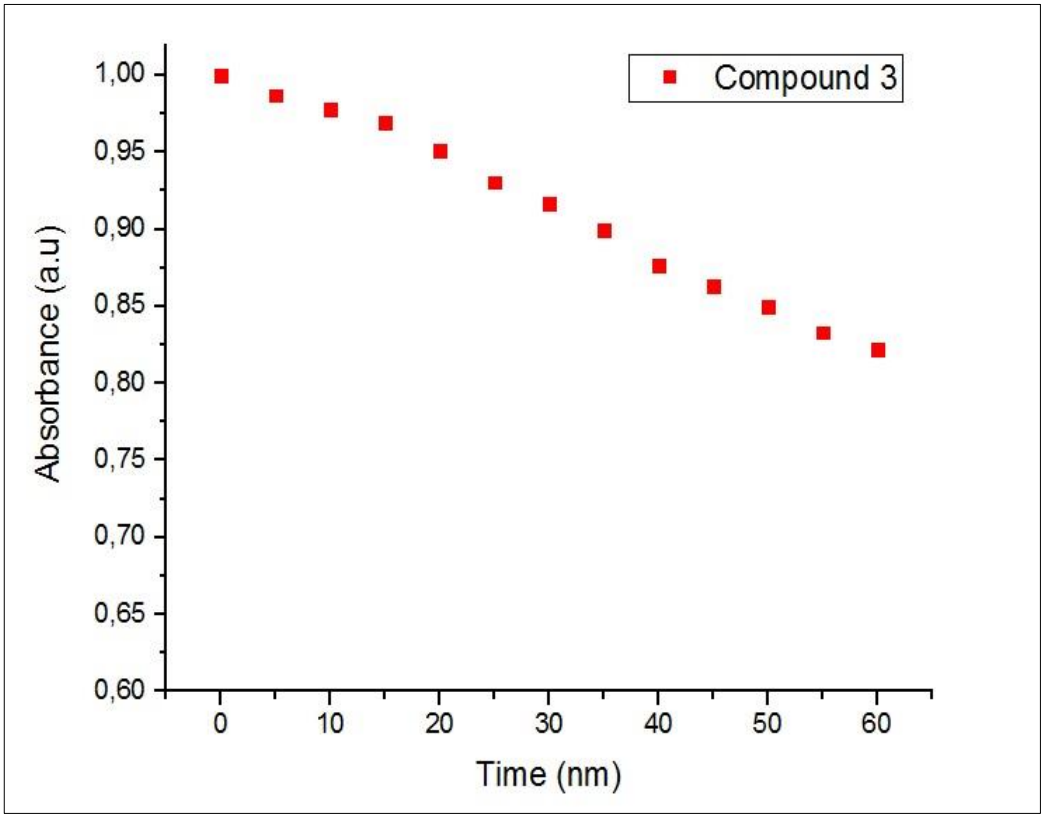

Figure 83 : Absorbance decrease of trap molecule at 378 nm with time in aqueous solution in the presence of Compound **3**

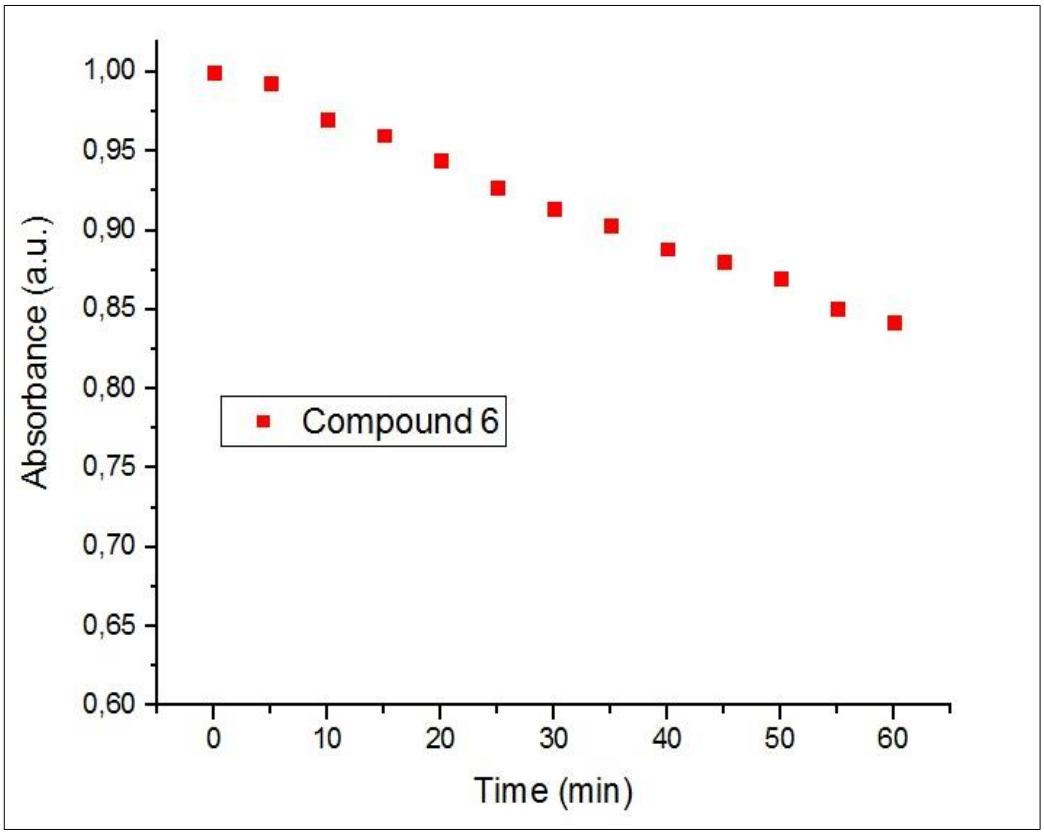

Figure 84: Absorbance decrease of trap molecule at 378 nm with time in aqueous solution in the presence of Compound **6**

5.4 Conclusion

In a nutshell, we have successively synthesized and characterized a series of novel photosensitizing agents that are effective in aqueous media when they are embedded into micelles. They are relatively effective singlet oxygen generator.

We performed singlet oxygen generation experiments in aqueous media by using micelle embedded-BODIPYs. Micelles of the target compounds were prepared according to the procedure in the literature [121].

It is noteworthy that target molecules of this project are effective photodynamic therapy agents in aqueous media according to the results of the singlet oxygen generation experiments

Our aim was to obtain photosensitizers that are biocompatible and effective in aqueous media. For this reason, we introduced long alkyl chains to the meso-position of the BODIPY cores in order to enhance stability of the micelles. In this particular work, we demonstrated that use of long alkyl chains to the meso position of the BODIPY cores enhanced stability of the micelles and they are relatively effective singlet oxygen generator. Excitation of the target compounds were performed outside the therapeutic window of the electromagnetic spectrum. However, this issue can be addressed by extending the conjugation of the dyes and obtain near-IR absorbing derivatives or by using secondary excitation sources which are persistence nanoparticles and upconverting materials.

5.5. Experimental Procedures

General: ^{1}H NMR and ^{13}C NMR spectra were recorded on Bruker DPX-400 (operating at 400 MHz for 1H NMR and 100 MHz for 13C NMR) in $CDCl_3$ with tetramethylsilane as internal standard. All spectra were recorded at 25^0C and coupling constants (J values) are given in Hz. Chemical shifts are given in parts per million (ppm). Absorption spectra were performed by using a Varian Cary-100 spectrophotometer. Fluorescence measurements were conducted on a Varian Eclipse spectrofluorometer. Mass spectra were recorded on Agilent Technologies 6530 Accurate-Mass Q-TOF LC/MS. Reactions were monitored by thin layer chromatography using Merck TLC Silica gel 60 F254. Silica gel column chromatography was performed over Merck Silica gel 60 (particle size: 0.040-0.063 mm, 230-400 mesh ASTM). All other reagents and solvents were purchased from Aldrich and used without further purification. Micelles of the target compounds have been prepared according to the literature[121].

Synthesis of compound 1

4-Hydroxybenzaldeyhde (2g, 16.4 mmol) and 1-bromodecane (5.2 ml, 32.8 mmol) were dissolved (150 ml) in acetonitrile. K_2CO_3 (6.88g, 49.2 mmol) and a few crystals of 18-crown-6 were added. The reaction mixture was refluxed for 48 h. The acetonitrile was evaporated in vacuum and extracted with water and chloroform. Organic phase was dried over Na_2SO_4. After the evaporation of the solvent, silica gel column chromatography using $CHCl_3$/ Hexane (5:1, v/v) as the eluent was performed in order to purify the residue (2.4 g, 51%).

^{1}H NMR (400 MHz, $CDCl_3$, 300K): δ_H = 9.80 (s, 1H), 7.79 (d, *J*= 8.8 Hz ,2H), 6.91 (d, *J*= 8.7 Hz, 2H), 4.05(-t, *J*= 6.4 Hz, 2H), 1.80 (q, 2H), 1.35(m,14H), 0.89(3H) .

^{13}C NMR (100 MHz, $CDCl_3$) δ 190.6, 164.2, 131.8, 129.7, 114.7, 68.3, 31.8, 29.5 ,29.3, 29.3, 29.0, 25.9, 22.6, 14.0

HRMS (ESI) calcd for $C_{17}H_{26}O$ (M+H) 263.2033, found 263.2019 Δ = 5.16 ppm.

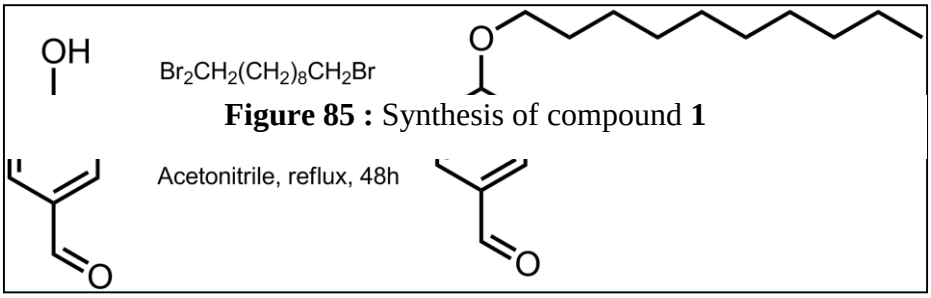

Figure 85 : Synthesis of compound **1**

Synthesis of compound 2

2,4-dimethyl pyrrole (5.033 mmol, 408.2 mg) and 4-decyloxybenzaldeyde (2.288 mmol, 300 mg) were dissolved in a 500 mL round-bottomed flask containing 350 mL argon-degassed CH_2Cl_2. To the reaction solution TFA (one drop) was added and stirred at r.t. for 24h.

After that, a solution of DDQ (2.29 mmol, 519.4 mg) in 100 mL CH_2Cl_2 was added to the reaction mixture. After addition of a DDQ solution, the reaction solution was stirred for additional 1 h. Then, 3 mL NEt_3 and 3 mL $BF_3.OEt_2$ were added respectively. TLC was used to monitor the reaction. (eluent $CHCl_3$)

The reaction mixture was additionally stirred for 30 min. Thereafter, the resulting solution was washed three times with water and dried over anhydrous Na_2SO_4. After the evaporation of the solvent, silica gel column chromatography using $CHCl_3$ as the eluent was performed in order to purify the residue (0.5 g, 46 %).

^{1}H NMR (400 MHz, $CDCl_3$, 300K): δ_H = 7.16 (d, J=8.68 Hz, 2H), 7.02 (d, J=8.68 Hz, 2H) 5.99 (s, 2H), 4.02 (t, J=6.58 Hz, 2H), 3.01 (s, 6H) , 1.84 (m,2H), 1.45 (s, 6H), 1.32(m, 14H) , 0.91 (t , J=6.80 Hz, 3H)

^{13}C NMR (100 MHz, $CDCl_3$): δ_C = 159.7, 155.1, 143.2, 142.0, 131.9, 129.1, 126.8, 121.1, 115.1, 68.2, 32.0, 29.6, 29.6, 29.5, 29.3, 29.3, 26.1, 22.7, 14.6, 14.5, 14.1

HRMS (ESI) calcd for $C_{29}H_{39}BF_2N_2O$ (M+H) 478.30371, found 478.30871 Δ = 1.05 ppm.

Figure 86 : Synthesis of compound **2**

Synthesis of compound 3

Compound **2** (0.23 mmol, 75 mg)) was dissolved in a mixture of DMF/DCM (25 ml/25ml). Then N-bromo succinimide (370 mg, 2.05 mmol) was dissolved in DCM (25ml). NBS in DCM solution was added to the reaction solution dropwise in 15 min. The reaction mixture was stirred at room temperature for 2 hours. Followed by thin layer chromatography the reaction was stopped and the extraction was done with water and DCM. The organic phase was dried with Na_2SO_4 and evaporated by using rotary evaporator. Silica gel column chromatography was carried out to purify the residue by using $CHCl_3$/ Hexane mixture (3:1 v/v) (165 mg, 94.66%).

^{1}H NMR (400 MHz, $CDCl_3$, 300 K): δ_H = 7.15 (d , *J*=8.72 Hz, 2H), 7.03 (d, J=8.72 Hz, 2H), 4.04 (t, J=6.60 Hz, 2H), 2.62 (s, 6H) , 1.85 (m,2H), 1.53(m, 2H), 1.45 (s, 6H), 1.32 (m, 12H) , 0.91 (t, J=6.80 Hz, 3H)

^{13}C NMR (100 MHz, $CDCl_3$): δ_C = 160.2, 153.7, 142.5, 140.7, 130.8, 129.0, 126.1, 115.4, 111.6, 68.3, 31.9, 29.6, 29.6, 29.4, 29.3, 29.2, 26.1, 22.69, 14.12, 13.9, 13.6

HRMS (ESI) calcd for $C_{29}H_{37}BBr_2F_2N_2O$ (M-H) 635.1244, found 635.12963 Δ = 8.23 ppm.

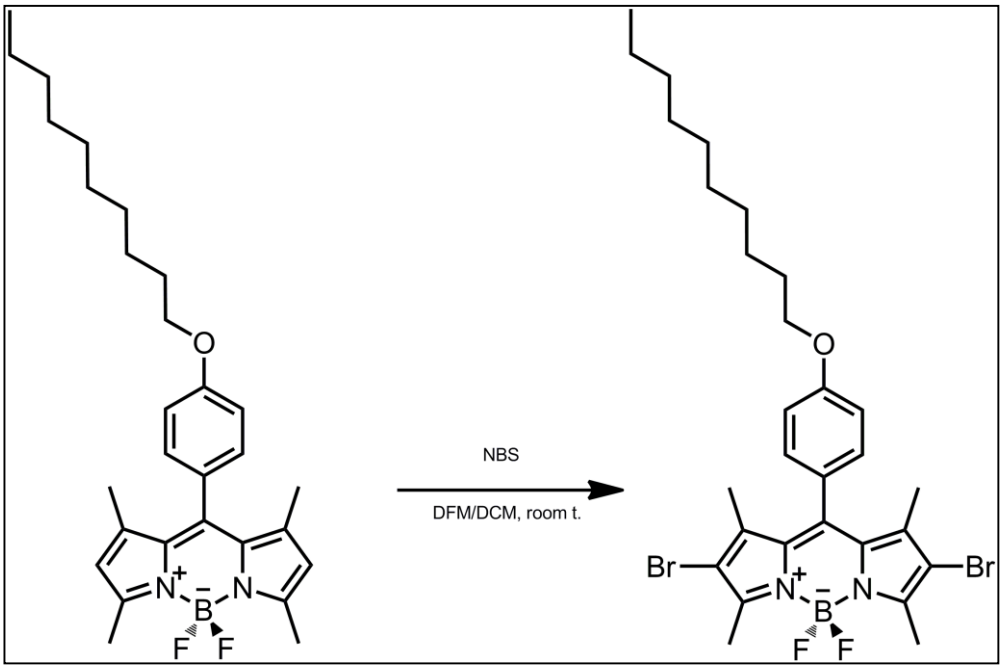

Figure 87 : Synthesis of compound **3**

Synthesis of compound 4

Compound **3** (0.189 mmol, 90 mg) and Iodine (0.78 mmol, 200 mg) were added to a 250 mL round bottomed flask and to this solution was added Iodic acid (0.63 mmol, 111.18 mg) dissolved in 2 mL of water. The reaction mixture was stirred at 60 ^{o}C and was monitored by TLC 1:1 $CHCl_3$: Hexanes. When all the starting material had been consumed, saturated $Na_2S_2O_3$ solution in water was added and the product was extracted into $CHCl_3$. The solvent was evaporated and the residue was purified by silica gel column chromatography using 1:1 $CHCl_3$: Hexanes as the eluant. Red solid (80 mg, 70%).

^{1}H NMR (400 MHz, $CDCl_3$, 300K): δ_H = 7.14 (d, J=8.48 Hz, 2H), 7.05 (d, J=8.48 Hz, 2H), 4.04 (t, J=6.50 Hz, 2H), 2.66 (s, 6H) , 1.84 (m,2H), 1.52(s, 6H), 1.47(m,2H), 1.32(m, 12H) , 0.91 (t, J=6.66 Hz, 3H)

^{13}C NMR (100 MHz, $CDCl_3$): δ_C = 160.2, 156.5, 145.4, 141.8, 129.0, 126.4, 115.4, 85.6, 68.3, 31.1, 29.6, 29.5, 29.4, 29.3, 26.1, 22.7, 17.2, 16.04, 14.20

HRMS (ESI) calcd for $C_{29}H_{37}BF_2I_2N_2O$ (M-H) 730.10199, found 730.10249

Δ = 0.68 ppm

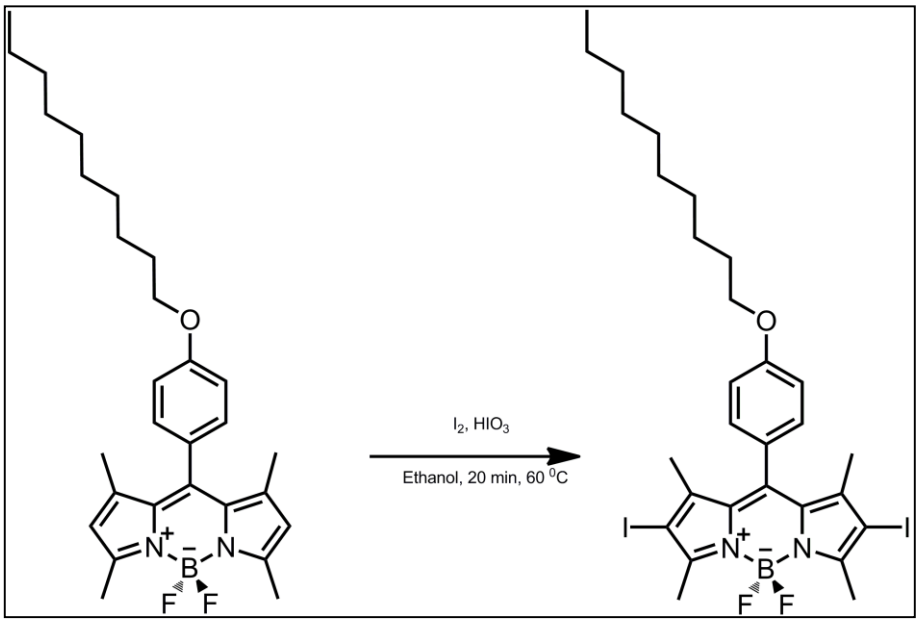

Figure 88 : Synthesis of compound **4**

Synthesis of compound 5

2,4-dimethyl pyrrole (10.34 mmol, 1 g) and palmitoylchrolide (5.17 mmol, 1.44 g) were added into a round bottom flask (500 ml) containing 300 ml CH_2Cl_2. The solution was refluxed for 1 day at 80 ^{0}C. Then, 5mL of Et_3N and 5 mL of $BF_3.OEt_2$ were successively added and after 30 minutes, the reaction mixture was washed three times with water (3x 75 mL). It was then extracted into the CH_2Cl_2 (3x 75mL) and dried over anhydrous Na_2SO_4. The solvent was evaporated and the residue was purified by silica gel column chromatography using (2 DCM: 1 Hexane) as the eluent. Orange solid (1.45 g, 59%).

^{1}H NMR (400 MHz, $CDCl_3$, 300 K): δ_H = 7.69-7.61 (m, 6H), 7.41 (d, J= 16.0 Hz, 2H), 7.28 (d, J= 21.3 Hz, 2H), 7.03 (d, 4.8 Hz, 2H), 6.95 (d, 8.7 Hz, 4H), 3.92 (d, 5.6 Hz, 4H), 1.82-1.73 (m, 2H), 1.60-1.27 (m, 16H), 1.00-0.88 (m , 12H)

^{13}C NMR (100 MHz, $CDCl_3$): δ_C = 161.1, 157.0, 139.0, 133.4, 129.6, 128.8, 128.4, 128.3, 117.9, 116.7, 115.0, 70.7, 39.3, 30.5, 29.1, 23.8, 23.0, 14.0, 11.1

HRMS (ESI) calcd for $C_{28}H_{45}BF_2N_2$ (M-H) 456.37, found 456.35712

Δ =6.3 ppm.

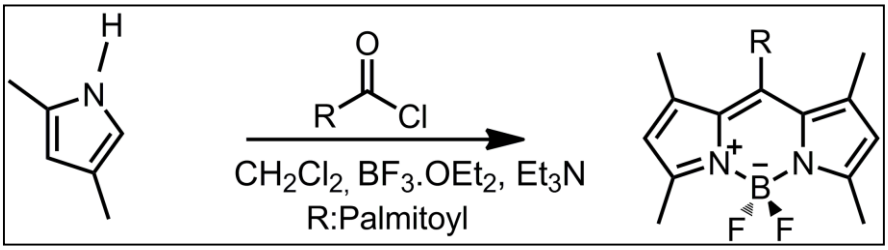

Figure 89 : Syntesis of compound **5**

Synthesis of compound 6

Compound **5** (0.80 mmol, 400 mg) and Iodine (1.78 mmol, 500 mg) were added to a 250 mL round bottomed flask and to this solution was added Iodic acid (2.27 mmol, 400 mg) dissolved in 3 mL of water. The reaction mixture was stirred at 60 ^{o}C and was monitored by TLC 1:1 $CHCl_3$: Hexanes. When all the starting material had been consumed, saturated $Na_2S_2O_3$ solution in water was added and the product was extracted into $CHCl_3$. The solvent was evaporated and the residue was purified by silica gel column chromatography using 1:1 $CHCl_3$: Hexanes as the eluant. Red solid (500 mg, 80%).

^{1}H NMR (400 MHz, $CDCl_3$, 300 K): δ_H = 3.01 (t, J=8.40 Hz, 2H), 2.63 (s, 6H), 2.49 (s, 6H) , 1.63 (m,2H), 1.52(m, 2H), 1.29(m, 22H) , 0.91 (t, J=6.82 Hz, 3H)

^{13}C NMR (100 MHz, $CDCl_3$): δ_C = 155.2, 146.4, 142.2, 131.4, 86.3, 31.9, 31.70, 30.3, 29.7, 29.66, 3.6, 29.6, 29.5, 29.4, 29.4, 29.3, 22.7, 18.9, 16.10, 14.12

HRMS (ESI) calcd for $C_{28}H_{43}BF2I_2N_2$ (M-H) 709.16, found 709.16034 Δ = 0.56 ppm

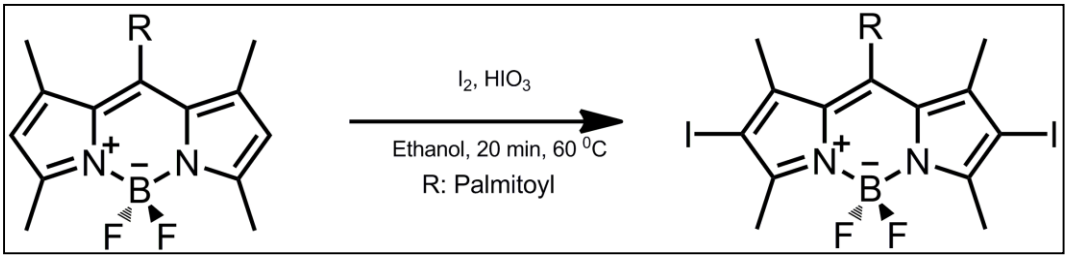

Figure 90 : Synthesis of compound **6**

CHAPTER 6

CONCLUSION

This thesis includes three main projects that have common aim which is to make a further progress in the development of photodynamic therapy. The efficacy of the photosensitizers is of paramount importance in terms of outcomes of the photodynamic therapy action. Many efforts have been devoted to develop more effective photosensitizers over the past few decades. However, they have several drawbacks, including low absorbance, skin photosensitivity, low extinction coefficients, low singlet oxygen quantum yields, high toxicity in the absence of light and low stability under illumination.

In chapter 3, with this consideration in mind, we reported herein the synthesis and characterization of the novel series of BODIPY dyes. Photophysical properties of the target molecules were also reported. An attempt was made to tune the absorption wavelength of the meso-CF_3 substituted BODIPYs to the near-IR range of the electromagnetic spectrum by performing knoevenagel condensation reaction with two different benzaldehyde derivatives. Introduction of the benzaldehyde groups to the 3 and 5-position of the BODIPY core gave rise to the spectacular red shift. Our target compounds have absorption maximum in the near-IR region of the electromagnetic spectrum. The absorption λ_{max} of compound 4 (Target molecule 1), compound 5 (Target molecule 2), compound 6 (Target molecule 3), compound 7 (target molecule 4) are at 890 nm, 886 nm, 759nm and 760 nm respectively. As mentioned before, deep tissue penetration is highly desirable in the photodynamic therapy application. By using these synthesized novel BODIPY based photosensitizers that have absorption maxima exactly in the therapeutic window, deep tissue penetration can be achieved and one of the most widely encountered side effect of the photo dynamic therapy can be overcome. Singlet oxygen generation experiments showed that these BODIPY-based

photosensitizers are effective and promising singlet oxygen generators even at low level of concentrations.

In chapter 4, we introduced the new concept and derivatives of the BODIPY dyes with the aim of overcoming the dark toxicity of the photosensitizers. It was done by handling the excited state of the BODIPY dye, resulting in generation of the putative cytotoxic singlet oxygen. A series of orthogonal BODIPY derivatives were synthesized and characterized. According to the computational studies of these orthogonal BODIPY derivatives, a new excited state configuration was defined for these derivatives. It was named as doubly substituted tetra radical state (DS-TR). This newly defined excited state of the orthogonal BODIPYs gives rise to the intersystem crossing. Namely, this property confers BODIPYs to generate cytotoxic singlet oxygen without incorporation of any heavy atoms to their core. Singlet oxygen generation of these BODIPY derivatives was proved by performing singlet oxygen trap experiments, cell culture studies and singlet oxygen phosphorescence experiments.

In chapter 5, we have reported examples of BODIPY based photosensitizing agent, containing micelle embedding side-chains. It was shown that in aqueous solutions, stable micelles of such compounds can be prepared which can act as effective photosensitizers. We are confident that similarly functionalized Bodipy dyes will find practical applications within the context of photodynamic therapy.

In conclusion, in this thesis, I attempted to combine organic synthesis with photochemistry, biochemistry and oncology in order to make a further progress in the photodynamic milieu and development of novel and effective photosensitizers.

BIBLIOGRAPHY

(1) Dolmans, D. E. J. G. J.; Fukumura, D.; Jain, R. K. Photodynamic therapy for cancer. *Nat. Rev. Cancer* **2003**, *3*, 380-387.

(2) Gomer C, Rucker N, Ferrario A, Wong S. Properties and applications of photodynamic therapy. Rad Res **1989**, *120*, 1

(3) Turan, I.S. , Cakmak, F.P., Yildirim, D.C., Cetin-Atalay, R., Akkaya,E.U, Near-IR absorbing BODIPY derivatives as Glutathione-Activated Photosensitizers for selective photodynamic action, Chem. Eur. J. **2014**, *20*, 16088-16092

(4) Lovell, J. F.; Liu, T. W. B.; Chen, J.; Zheng, G. Activatable Photosensitizers for Imaging and Therapy. *Chem. Rev.* **2010**, *110*, 2839-285

(5) Richards-Kortumr,R. amd Muraca, S. Quantitative optical spectroscopy for tisse diagnosis. E. *Annu. Re*V. *Phys. Chem* **1996**, *47*, 555-606

(6) Daniell M D and Hill J S A history of photodynamic therapy Aust. NZ J Surg **1991**,61, 340-348

(7) O. Raab , Z. Biol. **1900**, **39**,524-546

(8) Spikes, J. D. in primary photoprocesses in Biology and Medicine **1985** newyork

(9) Prime.J Les accidents toxiques par l"eosinate de sodium (Jouve and Boyer Paris 1900

(10) Finsen, N. R.: *Phototherapy*; Edward Arnold: London, **1901**.

(11) von Tappeiner, H.; Jodlbauer, A.: Die sensiblilisierende Wirkung fluoreszierender Substanzer Gesammte Untersuchungen uber die photodynamische Erscheinerung; Voger, F. C.: Leipzig, **1907**

(12) Hausmann, W. Die sensiblisierende Wirkung des Hematoporphyrins. *Biochem. Zeitung* **1911**, *30*, 276-316.

(13) Meyer–Betz, F. Untersuchungen uber die biologische photodynamische Wirkung des Hematoporphyrins und anderer Derivative des Blut und Galenafarbstoffs. *Dtsch. Arch. Klin.* **1913**, *112*, 476-503

(14) Szeimies RM, Draeger J, Abels C, Landthaler M. History of photodynamic therapy in dermatology. Photodynamic therapy and fluorescence diagnosis in dermatology. Amsterdam: Elsevier**, 2001**; 3–16.

(15) Schwartz, S. K., Abolon, K. & Vermund, H. Some relationships of porphyrins, X-rays and tumors. *Univ. Minn. Med. Bull.* **1955**,27, 7–8

(16) Lipson, R. L., Baldes, E. J. & Olsen, A. M. Hematoporphyrin derivative: a new aid for endoscopic detection of malignant disease. *J. Thorac. Cardiovasc. Surg.* **1961**,*42*, 623–629

(17) Lipson, R. L. & Baldes, E. J. The photodynamic properties of a particular hematoporphyrin derivative. *Arch. Dermatol.* **1960**,82, 508–516

(18) Diamond, I. Photodynamic therapy of malignant tumours. *Lancet* **1972**, *2*, 1175-1177

(19) Kelly, J. F., Snell, M. E. & Berenbaum, M. C. Photodynamic destruction of human bladder carcinoma. *Br. J. Cancer* **1975**,*31*, 237–244

(20) Dougherty, T. J. Photoradiation therapy for the treatment of malignant tumors. *Cancer Res.* **1978**, *38*, 2628-2635.

(21) Hayata, Y.; Kato, H.; Konaka, C.; Ono, J.; Takizawa, N. Hematoporphyrin derivative and laser photoradiation in the treatment of lung cancer. *Chest*. **1982**, *81*, 269–277

(22) McCaughan, J. S. Jr, Hicks, W., Laufman, L., May, E. & Roach, R. Palliation of esophageal malignancy with photoradiation therapy. *Cancer* **1984**,*54*, 2905–2910

(23) Hayata, Y., Kato, H., Okitsu, H., Kawaguchi, M. & Konaka, C. Photodynamic therapy with hematoporphyrin derivative in cancer of the upper gastrointestinal tract. *Semin. Surg. Oncol.* **1985**,1, 1–11

(24) Bown, S. G. *et al.* Photodynamic therapy for cancer of the pancreas. *Gut* **2002**,*50*, 549–557.

(25) Pass, H. I. *et al.* Intrapleural photodynamic therapy: results of a phase I trial. *Ann. Surg. Oncol.* **1994**, 1, 28–37

(26) Allison, R. R., Mang, T. S. & Wilson, B. D. Photodynamic therapy for the treatment of nonmelanomatous cutaneous malignancies. *Semin. Cutan. Med. Surg.* **1998**, 17, 153–163

(27) Schweitzer, V. G. Photodynamic therapy for treatment of head and neck cancer. *Otolaryngol. Head Neck Surg.* **1990**,102, 225–232

(28) Popovic, E. A., Kaye, A. H. & Hill, J. S. Photodynamic therapy of brain tumors. *J. Clin. Laser Med. Surg.* **1996**, 14,251–261

(29) Daniell, M. D.; Hill, J. S. A History of Photodynamic Therapy. *Aust. Nz. J. Surg.* **1991**, *61*, 340-348

(30) Star, W. M. *et al.* Destruction of rat mammary tumor and normal tissue microcirculation by hematoporphyrin derivative photoradiation observed *in vivo* in sandwich observation chambers. *Cancer Res.***1986** *46*, 2532–2540.

(31) Henderson, B. W. & Fingar, V. H. Relationship of tumor hypoxia and response to photodynamic treatment in an experimental mouse tumor. *Cancer Res.***1987** 47, 3110–3114

(32) Daniell, M. D.; Hill, J. S. A History of Photodynamic Therapy. *Aust. Nz. J. Surg.* **1991**, *61*, 340-348.

(33) M. O. Senge and J. C. Brandt, Photochem. Photobiol., **2011**, *87*, 1240–1296

(34) Josefsen, L. B.; Boyle, R. W. *Met. Based Drugs* **2008**, 276109

(35) Foote CS. Definition of type I and type II photosensitized oxidation. Photochem Photobiol **1991**, *54*, 659.

(36) Bilski P, Motten AG, Bilska M, Chignell CF. The photooxidation of diethylhydroxylamine by rose bengal in micellar and nonmicellar aqueous solutions. Photochem Photobiol **1993**, *58*,11-8

(37) Ma J, Jiang L. Photogeneration of singlet oxygen ($^1O_2$) and free radicals by tetra-brominated hypocrellin B derivative. Free Radic Res **2001**, *35*, 767-767

(38) Gomer, C., J. Razum, N. J. Acute skin response in albino mice following porphyrin photosensitization under oxic and anoxic conditions. *Photochem. Photobiol.* **1984,**40,435–439

(39) Dolmans, D. E. J. G. J.; Fukumura, D.; Jain, R. K. Photodynamic therapy for cancer. *Nat. Rev. Cancer* **2003**, *3*, 380-387

(40) Roberts WG, Smith KM, McCullough JL, Berns MW. Skin photosensitivity and photodestruction of several photodynamic sensitizers. Photochem Photobiol **1989**, 49, 431-439.

(41) Cairnduff, F., Stringer, M.R., Hudson, J.E., Ash, D.V., Brown, S.B., Superficial photodynamic therapy with topical 5-aminolaevulinic acid for superficial primary and secondary skin cancer, Br. J. Cancer, **1994**, *69*, 605-608

(42) Davies M . Singlet oxygen-mediated damage to proteins and its consequences Biochem Biophys Res Commun **2003**, 305,761-770

(43) Pervaiz, S.; Olivo, M. *Clin. Exp. Pharmacol. Physiol.* **2006**, *33*, 551

(44) Wilson, B. C.; Patterson, M. S. *Phys. Med. Biol.* **2008**, *53*, R61

(45) Castano, A. P.; Mroz, P.; Hamblin, M. R. *Nat. Re*V. *Cancer* **2006**, *6*,535

(46) Aina, O. H.; Sroka, T. C.; Chen, M.; Lam, K. S. *Pept. Sci.* **2002**, *66*,184.

(47) DeRosa, M. C.; Crutchley, R. J. *Coord. Chem. Re*V. **2002**, *233-234*, 351

(48) Konig, K., Multiphoton microscopy in life sciences, **2000**,200(2), 83-104

(49) Agostinis, P.; Berg, K.; Cengel, K. A.; Foster, T. H.; Girotti, A. W.; Gollnick, S. O.; Hahn, S. M.; Hamblin, M. R.; Juzeniene, A.; Kessel, D.; Korbelik, M.; Moan, J.; Mroz, P.; Nowis, D.; Piette, J.; Wilson, B. C.; Golab, J. Photodynamic Therapy of Cancer: An Update. *Ca-Cancer J. Clin.* **2011**, *61*, 250-281

(50) He, H.; Lo, P. C.; Ng, D. K. P. A Glutathione-Activated Phthalocyanine-Based Photosensitizer for Photodynamic Therapy. *Chem-Eur. J.* **2014**, *20*, 6241-6245

(51) Wood, T. E.; Thompson, A. Advances in the chemistry of dipyrrins and their complexes. *Chem. Rev.* **2007**, *107*, 1831-1861.

(52) Lim, S. H.; Thivierge, C.; Nowak-Sliwinska, P.; Han, J. Y.; van den Bergh, H.; Wagnieres, G.; Burgess, K.; Lee, H. B. In Vitro and In Vivo Photocytotoxicity of Boron Dipyrromethene Derivatives for Photodynamic Therapy. *J. Med. Chem.* **2010**, *53*, 2865-2874.

(53) Ulrich, G.; Ziessel, R.; Harriman, A. The chemistry of fluorescent bodipy dyes: Versatility unsurpassed. *Angew. Chem. Int. Ed.* **2008**, *47*, 1184-1201.

(54) Kolemen, S.; Bozdemir, O. A.; Cakmak, Y.; Barin, G.; Erten-Ela, S.; Marszalek, M.; Yum, J. H.; Zakeeruddin, S. M.; Nazeeruddin, M. K.; Gratzel, M.; Akkaya, E. U. Optimization of distyryl-Bodipy chromophores for efficient panchromatic sensitization in dye sensitized solar cells. *Chem. Sci.* **2011**, *2*, 949-954

(55) Ehrenschwender, .T.; Wagenknechet, H.A. 4,4-Difluoro-4-bora-3a,4a-diaza-*s*-indacene as a Bright Fluorescent Label for DNA. *J. Org. Chem*. **2011**, *76*,2301-2304

(56) Isik, M.; Ozdemir, T.; Turan, I. S.; Kolemen, S.; Akkaya, E. U. Chromogenic and Fluorogenic Sensing of Biological Thiols in Aqueous Solutions Using BODIPY-Based Reagents. *Org. Lett.* **2013**, *15*, 216-219.

(57) Buyukcakir, O.; Bozdemir, O. A.; Kolemen, S.; Erbas, S.; Akkaya, E. U. Tetrastyryl-Bodipy Dyes: Convenient Synthesis and Characterization of Elusive Near IR Fluorophores. *Org. Lett.* **2009**, *11*, 4644-4647.

(58) Harriman, A.; Izzet, G.; Ziessel, R. Rapid energy transfer in cascade-type bodipy dyes. *J. Am. Chem. Soc.* **2006**, *128*, 10868-10875.

(59) Ziessel, R.; Ulrich, G.; Harriman, A. The chemistry of Bodipy: a new El Dorado for fluorescence tools. *New J. Chem.* **2007**, *31*, 496-501

(60) Kolemen, S.; Cakmak, Y.; Kostereli, Z.; Akkaya, E. U. Atropisomeric Dyes: Axial Chirality in Orthogonal BODIPY Oligomers. *Org. Lett.* **2014**, *16*, 660-663

(61) Zheng,Q.; Xu,G. and Prasad, P.N. Conformationally Restricted Dipyrromethene Boron Difluoride (BODIPY) Dyes: Highly Fluorescent, Multicolored Probes for Cellular Imaging *Chem- Eur J* **2008**, 14,5812-5819

(62) Kamkaew, A.; Lim, S. H.; Lee, H. B.; Kiew, L. V.; Chung, L. Y.; Burgess, K. BODIPY dyes in photodynamic therapy. *Chem. Soc. Rev.* **2013**, *42*, 77-88.

(63) Yogo, T.; Urano, Y.; Ishitsuka, Y.; Maniwa, F.; Nagano, T. Highly efficient and photostable photosensitizer based on BODIPY chromophore. *J. Am. Chem. Soc.* **2005**, *127*, 12162-12163.

(64) Ortiz, M.J.: Agarrabeitia, A.R.; Duran-Sampedro, G.; Prieto ,J.B.; Lopez, T.A.; Massad, W.A.; Montejano, H.A.; Garcia, N.A. and Arbeola, I.L.;

Synthesis and functionalization of new polyhalogenated BODIPY dyes. Study of their photophysical properties and singlet oxygen generation, *Tetrahedron*, **2012**, *68*,1153-1162

(65) Umezawa, K.; Nakamura, Y.; Makino, H.; Citterio, D.; Suzuki, K. Bright, color-tunable fluorescent dyes in the visible-near-infrared region. *J. Am. Chem. Soc.* **2008**, *130*, 1550-1551.

(66) Atilgan, S.; Ekmekci, Z.; Dogan, A. L.; Guc, D.; Akkaya, E. U. Water soluble distyryl-boradiazaindacenes as efficient photosensitizers for photodynamic therapy. *Chem. Commun.* **2006**, 4398-4400

(67) He, H.; Lo,P.-C.; Yeung,S.-L., Fong, W.-P. and Ng, K.P.; Preparation of unsymmetrical distyryl BODIPY derivatives and effects of the styryl substituents on their *in vitro* photodynamic properties. *Chem Commun*. **2011**, 4748-4750

(68) Killoran, J.; Allen, L.; Gallagher, J.F.; Gallagher, W.M. and O'Shea. D.F.; Synthesis of BF2 chelates of tetraarylazadipyrromethenes and evidence for their photodynamic therapeutic behavior. *Chemm Commun.* **2002**, 1862-1863

(69) Gallagher, W.M.; Allen, L.T.; O'Shea, F.; Kenna,T.; Hall, M.; Gorman, A., Killoran, J. and O'Shea, D.F. A potent nonporphyrin class of photodynamic therapeutic agent: cellular localisation, cytotoxic potential and influence of hypoxia. *Br J Cancer.* **2005**, 92, 1702-1710

(70) Kolemen, S.; Işık, M.; Kim, G.M.; Kim, D.;,Geng, H.; Buyuktemiz, M.; Karatas, T., Zhang, X., F.; Dede, Y.; Yoon, J. and Akkaya, E.U. *Angew. Chem. Int. Ed.* **2015,** *54*, 5340-5344

(71) Tian, Y.Y.; Wang, L.L. and Wang, W. Progress in Photodynamic Therapy on Tumors. *Laser Physics.* **2008**, *18*,1119-1123

(72) Brunner, H.; Hausmann, F. and Krieg, R.C. The Effects of 5-Aminolevulinic Acid Esters on Protoporphyrin IX Production in Human Adenocarcinoma Cell Lines *Photochem. Photobiol.* **2001,** *74*,721-725

(73) Sessler, J.L.; Murai, T.; Lynch; V. and Cyr, M. An 'expanded porphyrin': the synthesis and structure of a new aromatic pentadentate ligand. *J. Am. Chem. Soc,* **1988**, *110*, 5586–5588.

(74) Sessler, J.L. and Miller, R.A., Texaphyrins: New drugs with diverse clinical applications in radiation and photodynamic therapy. *Biochemical Pharmacology,* **2000** , *59*, 733-739

(75) Woodburn KW, Fan Q, Kessel D, Luo Y and Young SW, Photodynamic therapy of B16F10 murine melanoma with lutetium texaphyrin. *Invest Dermatol,* **1998,**746–751

(76) Bellnier, D.A. and Dougherty, T.J. A preliminary pharmacokinetic study of intravenous photofrin in patients. *J Clin Laser Med Surg* **1996**,14, 311–314

(77) Maiya BG, Mallouk TE, Hemmi G, Sessler JL. Effects of substituents on the spectral and redox properties of cadmium(II) texaphyrins. Inorganic Chemistry **1990**, *29*, 3738–3745.

(78) Sutton, J.M.; Fernandez, N.; Boyle, R.W. Functionaliazed diphenylchlorins and bacteriochlorins: their synthesis and bioconjugate for targeted photodynamic therapy and tumor cell imaging, *J. Porphyr. Phthalocya*. **2000**, *4* ,655–658

(79) Shan, X.; Wang, T.; Li, S.; Yang, L.; Fu, L. and Yang, G. Photophysical properties of diphenyl-2,3- dihydroxychlorin and diphenylchlorin. *Journal of Photochemistry and Photobiology, B: Biology,* **2006**, *82*,140–145.

(80) Sharonov, G.V.; Karmakova, T.A.; Kassies, R.; Pljutinskaya, A.D.; Grin, M.A.; Refregiers,M.; Yakubovskaya, R.I.; Miranov, F.A.; Maurizot, J. D.; Vigny, P.; Otto, C. and Feafanov, A.V. Cycloimide bacteriochlorin p derivatives: photodynamic properties and cellular and tissue distribution. *Free Radical Biology and Medicine,* **2006** , *40,* 407-419.

(81) Triesscheijn, M.; Baas, P.; Schellens, J.H.M.; Stewart, F.A. Photodynamic Therapy in Oncology, *Radiation Oncology*, **2006,** *11*, 1034-1044

(82) Kato, H. Photodynamic therapy for lung cancers a review of 19 years' experience. J. Photochem. Photobiol., *B.* **1998**, *42*, 96-99

(83) Puolakkainen, P.; Schroder, T. Photodynamic therapy of gastrointestinal tumors: a review. *Dig. Dis.* **1992**, *10*, 53-60

(84) Jichlinski, P.; Leisinger, H.-J. Photodynamic therapy in superficial bladder cancer: Past, present and future. *Urol. Res.* **2001**, *29*, 396-405

(85) Prosst, R. L.; Wolfsen, H. C.; Gahlen, J. Photodynamic therapy for esophageal diseases: a clinical update. *Endoscopy* **2003**, *35*,1059-1068

(86) Dilkes, M. G.; Benjamin, E.; Ovaisi, S.; Banerjee, A. S. Treatment of primary mucosal head and neck squamous cell carcinoma using photodynamic therapy: results after 25 treated cases. *J. Laryngol. Otol.* **2003**, *117*, 713-717

(87) Baas, P.; Saarnak, A.; Oppelaar, H.; Neering, H.; Stewart, F. A. Photodynamic therapy with meta-tetrahydroxyphenylchlorin for basal cell carcinoma: a phase I/II study. *Br. J. Dermatol.* **2001**,*145*, 75-78.

(88) Schweitzer, V. G. Photofrin-mediated photodynamic therapy for treatment of aggressive head and neck nonmelanomatous skin tumors in elderly patients. *Laryngoscope* **2001**, *111*, 1091-1098

(89) Zeitouni, N.; Oseroff, A. R.; Shieh, S. Photodynamic Therapy for nonmelanoma skin cancers. Current review and update. *Mol. Immunol.* **2003**, *39*, 1133-1136.

(90) Pariser, D. M.; Lowe, N. J.; Stewart, D. M.; Jarratt, M. T.; Luck, A. W.; Pariser, R. J.; Yamauchi, P. S. Photodynamic therapy with topical methylaminolevulinate for actinic keratosis: results of a prospective randomized multicenter trial. *J. Am. Acad. Dermatol.* **2003**, *48*, 227-232.

(91) Freeman, M.; Vinciullo, C.; Francis, D.; Spelman, L.; Nguyen, R.; Fergin, P.; Thai, K.-E.; Murrell, D.; Weightman, W.; Anderson, C.; Reid, C.; Watson, A.; Foley, P. A comparison of photodynamic therapy using topical methyl aminolevulinate (Metvix) with single cycle cryotherapy in patients with actinic keratosis: a prospective, randomized study. *J. Dermatol. Treat.* **2003**, *14*, 99-106.

(92) Wong, T.-W.; Aizawa, K.; Sheyhedin, I.; Wushur, C.; Kato, H. Pilot study of topical delivery of mono-L-aspartyl chlorin e6 (NPe6): Implication of topical NPe6-photodynamic therapy. *J. Pharmacol. Sci.* **2003**, *93*, 136-142.

(93) Anderson, G. S.; Miyagi, K.; Sampson, R. W.; Sieber, F. Antitumoreffect of Merocyanine 540-mediated photochemotherapycombined with Edelfosine: potential implications for the ex vivopurging of hematpoietic stem cell grafts from breast cancerpatients. *J. Photochem. Photobiol., B* **2002,** *63*, 101-108.

(94) Brasseur, N.; Menard, I.; Forget, A.; El Jastimi, R.; Hamel, R.;Molfino, N. A.; van Lier, J. E. Eradication of multiple myelomaand breast cancer cells by TH9402-mediated photodynamictherapy: implication for clinical *ex vivo* purging of autologousstem cell transplants. *Photochem. Photobiol.* **2000**, *72*, 780-787

(95) Daziano, J. P.; Humeau, L.; Henry, M.; Mannoni, P.; Chanon,M.; Chabannon, C.; Juillard, M. Preferential photoinactivationof leukemia cells by aluminum phthalocyanine. *J. Photochem.Photobiol., B.* **1998**, *43*, 128-135.

(96) Onu, P.; LaMuraglia, G. M.; Robert, W. G.; Hasan, T. Photodynamic therapy of arteries. A novel approach for treatment of intimal hyperplasia. *Circulation* **1992**, *85*, 1189-1196.

(97) Onu, P.; LaMuraglia, G. M.; Robert, W. G.; Hasan, T. Photodynamic therapy of arteries. A novel approach for treatment of intimal hyperplasia. *Circulation* **1992**, *85*, 1189-1196.

(98) Boris, A.T, et al., General Route to Symmetric and Asymmetric *meso*-CF_3-3(5)-Aryl(hetaryl)- and 3,5-Diaryl(dihetaryl)-BODIPY Dyes, Org. Lett. **2011**, *13*, 2524-2527

(99) Li, L., Nguyen, B., Burgess, K., Functionalization of the 4,4-difluoro-4-bora-3a,4a-diaza-s-indacene (BODIPY) core *Bioorg. Med. Chem. Lett*. **2008**, *18*, 3112-3116

(100) Tang, C., Hu, P., Huang, M., Zheng, Q., Heavy atom enhanced generation of singlet oxygen in novel indenofluorene-based two-photon absorbing chromophores for photodynamic therapy. *Dyes and Pigments* **2015**, 117, 7-15

(101) Y. Cakmak, S. Kolemen, S. Duman, Y. Dede, Y. Dolen, B. Kilic, Z. Kostereli, L. T. Yildirim, A. L. Dogan, D. Guc, E. U. Akkaya, *Angew. Chem*. **2011**, 123, 12143 –12147; *Angew. Chem. Int. Ed*. **2011**, 50, 11937 – 11941

(102) W. Pang, X.-F. Zhang, J. Zhou, C. Yu, E. Hao, L. Jiao, *Chem. Commun*. **2012**, 48, 5437 –5439

(103) Adarsh, N.; Avirah, R. R.; Ramaiah, D. Tuning Photosensitized Singlet Oxygen Generation Efficiency of Novel Aza-BODIPY Dyes. *Org. Lett.* **2010**, *12*, 5720-5723

(104) Salem, L.; Rowland, C. The Electronic Properties of Diradicals. *Angew. Chem. Int. Ed.* **1972**, *11*, 92-111

(105) Michl, J. Spin-orbit coupling in biradicals .1. The 2-electrons-in-2-orbitals model revisited. *J. Am. Chem. Soc.* **1996**, *118*, 3568-3579

(106) Bozdemir, O. A.; Guliyev, R.; Buyukcakir, O.; Selcuk, S.; Kolemen, S.; Gulseren, G.; Nalbantoglu, T.; Boyaci, H.; Akkaya, E. U. Selective Manipulation of ICT and PET Processes in Styryl-Bodipy Derivatives: Applications in Molecular Logic and Fluorescence Sensing of Metal Ions. *J. Am. Chem. Soc.* **2010**, *132*, 8029-8036

(107) Loudet, A.; Burgess, K. BODIPY dyes and their derivatives Syntheses and spectroscopic properties. *Chem. Rev.* **2007**, *107*, 4891-4932

(108) Ozlem, S.; Akkaya, E. U. Thinking Outside the Silicon Box:Molecular AND Logic As an Additional Layer of Selectivity in Singlet Oxygen Generation for Photodynamic Therapy. *J. Am. Chem. Soc.* **2009**, *131*, 48-49

(109) Ventura, B.; Marconi, G.; Broring, M.; Krugerb, R.; Flamigni, L. Bis(BF2)-2,2 '-bidipyrrins, a class of BODIPY dyes with new spectroscopic and photophysical properties. *New J. Chem.* **2009**, *33*, 428-438

(110) Jiao, L. J.; Yu, C. J.; Li, J. L.; Wang, Z. Y.; Wu, M.; Hao, E. H. beta175 Formyl-BODIPYs from the Vilsmeier-Haack Reaction. *J. Org. Chem.* **2009**, *74*, 7525-7528

(111) Krumova, K.; Cosa, G. Bodipy Dyes with Tunable Redox Potentials and Functional Groups for Further Tethering: Preparation, Electrochemical, and Spectroscopic Characterization. *J. Am. Chem. Soc.* **2010**, *132*, 17560-17569

(112) Mirenda, M.; Strassert, C. A.; Dicelio, L. E.; Roman, E. S. Dye-Polyelectrolyte Layer-by-Layer Self-Assembled Materials: Molecular Aggregation, Structural Stability, and Singlet Oxygen Photogeneration. *ACS Appl. Mater. Inter.* **2010**, *2*, 1556-1560.

(113) Duman, S.; Cakmak, Y.; Kolemen, S.; Akkaya, E. U.; Dede, Y. Heavy Atom Free Singlet Oxygen Generation: Doubly Substituted Configurations Dominate S-1 States of Bis-BODIPYs. *J. Org. Chem.* **2012**, *77*, 4516-4527.

(114) Martinez, G. R.; Garcia, F.; Catalani, L. H.; Cadet, J.; Oliveira, M. C. B.; Ronsein, G. E.; Miyarnoto, S.; Medeiros, M. H. G.; Di Mascio, P. Synthesis of a hydrophilic and non-ionic anthracene derivative, the N,N '-di-(2,3-dihydroxypropyl)- 9,10-anthracenedipropanamide as a chemical trap for singlet molecular oxygen detection in biological systems. *Tetrahedron* **2006**, *62*, 10762-10770

(115) Tram, K.; Yan, H. B.; Jenkins, H. A.; Vassiliev, S.; Brucec, D. The synthesis and crystal structure of unsubstituted 4,4-difluoro-4-bora-3a, 4a-diaza-sindacene (BODIPY). *Dyes Pigments* **2009**, *82*, 392-395.

(116) Schmitt, A.; Hinkeldey, B.; Wild, M.; Jung, G. Synthesis of the Core Compound of the BODIPY Dye Class: 4,4'-Difluoro-4-bora-(3a,4a)-diaza sindacene. *J. Fluoresc.* **2009**, *19*, 755-758.

(117) Arroyo, I. J.; Hu, R. R.; Merino, G.; Tang, B. Z.; Pena-Cabrera, E. The Smallest and One of the Brightest. Efficient Preparation and Optical Description of the Parent Borondipyrromethene System. *J. Org. Chem.* **2009**, *74*, 5719-5722

(118) Tsien, R. Y. New Calcium Indicators and Buffers with High Selectivity against Magnesium and Protons - Design, Synthesis, and Properties of Prototype Structures. *Biochemistry-Us* **1980**, *19*, 2396-2404.

(119) Yakubovskyi, V. P.; Shandura, M. P.; Kovtun, Y. P. Boradipyrromethenecyanines. *Eur. J. Org. Chem.* **2009**, 3237-3243.

(120) Turro, N. J.; Ramamurthy, V.; Scaiano, J. C.: Principles of Molecular

Photochemistry: An Introduction; University Science Books: Sausalito, 2009.

(121) McDonnell, S. O.; Hall, M. J.; Allen, L. T.; Byrne, A.; Gallagher, W.M.; O'Shea, D. F. Supramolecular photonic therapeutic agents. *J. Am. Chem. Soc.* **2005**, *127*, 16360-16361

(122) Buggins, T. R.; Dickinson, P. A.; Taylor, G. The effects of pharmaceutical excipients on drug disposition. *Adv. Drug Delivery Rev*. **2007**, 59, 1482−1503

(123) Berthod, A.; Tomer, S.; Dorsey, J. G. Polyoxyethylene Alkyl Ether Nonionic Surfactants: Physicochemical Properties and Use for Cholesterol Determination in Food. *Talanta.* **2001**, 55, 69-83

(124) Bazylińska, U.; Pietkiewicz, J.; Saczko, J.; Nattich-Rak, M.; Rossowska, J.; Garbiec, A.; Wilk, K. A. Nanoemulsion-templated multilayer nanocapsules for cyanine-type photosensitizer delivery to human breast carcinoma cells. *Eur. J. Pharm. Sci*. **2012**, 47, 406−420

(125) Bonacin, J. A.; Engelmann, F. M.; Severino, D.; Toma, H. E.; Baptista, M. S. Singletoxygen quantum yields (Φd) in water using beetroot extract and an array of LEDs. *Journal of theBrazilian Chemical Society* **2009**, *20*, 31-36.

(126) Ronzani, F.; Trivella, A.; Arzoumanian, E.; Blanc, S.; Sarakha, M.; Richard, C.; Oliveros,E.; Lacombe, S. Comparison of the photophysical properties of three phenothiazine derivatives:transient detection and singlet oxygen production. *Photochemical & Photobiological Sciences* **2013**,*12*, 2160-2169.

APPENDIX

A. 1. Novel Near-IR Photosensitizers for photodynamic therapy

A.1.1. ^{1}H and ^{13}C NMR Spectra

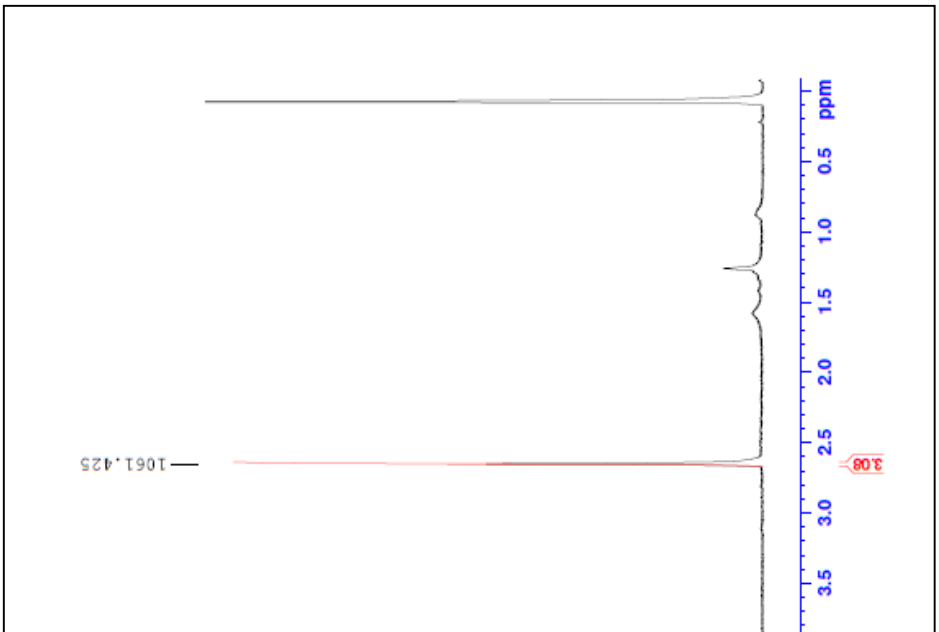

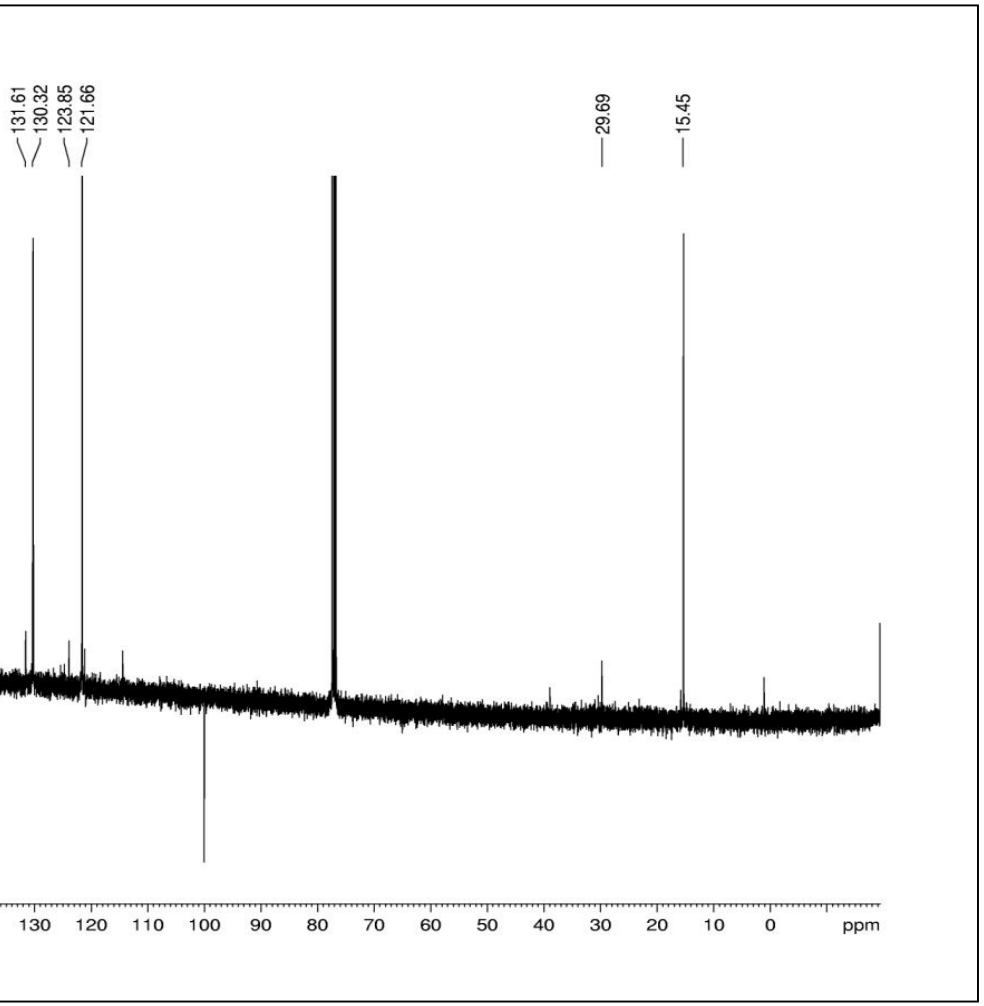
131.61
130.32
123.85
121.66
29.69
15.45
130
120
110
100
90
80
70
60
50
40
30
20
10
0
ppm

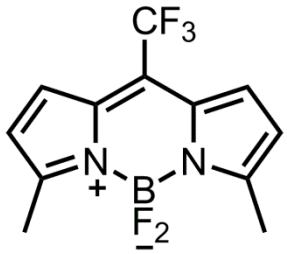
CF3
N
+
B
N
F2
−

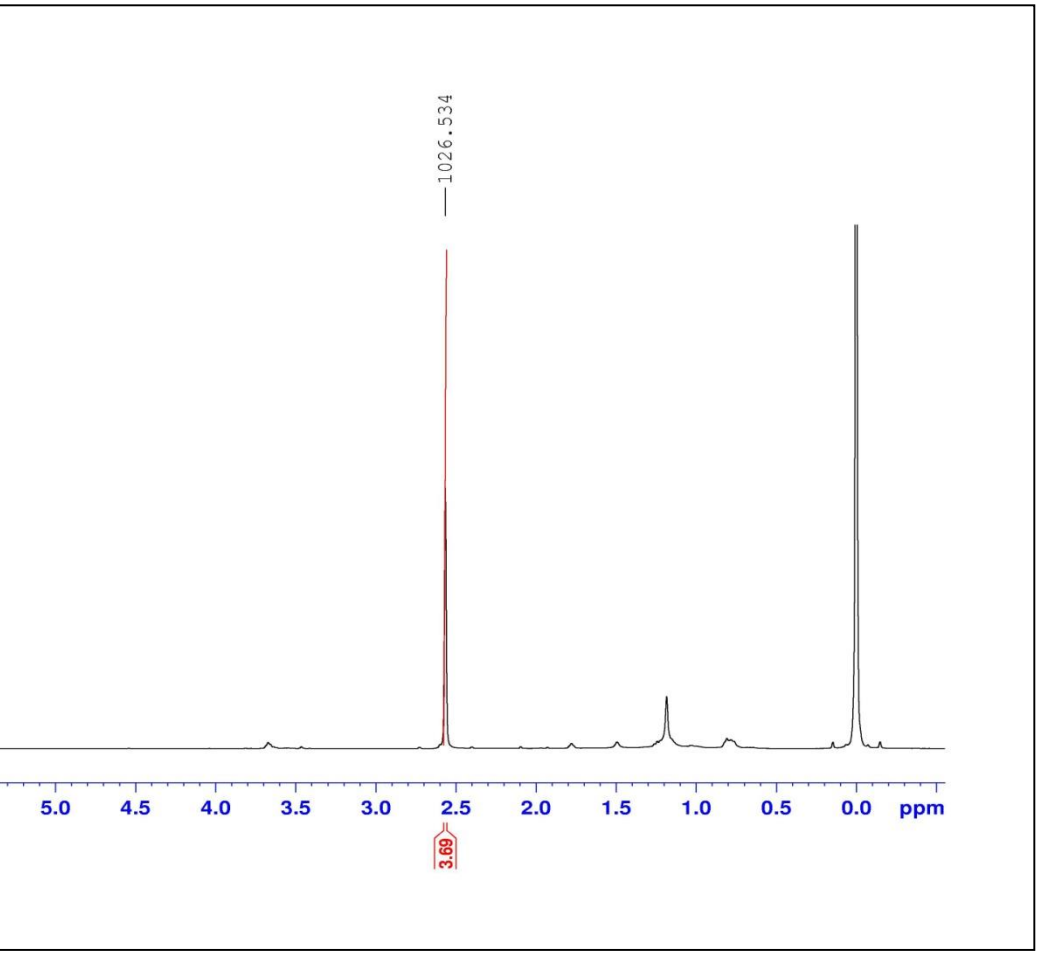
1026.534
5.0
4.5
4.0
3.5
3.0
2.5
2.0
1.5
1.0
0.5
0.0
ppm
3.69

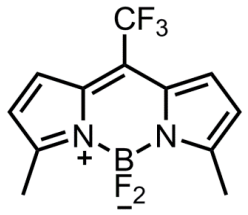
CF3
N
+
B
N
F2
−

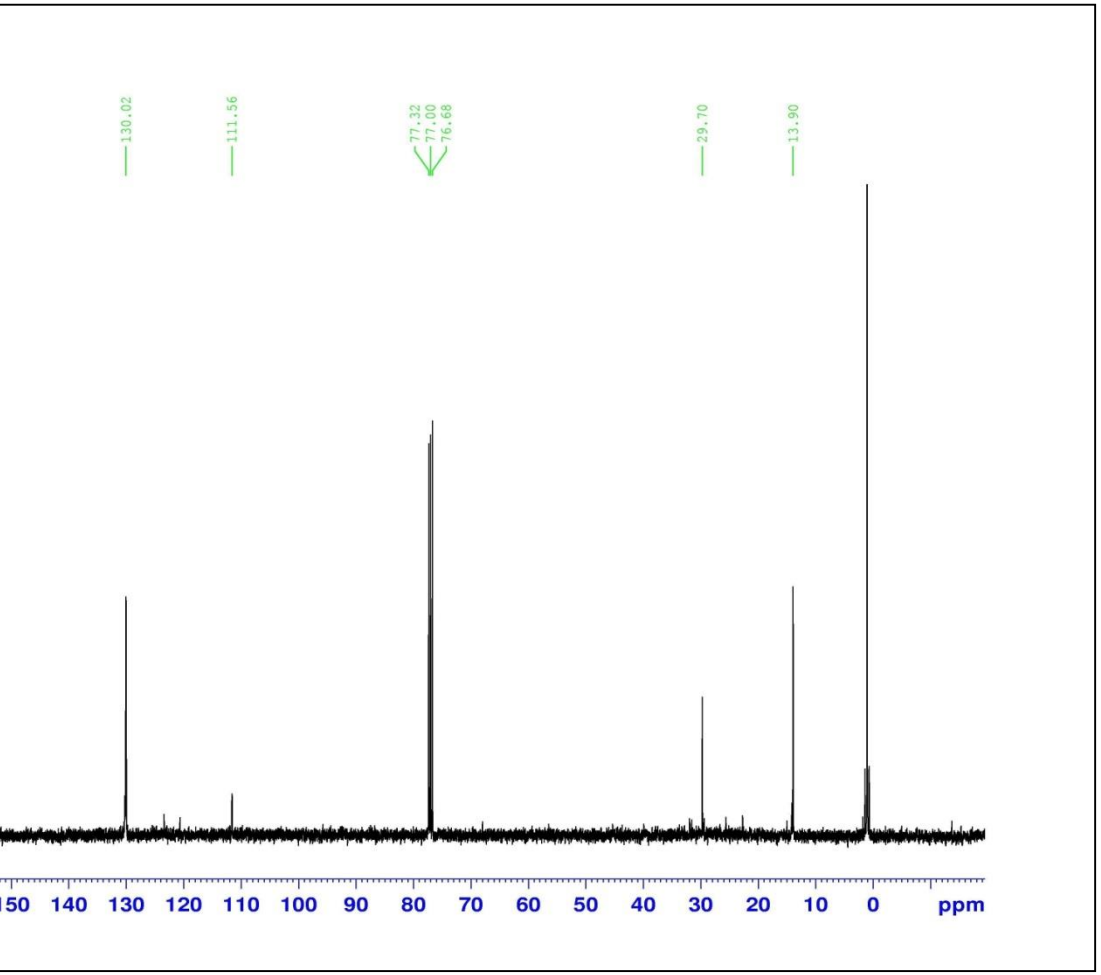
130.02
111.56
77.32
77.00
76.68
29.70
13.90
150 140 130 120 110 100 90 80 70 60 50 40 30 20 10 0 ppm

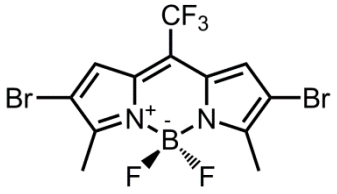
CF3
Br
Br
N+
B
N
F
F

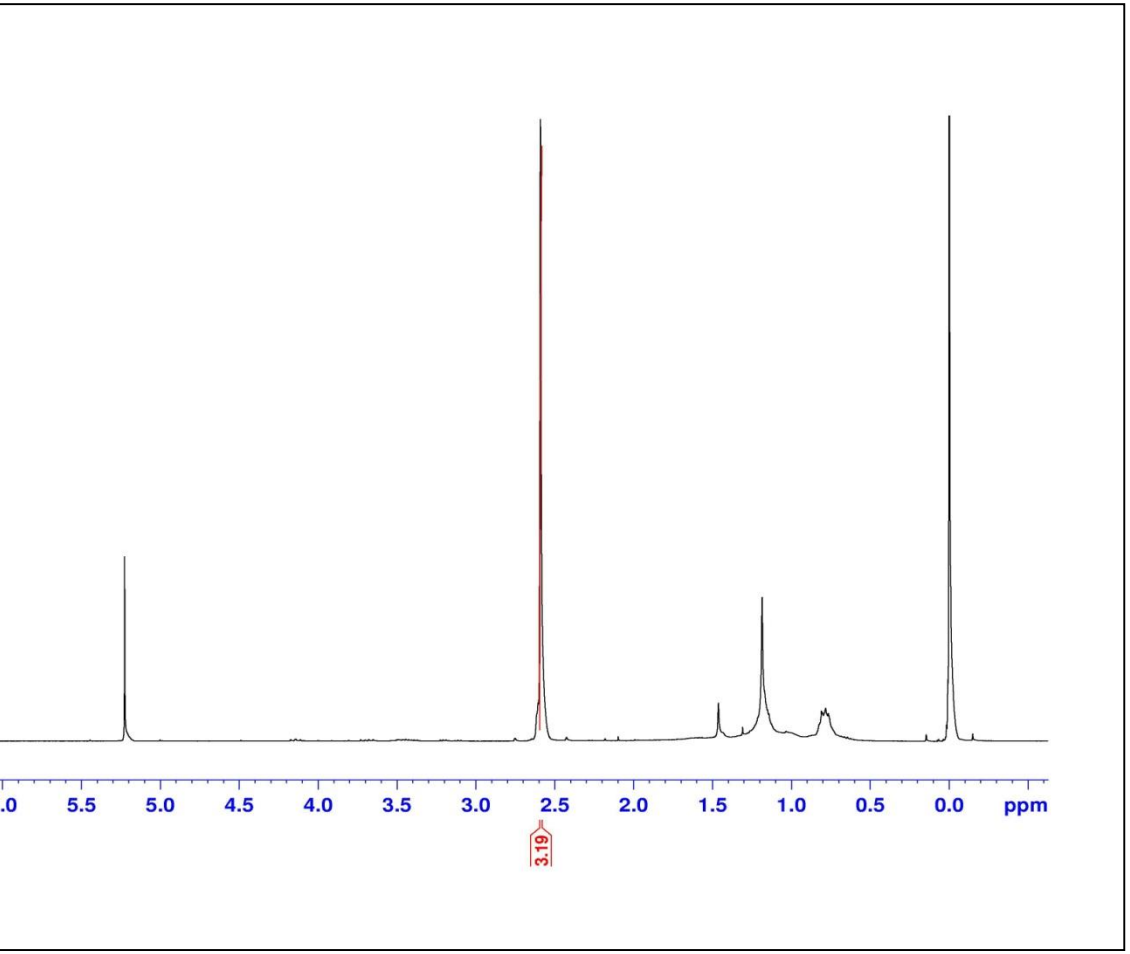
5.5
5.0
4.5
4.0
3.5
3.0
2.5
2.0
1.5
1.0
0.5
0.0
ppm
3.19


CF3
Br
Br
N+
B-
N
F
F

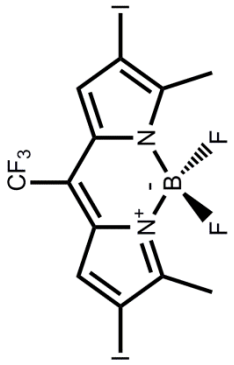
I
CF3
N
B
F
F
N+
-
I

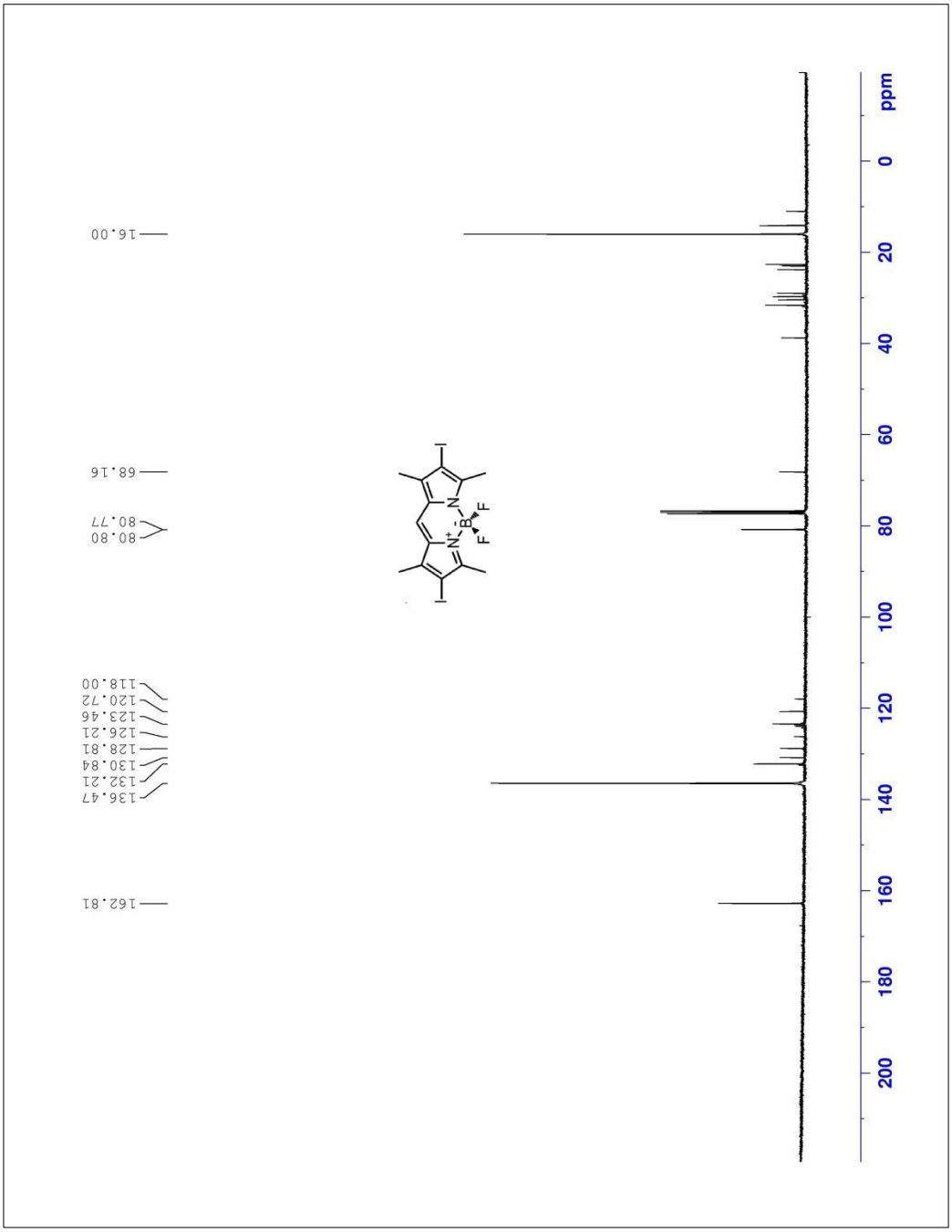
ppm
0
20
40
60
80
100
120
140
160
180
200
16.00
68.16
80.80
80.77
118.00
120.72
123.46
126.21
128.81
130.84
132.21
136.47
162.81

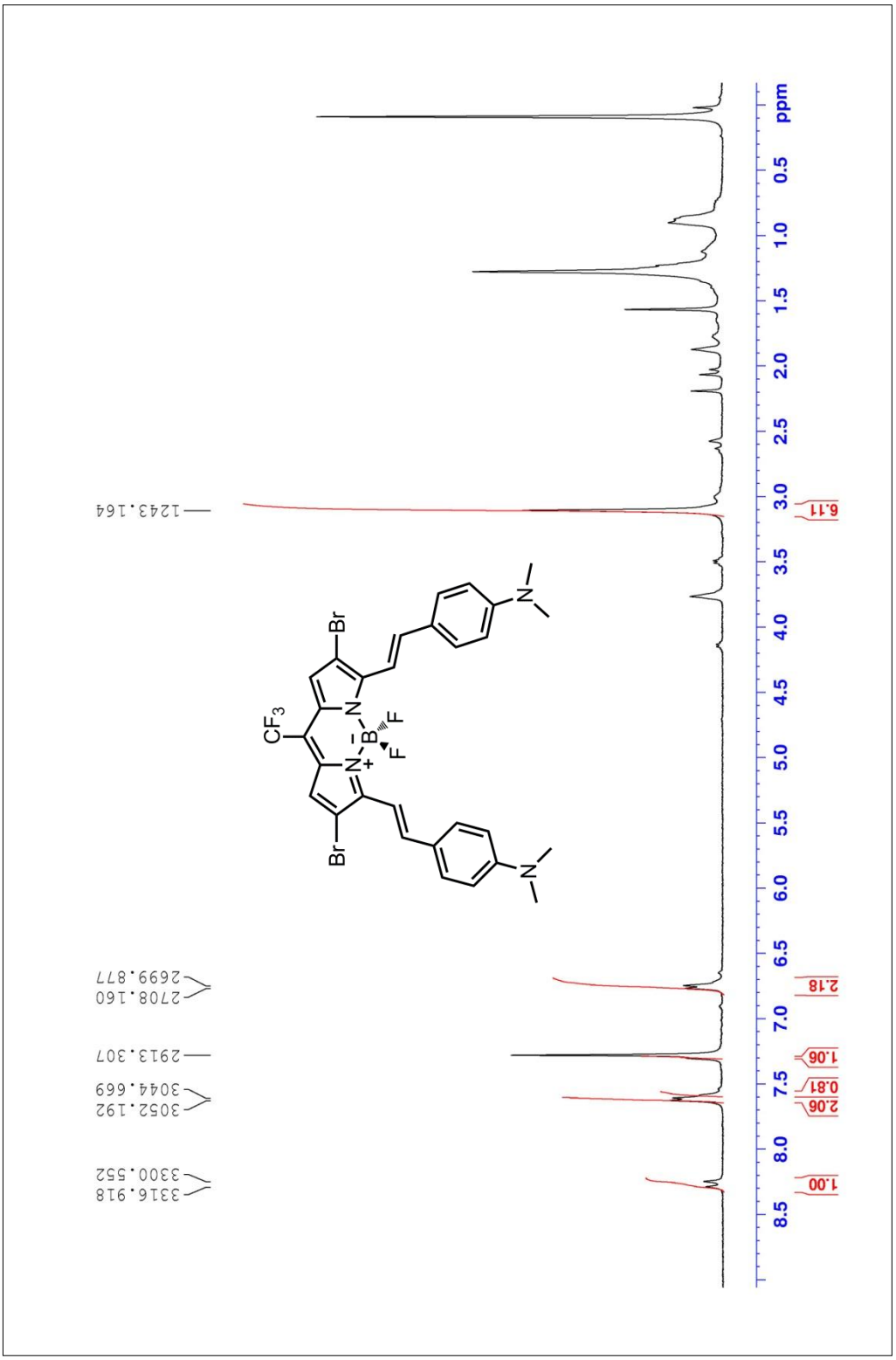
1243.164
2708.160
2699.877
2913.307
3052.192
3044.669
3316.918
3300.552
6.11
2.18
1.06
0.81
2.06
1.00
ppm
Br
Br
CF3
N
B
F
F

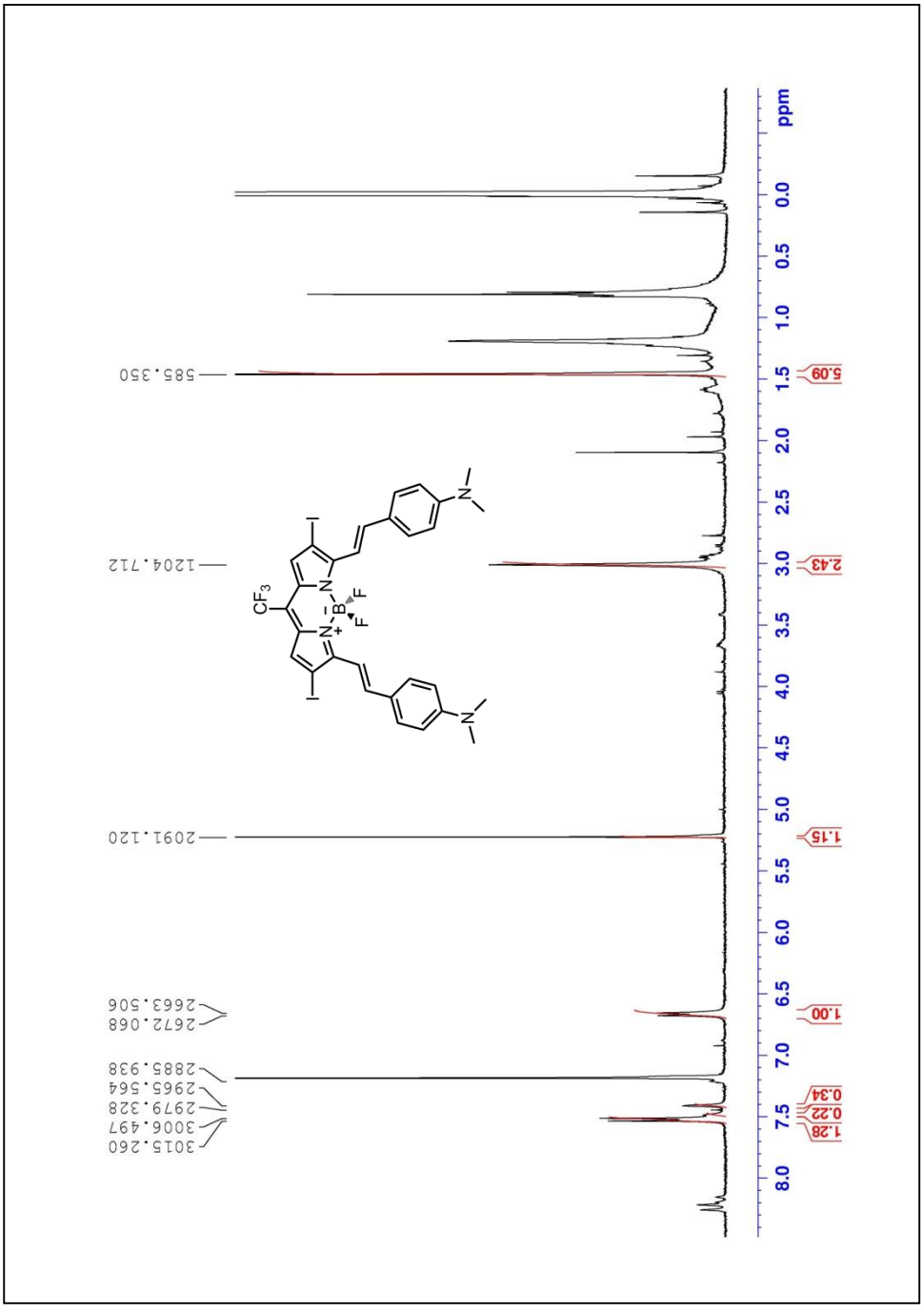
ppm
0.0
0.5
1.0
1.5
2.0
2.5
3.0
3.5
4.0
4.5
5.0
5.5
6.0
6.5
7.0
7.5
8.0
5.09
2.43
1.15
1.00
0.34
0.22
1.28
585.350
1204.712
2091.120
2663.506
2672.068
2885.938
2965.564
2979.328
3006.497
3015.260
CF3
B
F
F
N
N
I
I

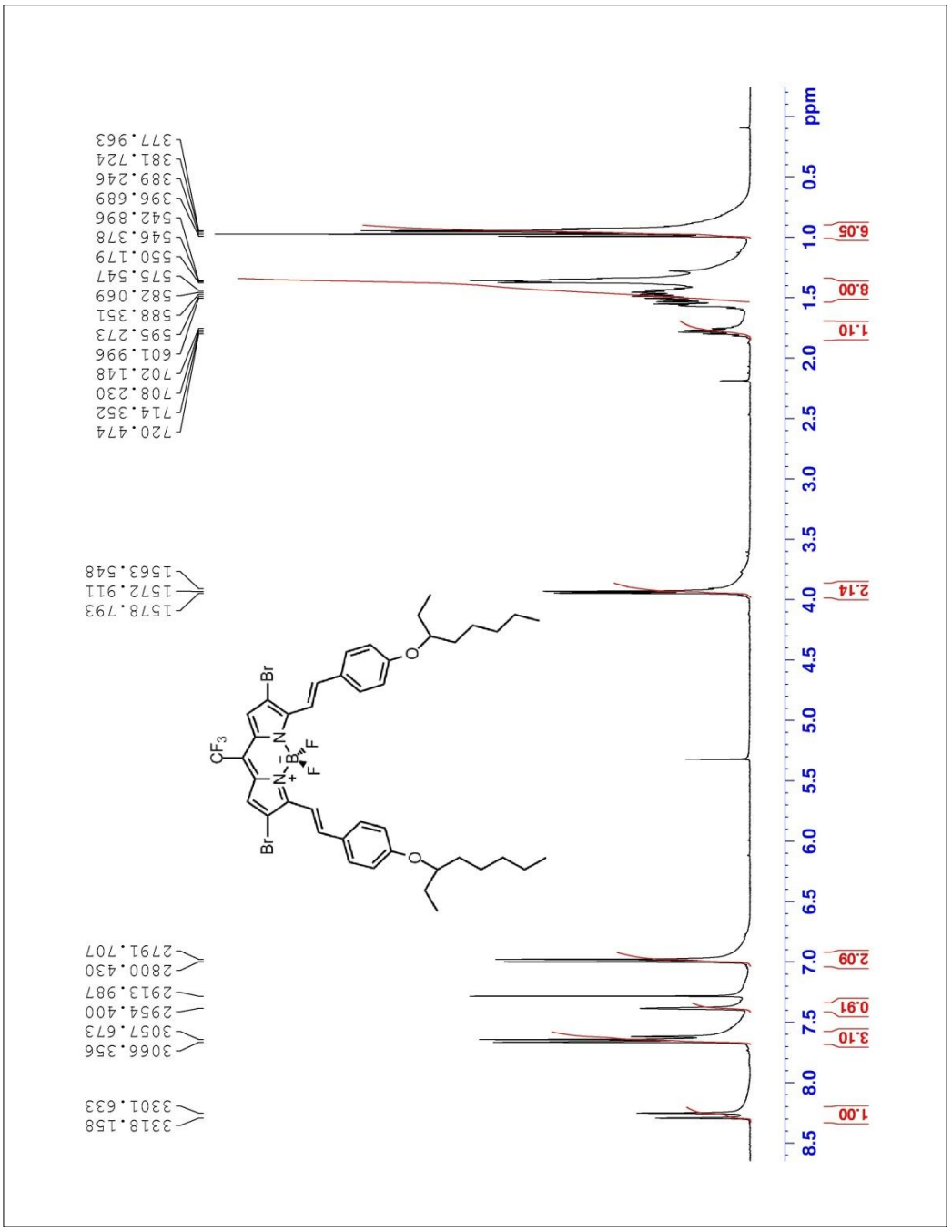
ppm
0.5
1.0
1.5
2.0
2.5
3.0
3.5
4.0
4.5
5.0
5.5
6.0
6.5
7.0
7.5
8.0
8.5
6.05
8.00
1.10
2.14
2.09
0.97
3.10
1.00
Br
Br
CF3
N
B
F
F
O
O
3318.158
3301.633
3066.356
3057.673
2954.400
2913.987
2800.430
2791.707
1578.793
1572.911
1563.548
720.474
714.352
708.230
702.148
601.996
595.273
588.351
582.069
575.547
550.179
546.378
542.896
396.689
389.246
381.724
377.963

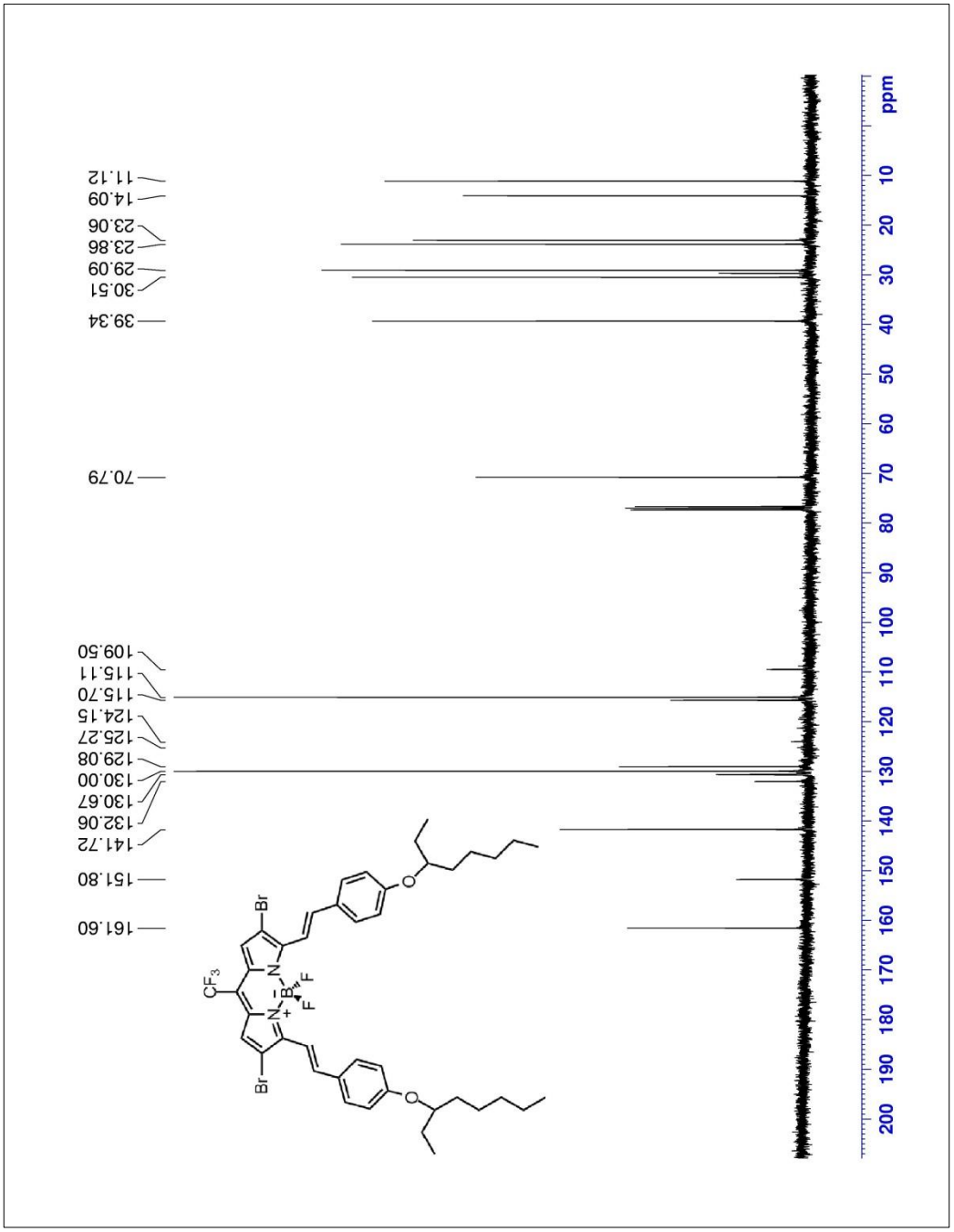
11.12
14.09
23.06
23.86
29.09
30.51
39.34
70.79
109.50
115.11
115.70
124.15
125.27
129.08
130.00
130.67
132.06
141.72
151.80
161.60
ppm
10
20
30
40
50
60
70
80
90
100
110
120
130
140
150
160
170
180
190
200
Br
Br
CF3
N
B
F
F
O
O

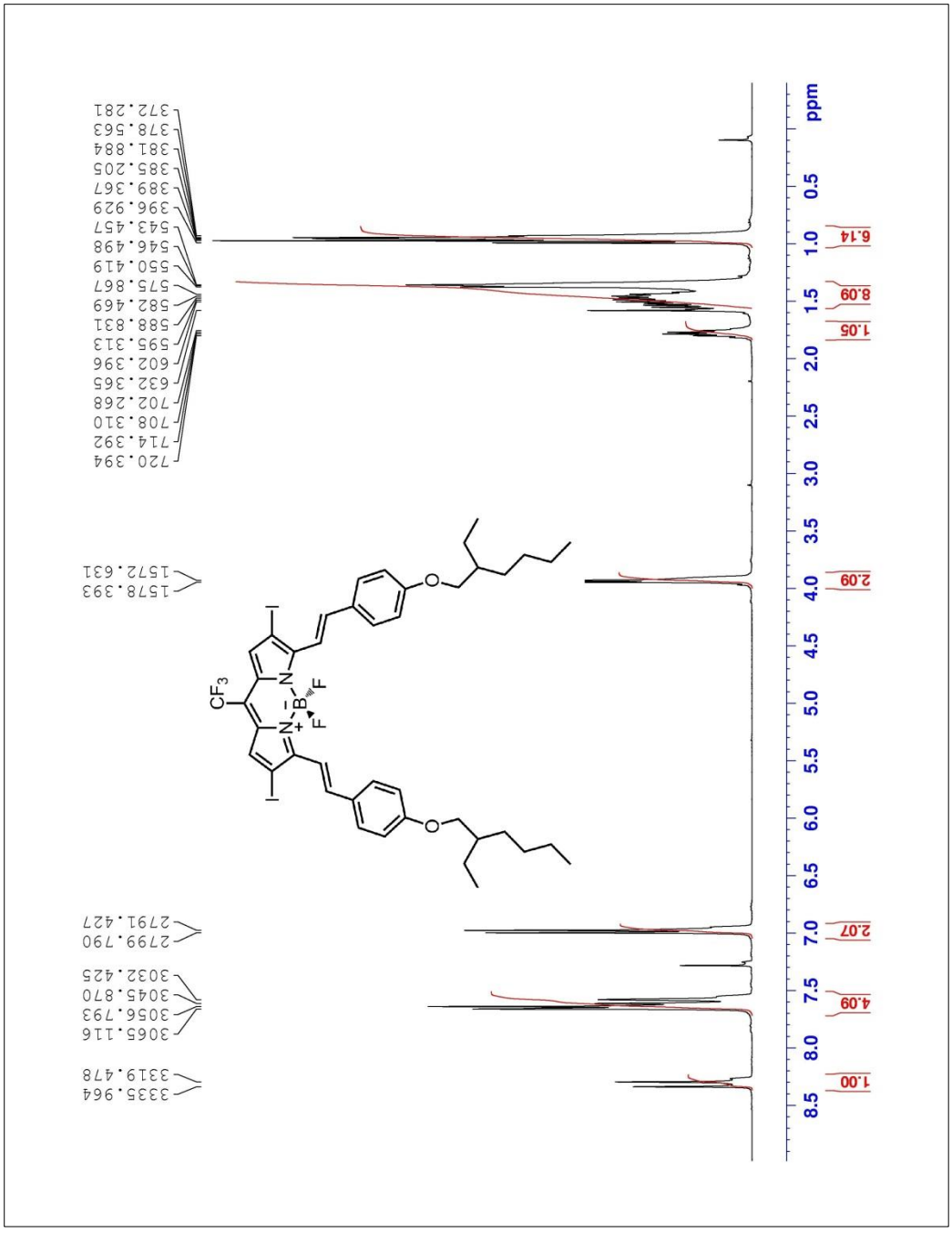
ppm
0.5
1.0
1.5
2.0
2.5
3.0
3.5
4.0
4.5
5.0
5.5
6.0
6.5
7.0
7.5
8.0
8.5
6.14
8.09
1.05
2.09
2.07
4.09
1.00
372.281
378.563
381.884
385.205
389.367
396.929
543.457
546.498
550.419
575.867
582.469
588.831
595.313
602.396
632.365
702.268
708.310
714.392
720.394
1572.631
1578.393
2791.427
2799.790
3032.425
3045.870
3056.793
3065.116
3319.478
3335.964
F
F
B
N
N
CF3

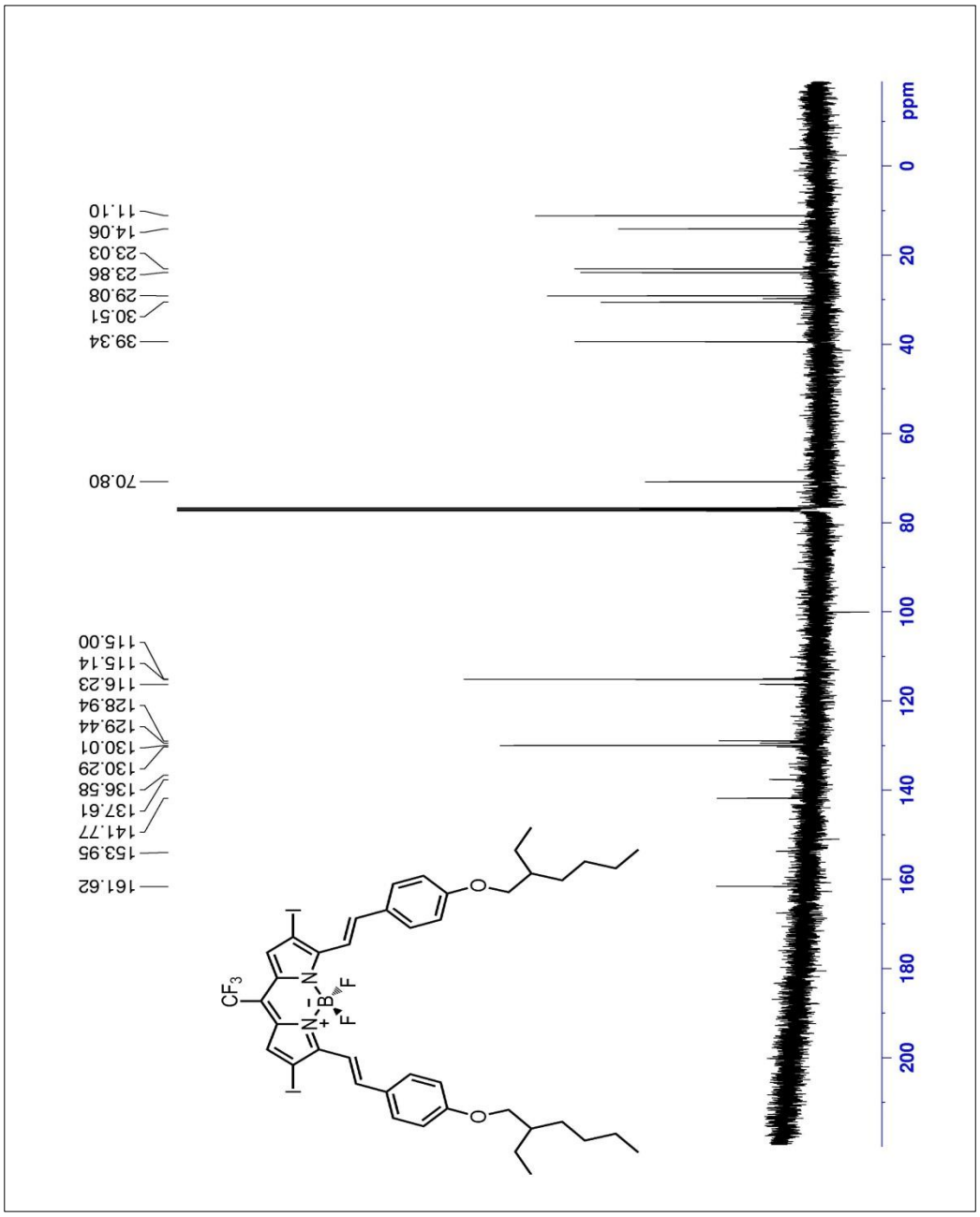

A.1.2. MASS SPECTRA

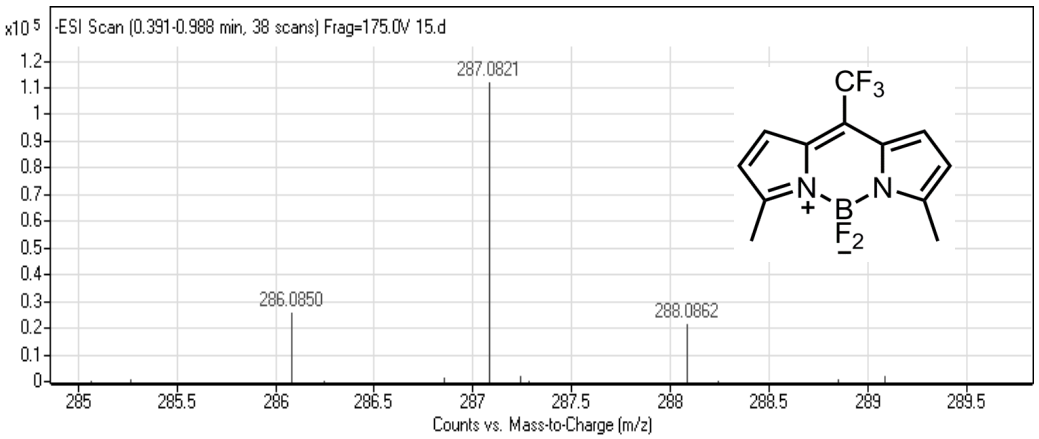
x10 5
-ESI Scan (0.391-0.988 min, 38 scans) Frag=175.0V 15.d
287.0821
286.0850
288.0862
CF3
N
B
N
F2
Counts vs. Mass-to-Charge (m/z)

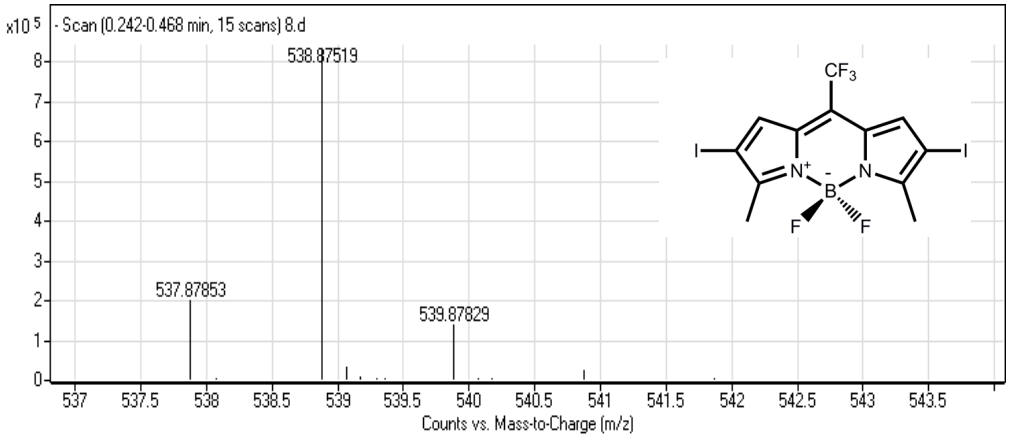
x10 5
- Scan (0.242-0.468 min, 15 scans) 8.d
538.87519
537.87853
539.87829
CF3
I
I
N
B
N
F
F
Counts vs. Mass-to-Charge (m/z)

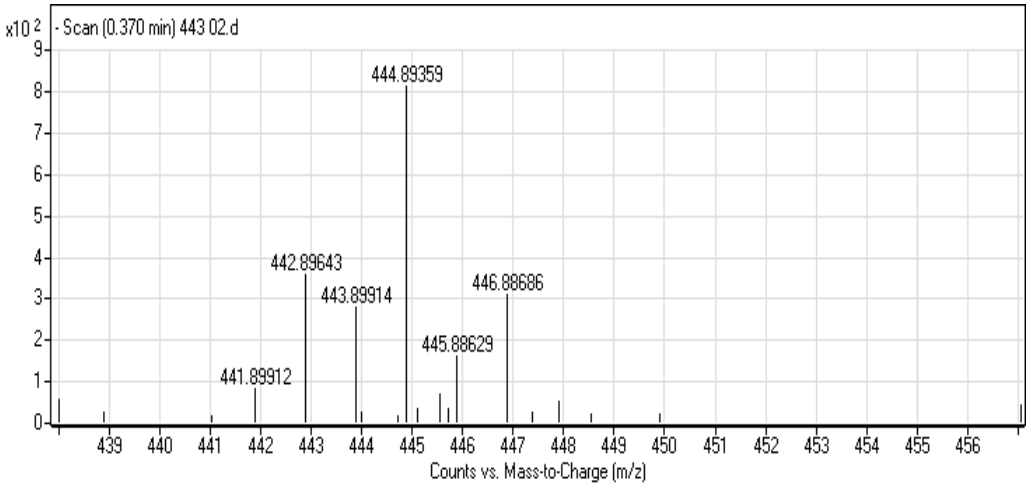
x10 2
- Scan (0.370 min) 443 02.d
444.89359
442.89643
443.89914
446.88686
445.88629
441.89912
Counts vs. Mass-to-Charge (m/z)

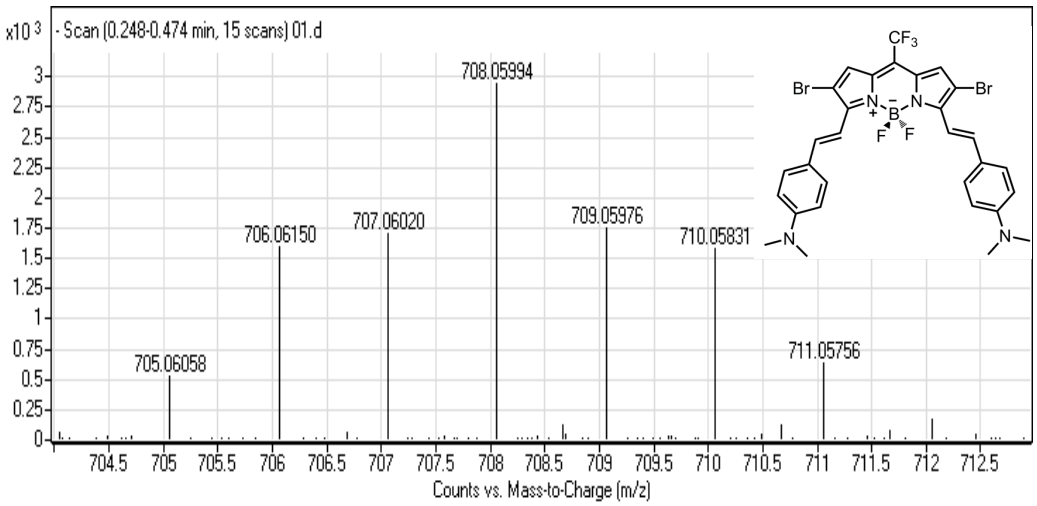
x10 3
- Scan (0.248-0.474 min, 15 scans) 01.d
708.05994
706.06150
707.06020
709.05976
710.05831
705.06058
711.05756
CF3
Br
Br
N
B
F
F
Counts vs. Mass-to-Charge (m/z)

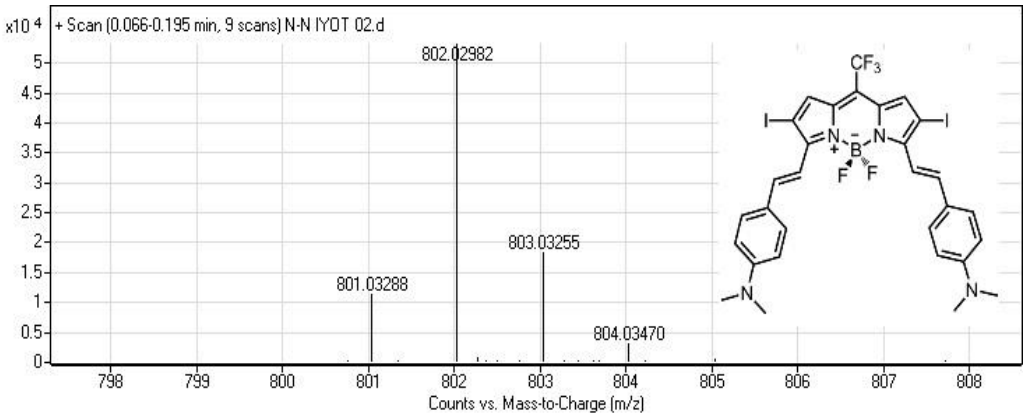
x10 4
+ Scan (0.066-0.195 min, 9 scans) N-N IYOT 02.d
802.02982
803.03255
801.03288
804.03470
CF3
I
I
F
F
N
Counts vs. Mass-to-Charge (m/z)

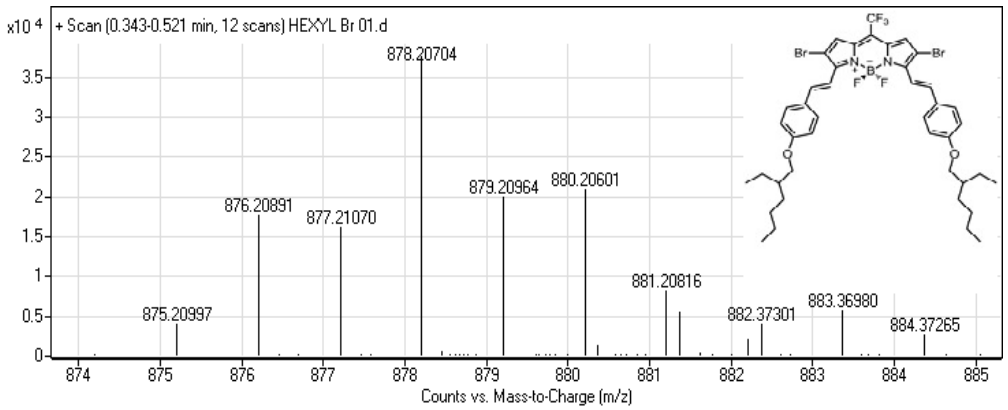
x10 4
+ Scan (0.343-0.521 min, 12 scans) HEXYL Br 01.d
878.20704
879.20964
880.20601
876.20891
877.21070
881.20816
875.20997
882.37301
883.36980
884.37265
CF3
Br
Br
F
F
O
Counts vs. Mass-to-Charge (m/z)

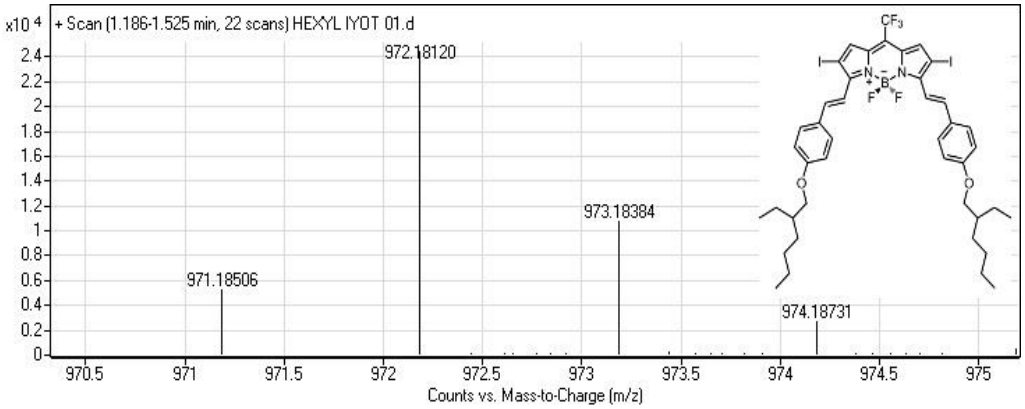
x10 4
+ Scan (1.186-1.525 min, 22 scans) HEXYL IYOT 01.d
2.4
2.2
2
1.8
1.6
1.4
1.2
1
0.8
0.6
0.4
0.2
0
972.18120
973.18384
971.18506
974.18731
970.5
971
971.5
972
972.5
973
973.5
974
974.5
975
Counts vs. Mass-to-Charge (m/z)
CF3
I
I
N
B
F
F
N
O
O

A. 2. Rational Design of Heavy Atom Free Anticancer Photosensitizer

A.2.1. ^{1}H and ^{13}C NMR Spectra

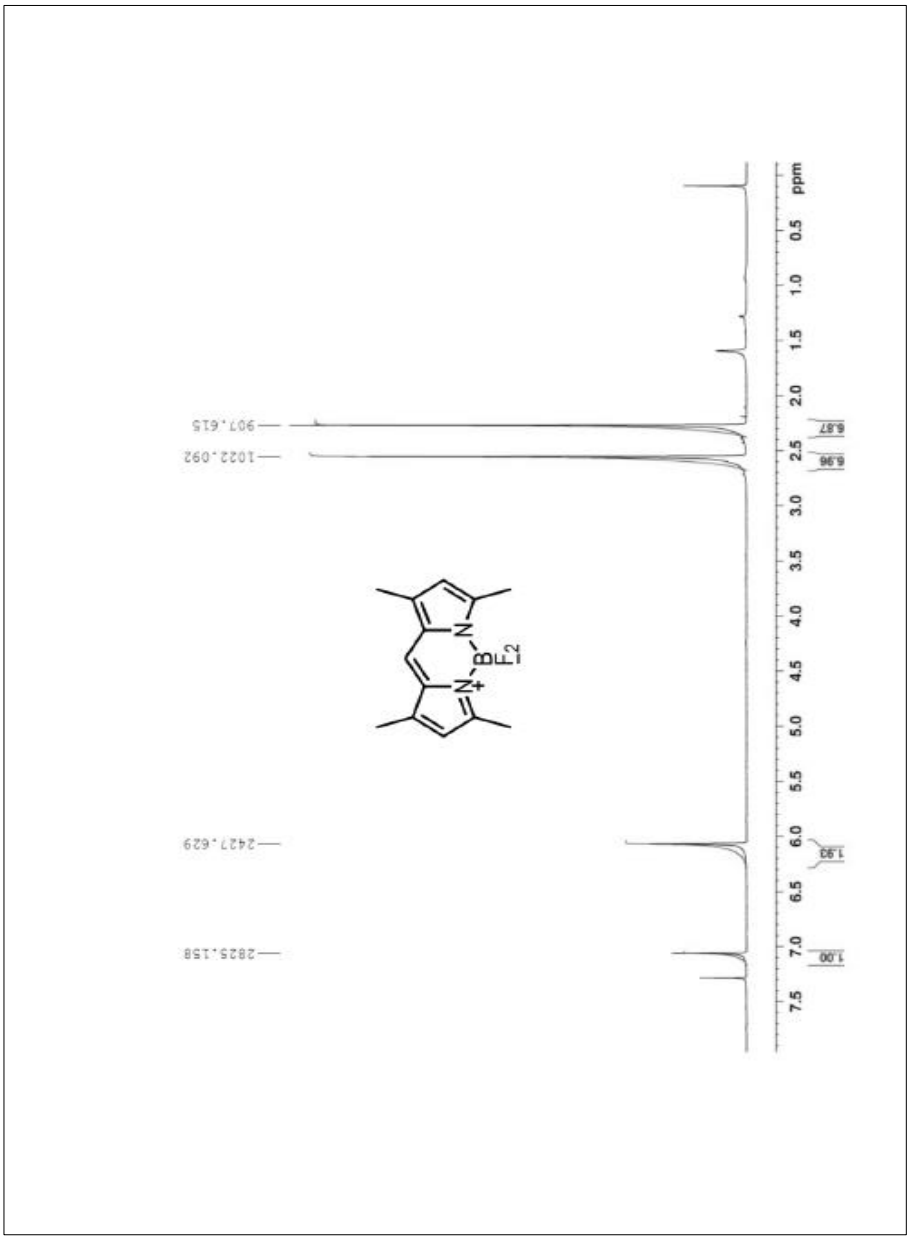

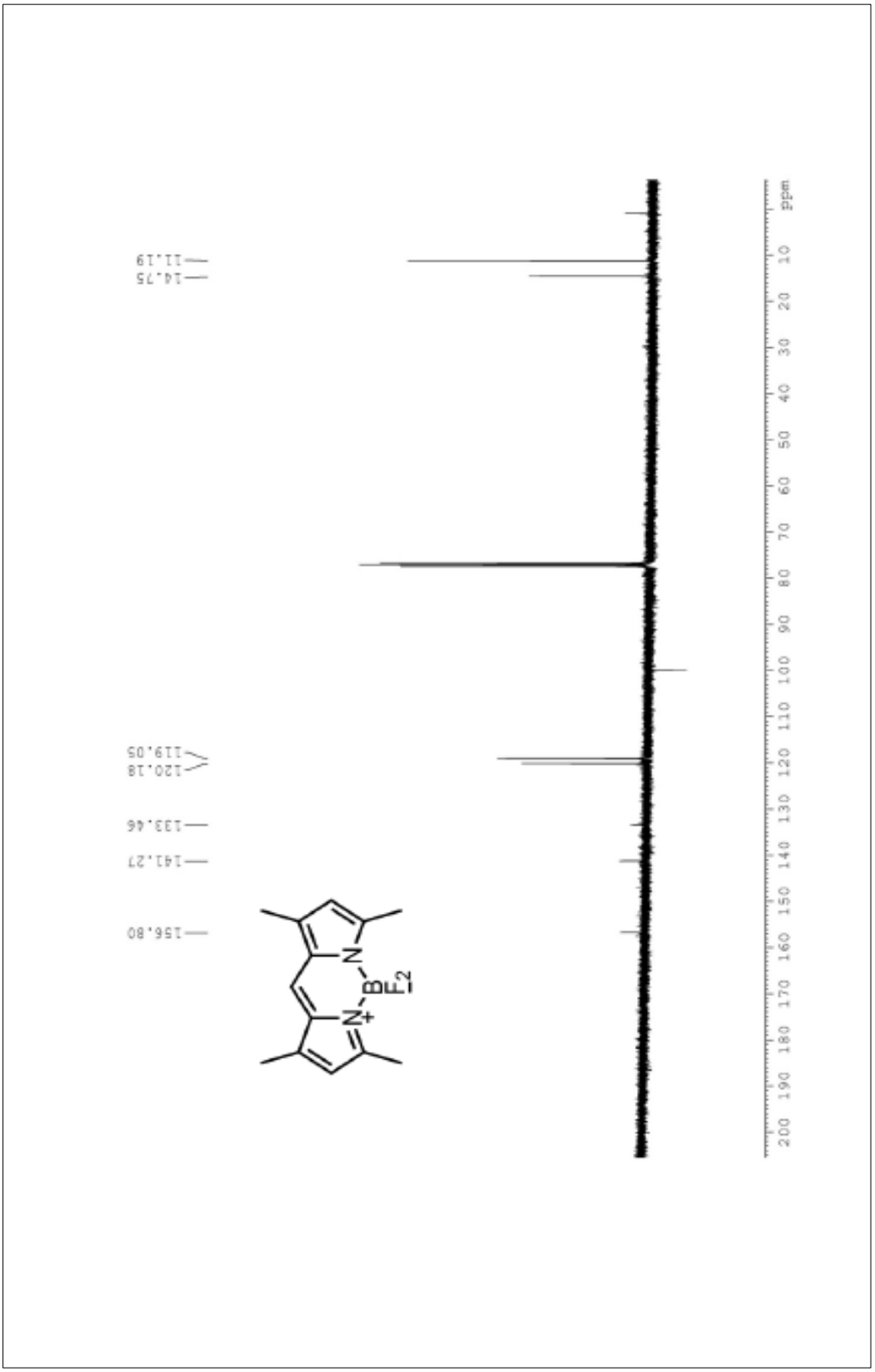
11.19
14.75
119.05
120.18
133.46
141.27
156.80
N
B
F2
N+
ppm

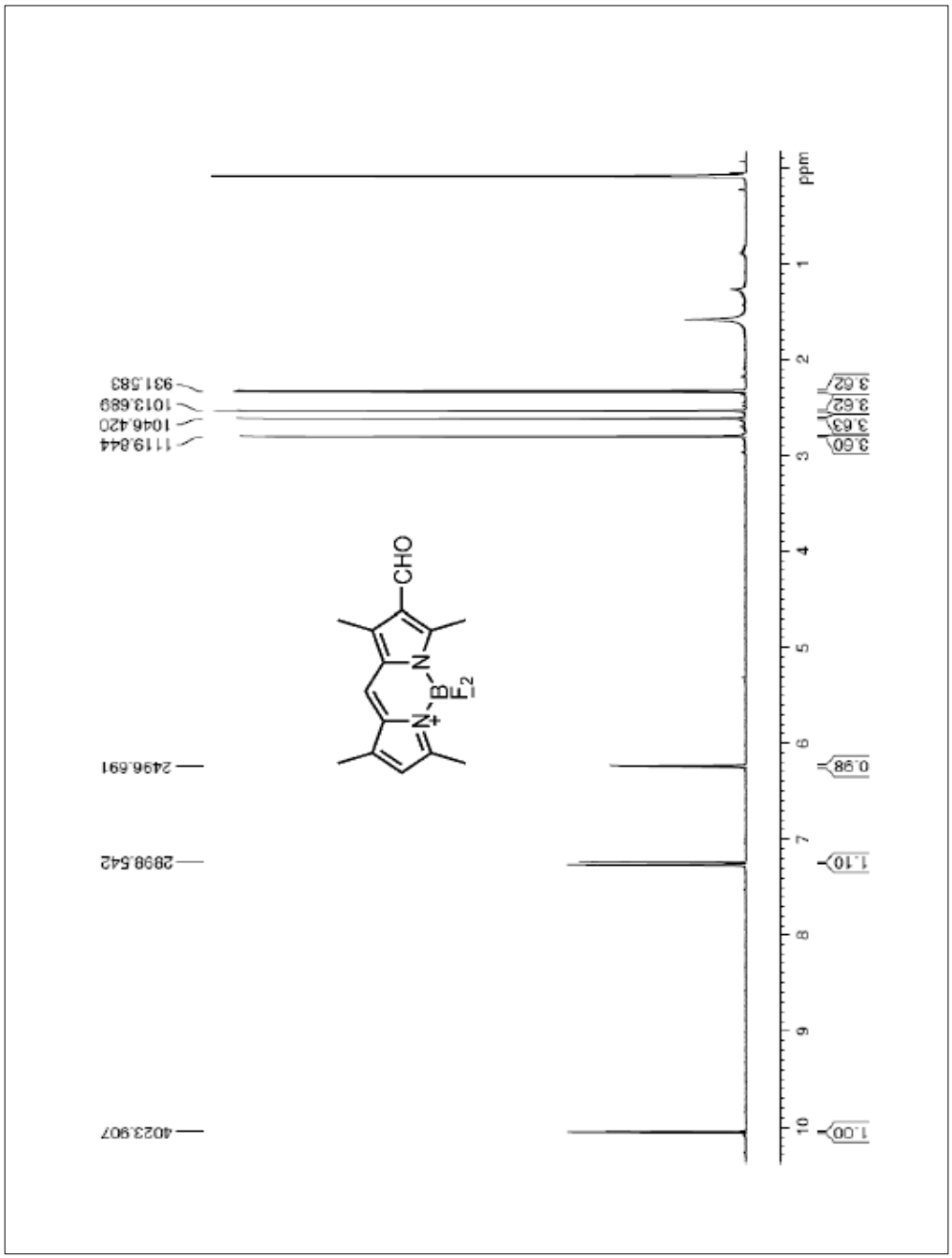
ppm
1.00
1.10
0.98
3.60
3.63
3.62
3.62
4023.907
2898.542
2496.691
1119.844
1046.420
1013.689
931.583
CHO
N
B
F2
N+

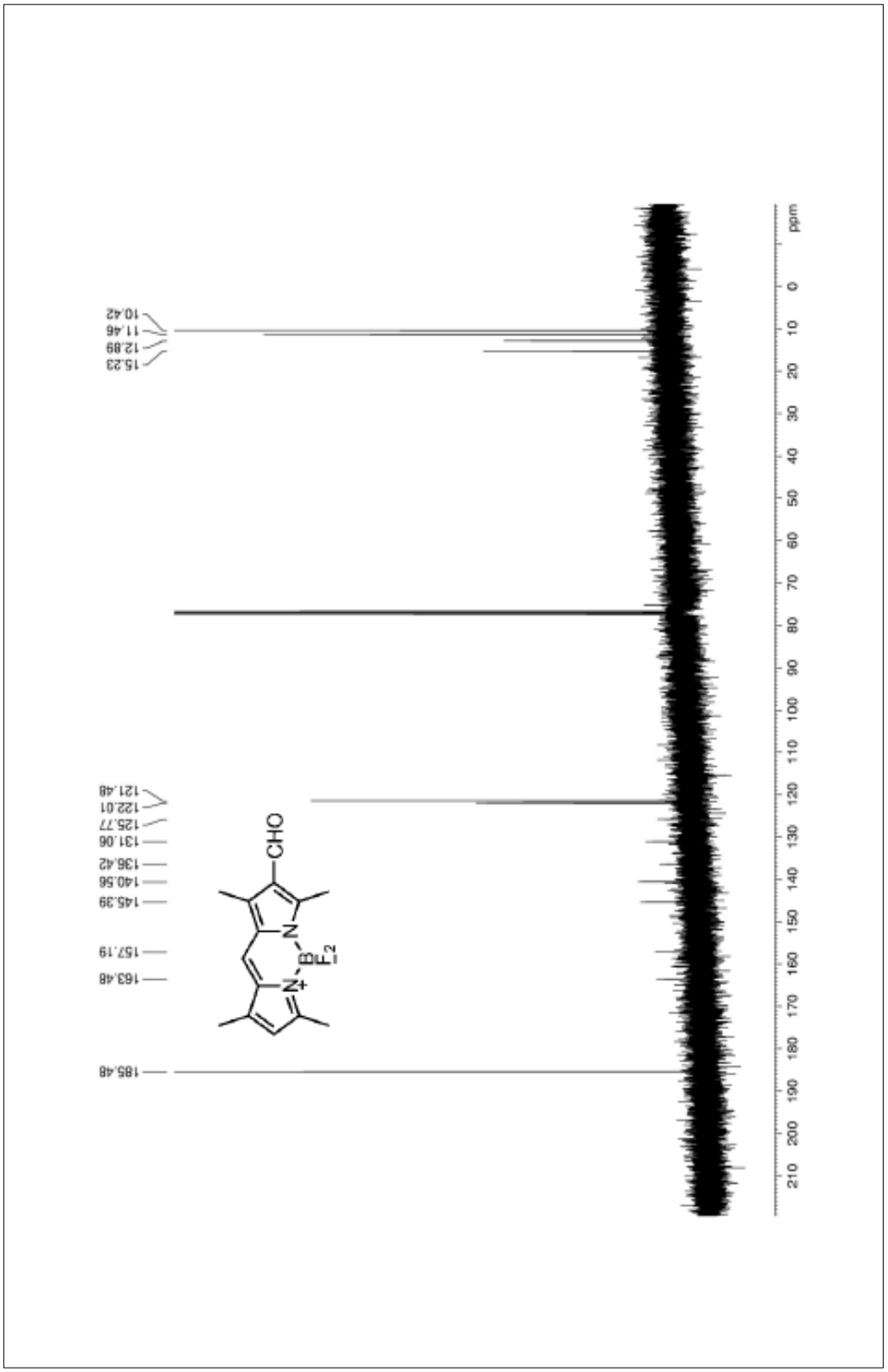
10.42
11.46
12.89
15.23
121.48
122.01
125.77
131.06
136.42
140.56
145.39
157.19
163.48
185.48
CHO
N
B
F2
N+
ppm
0
10
20
30
40
50
60
70
80
90
100
110
120
130
140
150
160
170
180
190
200
210

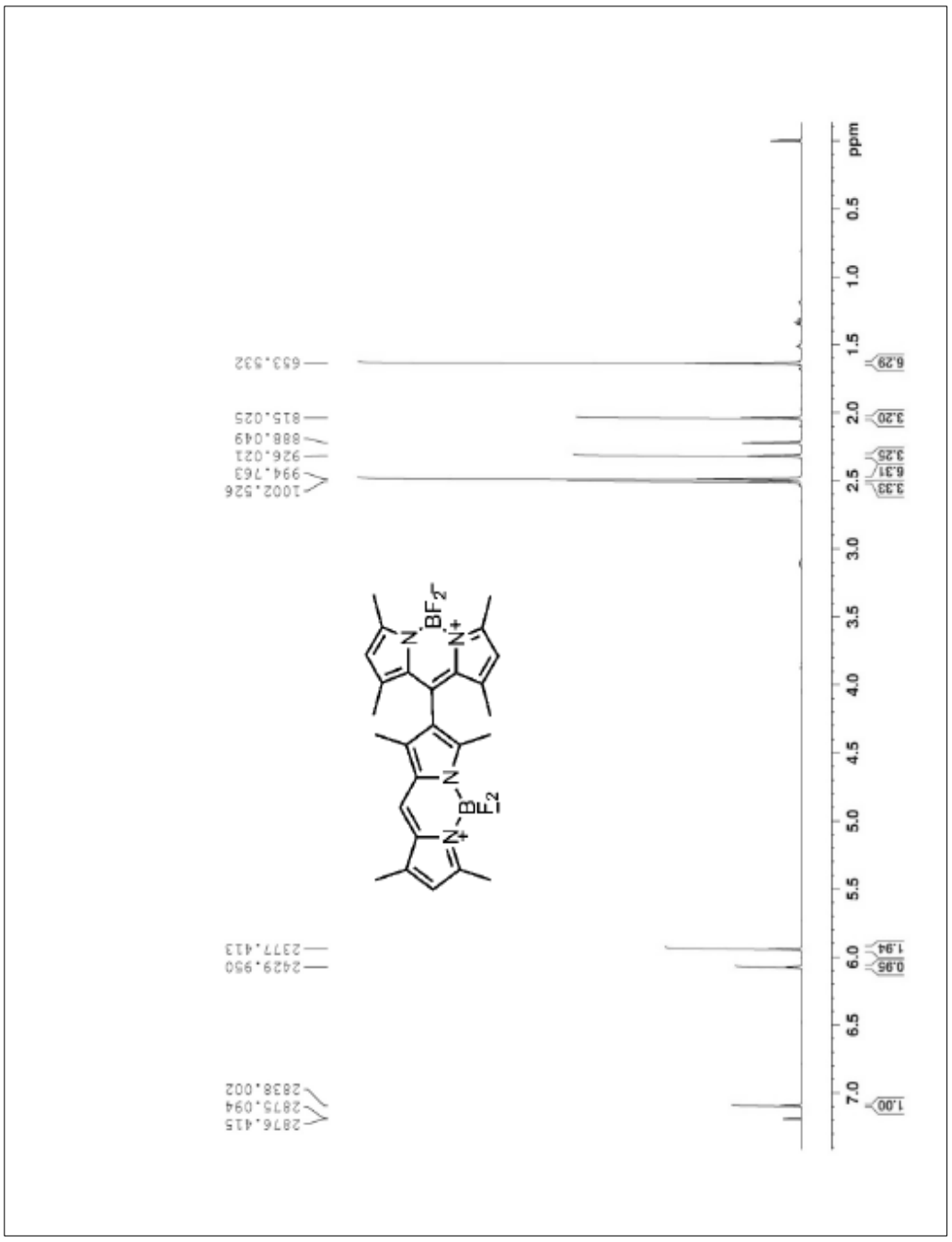
ppm
0.5
1.0
1.5
2.0
2.5
3.0
3.5
4.0
4.5
5.0
5.5
6.0
6.5
7.0
6.29
3.20
3.25
6.31
3.33
0.95
1.94
1.00
633.532
815.025
888.049
926.021
994.763
1002.526
2377.413
2429.950
2876.415
2875.094
2838.002

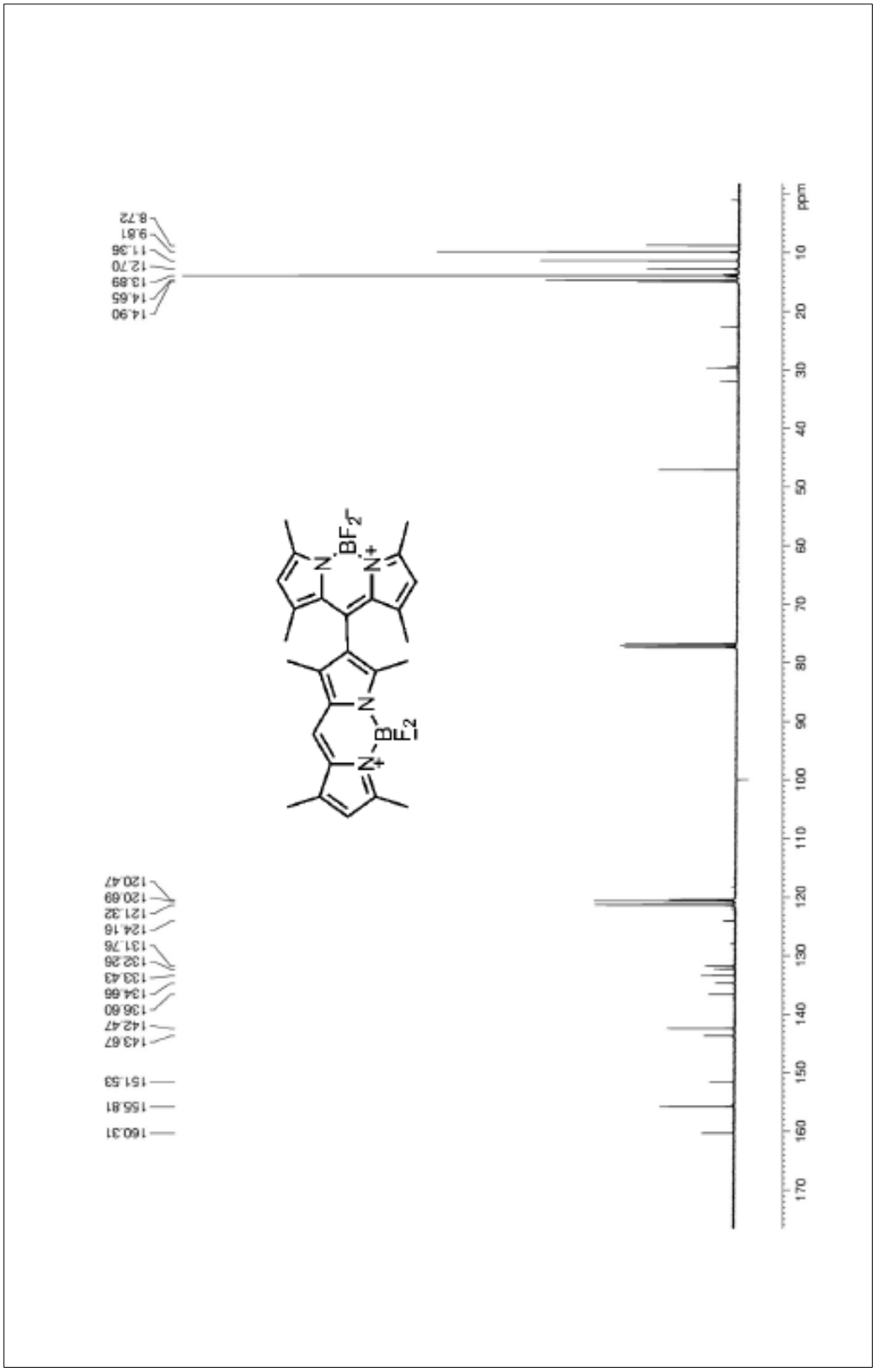
8.72
9.81
11.36
12.70
13.89
14.65
14.90
120.47
120.89
121.32
124.16
131.76
132.26
133.43
134.66
136.60
142.47
143.67
151.53
155.81
160.31
ppm
10
20
30
40
50
60
70
80
90
100
110
120
130
140
150
160
170
BF2
N
N+
B
F2

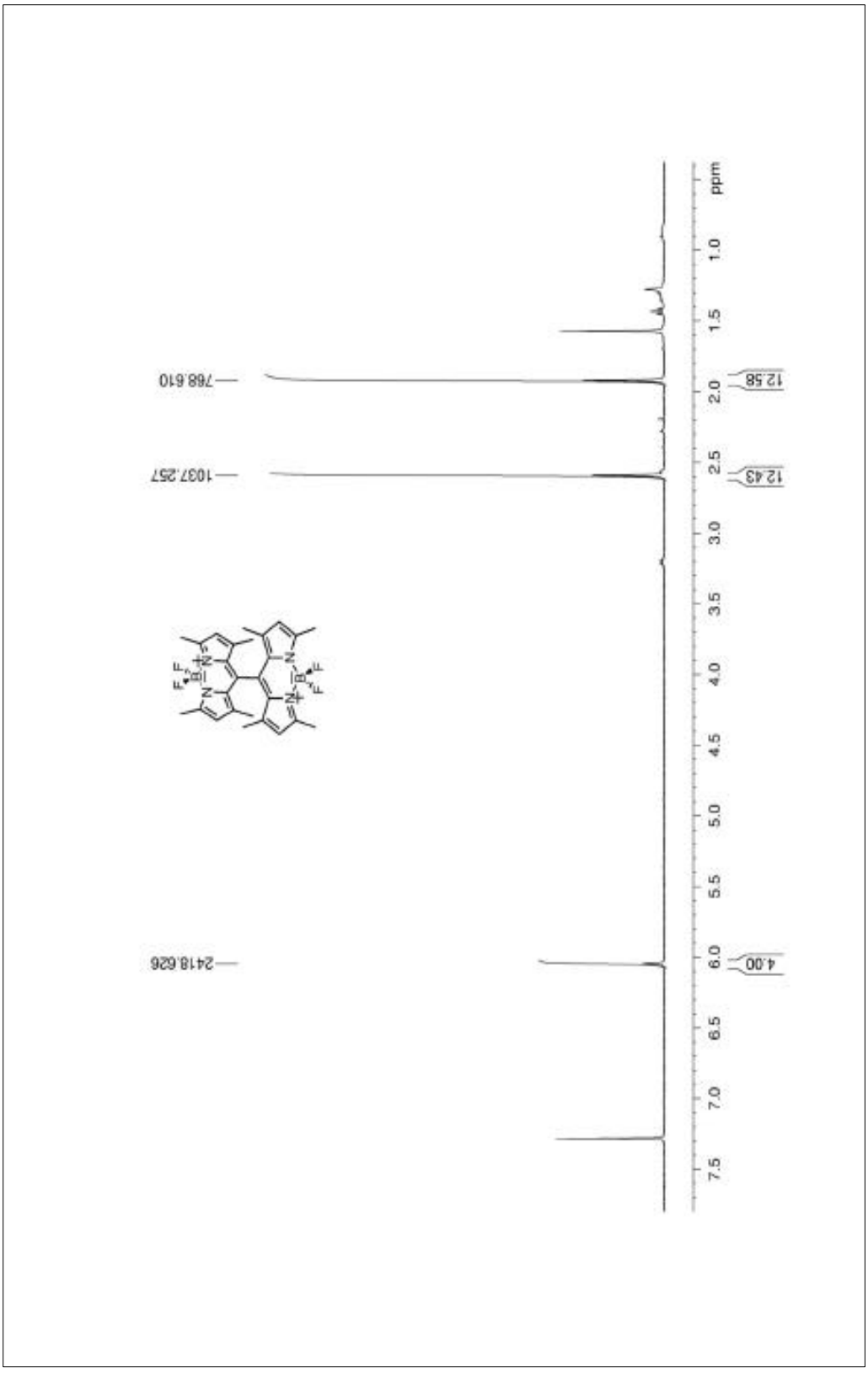
ppm
1.0
1.5
2.0
2.5
3.0
3.5
4.0
4.5
5.0
5.5
6.0
6.5
7.0
7.5
12.58
12.43
4.00
768.610
1037.257
2418.626

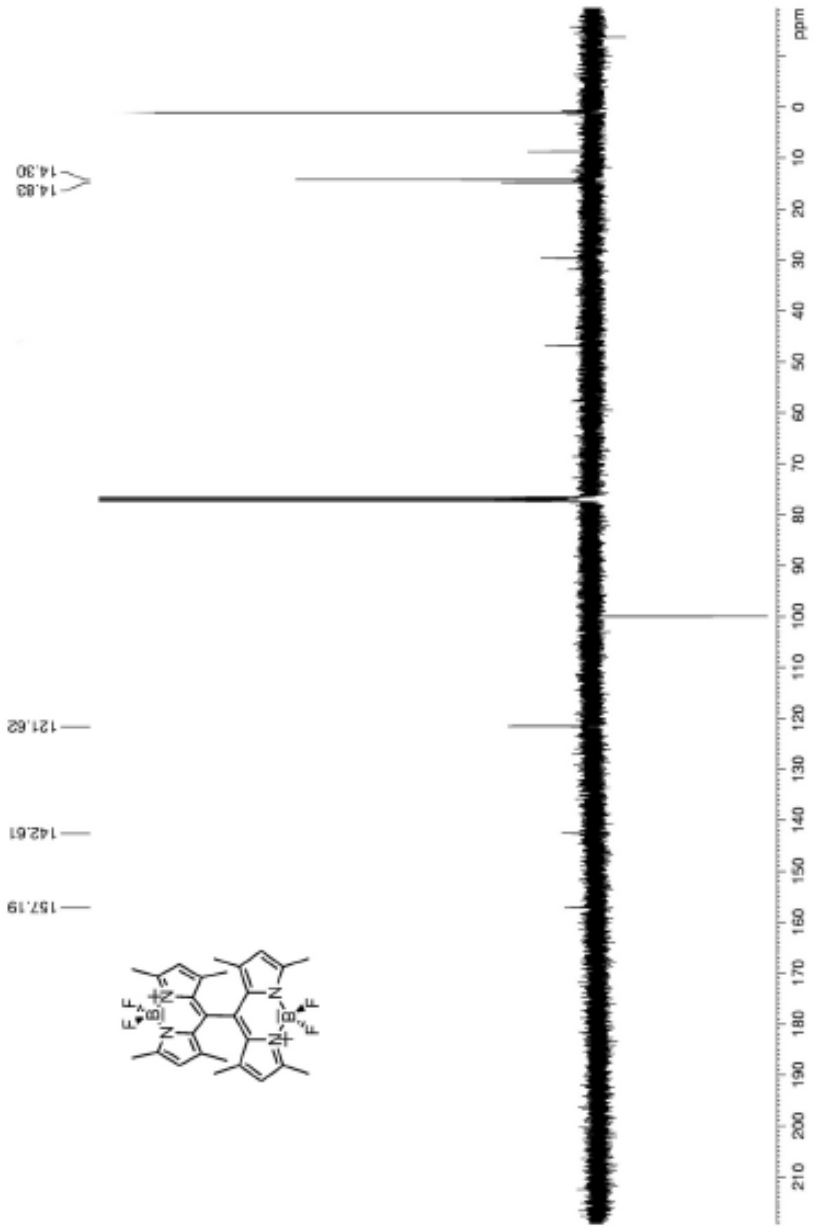
14.30
14.83
121.62
142.61
157.19
ppm
0
10
20
30
40
50
60
70
80
90
100
110
120
130
140
150
160
170
180
190
200
210

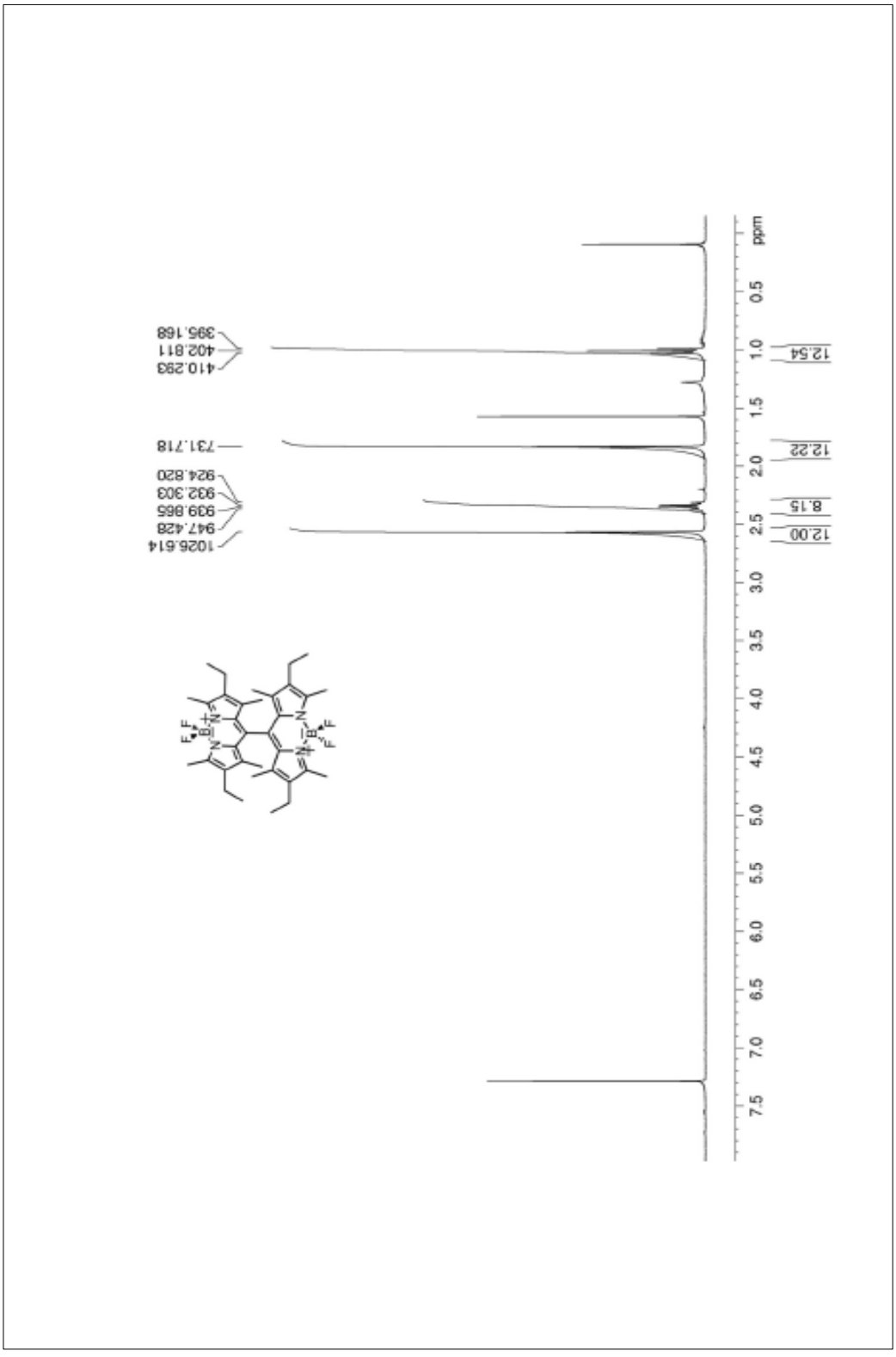
ppm
0.5
1.0
1.5
2.0
2.5
3.0
3.5
4.0
4.5
5.0
5.5
6.0
6.5
7.0
7.5
12.54
12.22
8.15
12.00
395.168
402.811
410.293
731.718
924.820
932.303
939.865
947.428
1026.614

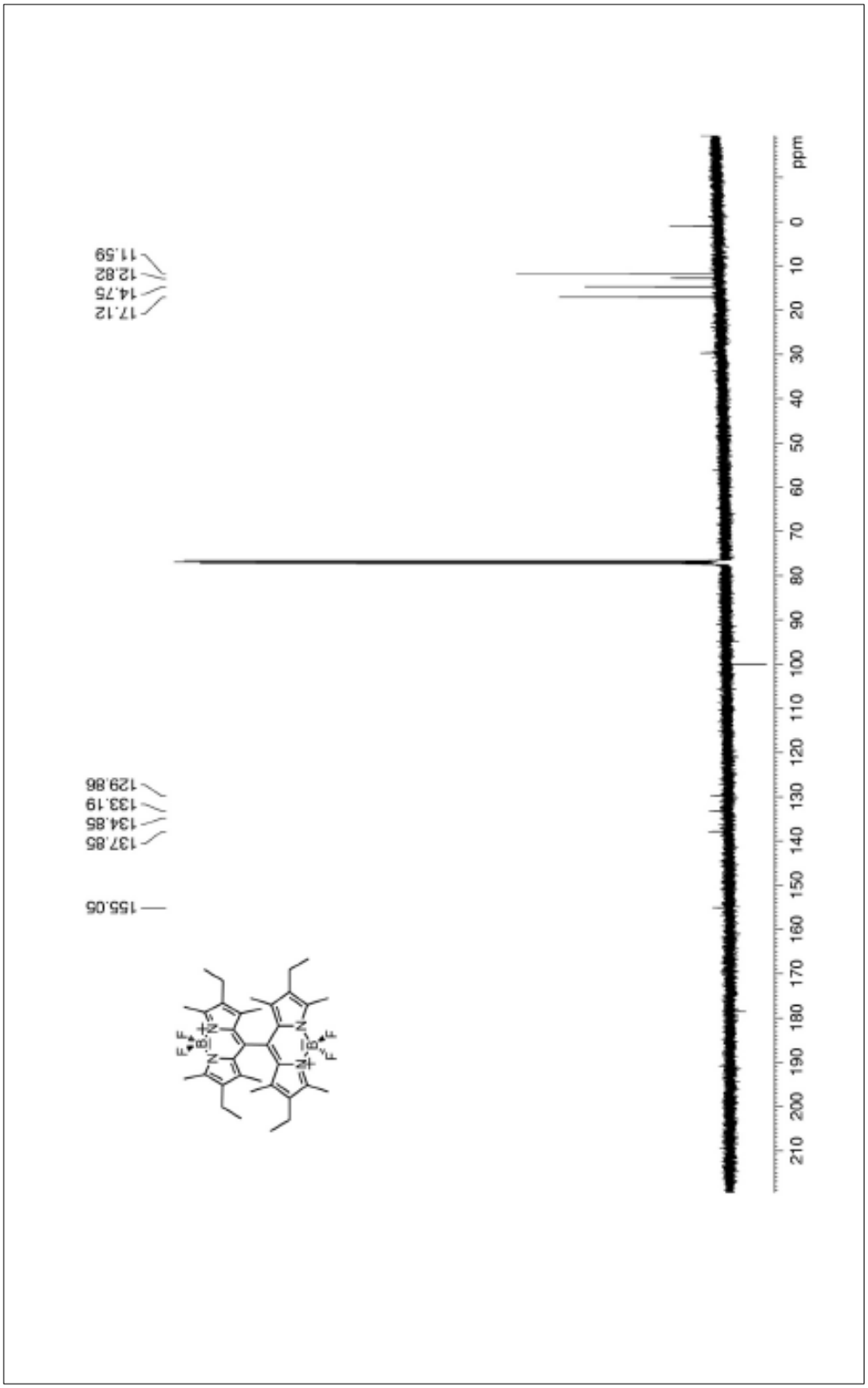
11.59
12.82
14.75
17.12
129.86
133.19
134.85
137.85
155.05
ppm

A.2.1.2 Mass Spectra

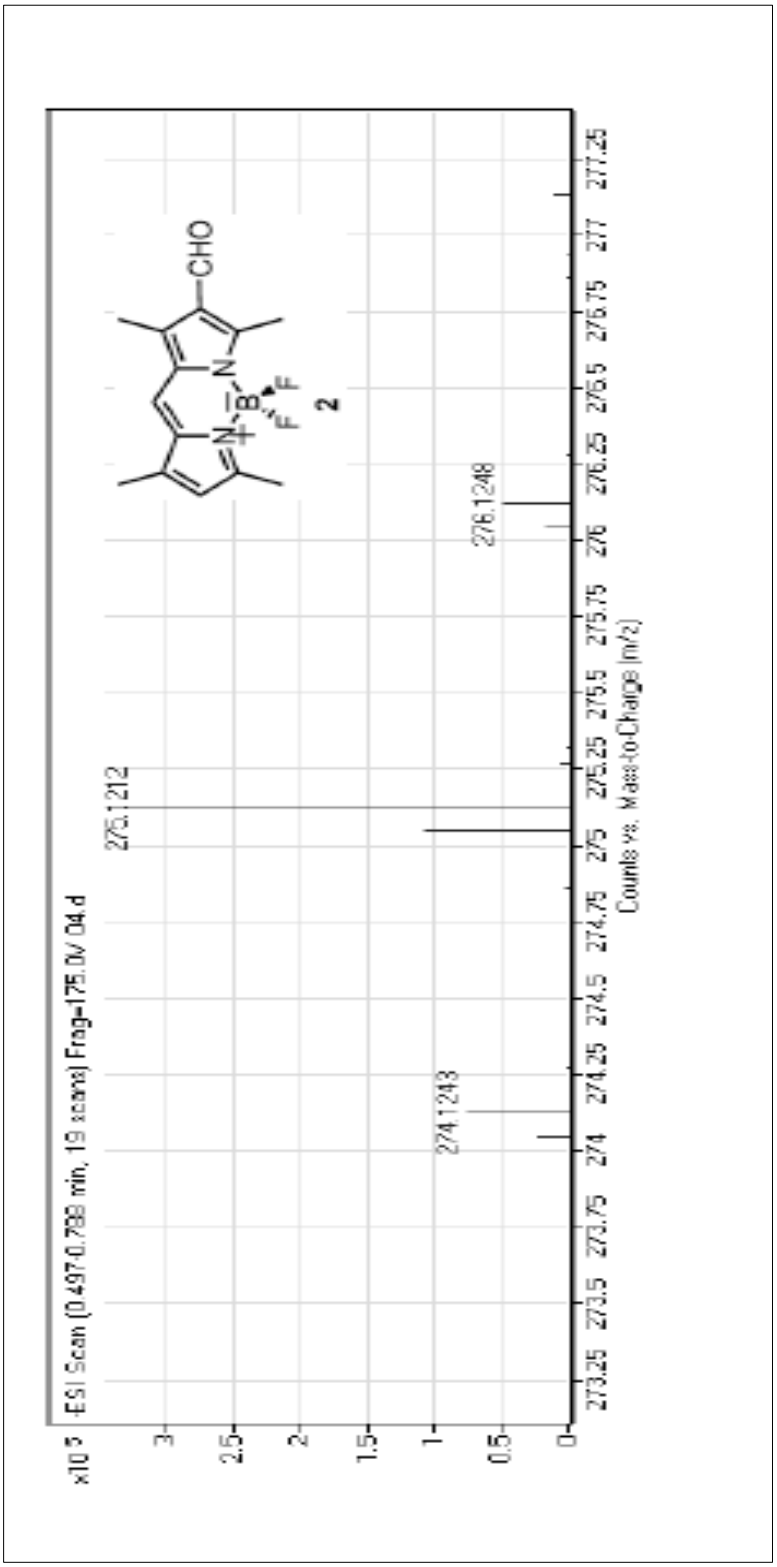

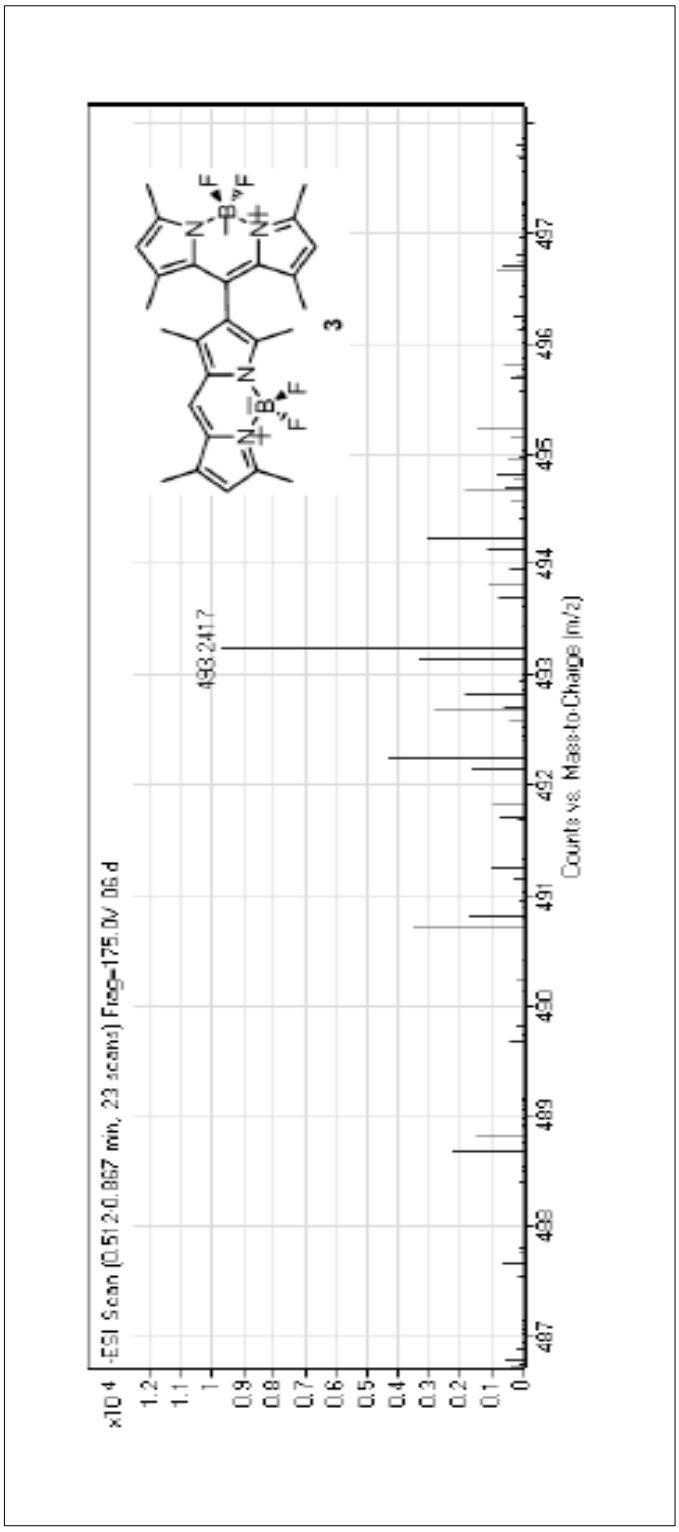
-ESI Scan (0.512:0.867 min, 23 scans) Frag=175.0V 06.d
x10 4
1.2
1.1
1
0.9
0.8
0.7
0.6
0.5
0.4
0.3
0.2
0.1
0
493.2417
487
488
489
490
491
492
493
494
435
496
497
Counts vs. Mass-to-Charge (m/z)
3

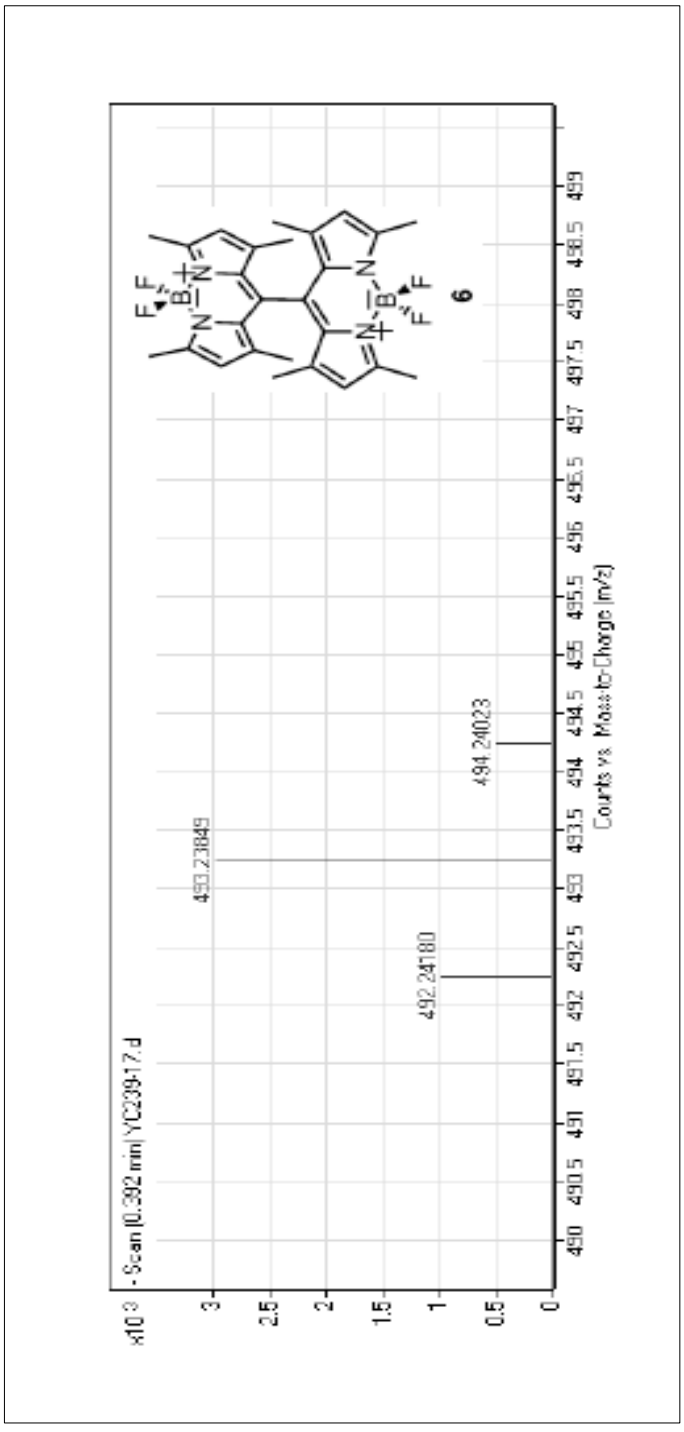
- Scan (0.392 min) YC239-17.d
x10 3
3
2.5
2
1.5
1
0.5
0
490
490.5
491
491.5
492
492.5
493
493.5
494
494.5
495
495.5
496
496.5
497
497.5
498
498.5
499
492.24180
493.23849
494.24023
Counts vs. Mass-to-Charge (m/z)
F
F
B
N
N
6

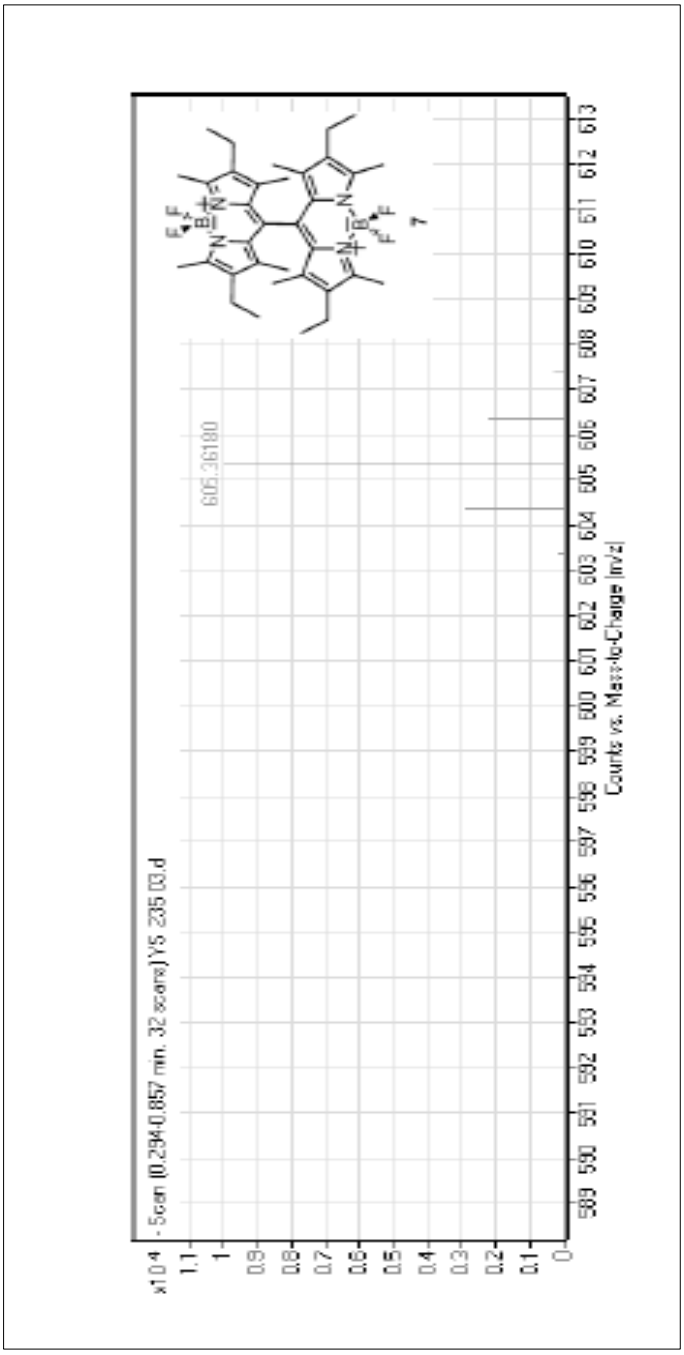
- Scan (0.294-0.857 min, 32 scans) YS 235 03.d
x10 4
1.1
1
0.9
0.8
0.7
0.6
0.5
0.4
0.3
0.2
0.1
0
589 590 591 592 593 594 595 596 597 598 599 600 601 602 603 604 605 606 607 608 609 610 611 612 613
Counts vs. Mass-to-Charge (m/z)
605.36180
7

A. 3 Designing Micelle-embedded BODIPY based photosensitizers for the Photodynamic Therapy

A.3.1. ^{1}H and ^{13}C NMR Spectra

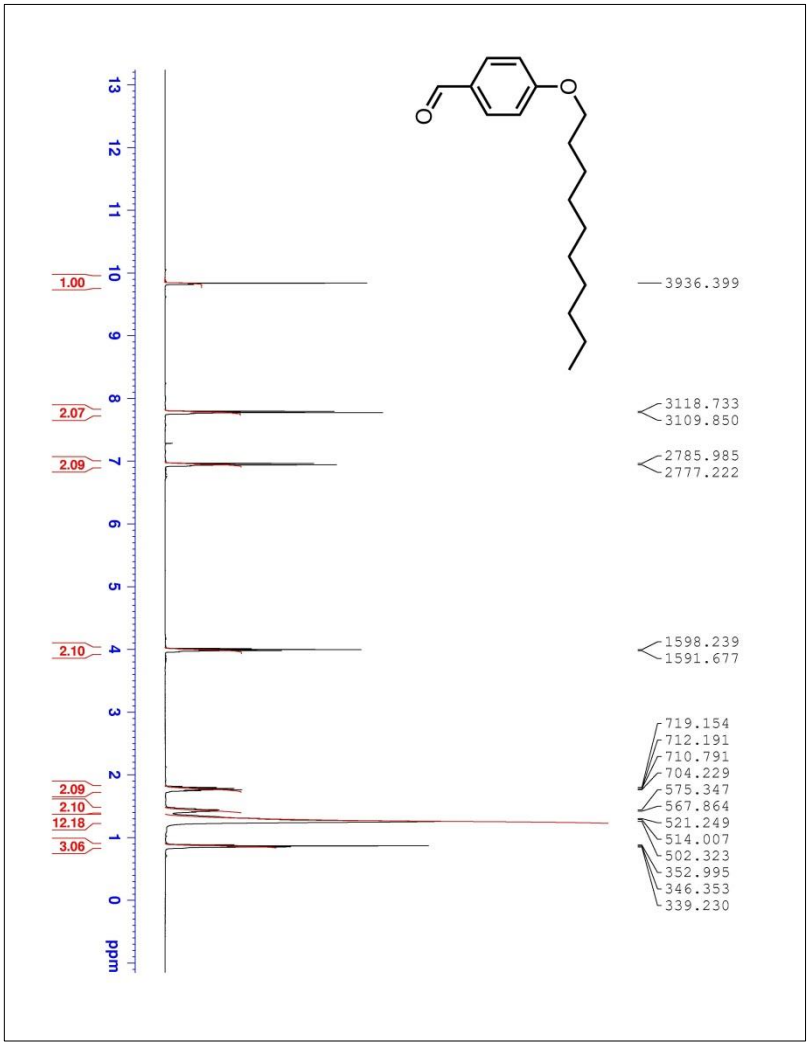

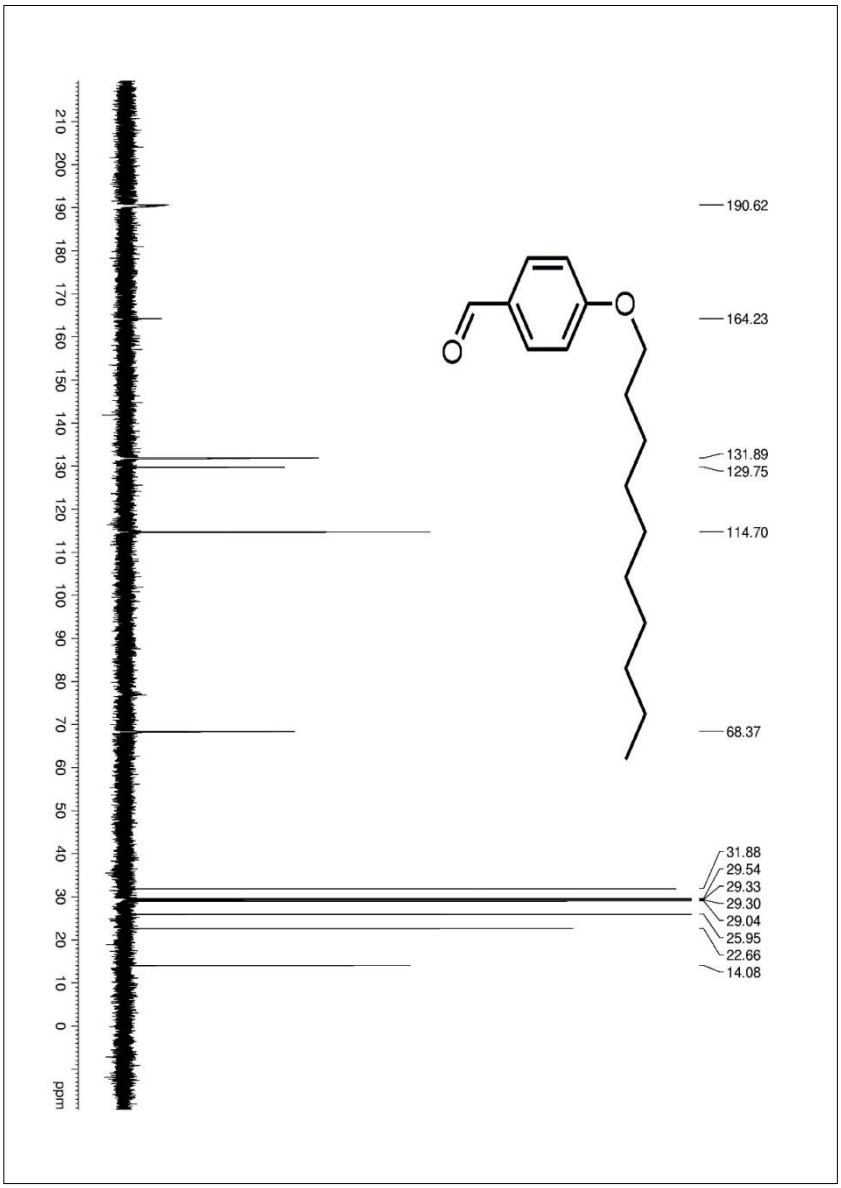
190.62
164.23
131.89
129.75
114.70
68.37
31.88
29.54
29.33
29.30
29.04
25.95
22.66
14.08
O
O
210 200 190 180 170 160 150 140 130 120 110 100 90 80 70 60 50 40 30 20 10 0
ppm

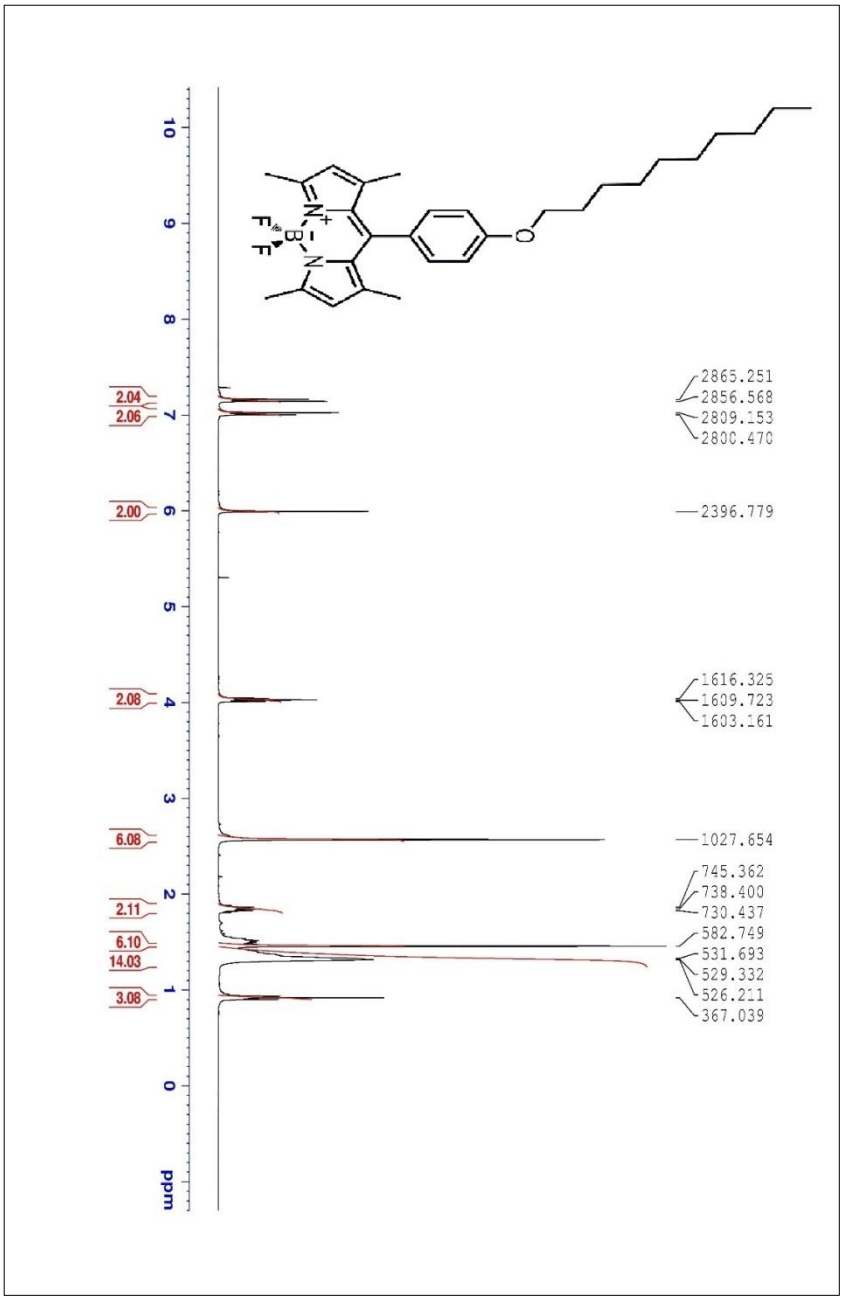
2865.251
2856.568
2809.153
2800.470
2396.779
1616.325
1609.723
1603.161
1027.654
745.362
738.400
730.437
582.749
531.693
529.332
526.211
367.039
2.04
2.06
2.00
2.08
6.08
2.11
6.10
14.03
3.08
ppm

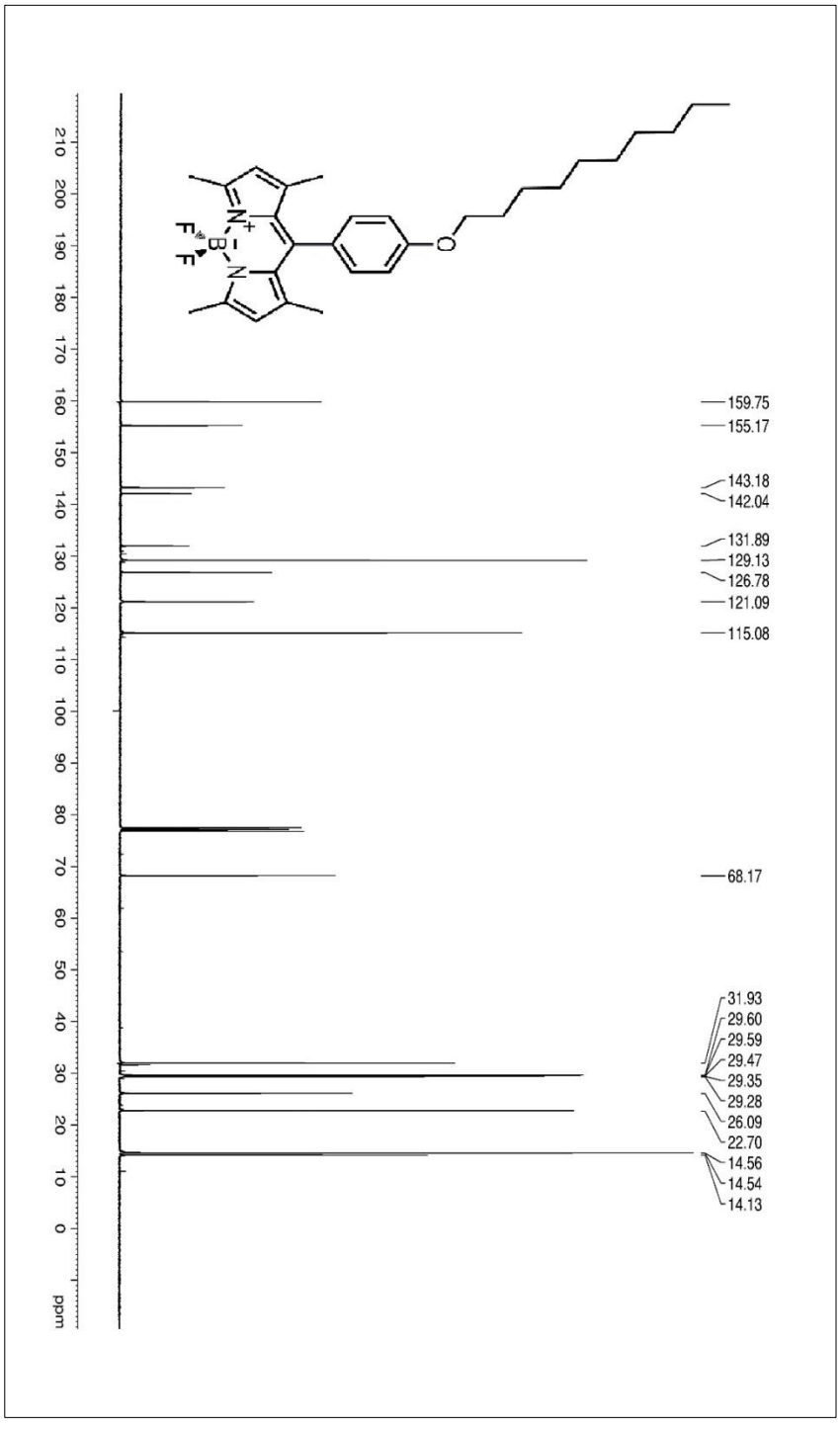
159.75
155.17
143.18
142.04
131.89
129.13
126.78
121.09
115.08
68.17
31.93
29.60
29.59
29.47
29.35
29.28
26.09
22.70
14.56
14.54
14.13
ppm

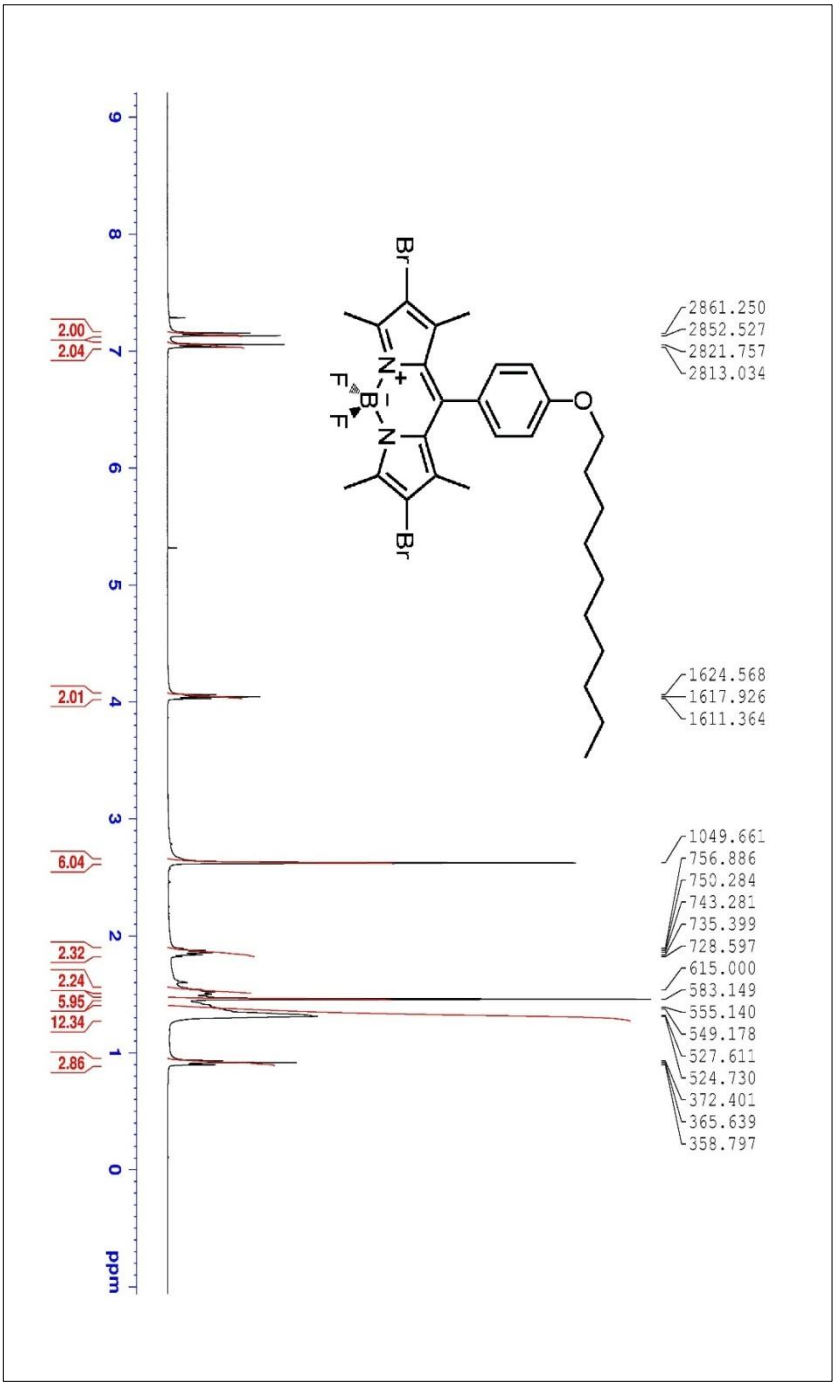
2.00
2.04
2.01
6.04
2.32
2.24
5.95
12.34
2.86
ppm
2861.250
2852.527
2821.757
2813.034
1624.568
1617.926
1611.364
1049.661
756.886
750.284
743.281
735.399
728.597
615.000
583.149
555.140
549.178
527.611
524.730
372.401
365.639
358.797

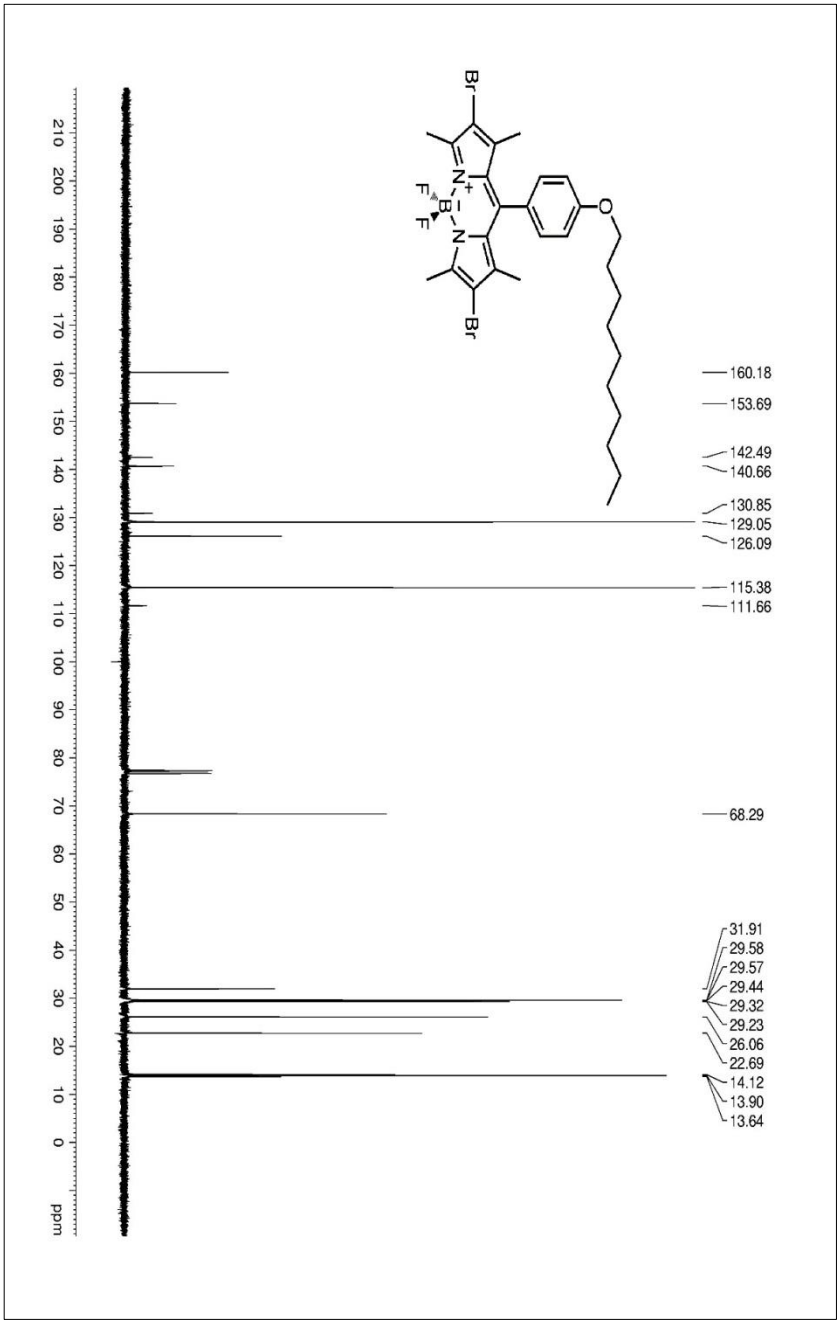
Br
N+
B−
F
F
N
O
Br
160.18
153.69
142.49
140.66
130.85
129.05
126.09
115.38
111.66
68.29
31.91
29.58
29.57
29.44
29.32
29.23
26.06
22.69
14.12
13.90
13.64
210 200 190 180 170 160 150 140 130 120 110 100 90 80 70 60 50 40 30 20 10 0 ppm

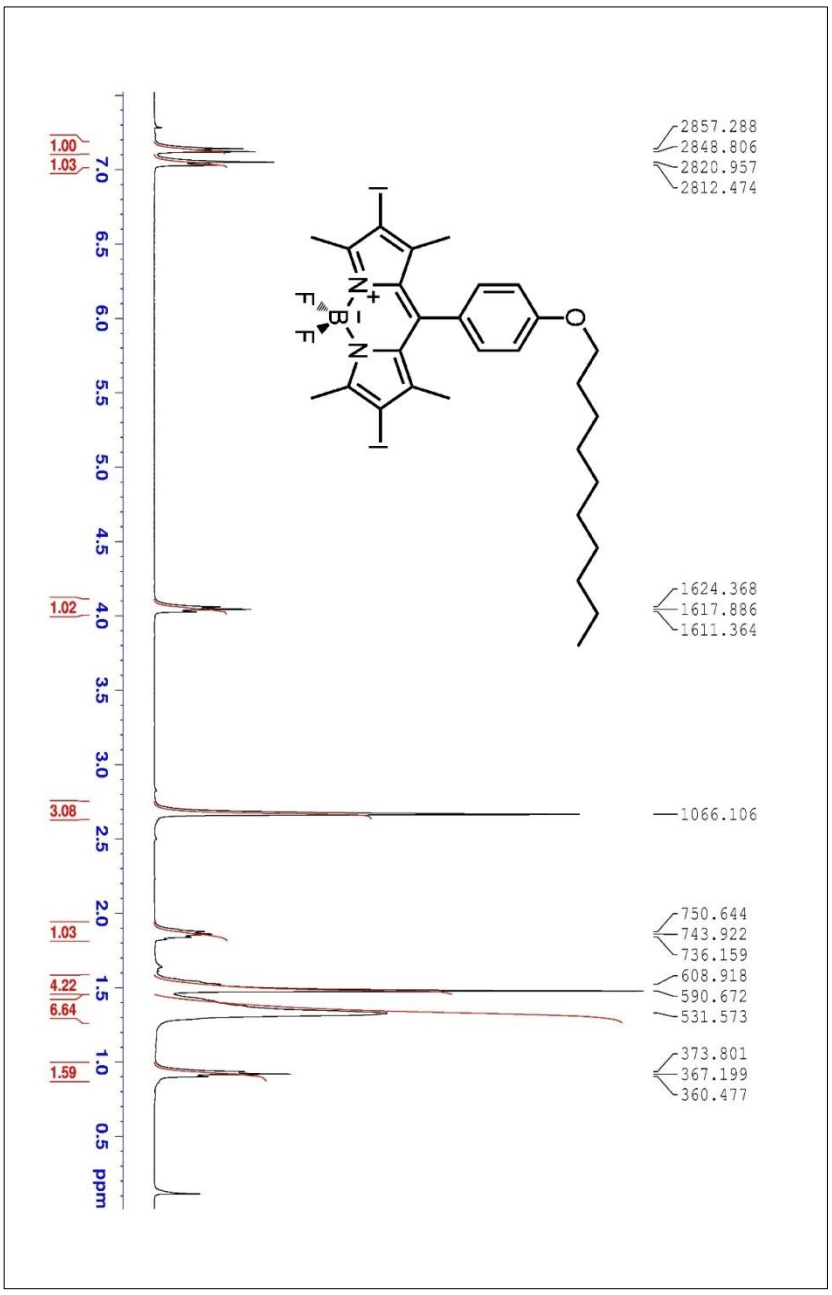
2857.288
2848.806
2820.957
2812.474
1624.368
1617.886
1611.364
1066.106
750.644
743.922
736.159
608.918
590.672
531.573
373.801
367.199
360.477
1.00
1.03
1.02
3.08
1.03
4.22
6.64
1.59
7.0
6.5
6.0
5.5
5.0
4.5
4.0
3.5
3.0
2.5
2.0
1.5
1.0
0.5
ppm

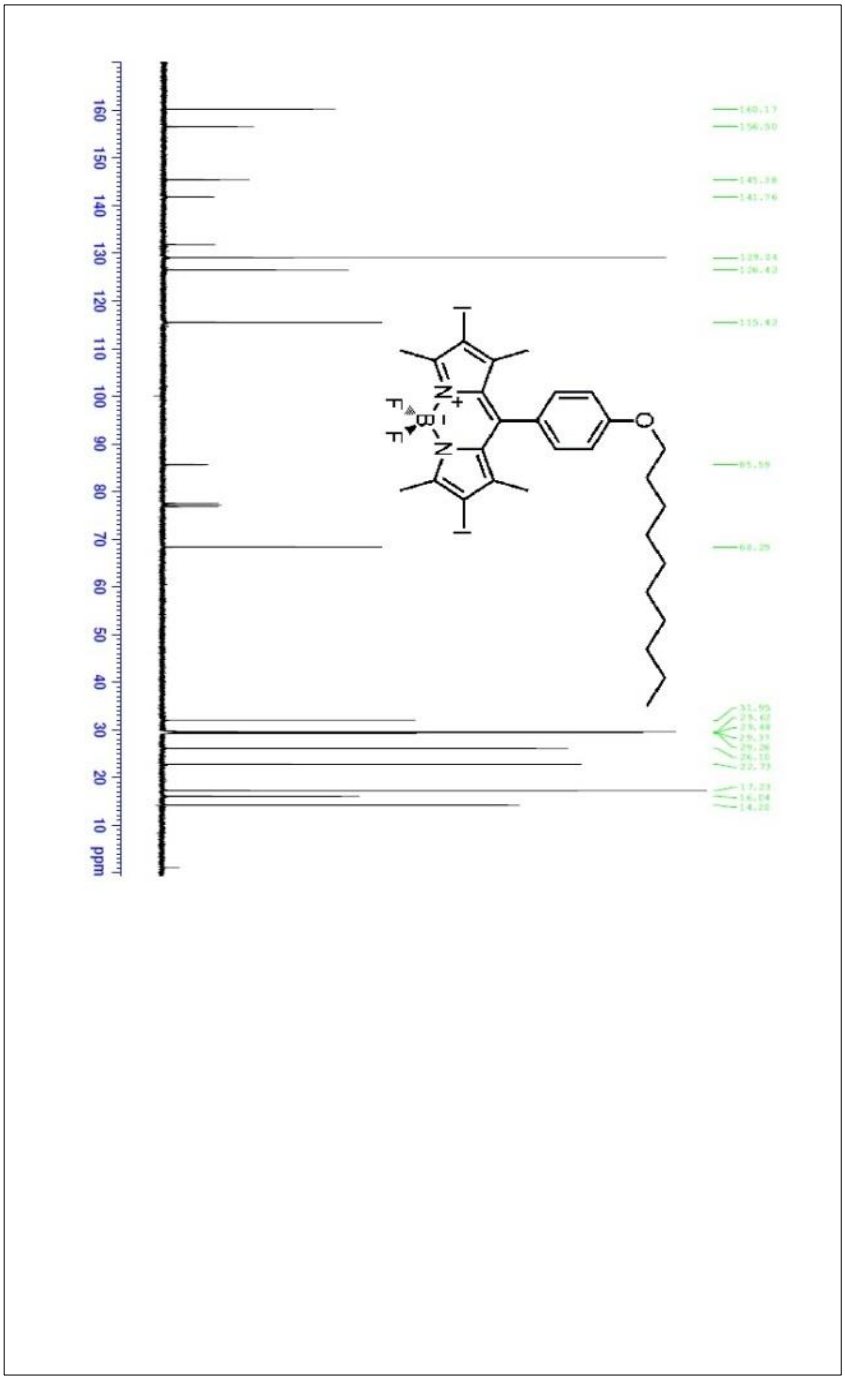
160
150
140
130
120
110
100
90
80
70
60
50
40
30
20
10
ppm
F
F
B
N
N

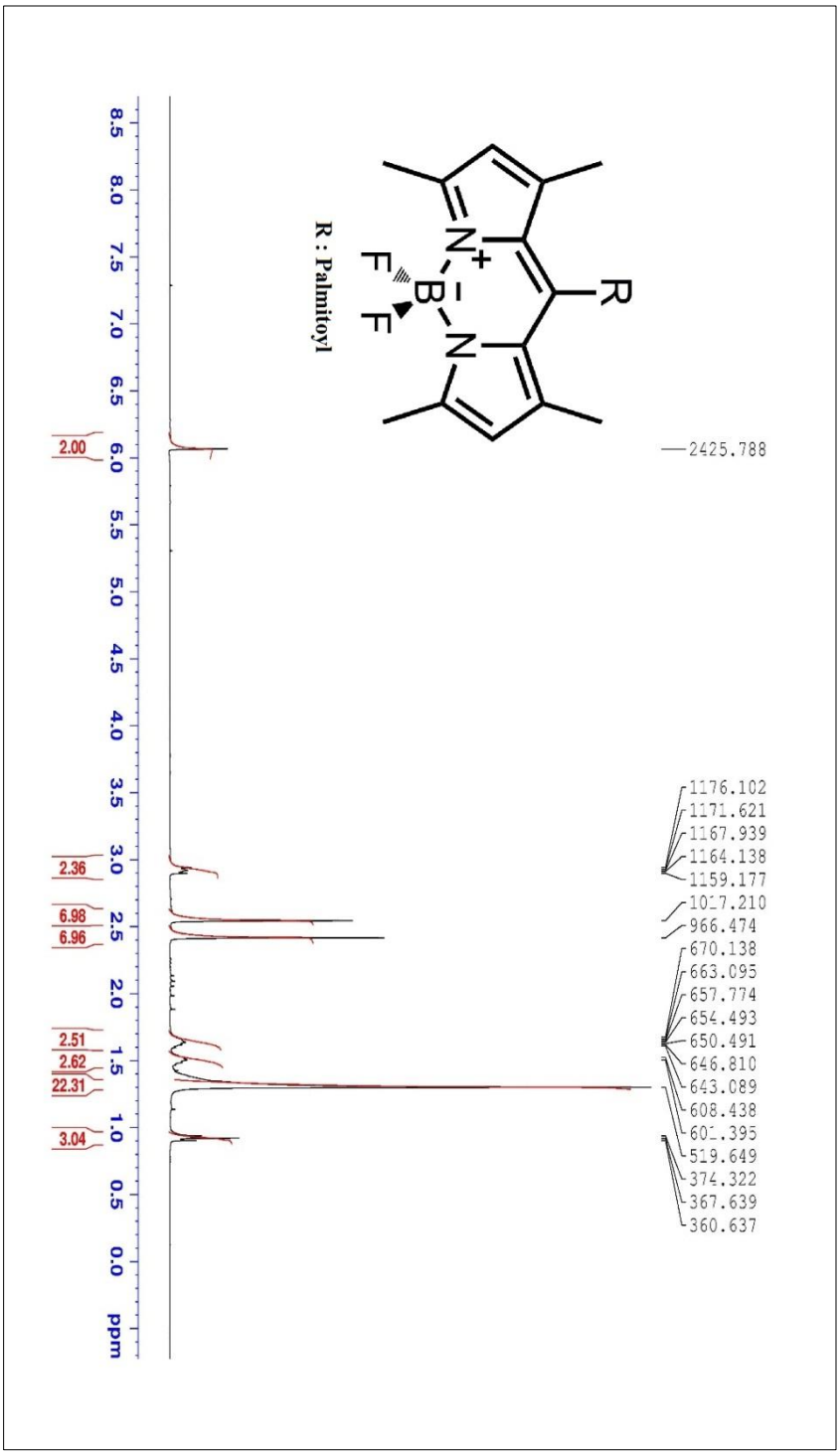
R : Palmitoyl
2425.788
1176.102
1171.621
1167.939
1164.138
1159.177
1017.210
966.474
670.138
663.095
657.774
654.493
650.491
646.810
643.089
608.438
601.395
519.649
374.322
367.639
360.637
2.00
2.36
6.98
6.96
2.51
2.62
22.31
3.04
ppm

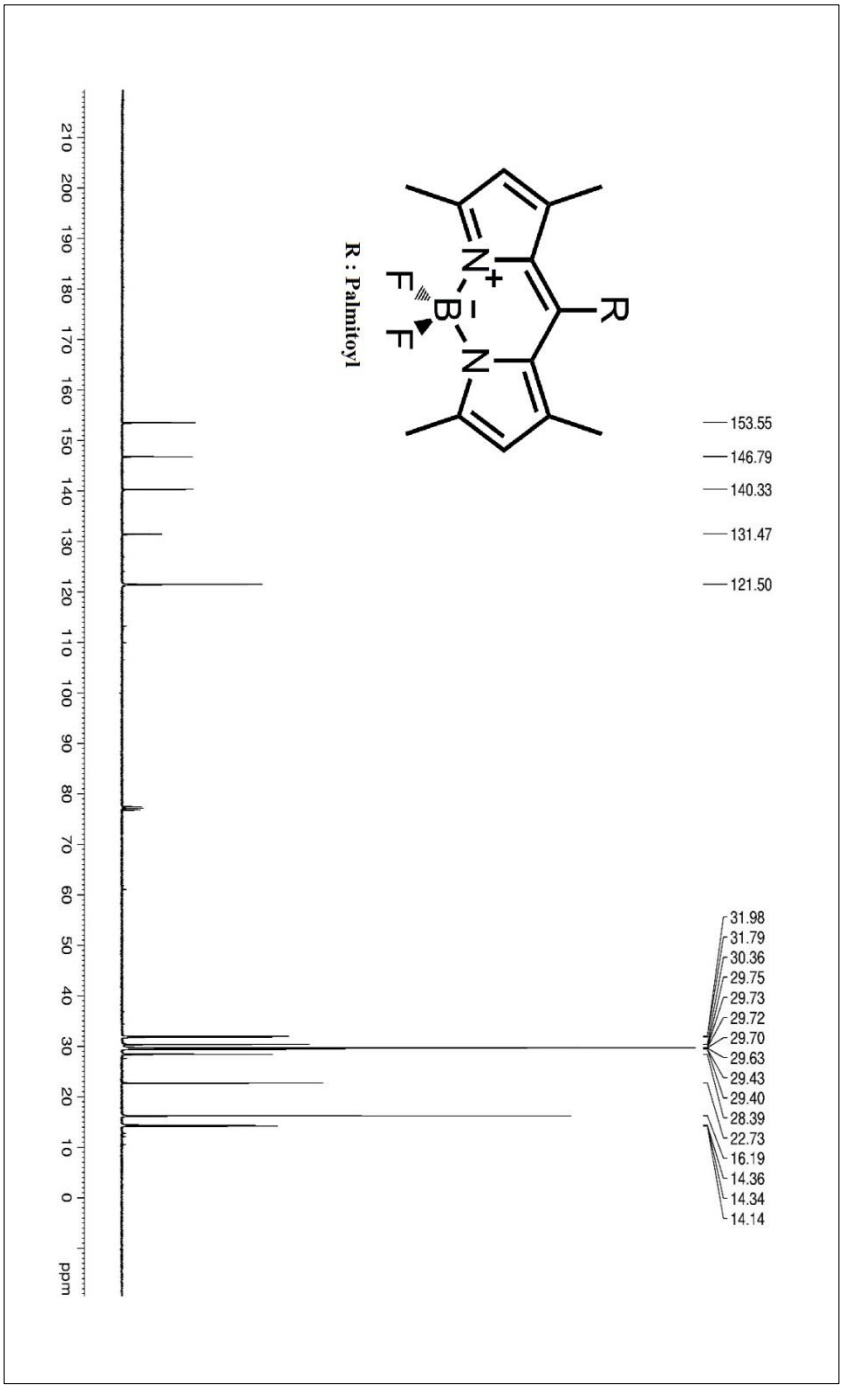
R : Palmitoyl
153.55
146.79
140.33
131.47
121.50
31.98
31.79
30.36
29.75
29.73
29.72
29.70
29.63
29.43
29.40
28.39
22.73
16.19
14.36
14.34
14.14
ppm

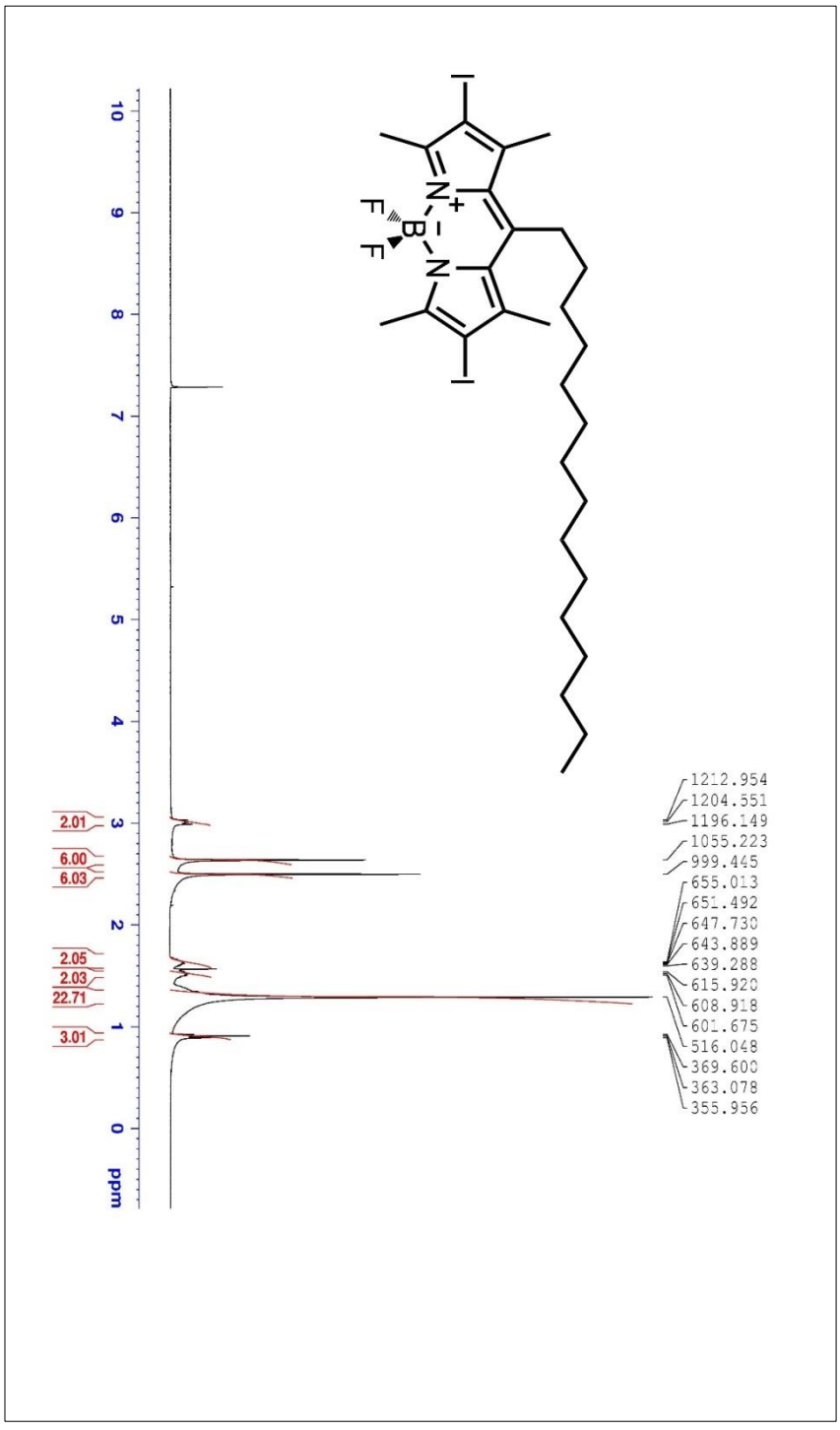
10
9
8
7
6
5
4
3
2
1
0
ppm
2.01
6.00
6.03
2.05
2.03
22.71
3.01
1212.954
1204.551
1196.149
1055.223
999.445
655.013
651.492
647.730
643.889
639.288
615.920
608.918
601.675
516.048
369.600
363.078
355.956

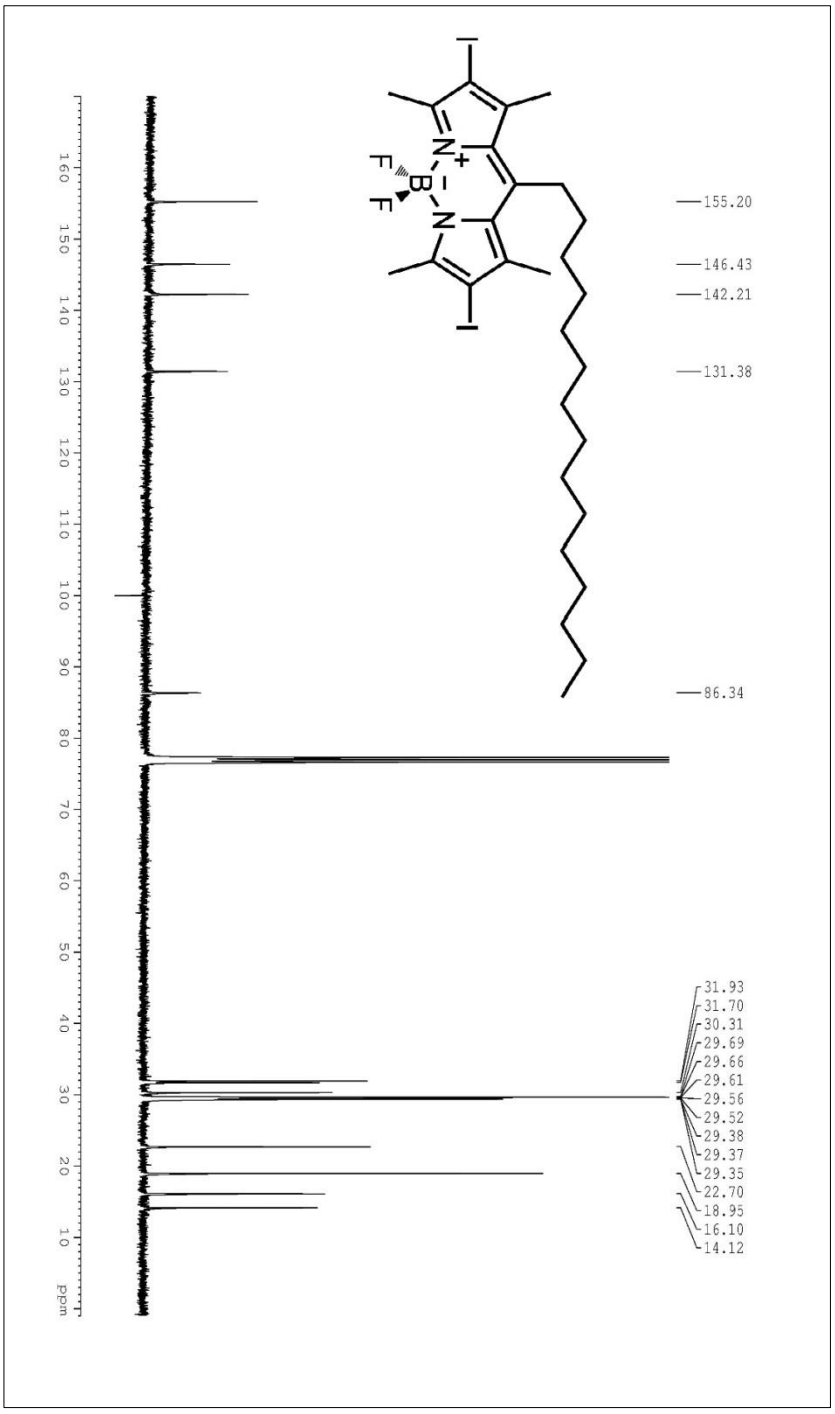
155.20
146.43
142.21
131.38
86.34
31.93
31.70
30.31
29.69
29.66
29.61
29.56
29.52
29.38
29.37
29.35
22.70
18.95
16.10
14.12
ppm

A.3.2. MASS SPECTRA

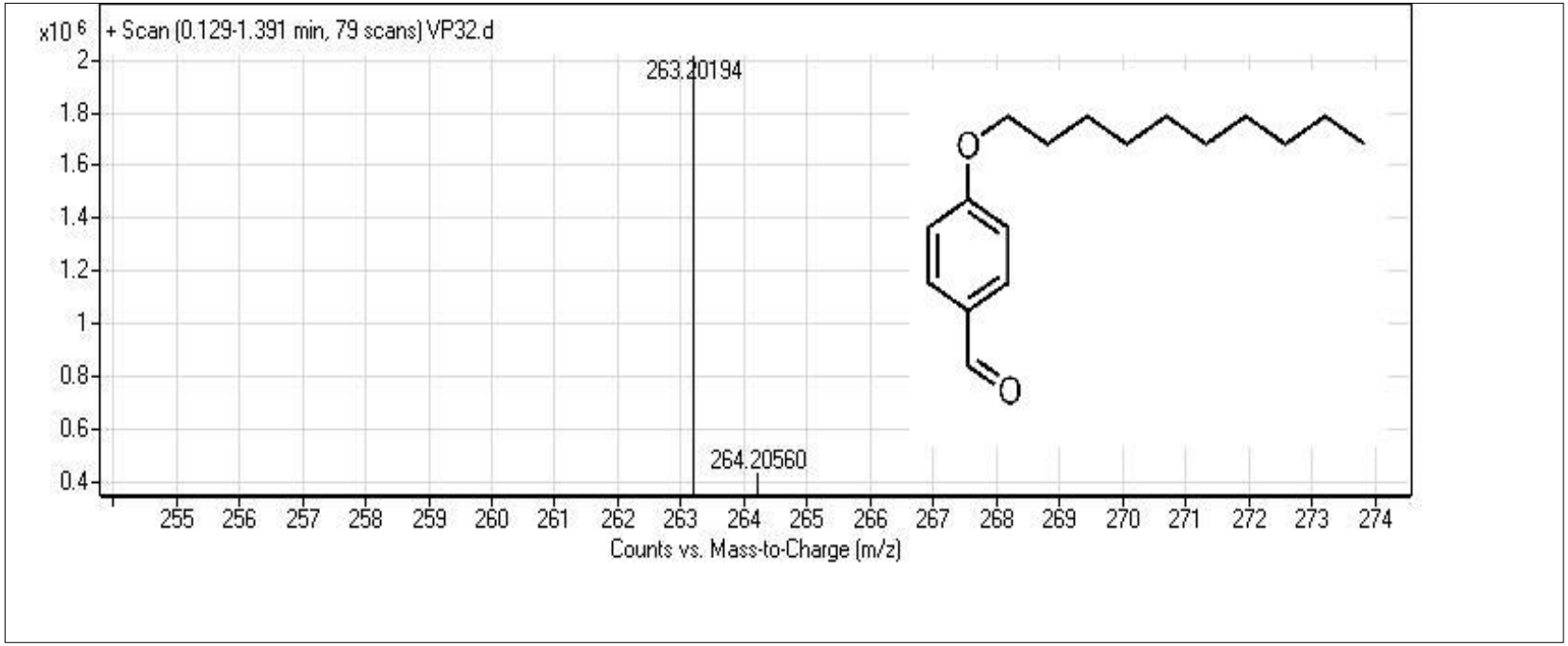
x10 6
+ Scan (0.129-1.391 min, 79 scans) VP32.d
263.20194
264.20560
2
1.8
1.6
1.4
1.2
1
0.8
0.6
0.4
255 256 257 258 259 260 261 262 263 264 265 266 267 268 269 270 271 272 273 274
Counts vs. Mass-to-Charge (m/z)
O
O

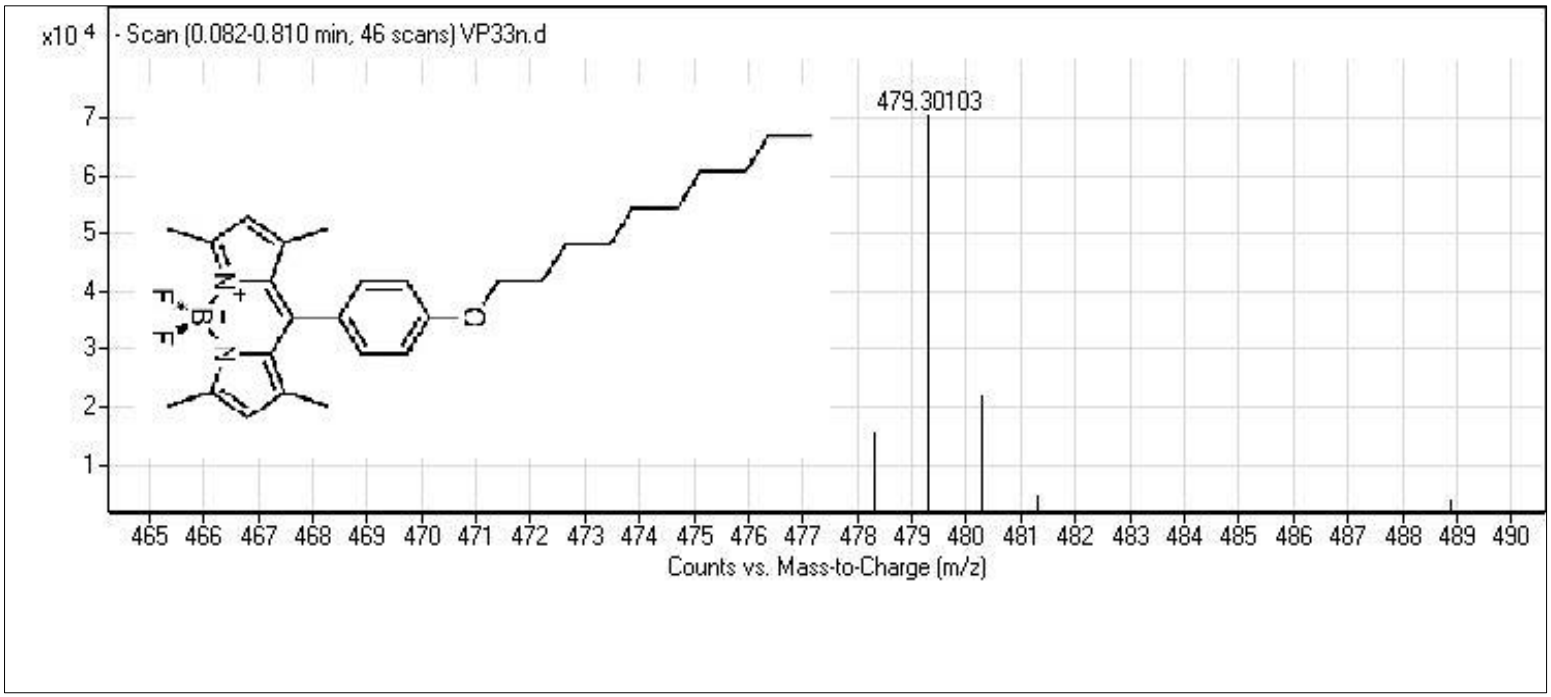
x10 4
- Scan (0.082-0.810 min, 46 scans) VP33n.d
479.30103
7
6
5
4
3
2
1
465 466 467 468 469 470 471 472 473 474 475 476 477 478 479 480 481 482 483 484 485 486 487 488 489 490
Counts vs. Mass-to-Charge (m/z)

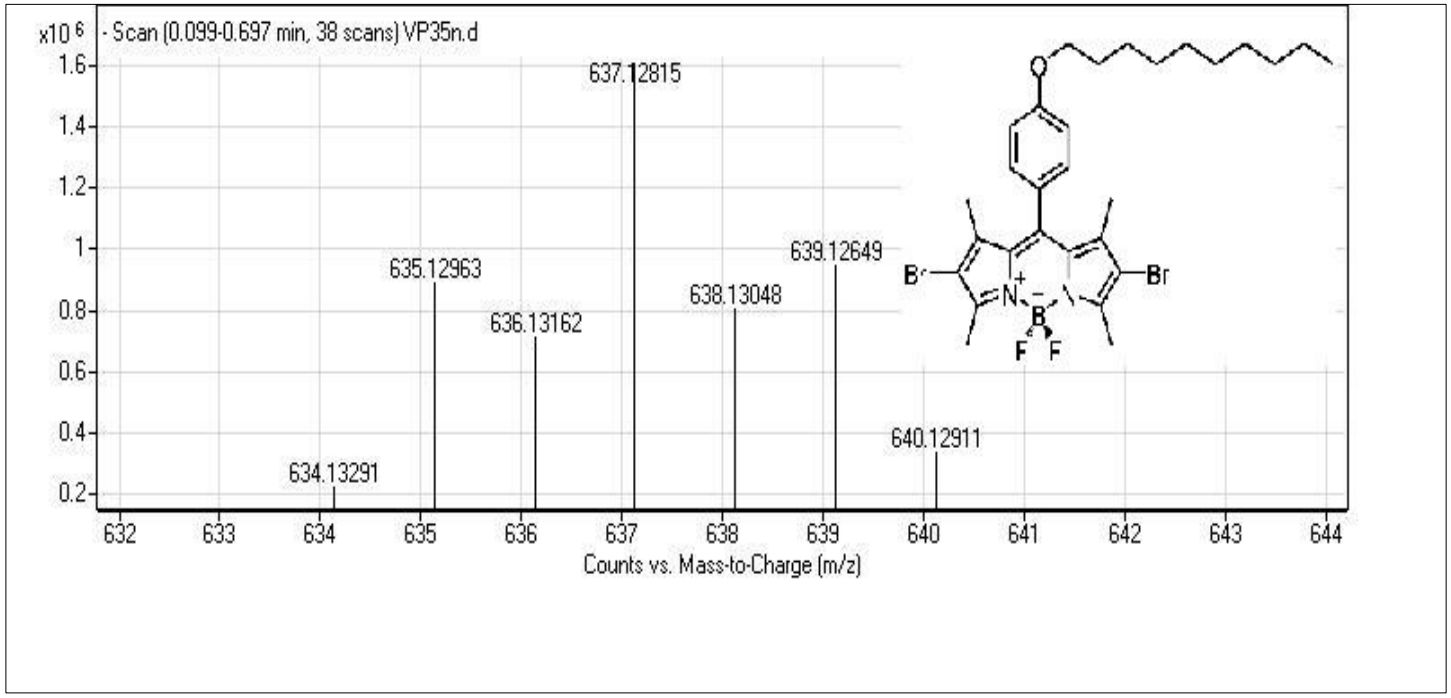
x10 6
- Scan (0.099-0.697 min, 38 scans) VP35n.d
1.6
1.4
1.2
1
0.8
0.6
0.4
0.2
637.12815
635.12963
639.12649
638.13048
636.13162
634.13291
640.12911
632
633
634
635
636
637
638
639
640
641
642
643
644
Counts vs. Mass-to-Charge (m/z)
O
Br
Br
N
B
F
F

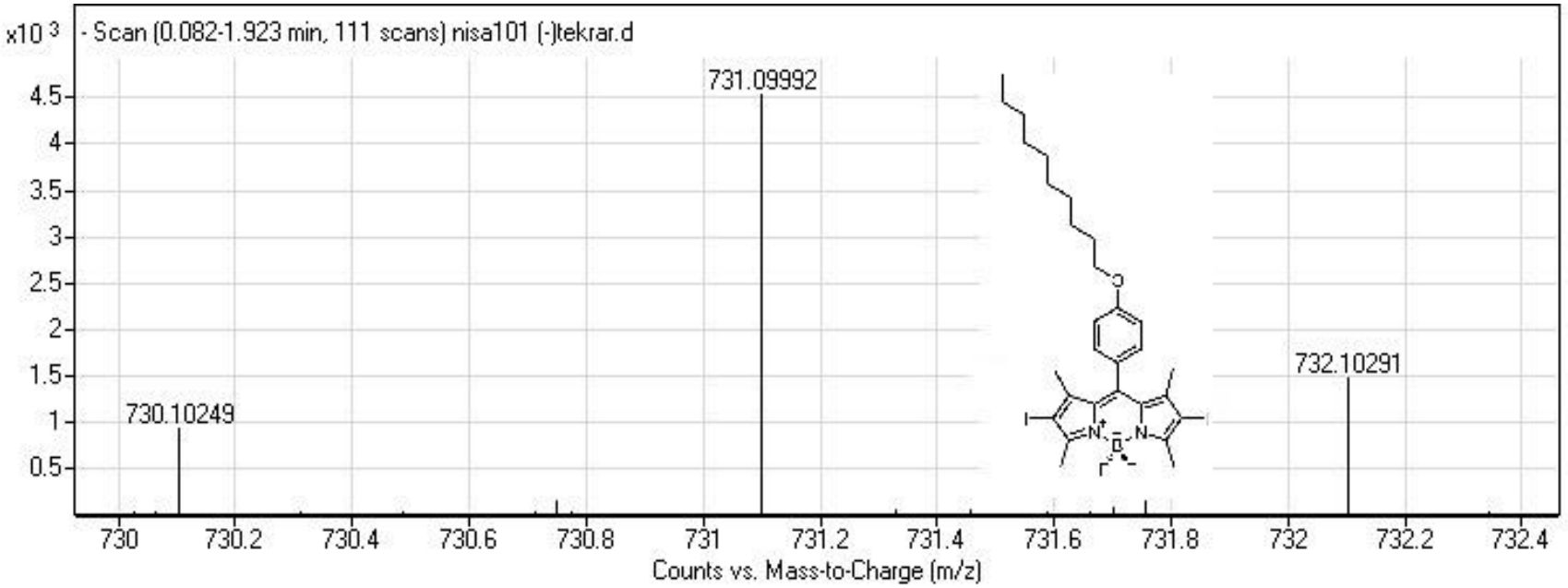
x10 3
- Scan (0.082-1.923 min, 111 scans) nisa101 (-)tekrar.d
731.09992
730.10249
732.10291
4.5
4
3.5
3
2.5
2
1.5
1
0.5
730
730.2
730.4
730.6
730.8
731
731.2
731.4
731.6
731.8
732
732.2
732.4
Counts vs. Mass-to-Charge (m/z)

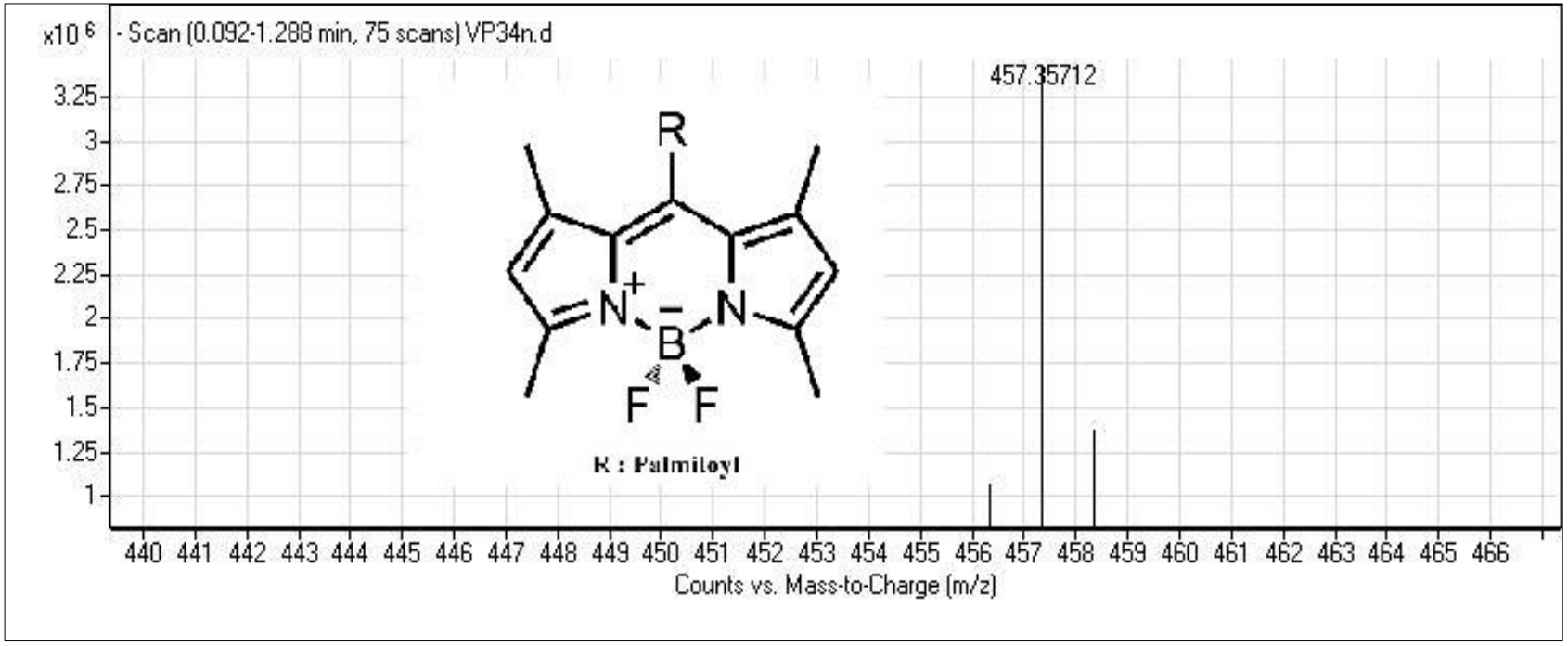
x10 6
- Scan (0.092-1.288 min, 75 scans) VP34n.d
457.35712
3.25
3
2.75
2.5
2.25
2
1.75
1.5
1.25
1
R
N+
B
N
F
F
R : Palmitoyl
440 441 442 443 444 445 446 447 448 449 450 451 452 453 454 455 456 457 458 459 460 461 462 463 464 465 466
Counts vs. Mass-to-Charge (m/z)

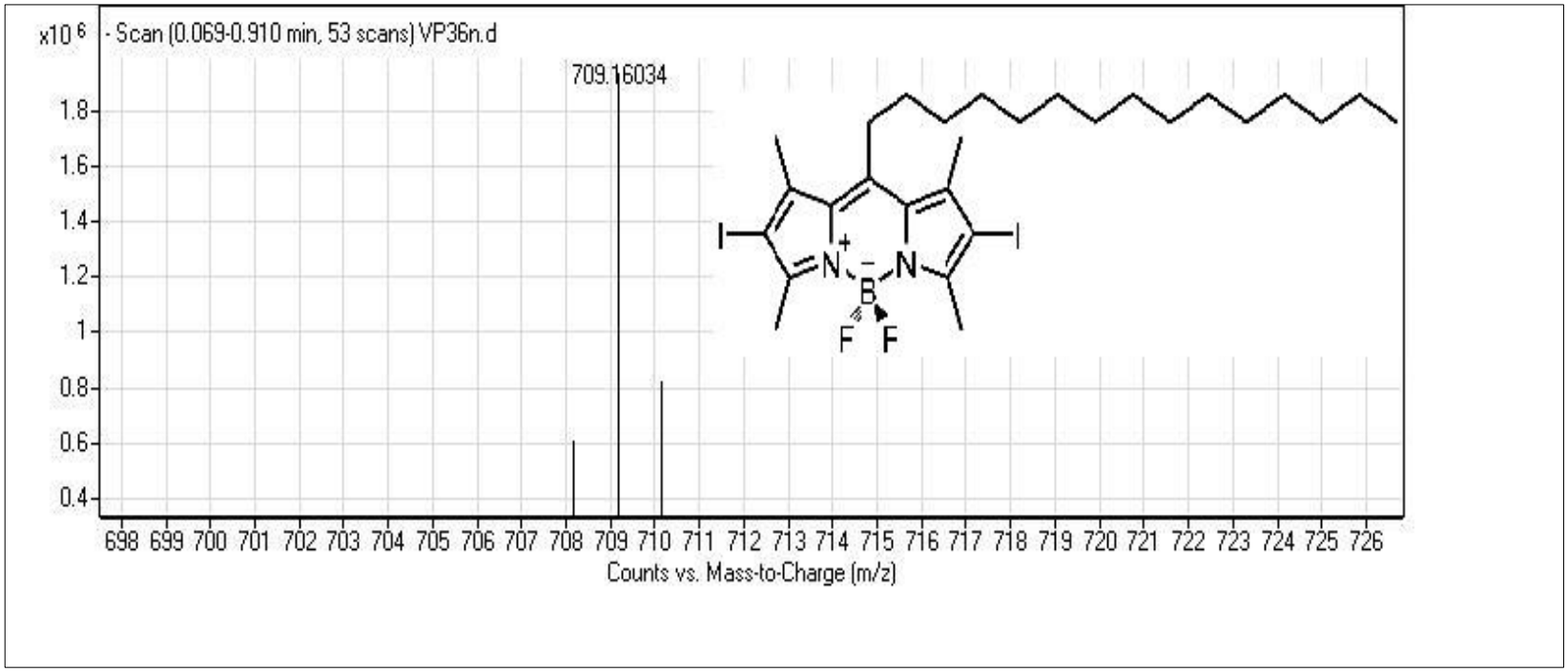
x10 6
- Scan (0.069-0.910 min, 53 scans) VP36n.d
709.16034
1.8
1.6
1.4
1.2
1
0.8
0.6
0.4
698 699 700 701 702 703 704 705 706 707 708 709 710 711 712 713 714 715 716 717 718 719 720 721 722 723 724 725 726
Counts vs. Mass-to-Charge (m/z)
I
I
N+
B
N
F
F